

Dissertation zur Erlangung des Doktorgrades
der Fakultät für Chemie und Pharmazie
der Ludwig-Maximilians-Universität München



**Loss of mitochondrial thioredoxin reductase
delays angiogenic switch and
impairs tumour growth**

Juliane Hellfritsch, geb. Hrdina
aus Bad Schlema

2011

Erklärung

Diese Dissertation wurde im Sinne von § 13 Abs. 3 bzw. 4 der Promotionsordnung vom 29. Januar 1998 von Herrn Professor Dr. Ulrich Pohl betreut und von Frau Professor Dr. Angelika Vollmar von der Fakultät für Chemie und Pharmazie vertreten.

Ehrenwörtliche Versicherung

Diese Dissertation wurde selbstständig, ohne unerlaubte Hilfe erarbeitet.

München, den 04.01.2011

.....
Juliane Hellfritsch

Dissertation eingereicht am:	04.01.2011
1. Gutachter:	Prof. Dr. Angelika Vollmar
2. Gutachter:	Prof. Dr. Ulrich Pohl
Mündliche Prüfung am:	11.02.2011

*"No one would have crossed the ocean
if he could have gotten off the ship in the storm."*

Charles F. Kettering

TABLE OF CONTENTS

1.	INTRODUCTION	1
1.1.	The mammalian thioredoxin family	1
1.1.1.	Thioredoxins	2
1.1.2.	Thioredoxin reductases	2
1.1.3.	Selenium is essential for thioredoxin reductase activity	3
1.2.	Mitochondrial thioredoxin reductase	5
1.2.1.	Structure and function of Txnrd2	5
1.2.2.	Implication of Txnrd2 in mitochondrial metabolism	7
1.2.3.	Targeted deletion of Trx2 and Txnrd2	9
1.3.	Tumour biology: How cancer arises	11
1.3.1.	The multi-step process of cancer	11
1.3.2.	Tumour vascularisation: the ‘angiogenic switch’	12
1.3.3.	Vascular endothelial growth factor in tumour angiogenesis	14
1.3.4.	Hypoxia and Hif-signalling in tumour biology	16
1.3.5.	Implication of mitochondria in tumour progression	22
1.4.	Thioredoxin reductases in relation to cancer and Hif-signalling	25
1.5.	Intention of the present work	27
2.	MATERIALS AND METHODS	28
2.1.	Materials	28
2.2.	Methods	38
2.2.1.	Cell culture techniques and related assays	38
2.2.2.	Flow cytometry	45
2.2.3.	High-resolution respirometry	48
2.2.4.	Molecular biology techniques	50
2.2.5.	Gene transfer methods	58
2.2.6.	Protein biochemistry	60
2.2.7.	Biochemical assays	64
2.2.8.	Tumour transplantation protocols	68
2.3.	Statistics	70

3.	RESULTS	71
3.1.	Long-term effects of Txnrd2-deletion in murine fibroblasts	71
3.1.1.	Characterisation of immortalised fibroblasts lacking Txnrd2	71
3.1.2.	GSH-depletion is associated with increased ROS levels in Txnrd2-deficient cells	72
3.1.3.	Cells respond to Txnrd2 deletion by upregulating other redox enzymes	73
3.1.4.	Structure and functionality of mitochondria in Txnrd2-deficient cells	76
3.1.5.	Respiratory capacity of Txnrd2-deficient cells	79
3.1.6.	Metabolic changes due to Txnrd2-deletion	81
3.2.	Studies of the impact of Txnrd2-deletion in transformed cells <i>in vitro</i>	85
3.2.1.	Generation of transformed Txnrd2-knockout cells	85
3.2.2.	Deletion of Txnrd2 impairs colony formation capacity of tumour cells	86
3.2.3.	Generation and characterisation of clonal single-cell lines	90
3.2.4.	Analysis of mitochondrial parameters and cellular metabolism following transformation of Txnrd2-knockout cells	93
3.3.	Relevance of Txnrd2 for <i>in vivo</i> tumour growth	96
3.3.1.	Loss of Txnrd2 limits tumour growth	96
3.3.2.	Histological analysis of Txnrd2-deficient tumours	98
3.3.3.	Quantification of apoptotic cells and necrotic area in tumour sections	98
3.3.4.	Impaired tumour growth due to restricted proliferation of tumour cells	100
3.3.5.	Loss of Txnrd2 delays the angiogenic switch	101
3.3.6.	Investigation of angiogenic key players in Txnrd2-deficient tumours	105
3.3.7.	Starved Txnrd2-deficient cells express decreased Hif-1 α levels	108
3.3.8.	Hif-1 α translation is altered in Txnrd2-deficient cells	110
3.3.9.	Txnrd2-null tumours are susceptible to pharmacological GSH-inhibition	111
3.4.	Txnrd2-deficiency modifies function of endothelial cells	114
3.4.1.	Generation and characterisation of Txnrd2-deficient eEPCs	114
3.4.2.	Tamoxifen-inducible endothelial-specific Txnrd2 knockout mice	117
4.	DISCUSSION	119
4.1.	Immortalised MEFs compensate Txnrd2-deficiency by induction of other redox-regulating enzymes	119
4.2.	Txnrd2-deficient fibroblasts switch their energy metabolism from oxidative phosphorylation to anaerobic glycolysis	121
4.3.	Txnrd2 is necessary for colonigenic potential of transformed MEFs	126
4.4.	Transformed Txnrd2-deficient single cell-derived cells were still sensitive towards GSH-depletion	128

4.5.	Loss of Txnrd2 impairs tumour growth due to limited proliferation and diminished tumour vascularisation	131
4.6.	Angiogenic signalling is impaired in Txnrd2-deficient tumours and tumour cells	133
4.7.	Depletion of GSH de novo synthesis in Txnrd2-null tumours further diminishes tumour growth	134
4.8.	Txnrd2 impacts on eEPC proliferation and angiogenic function	135
4.9.	Future prospects	137
5.	SUMMARY	139
6.	REFERENCES	140
7.	APPENDIX	172
7.1.	Abbreviations	172
7.2.	Publications	178
7.2.1.	Poster presentations	178
7.2.2.	Oral communication	178
7.2.3.	Original publication	179
7.3.	Curriculum vitae	180
7.4.	Acknowledgements	181

INDEX OF FIGURES

Figure 1-1: Postulated mechanism for the reduction of Trx by mammalian Txnrd	4
Figure 1-2: Structure of mammalian mitochondrial thioredoxin reductase (Txnrd2)	6
Figure 1-3: Electron transfer from the NADPH/H ⁺ via the mitochondrial Trx-dependent system to H ₂ O ₂	7
Figure 1-4: Mitochondria structure	8
Figure 1-5: Conditional deletion of the Txnrd2 gene	10
Figure 1-6: The 'angiogenic switch' in tumour progression	14
Figure 1-7: Contribution of VEGF to tumour angiogenesis	16
Figure 1-8: Implication of hypoxia and Hif-1 α in tumour physiology	17
Figure 1-9: Gene domain structure of human Hif-1 α	19
Figure 1-10: Hif-1 α is regulated by oxygen availability	20
Figure 1-11: Involvement of reactive oxygen species in Hif-signalling	22
Figure 1-12: Implication of mitochondria in cancer cells and tumour progression	24
Figure 2-1: Oxygraph-2k	48
Figure 2-2: High-resolution respirometry in permeabilised murine fibroblasts	49
Figure 2-3: Map of the intermediate vector 141pCAG-3SIP-mXCT	56
Figure 2-4: Map of the expression vector 141pCAG-3SIP-N'TAPe-mito-mTxnrd2-puro	57
Figure 2-5: Reduction of glutathione	65
Figure 2-6: GSH recycling mechanism by Tietze ³⁰⁹	66
Figure 2-7: Bioluminescent determination of ATP	68
Figure 2-8: Dorsal skinfold chamber implanted on a nude mouse ²⁸	69
Figure 3-1: Analysis of Txnrd2 expression in immortalised murine fibroblasts	72
Figure 3-2: Proliferation and intracellular ROS level of Txnrd2-deficient fibroblasts	73
Figure 3-3: Activity and expression of redox-regulating enzymes	75
Figure 3-4: Structural analysis of mitochondria in Txnrd2-deficient fibroblasts	76
Figure 3-5: Quantitative evaluation of mitochondria in Txnrd2-deficient fibroblasts	78
Figure 3-6: Functional analysis of respiratory chain complexes	80
Figure 3-7: Quantification of respiratory capacity in Txnrd2-deficient fibroblasts	81
Figure 3-8: Changes in energy metabolism due to Txnrd2-deletion	83
Figure 3-9: Expression of <i>GLUT-1</i> and <i>PGC1α</i>	84
Figure 3-10: Transformation of Txnrd2 wild-type and knockout fibroblasts with <i>c-myc</i> and <i>Ha-ras</i> ^{v12}	86
Figure 3-11: Txnrd2-deletion impairs colony formation capacity	88

Figure 3-12: Influence of NAC and restoration of a redox-inactive Txnrd2 on colonogenic capacity	89
Figure 3-13: Proliferation and colonogenic potential of single-cell clones	91
Figure 3-14: Analysis of ROS and redox-regulating systems following transformation	92
Figure 3-15: Mitochondria shape and energy metabolism of transformed fibroblasts	94
Figure 3-16: Activity of the respiratory chain in transformed fibroblasts	95
Figure 3-17: Observation of tumour growth <i>in vivo</i>	97
Figure 3-18: Morphological analysis of tumour sections	99
Figure 3-19: Number of cleaved-caspase 3 positive cells in tumour sections	100
Figure 3-20: Analysis of proliferation in tumour sections	101
Figure 3-21: Analysis of tumour vascularisation	103
Figure 3-22: Intravital microscopy of tumor vessel network	104
Figure 3-23: Analysis of Hif-1 α in tumour tissue	105
Figure 3-24: Quantification of VEGF in tumour samples	106
Figure 3-25: Quantification of PHD2 in tumours on day three and 11	107
Figure 3-26: Expression of Hif-1 α in Txnrd2-deficient tumour cells	108
Figure 3-27: Quantitative analysis of <i>Hif-1α</i> mRNA-level	109
Figure 3-28: Analysis of PHD2 in transformed cells	110
Figure 3-29: Phosphorylation of Akt	111
Figure 3-30: Inhibition of GSH synthesis further limits tumour growth of Txnrd2-null tumours	113
Figure 3-31: Generation of eEPC Txnrd2 wild-type and Txnrd2-deficient cell lines	115
Figure 3-32: Limited pro-angiogenic potential of Txnrd2-deficient eEPCs	116
Figure 3-33: Breeding scheme for endothelial-specific Txnrd2-null mice	118

INDEX OF TABLES

Table 1-1: Stages of tumour development	12
Table 2-1: PCR standard protocol	51
Table 2-2: Real-time PCR standard protocol	52
Table 2-3: Composition of acrylamid stacking and separating gel	61
Table 2-4: Primary antibodies for immunoblotting	62
Table 2-5: Secondary antibodies for immunoblotting	62

1. INTRODUCTION

Extensive research in the field of redox regulation particularly during the last couple of years has reshaped the mainly 'bad-guy' image of reactive oxygen species (ROS) and has provided a clearer understanding of thiol-based redox chemistry in living organisms. Previously, ROS have been mainly considered to compromise cell survival by damaging cellular macromolecules and exerting cell-death-promoting effects. But cells also express systems that deliberately produce ROS to mediate numerous physiological processes, including cell cycle progression, cell survival and redox-regulated transcription regulation. Cells have developed versatile and sophisticated mechanisms to ensure an appropriate redox balance. To maintain cellular redox balance, cells rely on non-enzymatic antioxidants as well as on enzymatic antioxidant systems. Endogenous and nutritional compounds such as glutathione (GSH), cysteine, uric acid, coenzyme Q, ascorbic acid (vitamin C), α -tocopherol (vitamin E) and carotenoids may directly interact with ROS to detoxify them. Enzymes involved in the regulation of the cellular redox state are superoxide dismutases (SOD), catalases, peroxiredoxins (Prx), and enzymes of the glutathione-dependent system and the thioredoxin-dependent system. The two major factors that keep the cytosol and cellular compartments in a reduced state are the tripeptide GSH and the oxidoreductase thioredoxin (Trx). Thioredoxin and its co-operating molecules are ubiquitous in archaea, bacteria and eukarya. Various pathologies and chronic diseases result from an imbalance between the cellular ROS production and their clearance by antioxidant defense systems. Atherosclerosis, Alzheimer's disease and cancer represent only few of a wide range of disorders, which are believed, at least in part, to be caused by pathologically elevated intracellular ROS levels. The present study aims to elucidate functions of the mammalian mitochondrial thioredoxin reductase (Txnrd2), particularly in tumour pathologies.

1.1. The mammalian thioredoxin family

Due to their intracellular localisation, two main thioredoxin-dependent systems are described in mammals. The most studied system is localised in the cytosol consisting of thioredoxin 1 (Trx1) and the thioredoxin reductase 1 (Txnrd1)³⁰⁶. The second less characterised system is mainly confined to mitochondria and consists of thioredoxin 2 (Trx2) and thioredoxin reductase 2 (Txnrd2)¹⁰⁷. Both systems in their respective compartment exert similar mechanisms to keep proteins of these cellular compartments in a reduced state. Furthermore, a third thioredoxin reductase, also named thioredoxin/glutaredoxin reductase (Txnrd3/TGR), was discovered that is predominantly expressed in testis. This enzyme differs from the other

two Txnrds in that it is able to reduce oxidised glutathione (GSSG) and glutathione-related disulfides besides the main substrate, oxidised thioredoxin (Trx-S₂)³⁰².

1.1.1. Thioredoxins

Thioredoxins are relatively small proteins (10 to 12 kDa) that contain two conserved cysteinyl residues in the active site sequence -Cys-Gly-Pro-Cys-³³⁴. These two cysteines are essential for the ability of thioredoxins to reduce other proteins. During the thiol-disulfide exchange reaction they undergo reversible oxidation and reduction. Thioredoxin (Trx-(SH)₂) reduces disulfide bonds in proteins. The oxidised form of thioredoxin (Trx-S₂) is in turn reduced by thioredoxin reductase in an NADPH-dependent reaction (Figure 1-1). Genetic deletion of Trx1 and Trx2 is embryonic lethal, reflecting the essential role of both in murine embryogenesis^{200, 233}.

Both thioredoxins are essential for keeping intracellular proteins in a reduced state. Depending on their subcellular localisation, both thioredoxins fulfil different tasks and participate in a broad range of signalling pathways. Thioredoxins supply reducing equivalents to enzymes like ribonucleotide reductase¹⁷⁷ and some thioredoxin peroxidases⁵¹. Through thiol-disulfide exchange reactions they may reduce Cys in transcription factors, thereby regulating the expression of stress response genes and oxidative stress-related apoptosis²²⁶. It has also been reported that thioredoxins function as growth factors in cells¹⁰⁶ and have the ability to inhibit the process of apoptosis¹⁴. Thus, it seems likely that thioredoxins may also contribute to pathological changes in living organisms. After infections, myocardial ischemia-reperfusion and oxidative stress, serum/plasma levels of thioredoxin were found to be elevated and expression levels positively correlated with the occurrence of cardiac diseases¹⁶³. In 2001 Nakamura *et al.* discovered increased levels of thioredoxin in the serum of human immunodeficiency virus (HIV)-patients which was shown to be associated with poor prognosis²²⁵.

1.1.2. Thioredoxin reductases

Thioredoxin reductases fundamentally differ between lower and higher organisms. In complex eukaryotes these enzymes are more closely related to glutathione reductase (GR) than to bacterial thioredoxin reductase. For instance, the enzyme is larger and displays broader substrate specificity compared to their bacterial counterparts. Additional to the N-terminal active site mammalian thioredoxin reductases have an additional redox active site at the conserved C-terminus sequence containing selenocysteine (Sec) (-Gly-Cys-Sec-Gly-) (Figure 1-2).

Thioredoxin reductases belong to the family of flavoproteins and are homodimeric proteins of 55 to 56 kDa. Each monomer contains an active site coupled with a redox-active disulfide, FAD as a prosthetic group and an NADPH binding site (Figure 1-2). The enzymes are named thioredoxin reductases due to their ability to reduce oxidised thioredoxin (Trx-S₂). The postulated mechanism for the reduction of thioredoxin by mammalian thioredoxin reductase is displayed in figure 1-1³⁵⁷.

In addition to thioredoxin, other substrates have been shown to be reduced by thioredoxin reductases. The substrate spectrum depends on the subcellular localisation of the enzyme. Txnrd1 is known to interact with lipid hydroperoxides³⁰, dehydroascorbic acid²⁰¹ and the ascorbyl free radical²⁰². Substrates of the Txnrd2 shall be discussed in a subsequent section (see chapter 1.2.1).

Similar to Trx1 and Trx2, targeted deletion of either Txnrd1 or Txnrd2 is embryonic lethal in mice, albeit at different embryonic stages^{61, 151}.

1.1.3. Selenium is essential for thioredoxin reductase activity

Selenium is a non-metal chemical element, which is in its properties related to sulphur and tellurium. Selenium salts are toxic in large amounts, but in trace amounts selenium is essential for cellular function. As selenocysteine (Sec) it is incorporated in the active site of enzymes, e.g. glutathione peroxidases, thioredoxin reductases or iodide peroxidases.

During the conversion of inorganic selenium to organic forms, many different metabolites are formed in animals. Hydrogen selenite is a key metabolite of selenium. It provides selenium for the synthesis of selenoproteins including thioredoxin reductases. Selenium is essential for the activity of thioredoxin reductases. The addition of 1 µM sodium selenite to the culture medium increased the cellular activity of thioredoxin reductase 37-fold in MCF-7 breast cancer cells, 19-fold in HT-29 colon cancer cells and 8-fold in A549 lung cancer cells. This increase in activity was accompanied with a slight elevation of mRNA and protein amount of the enzyme¹⁰¹. *In vivo*, dietary supplementation of rats with supra-nutritional levels of selenium causes a transient increase in activity without affecting protein levels of thioredoxin reductase²⁵. These results indicate that the elevated activity is due to increased selenium incorporation.

Selenium is incorporated in thioredoxin reductases in form of the 21st amino acid Sec. Sec is encoded by the opal codon UGA, which is normally recognised as a signal for termination of protein synthesis¹⁹¹. But in the presence of a specific cis-acting element in the 3'untranslated region (UTR), a mRNA secondary structure termed SECIS (selenocysteine insertion sequence) element, the UGA is decoded as Sec¹⁰⁷. Sec is essential for the catalytic activity of thioredoxin reductases. A truncated enzyme lacking the Sec-Gly peptide

or with Sec replaced by Ser resulted in an inactive enzyme. Mutation of the Sec to Cys resulted in a decreased activity, increased binding of thioredoxin and a change in pH optimum³⁵⁸. Removal of the C-terminus, where Sec is located, either by enzymatic treatment (carboxypeptidase), alkylation, or Cre-mediated deletion resulted in inactivation of thioredoxin reductases^{61, 118, 151, 356}.

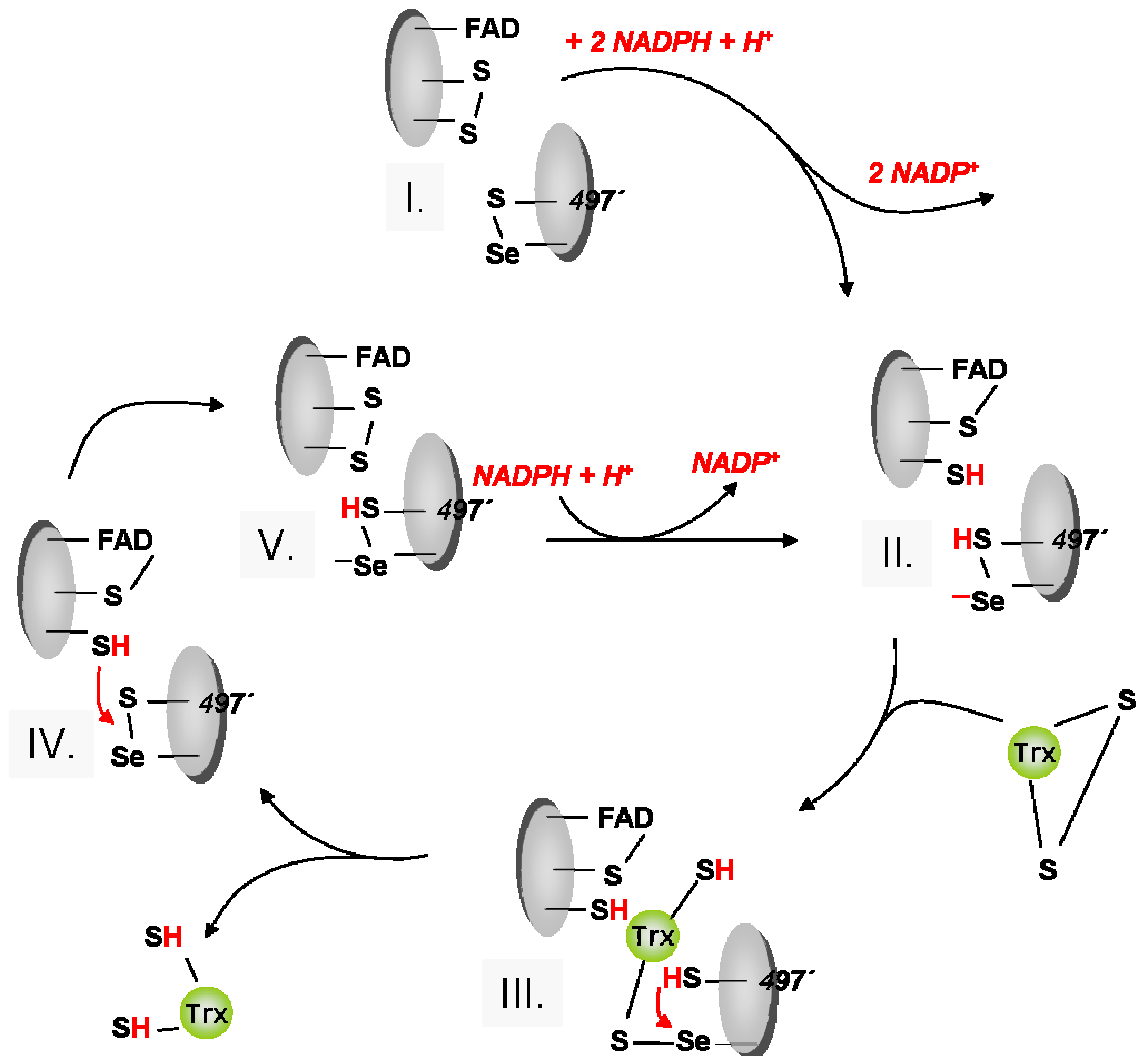


Figure 1-1: Postulated mechanism for the reduction of Trx by mammalian Txnrd

The catalytic reaction starts with the reduction of the selenenylsulfide (I.) to the selenolate anion (-Se⁻) (II.). The selenolate anion attacks the disulfides of Trx and the resulting enzyme-Trx-mixed selenenylsulfide is attacked by Cys497 to regenerate the selenenylsulfide (III.). The latter is reduced again by the active site thiolate of the other subunit (IV.). During the reaction the active site dithiol maintains the selenol in the reduced state. In general, the selenolate anion represents a better nucleophilic and leaving group than the thiolate anion. The scheme was adapted from Zhong *et al.*, 2000³⁵⁷.

1.2. Mitochondrial thioredoxin reductase

In december 2010 a search for 'thioredoxin reductase' returns 1642 entries (thereof 128 reviews) in the free digital archive of biomedical and life sciences, Pubmed, starting in 1964. An extensive search for 'mitochondrial thioredoxin reductase' resulted in only 36 hits (including 2 reviews) starting in 1998.

The mammalian Txnrd1 was the first enzyme of the group to be discovered in 1996³⁰⁶. Hence structure, function and implication in physiological and pathological processes have been mainly elaborated for Txnrd1, whereas much less is known about Txnrd2, which predominantly localises to mitochondria.

1.2.1. Structure and function of Txnrd2

The discovery of a mitochondrial thioredoxin²⁹³ predicted the existence of a mitochondrial thioredoxin reductase that maintains this thioredoxin in its reduced form. The identification and initial characterisation of a novel human thioredoxin reductase included a different molecular mass and distinct pattern of tissue expression compared to the cytosolic form¹⁰⁷. This enzyme showed 54% homology with the cytosolic thioredoxin reductase and harbours the same catalytic sites. Moreover, it contains an 36 amino acid long N-terminal extension (absent in Txnrd1), which emerged to be a typical mitochondrial leader peptide (Figure 1-2). Almost simultaneously, mitochondria-specific thioredoxin reductase were described in *Saccharomyces cerevisiae*²⁴¹, mouse²¹⁴, rat²⁶⁷ and cow³³⁰. Except for the yeast enzyme, all reductases are selenoproteins. The human mitochondrial thioredoxin reductase consists of 18 exons and maps to chromosome 22q11.2²¹³. In mouse the gene maps to chromosome 16q11.2²¹⁴. The mRNA of Txnrd2 was found to be expressed in all human, mouse and rat tissues analysed, with highest expression levels in tissues with high energy demand (e.g. testis, skeletal muscle, heart, liver)¹⁸¹.

The mitochondrial electron-transport system consumes 85-90% of the oxygen required within cells. Due to incomplete reduction of oxygen to water in the mitochondrial respiratory chain, mitochondria are one of the sites with the highest ROS production in cells, in particular superoxide anion (O_2^-), hydrogen peroxide (H_2O_2) and hydroxyl radicals ($HO\bullet$)²⁹⁰.

Glutathione peroxidases (GPx), glutathione reductase (GR) and manganese superoxide dismutase (MnSOD)²⁵⁸ are located in mitochondria and are known to scavenge ROS generated by the respiratory chain. In the cytosol, catalase and glutathione peroxidases break-down H_2O_2 to H_2O . By now it is believed that catalase is absent in most mitochondria except in mitochondria of cardiomyocytes^{13, 259}. Txnrd2 is able to detoxify mitochondrial H_2O_2 either directly or indirectly via thioredoxins to maintain the peroxide scavenging mitochondrial thioredoxin-dependent peroxidases (Prx3 and Prx5) in their active state³²⁹ (Figure 1-3).

First reported for Txnrd1^{115, 303, 306}, various isoforms have been also described for Txnrd2¹⁸⁴. Lescure *et al.* used computer-based screens for the RNA hairpin directing Sec incorporation to discover novel selenoproteins and found two proteins (SelZf1 and SelZf2) that obviously arise from the same gene as Txnrd2 but show differences in domains at the N-terminus, probably due to alternative splicing¹⁸⁴. The observation that alternative first exon splicing of Txnrd2 results in the formation of predicted mitochondrial and cytosolic isoforms could be confirmed by further studies^{215, 302}. It is believed that this remarkable heterogeneity within thioredoxin reductases results from evolutionary conserved genetic mechanisms, conducted by complex regulation of expression and specific intracellular localisation of mammalian thioredoxin reductases. Only one of the discovered isoforms of the Txnrd2 resides in the mitochondria (mitochondrial matrix), whereas the others are predicted to reside also in the cytosol. These latter isoforms show no catalytic specificity towards mitochondrial Trx (Trx2) *versus* cytosolic Trx (Trx1), both could serve as substrates³¹⁵. Up to now it is less understood which functions the different isoforms perform.

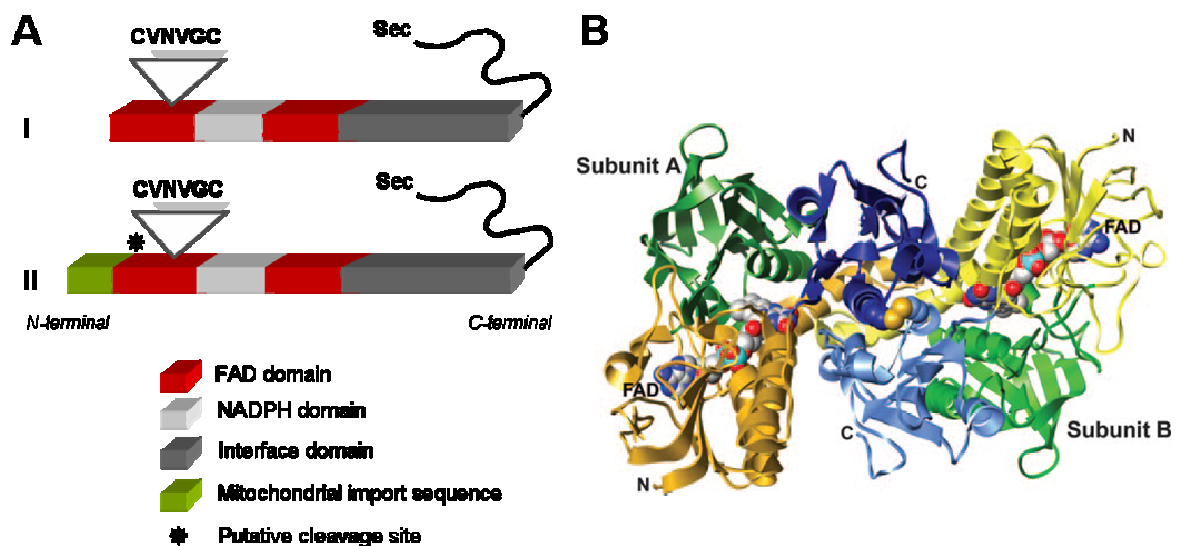


Figure 1-2: Structure of mammalian mitochondrial thioredoxin reductase (Txnrd2)

(A) Domain structures of the human cytosolic thioredoxin reductase (I) and the mitochondrial thioredoxin reductase (II). The various domains and the cleavage site of Txnrd2 are indicated in the keynotes. Triangles indicate the N-terminal catalytic active sites. The image was adapted from Mustacich *et al.*, 2000²²¹. (B) Ribbon representation of the crystal structure of the Txnrd2. Subunit A is shown in dark colours and subunit B in light colours. The FAD-domain is displayed in yellow, the NADPH-domain in green and the interface-domain in blue. Bound FAD molecules are represented with carbon atoms coloured in grey, nitrogen atoms in blue, oxygen atoms in red and phosphorus atoms in cyan. Sulphur atoms (yellow) represent side-chains of Cys483 located at the dimer interface. Adapted from Biterova *et al.*, 2005²⁹.

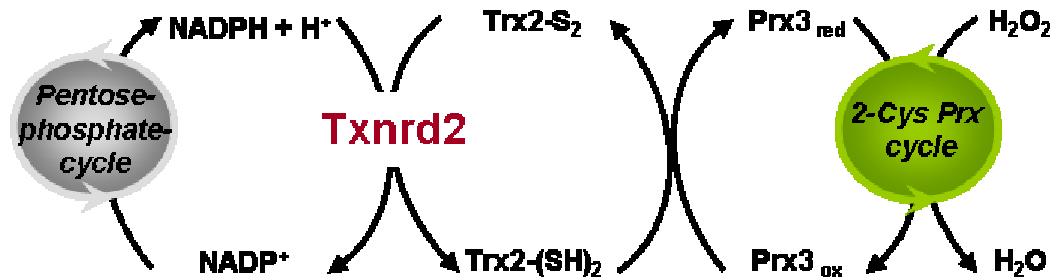


Figure 1-3: Electron transfer from the NADPH/H^+ via the mitochondrial Trx-dependent system to H_2O_2

The image depicts an electron transport system for peroxide reduction in mitochondria. Txnrd2 recovers oxidised Trx2 (Trx2-S_2), which, in turn restores oxidised peroxiredoxin 3 (Prx3_{ox}). Peroxiredoxins are homodimers that reduce H_2O_2 with a peroxidatic (catalytic) Cys which in turn oxidises to sulphenic acid (-SOH). The -SOH interacts with the resolving Cys of the other subunit to form a disulfide. Finally the disulfide is reduced by Trx2. Adapted from Watabe *et al.*, 1997 and D'Autreaux *et al.*, 2007^{67, 329}.

1.2.2. Implication of Txnrd2 in mitochondrial metabolism

Mitochondria are membrane-enclosed organelles ranging from 0.5 to 10 μm in size and are found in most eukaryotic cells¹³⁷. Through oxidative phosphorylation and the citric acid cycle they are the powerhouses of the cell and produce the majority of energy in a cell in form of adenosine triphosphate (ATP). Mitochondria are further involved in a wide range of cellular processes including cell growth, differentiation, control of the cell cycle, cellular signalling as well as apoptosis²⁰⁴. The number of mitochondria in a cell varies by organism and tissue type. Depending on their energy demand, some cells only have one mitochondrion whereas other cells have thousands of mitochondria. Mitochondria are composed of different compartments that carry out specialised functions (Figure 1-4). Depending on the tissue and species, mitochondrial proteins differ from each other. It is predicted that the mitochondrial proteome is regulated dynamically. Notably, some mitochondrially localised proteins and tRNAs are encoded by the mitochondrial genome, which displays substantial similarities to the bacterial genome.

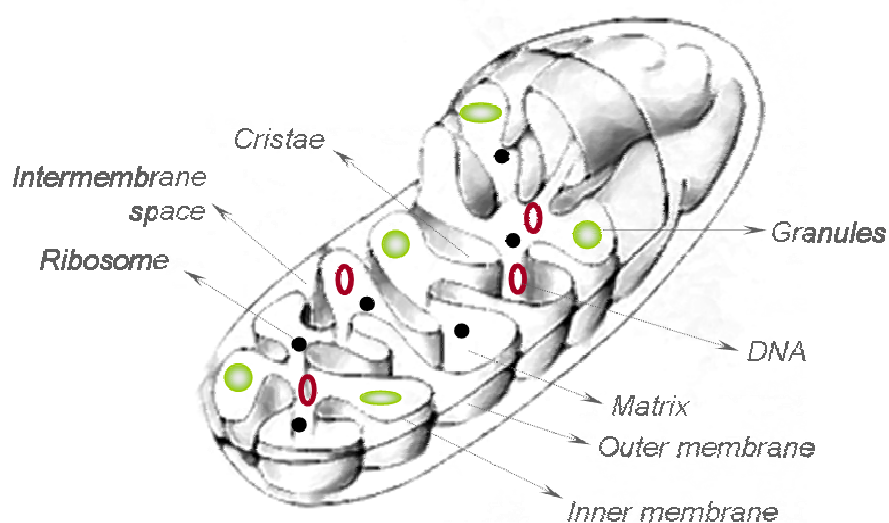


Figure 1-4: Mitochondria structure

The outer membrane of mitochondria contains channels and transport proteins that facilitate the exchange of molecules and ions with the cytosol. Large molecules can not pass the outer membrane of the mitochondria. The inner membrane is composed of various invaginations (=cristae), leading to a huge enlarged surface area. Most chemical reactions occur there and therefore the membrane contains the major protein complexes of the respiratory chain. The inner membrane encloses the mitochondrial matrix which contains ribosomes, granules, the mitochondrial nucleotides and enzymes, e.g. of the citric acid cycle. Image adapted from Frey and Mannella, 2000^{97, 237}.

As mentioned above, Txnrd2 functions as an electron donor for Trx2 and other substrates. In particular, Txnrd2 obtains reducing equivalents from NADPH/H⁺ in order to reduce and recycle mainly oxidised Trx2 (Figure 1-3). Trx2 itself catalyses reductions of protein disulfides (e.g. peroxiredoxins) at much higher rates than glutathione⁸.

Through this redox-recycling system, Txnrd2 has been suggested to control mitochondrial ROS levels as well as the redox state of mitochondrial proteins. It is known that ROS generated in mitochondria are involved in cell signalling and participate, for example, in apoptotic processes³⁰⁷. Mitochondrial ROS are e.g. considered to be involved in the opening of the mitochondrial permeability transition pore (PT), which is implicated in Ca²⁺ efflux³⁶². Opening of the PT has been shown to be dependent on redox-sensitive dithiol groups^{246, 267}. Several studies suggested that the mitochondrial thioredoxin reductase affects the regulation of the PT opening^{267, 269}.

Increased H₂O₂ generation due to stimulation with tumour necrosis factor- α (TNF- α) resulted in increased oxidation of oxidised Txnrd2. This, in turn, causes reduced scavenging of H₂O₂, resulting in induction of apoptosis. These results indicate that an accumulation of oxidised Txnrd2 accelerates TNF- α -induced apoptosis^{56, 159}. Furthermore, overexpression of an alternative splicing variant of Txnrd2 in HeLa cells resulted in the induction of apoptotic cell

death, confirming the involvement of the mitochondrial thioredoxin reductase in apoptotic signalling⁵⁴.

In vitro observations of cells overexpressing Txnrd2 revealed a reduced proliferation independent of selenium supplementation²²⁸. Overexpression of a dominant-negative Txnrd2 in HeLa cells increased ROS production, accompanied with extended protein tyrosine phosphorylation and accelerated progression of G1 to S phase in the cell cycle¹⁶¹. These studies are suggestive of an involvement of Txnrd2 in the regulation of cell proliferation.

Formation as well as reduction of disulfide bonds is a major regulatory mechanism for the function of numerous proteins. The redox balance in the mitochondrial matrix is indispensable for the proper function of the respiratory chain. The mitochondrial ATPase F0- F1 complex and cytochrome-c-oxidase, both participants in the respiratory chain, have been reported to be regulated by redox mechanisms³⁴⁶⁻³⁴⁷. It has been predicted that Txnrd2 may not only act as an antioxidant regenerator, but possibly also plays a role in directly reducing members of the respiratory chain. Indeed, it was demonstrated that Txnrd2 directly reduces cytochrome c. Furthermore, overexpression of Txnrd2 increased the resistance to cytotoxicity induced by antimycin A and myxothiazol, both inhibitors of complex III²²⁸.

To date, the entire impact of Txnrd2 on mitochondria function and the explicit underlying mechanisms are not fully understood.

1.2.3. Targeted deletion of Trx2 and Txnrd2

Mutational insertion leading to a homozygous silenced mouse gene for the mitochondrial thioredoxin caused early embryonic lethality. The embryos displayed an open anterior neural tube and showed massively increased apoptosis. The time point of embryonic lethality (E12.5) is accompanied by the maturation of mitochondria and initial oxidative phosphorylation. Embryonic fibroblasts with homozygous deletion of Trx2 are also not viable. This demonstrates that Trx2 is indispensable for mouse development and also for respiring cells²³³.

Previously, different mouse models with targeted inactivation of Txnrd2 were established in our laboratory. The ubiquitous Cre-mediated deletion of Txnrd2 (Figure 1-5) was lethal around embryonic stage E13.5 - E15.5^{62, 61}. Reduced proliferation of cardiac cells and increased apoptosis of fetal blood cells in the liver are the major reasons for the severe anaemic phenotype and partial growth retardation of *Txnrd2*^{-/-} embryos. In contrast to Trx2-null cells²³³, Txnrd2-null fibroblasts could be isolated and cultured from E12.5 embryos. *In vitro* Txnrd2-null fibroblasts demonstrated decreased proliferation and increased sensitivity to experimental glutathione depletion. Since Txnrd2-null embryos displayed a thinner ventricular heart wall and a decreased proliferation of cardiomyocytes, a mouse with cardiac

tissue-restricted ablation for *Txnrd2*, which resulted in fatal dilated cardiomyopathy, was investigated^{62, 61}. The newborn mice died within several hours after birth due to congestive heart failure accompanied with generalised edema, liver congestion, globular heart shape and atrial dilatation. Cardiomyocytes displayed swelling and destruction of mitochondrial cristae. These results demonstrated that the *Txnrd2* obviously plays an indispensable part in early embryogenesis, haematopoiesis as well as heart function.

To bypass embryonic and postnatal lethality of *Txnrd2*-null mice, a tamoxifen-inducible cardiac tissue-specific knockout mouse for *Txnrd2* was generated¹⁵⁷. Unexpectedly, inducible adult heart-specific *Txnrd2*-null mice were fully viable and displayed no apparent signs of abnormalities in histopathological analysis of cardiac tissue. Referring to the anaemic phenotype of ubiquitous *Txnrd2*-null embryos, T- and B-lymphocyte-specific (CD4⁻ and CD19⁺ cells) deletion of *Txnrd2* was investigated¹⁰⁹. Development and differentiation of both cell types in thymus and bone marrow was not impaired. Also, proliferation and activation in response to CD40 and IL-4 was unaffected in B-cells. Furthermore, nervous system-specific deletion of *Txnrd2* revealed no apparent histopathological changes in any brain region²⁹². These findings support the consideration that *Txnrd2* has important tissue- and organ-specific functions depending on the developmental state. The established conditional knockout models for *Txnrd2* and cellular systems thus offer powerful tools for further investigations concerning the involvement of *Txnrd2* in cellular function and the underlying molecular mechanisms.

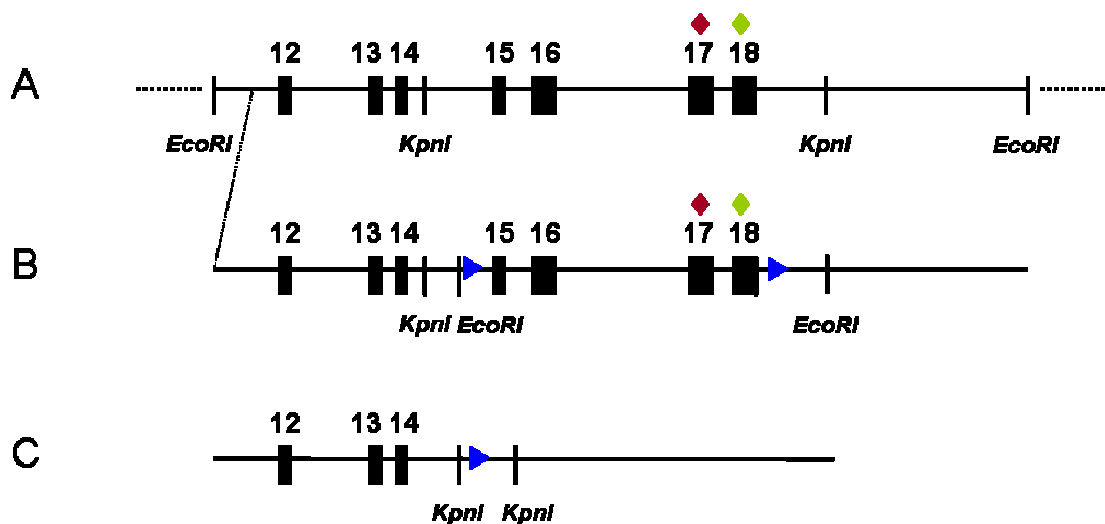


Figure 1-5: Conditional deletion of the *Txnrd2* gene

(A) The upper line shows the 3' region of the wild-type *Txnrd2* gene with Sec encoded by exon 17 (red diamond) and the SECIS element located on exon 18 (green diamond). (B) Exons 15 and 18 are flanked with loxP sites (blue triangles) for conditional gene targeting. (C) Deletion of the C-terminally located redox-center is mediated by Cre-Recombinase. Adopted from Conrad *et al.*, 2004⁶¹.

1.3. Tumour biology: How cancer arises

Cancer is a term used for diseases in which abnormal cells divide without control and are able to invade other tissues. Cancer is the second most frequent cause of death in Germany. In 2008, 29% men and 22% women died due to cancer in Germany¹⁷. Each day about 20,000 people worldwide die from cancer. Cancer constitutes a particularly challenging task for both research and clinical practice, it affects practically each and every organ in the human body (except myocardium) and each type of cancer has its own *modus operandi* and rules to develop and progress.

However, cancer treatment has improved in recent years and today more than half of all patients in Germany are still alive five years after the frightful diagnosis of cancer.

1.3.1. The multi-step process of cancer

As a reward of research over the last 30 decades, it is now well-known that cancer represents a disease involving dynamic changes in the genome and that multiple rate-limiting steps are required to turn a normal cell into a malignant cancer cell. The number of genes that are involved in this progression is large and their identification is still ongoing. The impact of one gene on the development of cancer can vary at different time points of the process.

As mentioned above, nearly all tissues in the body can develop malignancies, even different cell types in the same tissue. The basic processes that produce these diverse tumours appear to be quite similar. Normally cells reproduce only when instructed to do so by communication with adjacent cells. Thus, it is ensured that each tissue maintains a size and architecture appropriate to the organisms need. Tumour cells are able to violate this scheme and follow their own internal agenda for proliferation. They are furthermore able to migrate from the site of their origin and can thus invade other tissues, forming masses at distant sites in the organism. It is suggested that a normal cell has to undergo six essential alterations in their normal behaviour to dictate and manifest malignant growth. These six modifications are in particular (i) self-sufficiency in growth signals, (ii) insensitivity to growth-inhibitory signals, (iii) evasion of apoptosis (programmed cell death), (iv) limitless replicative potential, (v) sustained angiogenesis and (vi) tissue invasion and metastasis¹³¹. This indicates that the genomes of tumour cells are invariably altered at multiple sites. Furthermore tumour development occurs in five major stages: (i) genetically altered cell, (ii) hyperplasia, (iii) dysplasia, (iv) *in situ* cancer and (v) invasive cancer³³⁶ (Table 1-1).

It is proposed that so-called proto-oncogenes and tumour suppressor genes play pivotal roles in triggering tumour development and account for the uncontrolled cell proliferation. Under physiological conditions proto-oncogenes (e.g. *N-ras*, *c-myc*) and tumour suppressor

genes (e.g. *APC*, *p53*, *VHL*) are essential regulators of the life cycle of cells, the former prompting, the latter inhibiting growth. When mutated, proto-oncogenes become carcinogenic oncogenes that drive excessive proliferation. In contrast, tumour suppressor genes are inactivated and this loss of function deprives the cell of crucial brakes that prevent inappropriate growth^{144, 336}. Numerous other classes of genes were already identified to participate in the initiation and even more in the progression (see chapter 1.3.4.) of cancer malignancies and emerged essential for tumour cells to attract blood vessels (see chapters 1.3.2. and 1.3.3.) or to invade adjacent tissues and metastasise.

Table 1-1: Stages of tumour development

Adapted from Weinberg, 1996³³⁶.

i	Genetic mutation in one single-cell	one cell experiences a mutation that makes itself more likely to divide and proliferate
ii	Hyperplasia	the altered cell and its descendants grow and divide excessively
iii	Dysplasia	descendants keep on dividing excessively and begin to look abnormal
iv	<i>In situ</i> cancer	at the place of origin the single-cell and its descendants form a mass of exorbitant growing cells with an abnormal shape
v	Invasive cancer	some cells experience further mutations and start invading adjacent tissues, shed into the blood or lymph system and establish new tumors in distant organs: the tumour is now described as malignant.

1.3.2. Tumour vascularisation: the 'angiogenic switch'

In the early stage of tumour formation genetic and epigenetic alterations activate oncogenes and/or inhibit tumour suppressor genes, leading to uncontrolled proliferation. Once the tumour mass reaches a critical size, tumour cells distant to blood vessels lack appropriate supply with oxygen and nutrients. In the 1970s Judah Folkman hypothesised that vessels are an indispensable prerequisite for the expansion of the tumour beyond a diameter of 1-2 mm³⁹³. Without an appropriate vasculature cells either undergo apoptosis/necrosis and further tumour growth is impaired (tumour dormancy) (Figure 1-6 a). Unfortunately tumour cells can

overcome this inconvenience. The so called 'angiogenic switch' is controlled by changes in the balance between pro- and anti-angiogenic factors secreted by the tumour cells themselves or by cells of the tumour microenvironment. This multi-step process induces the formation of new blood vessels from pre-existing blood vessels and reconstitutes the supply with oxygen and nutrients (Figure 1-6 b-e). Furthermore, tumour vascularisation offers an effective way to remove waste products as well as the chance to metastasise. Numerous distinct angiogenic factors have been identified in the past decades. It is proposed that these factors directly or indirectly induce proliferation and differentiation of endothelial cells. The prototypic pro-angiogenic factor, and a major regulator of physiological and also pathological angiogenesis, is the vascular endothelial growth factor-A (VEGF-A) (see chapter 1.3.3)^{84, 145, 186, 286}. Fibroblast growth factor (FGF-1 and -2), platelet-derived growth factor (PDGF-B and -C) as well as the angiopoietins (Ang-1 and -2) are only some of a multitude of important positive regulators of tumour angiogenesis. However, a large number of anti-angiogenic factors have also been characterised so far. Thrombospondin (TSP1) and endostatin are extracellular matrix-associated anti-angiogenic factors, whereas a second group comprises soluble factors like interferon- α and $-\beta$ as well as angiostatin. In summary, the 'angiogenic switch' is a complex process in which genetic and epigenetic events within the tumour cells and the tumour stroma causes the balance to shift from pro- and anti-angiogenic factors towards the former. This in turn favours tumour angiogenesis and thus ongoing tumour growth^{11, 48, 126}.

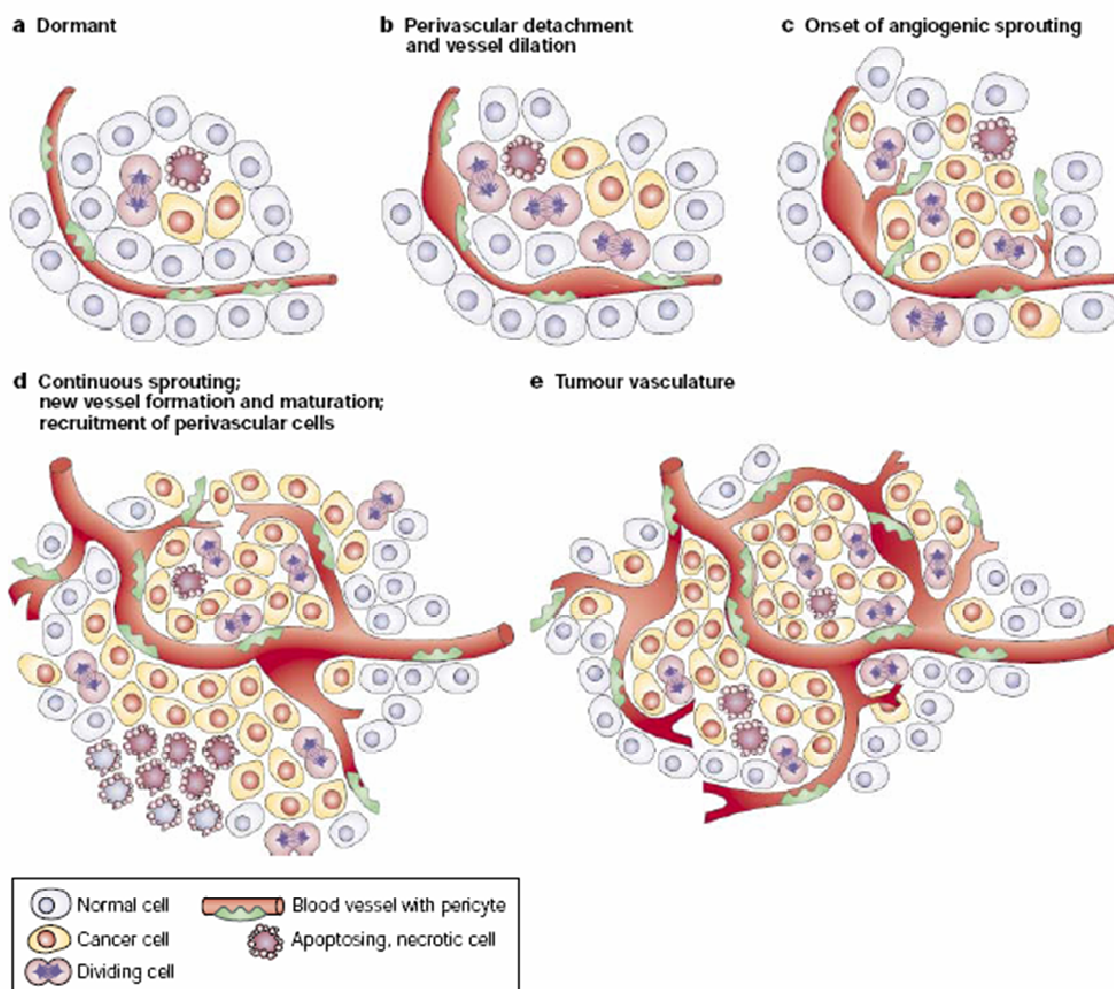


Figure 1-6: The 'angiogenic switch' in tumour progression

The 'angiogenic switch' is a crucial event in the development of a growing tumour. It can occur at different stages in the process of formation and is subject to the nature of the tumour and the surrounding microenvironment. Tumours mainly grow as avascular nodules (a) until they reach a critical size and a steady-state level of proliferating and apoptotic cells. To facilitate exponential tumour growth, the 'angiogenic switch' is indispensable. Starting with perivascular detachment and vessel dilation (b) the process continues with angiogenic sprouting (c), and formation and maturation of new vessels (d). Recruitment of perivascular cells completes this process of tumour vascularisation. As long as the tumour grows, the formation of new blood vessels continues. The vessels especially provide oxygen and nutrients to hypoxic and necrotic areas of the tumour. The image was taken from Bergers and Benjamin, 2003²².

1.3.3. Vascular endothelial growth factor in tumour angiogenesis

Recent evidence indicates that angiogenesis and vessel maturation are highly complex and coordinated processes, requiring the sequential activation of a series of receptors by numerous ligands in endothelial and mural cells^{49, 150, 349}. However, VEGF, as a major regulator of blood vessel formation and function, often represents a rate-limiting step in physiological angiogenesis. VEGF is an essential survival factor for endothelial cells, *in vitro* and *in vivo*. Loss of a single *VEGF* allele resulted in defective vascularisation and early embryonic lethality^{47, 85}.

The history of isolation of a tumour 'vascular permeability factor', the identification of VEGF and discovery of other VEGF-related molecules and their receptors is reported in several reviews by Ferrara *et al*^{88-89, 87}. This chapter aims to briefly mention the activities of VEGF and its relevance to tumour biology.

Several studies demonstrated that VEGF has the ability to promote growth of vascular endothelial cells derived from arteries, veins and lymphatics^{86, 186, 232, 243-244, 250}. Furthermore, it was shown that VEGF induces lymphangiogenesis *in vivo*²²²⁻²²³. VEGF is also known to be an essential survival factor for endothelial cells. VEGF prevents endothelial cell apoptosis mediated by the phosphoinositide 3-kinase (PI3K)-pathway^{98, 113} and, furthermore, induces the expression of the anti-apoptotic proteins Bcl-2, A1¹¹², XIAP³¹² and survivin³¹³. Inhibition of VEGF resulted in extensive apoptotic changes in the vasculature of neonatal mice¹¹⁴. Furthermore, numerous studies demonstrated that VEGF impacts on bone marrow cells and haematopoiesis, and influences vascular permeability and haemodynamic effects (for review see Ferrara *et al*⁸⁸).

Considering with its versatile functions, it is not surprising that VEGF plays a role in several pathological conditions. VEGF is reported to be involved in haematological pathologies, intraocular neovascular syndromes, inflammatory disorders and brain edema as well as pathologies of the female reproductive tract⁸⁸. Notably, VEGF mRNA is expressed in the vast majority of human tumours^{42, 40-41, 124, 249, 318} and it was demonstrated that many tumour cells secrete VEGF *in vitro*⁸⁴, indicating VEGF as a mediator of tumour angiogenesis. But not only tumour cells produce and deliver VEGF, it was also reported that tumour cells chemotactically attract tumour-surrounding stromal cells which also produce and secrete paracrine factors like VEGF (Figure 1-7)^{70, 99, 139, 153, 160}.

The concept of anti-angiogenic therapy has been validated in numerous cancer cell lines, traditional transplant tumour models as well as genetically engineered mouse models of cancer, beginning in the mid-1990s and continuing to the present^{10, 32-33, 31, 146, 160, 208, 328}. Several clinical trials already led to the approval of a number of anti-angiogenic therapies targeting the VEGF/VEGFR2 pathway in certain types of cancer that are commercially available since 2005. The FDA (Food and drug administration)-approved agents include bevacizumab (Avastin®), a humanised monoclonal antibody for VEGF, as well as several small molecule tyrosine kinase inhibitors of VEGF receptors and other key growth factor receptors^{66, 141, 256-257, 333, 345}.

Notably, the anti-angiogenic therapy alone is not beneficial for cancer patients unless combined with chemotherapy or radiation therapy^{149, 164, 168, 178}. The paradox that cytotoxic or radiation therapies require blood vessels for delivering drugs and oxygen but anti-angiogenic therapies kill blood vessels, could be resolved by Jain *et al*. He postulated in 2001 that the

application of anti-angiogenic agents can 'normalise' the abnormal vasculature, resulting in more efficient delivery of drugs and oxygen to the targeted cancer cells ¹⁴⁹.

Indeed tumour blood vessels are leaky, tortuous, dilated, saccular and have a chaotic pattern of interconnection which can result in an inappropriate drug supply. However, it is noteworthy that anti-angiogenic drugs have not produced long-term effects in terms of tumour shrinkage, dormancy or long-term survival. The common result is a delayed progression following a period of clinical benefit, suggesting an emerging resistance against the therapy ²³.

Besides, experimental data could demonstrate that targeting the VEGF pathway resulted in tumour adaptation and progression to stages of greater malignancy including increasing invasion and metastasis ²³⁶.

Altogether, anti-angiogenesis therapies emerged as significant advancements in cancer treatment though the high expectations had to be scaled down.

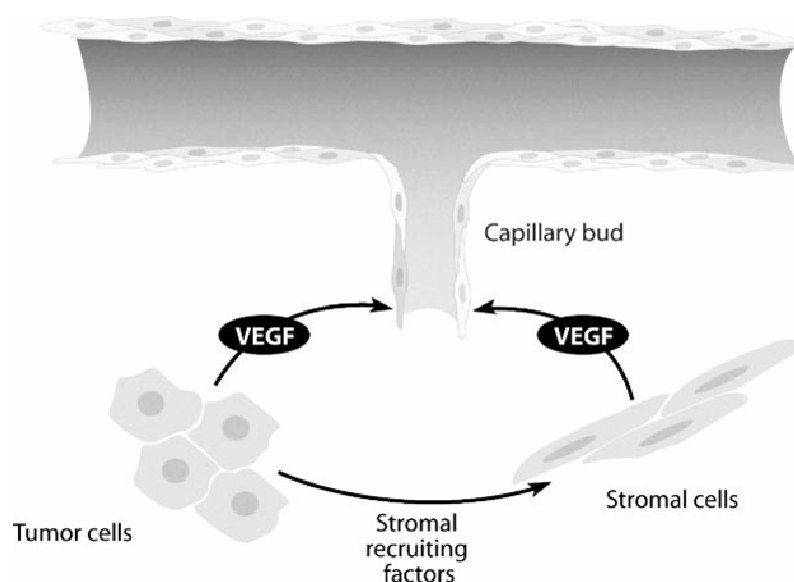


Figure 1-7: Contribution of VEGF to tumour angiogenesis

Tumour cells itself produce VEGF, but also tumour-associated stromal cells are an important source of VEGF. In response to chemotactic stimuli, stromal cells are recruited to the tumour and deliver VEGF and other angiogenic factors. Image adapted from Ferrara, 2004 ⁸⁸.

1.3.4. Hypoxia and Hif-signalling in tumour biology

Hypoxia defines a cellular condition in which oxygen becomes restricted and the supply is unable to meet the demand. Obviously, hypoxia is linked to the pathology of several diseases like cardiovascular diseases, stroke or cancer. Numerous reports on the relevance of hypoxia in the progression of tumours were published in the last decade, reflecting the eminent implication of this biological phenomenon in malignant processes ^{1, 3, 35-36, 156}. To understand how hypoxic conditions are generated in the tumour and in which way cells respond to the decreased availability of oxygen, it is essential to understand tumour

progression and metastasis. As already mentioned, cells have to undergo various changes in their metabolism to become malignant¹³¹. However, hypoxia seems to be involved in the progression of nearly all types of cancer. Massive proliferation of tumour cells disconnects cells from the vascular network, leading to restriction in oxygen supply and nutrient availability. Histological observations of malignant tissue revealed a central core of necrotic cells in numerous tumours. An oxygen partial pressure (pO_2) at low levels between 1-10 mmHg has been observed in solid tumours³⁰⁸. Together with restricted glucose supply, it seems obvious that this contributes to necrotic cell death in the middle of the tumour tissue (Figure 1-8). Hypoxic zones are postulated to have a reduced response to radiotherapy and several chemotherapy resistances due to limited deliverance of drugs^{100, 108, 140, 176}.

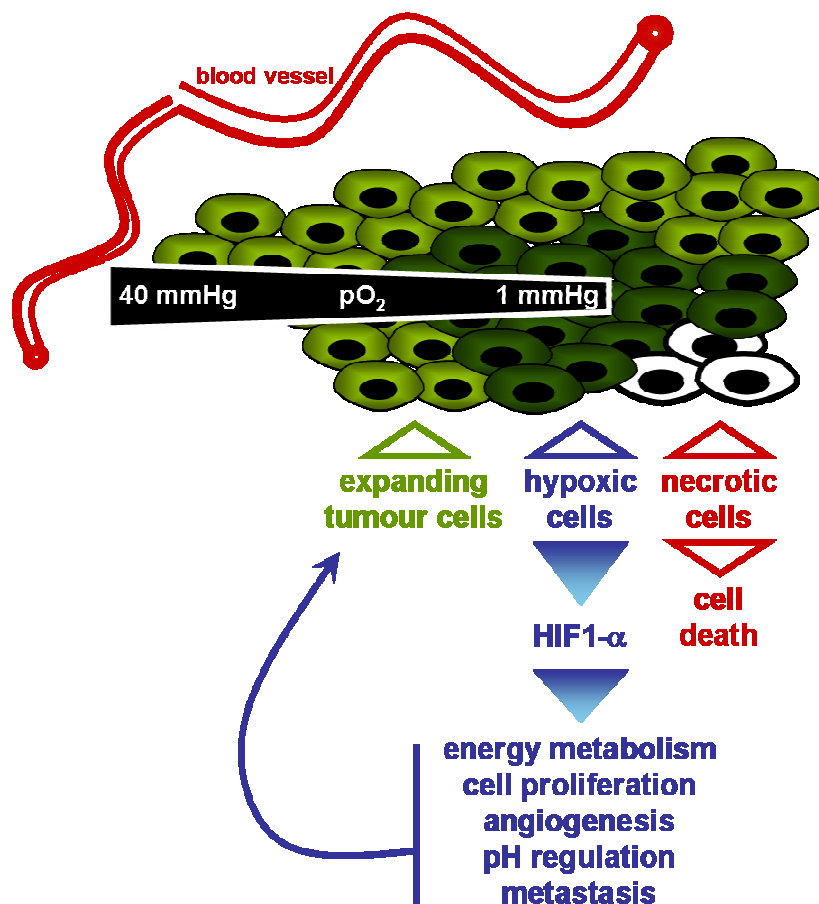


Figure 1-8: Implication of hypoxia and Hif-1 α in tumour physiology

The pO_2 drops from blood vessels to the distant tumour tissue. Tumour cells residing close to the vessel are well oxygenated (light green) whereas cells that are more distant from the vessel are exposed to hypoxic stress (dark green). The latter stabilise Hif-1 α , leading to stimulation of expression of numerous target genes. The target genes encode factors that modulate adaptation to the hypoxic situation of the cell (blue arrows). Tumour cells which fail to stabilise Hif-1 α undergo necrosis or apoptosis (white cells). The image was adapted from Keith *et al.*, 2007¹⁵⁶.

Cells exposed to hypoxic conditions are able to respond by increasing rates of anaerobic glycolysis and/or induction of angiogenesis or in the last resort they undergo cell death via apoptosis/necrosis. A prominent family of transcription factors, the hypoxia inducible factors (Hifs), can activate adaptive processes that enhance the likelihood of survival.

In 1992, Hif-1 α was first described when the mechanism of hypoxia-induced erythropoietin expression was discovered²⁸³. Hif-1 α is a heterodimeric transcription factor consisting of two subunits, α and β . The β -subunit is also known as aryl hydrocarbon receptor nuclear translocator (ARNT). Whereas ARNT is constitutively expressed, the stability, subcellular localisation and transcriptional activity of the α -subunit is affected mainly by oxygen levels³²³. In order to act as a transcription factor, Hif-1 α translocates into the nucleus and dimerises with Hif-1 β . There are two more known members of the Hif-family that possess structural similarity with Hif-1 α , Hif-2 α and Hif-3 α . Whereas Hif-2 α also activates transcription and induces hypoxia-mediated gene expression, Hif-3 α was found to act as a Hif-1 α antagonist¹⁸⁰. However, up to now Hif-1 α has been studied most.

Under normoxic conditions, Hif-1 α is rapidly degraded via the pVHL-mediated ubiquitin-proteasome pathway. Post-translational Hif-1 α is hydroxylated by prolyl hydroxylases (PHDs) at two sites within its ODD domain and further acetylated by ARD1 acetyltransferase (Figure 1-9)¹⁷⁹. Thus, Hif-1 α is labelled to interact with an E3 ubiquitin-protein ligase complex composed of pVHL, elongin B&C and cullin 2. Upon polyubiquitination Hif-1 α is degraded by the 26S proteasome (Figure 1-10).

Under hypoxic conditions the PHDs become inactive, Hif-1 α is no longer hydroxylated and less acetylated¹⁷⁹. Hence, Hif-1 α can not be targeted by pVHL for proteasomal degradation, becomes stabilised and translocates into the nucleus (Figure 1-10). Once stabilised and translocated to the nucleus, Hif-1 α dimerises with Hif-1 β and binds to the hypoxia-response-element (HRE) in several genes (Figure 1-10). Subsequently, Hif-1 α acts as a master regulator of oxygen-regulated gene expression and targets more than 60 putative genes¹⁸⁰. Hif-1 α is known to regulate transcription and thereby influences events like angiogenesis (VEGF), cell proliferation (TGF- α , TGF- β 3, cyclin G2), cell survival (IGF2, NOS2), glucose metabolism (GLUT1, GAPDH), iron metabolism (transferrin) and erythropoiesis (EPO)^{121, 180}. Several target genes of Hif-1 α have been predicted to participate in malignant processes. Indeed, Hif-1 α is overexpressed in many different types of cancer³⁰⁵. This often correlates with increased angiogenesis, malignant progression and treatment failure³⁵⁵.

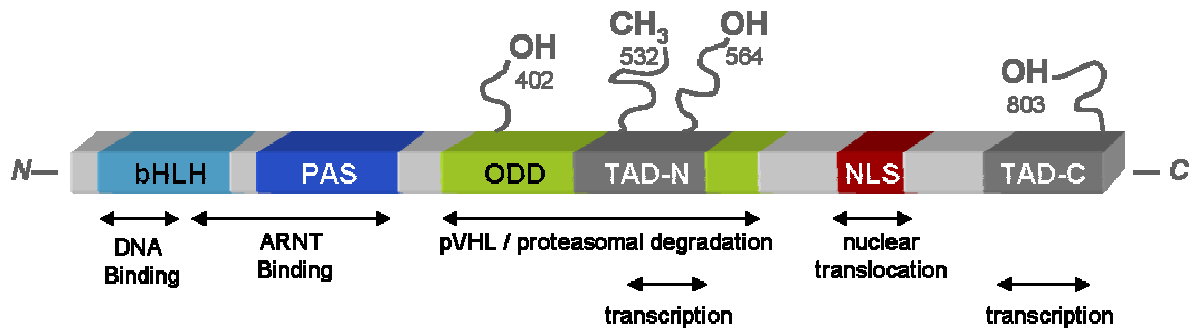


Figure 1-9: Gene domain structure of human Hif-1 α

The amino acid residues 402, 532 and 564 are targeted for hydroxylation by PHDs and acetylation by ARD under normoxia, leading to Hif-1 α destabilisation. The amino acid residue 803 is hydroxylated by FIH (factor inhibiting Hif-1 α) under normoxic conditions and inhibits the association with p300/CBP, essential for Hif-1 α stabilisation and DNA-binding. [bHLH = basic helix-loop-helix-PAS family-domain, PAS-domain = acronym for Per, ARNT and Sim (first recognised members of this family), ODD = oxygen-dependent degradation domain, TAD-N = N-terminal transcriptional domain, NLS = nuclear localisation signals, TAD-C = C-terminal transcriptional domain, OH = hydroxyl group, CH₃ = methyl group.] Image modified from Lee *et al.*, 2004¹⁷⁹.

However, oxygen-independent mechanisms that stabilise Hif-1 α under normoxic conditions also exist. This has been reported for many growth factors and cytokines^{136, 296, 353}. The mechanisms underlying this activation are proposed to rely on elevated ROS production²⁵³. Interference of ROS with the Hif-1 α pathway under normoxic conditions was first demonstrated by exposing cells to exogenous ROS. Stabilisation of Hif-1 α protein and activation of Hif-1 α target genes was induced by H₂O₂ or several other oxidative stressors^{37, 53, 71, 198}. These effects could be reversed by adding several antioxidant components like N-acetylcysteine, glutathione and vitamins E or C^{104, 128, 238, 270, 288, 361}. But prior to addressing the responsibility of ROS in Hif-signalling it is crucial to consider the intracellular kinetics of ROS in response to pO₂ changes. On the one hand, formation of ROS was found to be decreased under hypoxic conditions^{45, 190, 324} but on the other hand, cumulative reports document that hypoxia actually increases intracellular ROS production, predominantly via the mitochondria^{44, 58, 111, 127, 198, 234}. The latter is somewhat paradox as the substrate (oxygen) for the mitochondria to make ROS should be less abundant. While these discrepancies could be due to technical demands and limitations in ROS quantification², the exact mechanisms of mitochondrial ROS production during hypoxia still remain to be fully elucidated. Therefore, it might be useful to establish one general reliable, quantitative and sensitive method for measuring ROS.

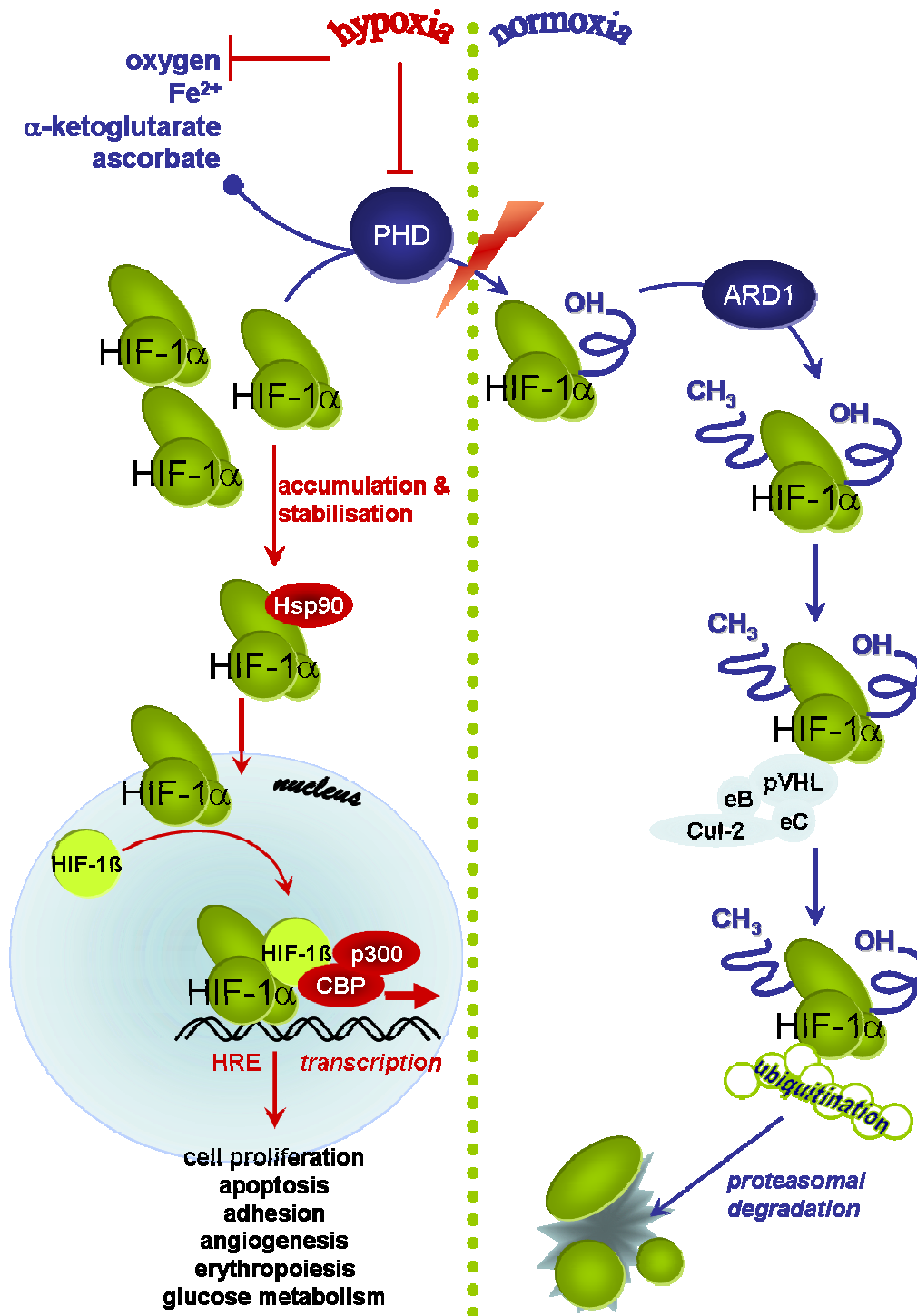


Figure 1-10: Hif-1 α is regulated by oxygen availability

Blue arrows indicate Hif-1 α signalling under normoxic conditions with hydroxylation through PHDs, acetylation through ARD1 and binding of further proteins for proteasomal degradation. Red arrows illustrate the signalling pathway under hypoxic conditions with stabilisation and accumulation of Hif-1 α , leading to the binding of several co-activator proteins (Hsp90 = heat shock protein 90, p300 and CBP) and translocation into the nucleus. In the nucleus, Hif-1 α binds to HRE (hypoxia-response element) of several genes that are involved in cell proliferation, apoptosis, angiogenesis and energy metabolism. The image was adapted from Lee *et al.*, 2007¹⁸⁰.

Though the changes in ROS production due to hypoxia are still controversial matters, over the last decade several feasible points of interaction of ROS in the pathway of Hif-1 α signalling are now considered clear (Figure 1-11). It has been already reported that redox-dependent pathways are involved in Hif-1 α stabilisation and DNA-binding^{143, 175, 324}. Further investigations revealed that ROS may have an impact on Hif-1 α expression via the activation of kinases. Tyrosine kinase inhibitors completely blocked Hif-1 α synthesis and DNA-binding activity under hypoxic conditions³²⁵.

In particular PHDs, which have a considerable regulatory impact on Hif-1 α under hypoxia, offer an attractive target for ROS to interfere with the Hif-1 α pathway. PHD2 has been reported to reside in the cytosol²¹⁰, where it is directly exposed to ROS derived from NADPH oxidases⁶. H₂O₂ produced in the mitochondrial matrix can relocate to the cytosol and influence PHD activity^{44, 127}. Activity of PHDs requires several co-factors. The availability of oxygen is an absolute determinant in PHD activity. Furthermore, the enzymes require α -ketoglutarate, ferrous iron (Fe²⁺), and ascorbate for full activity. Sustained production of ROS was found to reduce the cellular pool of Fe²⁺, thereby increasing the proportion of PHD in the inactive Fe³⁺ oxidation state¹¹¹. At physiological concentrations ascorbate was shown to enhance PHD activity, thereby promoting Hif-1 α degradation¹⁶⁶.

In summary, hypoxic areas in tumours even display the beginning of a hypoxic signalling cascade. Decreasing oxygen levels are accompanied by increasing stabilisation of Hif-1 α . Subsequently, a broad range of genes implicated in cell survival/death, metabolism, angiogenesis, pH regulation, adhesion, extracellular matrix remodelling, migration, and metastasis are targeted, leading to adaptive cellular reactions. It is also reported that hypoxic signalling seems to be crucially involved in promoting invasive potential of tumour cells³⁶.

Besides oxygen-dependent stabilisation of Hif-1 α in tumour cells also defects in the regulation of Hif-1 α degradation can contribute to malignant processes and promote tumour progression as well as invasiveness. Von Hippel Lindau (VHL) disease, a hereditary cancer syndrome, results from a mutation in the von Hippel-Lindau tumour suppressor gene, leading to loss of function. As a consequence, Hif-1 α is stable and acts as versatile transcription factor. This syndrome is characterised by the presence of highly vascularised tumours including renal angioma, renal cell carcinoma and pheochromocytoma. Therefore, a strong link between Hif-1 α , angiogenesis and tumour progression is provided^{91, 169}.

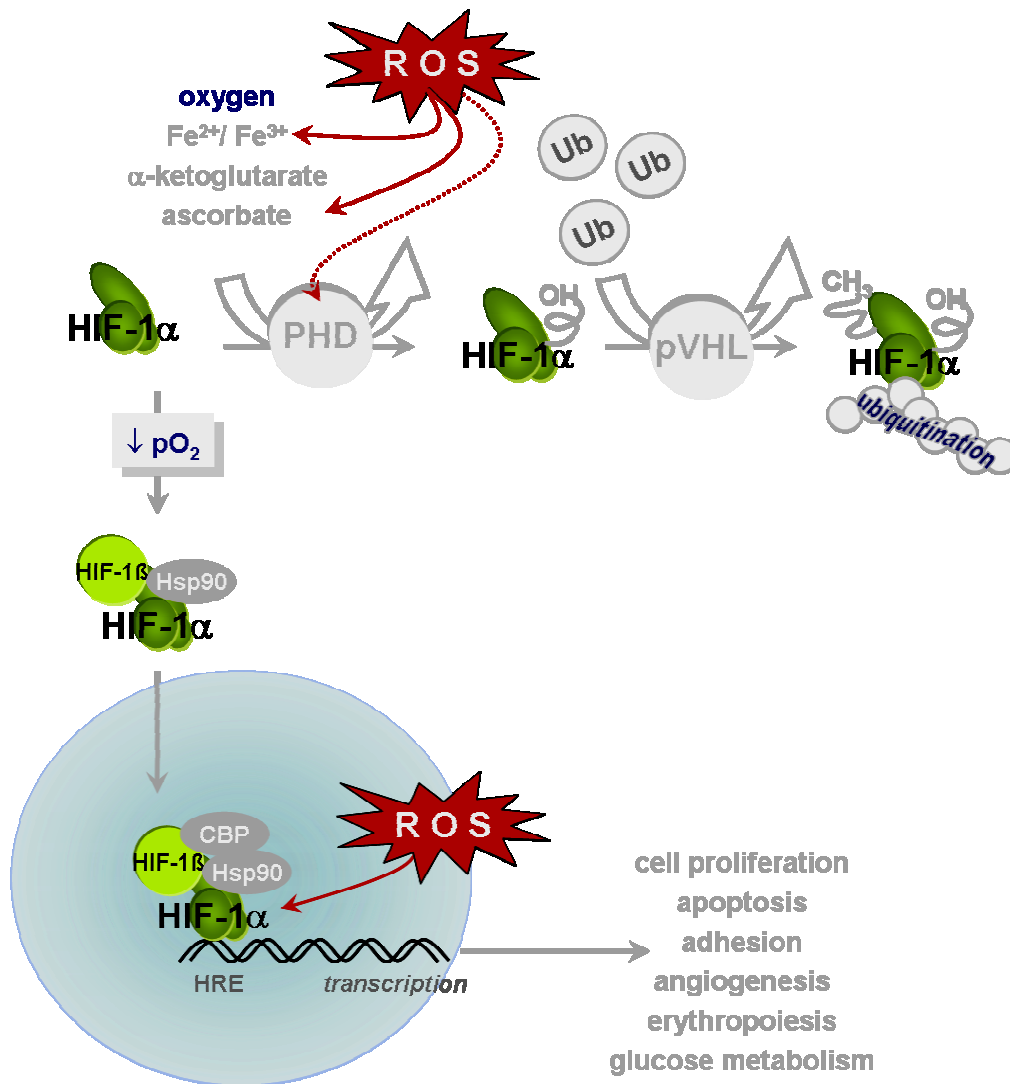


Figure 1-11: Involvement of reactive oxygen species in Hif-signalling

Stabilisation and DNA-binding of Hif-1 α revealed as ROS-sensitive processes (red arrows). Interaction of ROS with Fe²⁺ and ascorbate limits factors crucial for the activity of PHDs. Thus, degradation of Hif-1 α is interrupted. Once stabilised and translocated to the nucleus, the binding of Hif-1 α to the HRE of several genes occurs in a redox regulated manner. The illustration was adapted from Kaelin *et al.*, 2005 and Pouyssegur *et al.*, 2006^{152, 253}.

1.3.5. Implication of mitochondria in tumour progression

With their central position in cellular metabolism, mitochondria play a critical role in a broad range of diseases (Figure 1-12). Metabolic defects in Parkinson disease, neuronal injuries, cardiovascular diseases, mediated cell death in diabetes, and cancer depict only a few. A pivotal role for mitochondria has been predicted for the process of aging. Several mitochondrial functions decline with increasing age. Decreased membrane fluidity and intrinsic rate of proton leakage across the inner mitochondrial membrane are only some of these age-associated mitochondrial changes. It has been suggested that there is an age-dependent accumulation of ROS due to progressive dysfunctions of mitochondria²⁹⁰. In

many human diseases, chronically elevated levels of ROS contribute to the disease trigger and pattern. Oxidative stress is a conserved signal for cell death and mitochondria are the switchboard of the apoptotic machinery²³⁵. For instance ischemia-reperfusion and drug injuries are accompanied by increased ROS production, inducing mitochondrial dysfunction and increasing mitochondrial autophagy²⁶⁰.

As already mentioned (see chapter 1.3.4.), it has been proposed that mitochondria contribute to hypoxic signalling^{44, 111, 127, 198, 234}. Mitochondria generally represent a major source of ROS in the cells. Several groups could demonstrate that H₂O₂ is required for the induction of Hif-1 α target genes under hypoxic conditions^{52, 74, 81}. Moreover, three recent studies demonstrated that, under hypoxic conditions, mitochondria produce a burst of ROS that stabilises Hif-1 α , which could be impaired by blocking mitochondrial function either chemically or pharmacologically^{44, 198, 280}. An additional study demonstrated that Hif-1 α is also stabilised in cells lacking functional respiration, disproving the latter assumption¹⁹. Though, this subject is obviously inconsistent and requires further investigation.

One more controversial issue comprises the mitochondria and their relevance in malignant processes. In the 1930s Otto Warburg discovered a functional disruption of mitochondria in tumour cells. He observed elevated lactate levels in cancer cells compared to normal cells even though adequate oxygen for oxidative phosphorylation was available³²⁷. He could show that cancer cells can obtain approximately the same energy from fermentation (glycolysis) than from respiration. In contrast, normal cells obtain much more energy from respiration. Thus Warburg postulated that the disruption of respiration in cancer cells must be irreversible but not to such an extent that the cells are killed. Since he observed that cancer cells cannot regain normal respiration even if oxygen is available, he assumed that the destruction of respiration might be the origin of cancer cells³²⁷. Later on, studies challenged his thesis and revealed that the mitochondria of tumour cells are not dysfunctional, do respire and produce ATP¹¹⁹. However, it has been shown that many tumours contain somatic mutations in mitochondrial DNA^{46, 252}. One would assume that the outcome is probably a sub-optimal or non-functional oxidative phosphorylation and ATP synthesis, meaning that cells must accelerate anaerobic glycolysis. But the functional consequences of mitochondrial DNA mutations might be marginal and of peripheral importance to tumourigenesis. Limited evidence indicates that some of these mutations might directly promote tumour growth^{247, 289}. More recently, it was discovered that mitochondrial proteins can act as tumour suppressors. Somatic mutation of succinate dehydrogenase (SDH), member of the TCA, has been shown to lead to the development of pheochromocytoma or paraganglioma^{15, 75, 251}.

To this day Warburg's thesis has been neither completely confirmed nor absolutely disproved. However, it has been proven that cancer cells indeed exhibit a higher rate of anaerobic glycolysis. This extensive utilisation of glucose is currently used for visualisation of tumours

via positron emission tomography ¹⁰². During the last decade several studies suggested that the Warburg effect is less related to mitochondrial defects but even more to alterations in signalling. As mentioned above, mitochondria are more than a powerhouse for cells. They contribute to Ca²⁺ homeostasis, cell death signalling, redox signalling, as well as cell growth and survival (Figure 1-12). Obviously, these functions are crucial for tumour cell physiology and many extensive reports have examined these features faithfully ^{116, 203, 335}. Nearly 30 years ago, new therapeutic approaches started to specifically target mitochondria. Anti-cancer agents exclusively targeting these organelles are now termed ‘mitocans’. They aim to destabilise mitochondria, resulting in efficient cell death and long-term suppression of tumour growth. A redox silent vitamin E analogue epitomised by α -tocopheryl succinate (alpha-TOS) is proposed to be such a mitochondria-selective anti-cancer agent. It has been described to efficiently target complex II of the respiratory chain, thereby disrupting electron flow ²³¹. As already mentioned, normal cells have to undergo six major alterations in their properties to become a tumour cell ¹³¹. These days, many researchers include a seventh important alteration, a change in cellular metabolism in relation to mitochondrial functions ⁶⁹.

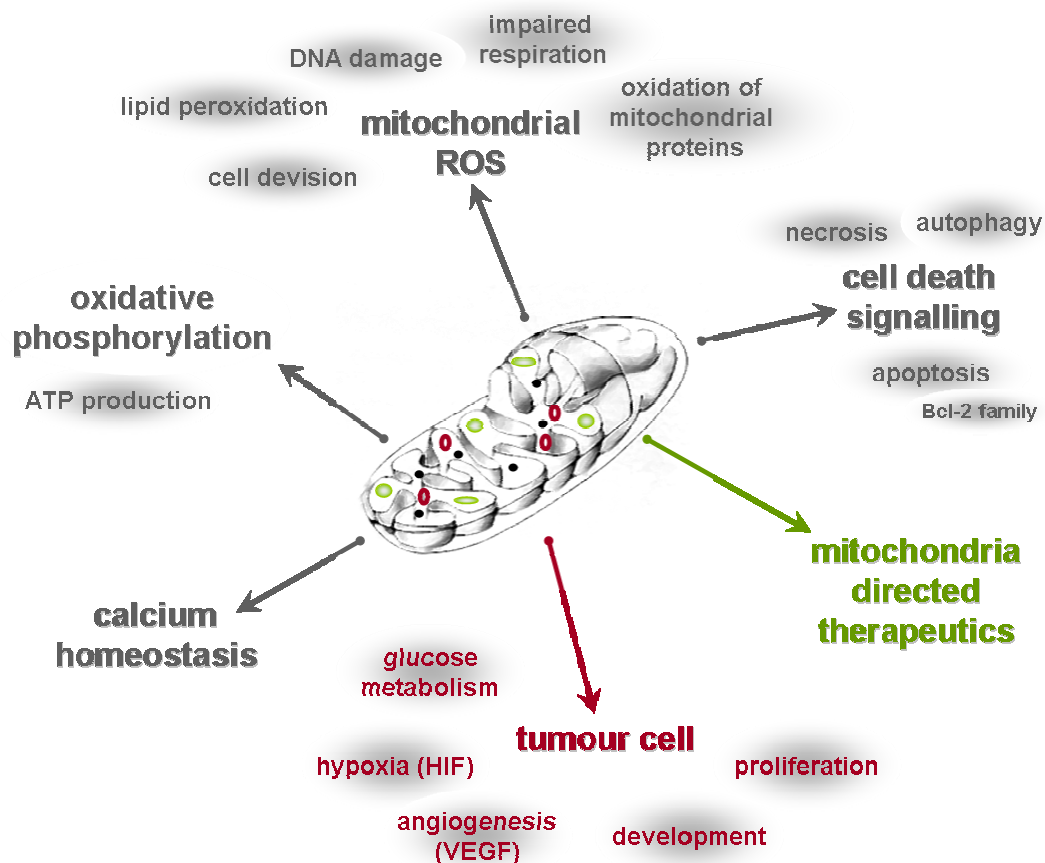


Figure 1-12: Implication of mitochondria in cancer cells and tumour progression

This illustration depicts the complex relationship between mitochondrial activities and malignant processes in a simplified way. The six issues are mentioned and partially discussed in the text. Image adapted from Mayevsky *et al.*, 2009 ²⁰³.

1.4. Thioredoxin reductases in relation to cancer and Hif-signalling

The literature suggests that the thioredoxin-dependent system may be involved in several, if not all stages of tumour development. However, the relative importance at the hallmarks of cancer (Hanahan and Weinberg, 2000) by the thioredoxin system and its individual elements is far from clear and certainly varies between different types of cancer. Most reports concerning the thioredoxin system in disease and mainly cancer refer to the cytosolic thioredoxin and thioredoxin reductase (Txnrd1)^{9, 16, 221}. Inhibition of Txnrd1 via siRNA in human hepatocellular carcinoma cells resulted in the accumulation of cells in cell cycle phase G₂/M. The anti-apoptotic Bcl-family member Bcl-2 was decreased and, in contrast, the tumour suppressor and regulator of cell cycle, p53, was increased¹⁰³. Overexpression of Txnrd1 has been reported for numerous cancer types, proposing the enzyme as a target for cancer therapy. Long-term knockdown of Txnrd1 in Lewis lung carcinoma cells via stable siRNA transfection revealed a change from a cancer cell phenotype to a normal cell phenotype³⁵⁰. *In vivo*, the knockdown of Txnrd1 resulted in reduced tumour progression and metastasis, even more Txnrd1 knockdown cells-derived tumours lost the targeting siRNA construct. These results indicate that the cytosolic form of thioredoxin reductases is pivotal for tumour promotion and is especially indispensable for self-sufficiency in growth signals of malignant cells³⁵¹. In contrast, recent work in our lab demonstrated that Txnrd1 is not essential for tumour growth. Txnrd1-deficient MEFs could be successfully transformed with the two proto-oncogenes *c-myc* and *Ha-ras*^{V12}, maintained in culture, and showed equal proliferative capacity. Furthermore, loss of Txnrd1 function had no impact on anchorage-independent growth *in vitro* and tumour growth *in vivo*¹⁹⁷.

Up to now, only one study reported about on elevated expression of the mitochondrial thioredoxin reductase (Txnrd2) in tumour tissue. Txnrd2 and a second mitochondrial protein, peroxiredoxin 3 (Prx3), were expressed to a significant higher degree in hepatocellular carcinoma tissue compared to adjacent healthy tissue⁵⁹.

For cells, the thioredoxin system offers one of several effective tools to scavenge free ROS, recover oxidised disulfides of proteins, and, most importantly, keep the cell in a more reduced state. Hif-1 α , as mentioned above, has recently been reported to respond to redox-dependent regulatory mechanisms. The cytosolic form of thioredoxin (Trx1) was found to be increased in several tumour tissues and has been linked to aggressive tumour growth. Moreover, the mRNA levels of Trx1 increased in cells exposed to hypoxia²⁴. Thus, the question arises whether there is any functional connection between thioredoxin and Hif-1 α . Stable transfection of human breast cancer cells with human Trx1 significantly increased Hif-1 α protein levels, Hif-1 α transactivation activity, and also caused an increase in protein

products of hypoxia-responsive genes (VEGF, iNOS). On the other hand, transfection of a redox-inactive Trx1 resulted in a decrease in Hif-1 α protein, Hif-1 α transactivation activity and VEGF protein levels³³⁸. Irreversible inhibition of Trx1 using two specific inhibitors (PX-12 and pleurotin) prevented hypoxia-induced Hif-1 α protein stabilisation, transactivation activity and furthermore reduced VEGF as well as iNOS levels³³⁹.

In a previous study, cells were stably transfected to overexpress either Trx1 or Trx2 and effects on Hif-1 α were investigated. Surprisingly, the results for these two thioredoxins produced opposite effects. Overexpression of Trx1 increased Hif-1 α protein and activity, whereas overexpression of Trx2 decreased Hif-1 α protein level and transactivation activity. Further investigations revealed that the differences are not due to altered transcription or degradation of Hif-1 α , but may depend on altered phosphorylation and activities of proteins of the Akt pathway, mitogen-activated protein kinases and ROS production³⁵⁹. Observation of nitric oxide (NO)-evoked Hif-1 α stabilisation offered similar results. Overexpression of Trx1 resulted in Hif-1 α accumulation accompanied by increased transactivation activity, phosphorylation of p42/44 mitogen-activated protein kinase and elevated intracellular ATP levels. Cells overexpressing Trx2 showed opposite effects which was also true for overexpression of Txnrd2³⁶⁰. Nevertheless, despite the underlying mechanisms for the controversial actions of thioredoxins in Hif-1 α signalling still requiring further investigation there is increasing evidence that the thioredoxin system interferes with Hif-1 α .

1.5. Intention of the present work

Our group could previously demonstrate that Txnrd2 is essential for embryogenesis, heart development and function, and especially haematopoiesis⁶¹. Subsequently, the impact of Txnrd2 knockout on cell proliferation was investigated *in vitro*, the reply to oxidative stress, as well as interactions with other redox-regulating enzymes, e.g. the glutathione-dependent system and peroxiredoxins, using primary Txnrd2-deficient MEFs²⁴⁵.

Over the last decades the function of cytosolic Txnrd (Txnrd1) has been investigated intensely. Besides its impact on cell proliferation, apoptosis and redox-signalling, Txnrd1 was found to be upregulated in many cancer cell lines and solid tumours. Less is known about Txnrd2 and its contribution to malignant processes. Up to now only one study could show that Txnrd2 in particular is highly expressed in hepatocellular carcinoma tissue⁵⁹.

Using immortalised MEFs, transformed MEFs and eEPCs, the present study aims to investigate Txnrd2 functions, particularly in normal cell physiology, tumour cell physiology and malignant processes with the following hypotheses:

- Txnrd2 deletion has long-term effects on cell metabolism.
- Txnrd2 deletion affects tumour cells *in vitro* and tumour growth *in vivo*.
- Txnrd2 knockout influences endothelial cell function.

2. MATERIALS AND METHODS

2.1. Materials

CHEMICALS	COMPANY
2-Log DNA ladder	NEB Biolabs GmbH, Frankfurt a.M., Germany
2-Propanol	Merck KGaA, Darmstadt, Germany
Acetic acid 100%	AppliChem GmbH, Darmstadt, Germany
Acrylamide 30% (Mix 37.5:1)	Genaxxon Bioscience GmbH, Ulm, Germany
ADP	Sigma-Aldrich GmbH, Taufkirchen, Germany
Agarose low EEO	AppliChem GmbH, Darmstadt, Germany
Agarose, TopVision™ LMGQ	Fermentas GmbH, St. Leon-Rot, Germany
Ammonium persulfate	AppliChem GmbH, Darmstadt, Germany
Ampicillin sodium salt	Sigma-Aldrich GmbH, Taufkirchen, Germany
Aqua ad iniectabilia	B. Braun Melsungen AG, Melsungen, Germany
Ascorbic acid	Sigma-Aldrich GmbH, Taufkirchen, Germany
Bacto agar	Applichem GmbH, Darmstadt, Germany
Bacto yeast extract	Sigma-Aldrich GmbH, Taufkirchen, Germany
Boric acid	Merck KGaA, Darmstadt, Germany
Bovine serum albumin (albumin fraction V)	AppliChem GmbH, Darmstadt, Germany
Bromophenol blue	Sigma-Aldrich GmbH, Taufkirchen, Germany
Calcium chloride	Sigma-Aldrich GmbH, Taufkirchen, Germany
Chloroquine diphosphate	Sigma-Aldrich GmbH, Taufkirchen, Germany
Crystal violet	Sigma-Aldrich GmbH, Taufkirchen, Germany
DCF, DCFDA	Invitrogen, Karlsruhe, Germany
Digitonin	Sigma-Aldrich GmbH, Taufkirchen, Germany
Disodium hydrogenphosphate	Merck KGaA, Darmstadt, Germany
D-Mannitol	Merck KGaA, Darmstadt, Germany
dNTPs for PCR, premixed	GE Healthcare, Freiburg, Germany
ECL™, Western Blotting Reagent	GE Healthcare, Freiburg, Germany
EDTA	AppliChem GmbH, Darmstadt, Germany
EGTA	AppliChem GmbH, Darmstadt, Germany
Eosin G, 0.5%	Roth Carl GmbH & Co., Heidelberg, Germany
ER-Tracker™ Green	Invitrogen, Karlsruhe, Germany
Ethanol	Merck KGaA, Darmstadt, Germany

Ethidium bromide	Sigma-Aldrich GmbH, Taufkirchen, Germany
Ethyl ether	Sigma-Aldrich GmbH, Taufkirchen, Germany
FITC-dextran	Sigma-Aldrich GmbH, Taufkirchen, Germany
Forene®	Abbott GmbH & Co KG, Wiesbaden, Germany
Glutamate	Sigma-Aldrich GmbH, Taufkirchen, Germany
Glycerol	AppliChem GmbH, Darmstadt, Germany
Glycin	AppliChem GmbH, Darmstadt, Germany
Hämalaun solution, acidic	Roth Carl GmbH & Co., Heidelberg, Germany
K-lactobionate	Sigma-Aldrich GmbH, Taufkirchen, Germany
L-Glutathione oxidised disodium salt	Sigma-Aldrich GmbH, Taufkirchen, Germany
Malate	Sigma-Aldrich GmbH, Taufkirchen, Germany
Magnesium chloride	AppliChem GmbH, Darmstadt, Germany
Magnesium sulphate	Merck KGaA, Darmstadt, Germany
Methanol	AppliChem GmbH, Darmstadt, Germany
Mitotracker® Green FM	Invitrogen, Karlsruhe, Germany
Mitotracker® Red CMH ₂ XRos	Invitrogen, Karlsruhe, Germany
MitoSOX™ Red	Invitrogen, Karlsruhe, Germany
MOPS	Sigma-Aldrich GmbH, Taufkirchen, Germany
NAD phosphate, reduced tetrasodium	Sigma-Aldrich GmbH, Taufkirchen, Germany
Nonfat dried milk powder	AppliChem GmbH, Darmstadt, Germany
Nonyl acridine orange	Invitrogen, Karlsruhe, Germany
Page Ruler™ Prestained Protein Ladder	Fermentas GmbH, St. Leon-Roth, Germany
Paraformaldehyde	Merck KGaA, Darmstadt, Germany
Perchloric acid 70%, absolute	AppliChem GmbH, Darmstadt, Germany
Phenol/Chloroform/Isoamyl alcohol	Roth Carl GmbH & Co., Karlsruhe, Germany
Phenylmethylsulfonyl fluoride	Merck KGaA, Darmstadt, Germany
Ponceau S	Sigma-Aldrich GmbH, Taufkirchen, Germany
Potassium acetate	Merck KGaA, Darmstadt, Germany
Potassium chloride	Merck KGaA, Darmstadt, Germany
Potassium cyanide	Sigma-Aldrich GmbH, Taufkirchen, Germany
Potassium dihydrogen phosphate	Merck KGaA Darmstadt, Germany
Rotenone	Sigma-Aldrich GmbH, Taufkirchen, Germany
Rubidium chloride	Sigma-Aldrich GmbH, Taufkirchen, Germany
Sodium chloride	AppliChem GmbH, Darmstadt, Germany
Sodium deoxycholate	Sigma-Aldrich GmbH, Taufkirchen, Germany
Sodium dodecyl sulfate	Sigma-Aldrich GmbH, Taufkirchen, Germany

Sodium fluoride	Merck KGaA, Darmstadt, Germany
Sodium orthovanadate	Enzo Life Sciences GmbH, Lörrach, Germany,
Succinate	Sigma-Aldrich GmbH, Taufkirchen, Germany
SuperSignal® West Femto Substrate	Fisher Scientific GmbH, Schwerte, Germany
Taurine	Sigma-Aldrich GmbH, Taufkirchen, Germany
Tetramethylethylenediamine (TEMED)	AppliChem GmbH, Darmstadt, Germany
Tetramethylphenylenediamine	Sigma-Aldrich GmbH, Taufkirchen, Germany
Thiazolylblau (MTT)	Roth Carl GmbH & Co., Heidelberg, Germany
Trichloroacetic acid	Sigma-Aldrich GmbH, Taufkirchen, Germany
Tris	AppliChem GmbH, Darmstadt, Germany
Triton X-100	AppliChem GmbH, Darmstadt, Germany
Tryptone	Difco Laboratories, Michigan, USA
Tween 20	AppliChem GmbH, Darmstadt, Germany
Xylene cyanol	Sigma-Aldrich GmbH, Taufkirchen, Germany

CELL CULTURE REAGENTSCOMPANY

Antimycin A	Sigma-Aldrich GmbH, Taufkirchen, Germany
Collagen G	Biochrom AG, Berlin, Germany
Dichloricacid sodium 98%	Sigma-Aldrich GmbH, Taufkirchen, Germany
Dimethyl sulfoxide	AppliChem GmbH, Darmstadt, Germany
Dulbecco´s Modified Eagle Medium, high glucose (4.5 g/l glucose)	Invitrogen, Karlsruhe, Germany
Dulbecco´s Modified Eagle Medium, low glucose (1 g/l glucose)	Invitrogen, Karlsruhe, Germany
Dulbecco´s Modified Eagle Medium, no glucose	Invitrogen, Karlsruhe, Germany
D-(+)-Galactose	Sigma-Aldrich GmbH, Taufkirchen, Germany
Fetal calf serum	Biochrom AG, Berlin, Germany
Fibronectin	Harbor Bio-Products, Norwood, USA
Gelatine from porcine skin	Sigma-Aldrich GmbH, Taufkirchen, Germany
HEPES	Invitrogen, Karlsruhe, Germany
L-Buthionine sulfoximine (BSO)	Sigma-Aldrich GmbH, Taufkirchen, Germany
L-Glutamine, 200 mM, liquid	Invitrogen, Karlsruhe, Germany
Matrigel™ Basement Membrane Matrix	BD Biosciences, Heidelberg, Germany
MEM non-essential amino acids (100x)	Invitrogen, Karlsruhe, Germany
N-Acetyl-L-cysteine (NAC)	Sigma-Aldrich GmbH, Taufkirchen, Germany

Penicillin-Streptomycin Solution, 100 mM	Invitrogen, Karlsruhe, Germany
Puradisc™ 25 AS Syring filter, 0.2 µM	Whatman GmbH, Dassel, Germany
Puromycin dihydrochloride	Sigma-Aldrich GmbH, Taufkirchen, Germany
Sodium Pyruvate MEM 100 mM, liquid	Invitrogen, Karlsruhe, Germany
Sodium selenite	Sigma-Aldrich GmbH, Taufkirchen, Germany
Trypan blue (0.4%)	Sigma-Aldrich GmbH, Taufkirchen, Germany
Trypsin 0.05% (1x), sodium EDTA, liquid	Invitrogen, Karlsruhe, Germany
α-Tocopherol (α-Toc)	Sigma-Aldrich GmbH, Taufkirchen, Germany
β-Mercaptoethanol	Invitrogen, Karlsruhe, Germany

ANTIBODIES**COMPANY**

anti-Akt	NEB GmbH, Frankfurt a.M., Germany
anti-CD31/PECAM1	Millipore GmbH, Schwalbach/Ts., Germany
anti-cleaved Caspase-3	NEB GmbH, Frankfurt a.M., Germany
anti-c-myc	Santa Cruz Biotechnology, Heidelberg, Germany
anti-FLAG	Sigma-Aldrich GmbH, Taufkirchen, Germany
anti-GAPDH	Millipore GmbH, Schwalbach/Ts., Germany
anti-Glutathione reductase	Santa Cruz Biotechnology, Heidelberg, Germany
anti-goat IgG H&L chain specific	Merck KGaA, Darmstadt, Germany
anti-HIF-1α	Acris Antibodies GmbH, Herford, Germany
anti-Ki-67	BD Biosciences, Heidelberg, Germany
anti-mouse IgG, H&L chain specific	Merck KGaA, Darmstadt, Germany
anti-PHD2	Acris Antibodies GmbH, Herford, Germany
anti-Peroxiredoxin 3	BioVendor R&D GmbH, Heidelberg, Germany
anti-Phospho-Akt (Ser473)	NEB GmbH, Frankfurt a.M., Germany
anti-rabbit IgG, H&L chain specific	Merck KGaA, Darmstadt, Germany
anti-Ras	NEB GmbH, Frankfurt a.M., Germany
anti-rat-HRP conjugat	Dianova GmbH, Hamburg, Germany
anti-Thioredoxin-2	R&D systems GmbH, Wiesbaden, Germany
anti-Txnrd1 polyclonal antisera	Dr. Vladim Gladyshev, University of Nebraska, Lincoln, USA
anti-Txnrd2 monoclonal antisera	Dr. Elisabeth Kremmer, Helmholtz Zentrum, München, Germany
anti-Txnrd2 polyclonal antisera	Dr. Vladim Gladyshev, University of Nebraska, Lincoln, USA
anti-VEGF-A	Acris Antibodies, Herford, Germany

anti- α -Tubulin	Sigma-Aldrich GmbH, Taufkirchen, Germany
anti- β -Actin	Sigma-Aldrich GmbH, Taufkirchen, Germany

The production of a monoclonal antibody against murine Txnrd2 was performed in collaboration with Dr. Elisabeth Kremmer and Dr. Tamara Perisic (Helmholtz Zentrum, München). Rats were immunised with a mouse thioredoxin-reductase 2-specific peptide (VKLHISKRSGLEPTVTG) coupled to ovalbumin (OVA)/ Keyhole limpet hemocyanin (KHL). The peptides were obtained from Peptide Specialty Laboratories (Heidelberg, Germany). More than 30 hybridoma clones were screened by immunoblotting until two being immunoreactive against Txnrd2 were found. The antibody-rich supernatant of the hybridoma clones #1C4 and #1D3 were used in the present study.

<u>ENZYMES</u>	<u>COMPANY</u>
Antarctic Phosphatase	NEB GmbH, Frankfurt a.M., Germany
Glutathione reductase, from bakers yeast	Sigma-Aldrich GmbH, Taufkirchen, Germany
RNase A	Qiagen GmbH, Hilden, Germany
Protease Inhibitor Cocktail	Roche Diagnostics GmbH, Heidelberg, Germany
Proteinase K	Roth Carl GmbH & Co., Karlsruhe, Germany
Restriction Endonucleases	NEB GmbH, Frankfurt a.M., Germany
T4 DNA Ligase	Promega GmbH, Mannheim, Germany
Taq DNA polymerase	Qiagen GmbH, Hilden, Germany
<u>KITS AND DISPOSABLES</u>	<u>COMPANY</u>
ApopTag® peroxidase in situ	Millipore GmbH, Schwalbach/Ts., Germany
Apoptosis Detection Kit	
BCA Protein Assay Kit	Fisher Scientific GmbH, Schwerte, Germany
EnzyLight™ ATP Assay Kit (EATP-100)	Biotrend Chemikalien GmbH, Cologne, Germany
Gel Extraction Kit	Qiagen GmbH, Hilden, Germany
Jetstar 2.0 Plasmid Purification System	Genomed GmbH, Loehne, Germany
Lactate Assay Kit II, Colorimetric (450nm)	BioCat GmbH, Heidelberg, Germany
Light Cycler® Fast Start ,	Roche Diagnostics GmbH, Mannheim, Germany
DNA Master ^{PLUS} Set, SYBR Green I	
Light Cycler Capillaries	Roche Diagnostics GmbH, Mannheim, Germany
Parafilm M®	Pechiney Plastic Packaging Company

Polypropylene tubes	Greiner Bio-One GmbH, Frickenhausen; Germany
QIAshredder	Qiagen GmbH, Hilden, Germany
Quantikine ELISA Kit (Mouse VEGF)	R&D systems GmbH, Wiesbaden, Germany
Reverse Transcription System	Promega GmbH, Mannheim, Germany
RNase-Free DNase Set	Qiagen GmbH, Hilden Germany
RNeasy Mini Kit	Qiagen GmbH, Hilden, Germany
SuperFrost® Plus slides	Fisher Scientific GmbH, Schwerte, Germany
Tissue-Tek® O.C.T.™	Sakura, Zoeterwonde, Netherlands

OLIGONUCLEOTIDESSEQUENCE

GENOTYPING

TR2_Del_for	5'-CACGACCAAGTGACAGCAATGCTG-3'
TR2_Del_rev	5'-CAGGCTCCTGTAGGCCCATTAAGGTGC-3'
TR2_Flox_for	5'-CAGGTCAGTACTAGGCTGTAGAGTTTGC-3'
TR2_Flox_rev	5'-TTCACGGTGGCGGATAGGGATGC-3'

REAL-TIME PCR

16S rRNA_for	5'-CCGCAAGGGAAAGATGAAAGAC-3'
16S rRNA_rev	5'-TCGTTTGGTTTCGGGGTTTC-3'
18S rRNA_for	5'-GGACAGGATTGACAGATTGATAG-3'
18S rRNA_rev	5'-CTCGTTCGTTATCGGAATTAAC-3'
Aldolase_for	5'-AGCTGTCTGACATCGCTCACCG-3'
Aldolase_rev	5'-CACATACTGGCAGCGCTTCAAG-3'
Glut-1_for	5'-CTAGAGCTTCGAGCGCAGCGC-3'
Glut-1_rev	5'-AGGCCAACAGGTTTCATCATC-3'
Glut-3_for	5'-TGTCACAGGAGAAGCAGGTG-3'
Glut-3_rev	5'-TCATGAAAACGGAGCAAACA-3'
Glut-4_for	5'-TCATTCTTGGACGGTTCCTC-3'
Glut-4_rev	5'-AGTGCGTCAGACACATCAGC-3'
Hexokinase_for	5'-GCCAGCCTCTCCTGATTTTAGTGT-3'
Hexokinase_rev	5'-GGGAACACAAAAGACCTCTTCTGG-3'
Hif-1 α _for	5'-CAGCGATGACACAGAACTG-3'
Hif-1 α _rev	5'-GGGGCATGGTAAAAGAAAGT-3'
PHD1_for	5'-GTCTGGTATTTTGGATGCCAAGGAAC-3'
PHD1_rev	5'-AGTGATACTTAGTGCCCTCCACACC-3'

PHD2_for	5'-GTTGATAACCCAAATGGAGATGGAA-3'
PHD2_rev	5'-AGTTCAACCCTCACACCTTTCTCAC-3'
PHD3_for	5'-GACTGTCTGGTACTTCGATGCTGAA-3'
PHD3_rev	5'-GTCGTCTGCAGGTATTTCTGGAGTT-3'
Pgc1 α _for	5'-AATGCAGCGGTCTTAGCACT-3'
Pgc1 α _rev	5'-TTTCTGTGGGTTTGGTGTGA-3'
Prx3_for	5'-GTCTGCCTCTGCCCAAGGAAA-3'
Prx3_rev	5'-CTTGGTGTGTTGATCCAGGCA-3'
Prx5_for	5'-AATCTCATCAAAGTTCCTGCC-3'
Prx5_rev	5'-ACCACAGAACTTGGCAGAGCTGC-3'
TrxR2E15_for	5'-TTCACGGTGGCGGATAGGGATGC-3'
TrxR2E18_rev	5'-TGCCCAGGCCATCATCATCTGACG-3'
VEGF_for	5'-CAAGTGGTCCCAGGCTGCACCC-3'
VEGF_rev	5'-CCCTGAGGAGGCTCCTTCCTGCC-3'
β -Actin_for	5'-CCAAGGCCAACCGCGAGAAGATGAC-3'
β -Actin_rev	5'-AGGGTACATGGTGGTGCCGCCAGAC-3'

All DNA-oligonucleotides were obtained from Eurofins MWG Operon, Ebersberg, Germany.

<u>VECTORS</u>	<u>VECTOR TYPE</u>
141pCAG-3SIP-mock-puro ¹	Expression
141pCAG-3SIP-mxCT ¹	Intermediate
141pCAG-3SIP-N'TAPe-mito-mTxnrd2-puro	Expression
391 pEcoEnv-IRES-puro ²	Expression
392 pMDLg_pRRE ²	Expression
393 pRSV_Rev ²	Expression
441 L1 <i>Ha-ras</i> ^{V12} -IRES-golgiVENUS ²	Expression
443 L1 <i>c-myc</i> IRES-mitoVENUS ²	Expression
442 L1-N'TAPe-mito-mTxnrd2-Stop(U524Stop)-IRES-puro ³	Expression
442 L1-N'TAPe-mito-mTxnrd2-IRES-puro ¹	Intermediate
442 L1-N'TAPe-IRES-puro ¹	Expression

Assigned vectors were kindly provided by ¹ Dr. Tamara Perisic, ² Dr. Pankaj Kumar Mandal and ³ Katja Möllmann (Helmholtz Zentrum, München).

BACTERIACOMPANY

TOP10 E.coli cells

Invitrogen, Karlsruhe, Germany

CELL LINES

MOUSE EMBRYONIC FIBROBLASTS (MEFs)

MEFs were isolated from mouse embryos derived from mice heterozygous for *Txnrd2* at embryonic day E12.5⁶¹. The cell lines used in the present study were analysed via genotyping and named *Txnrd2*^{+/+} for wild-type cells and *Txnrd2*^{-/-} for knockout cells. *Txnrd2*^{-/-} cells were stably transfected with the vectors pCAG-3SIP-mock and pCAG-NTAPe-mmitoTxnrd2 to generate the cell lines *Txnrd2*^{-/-}-mock and *Txnrd2*^{-/-}-add-back (reconstitution of Txnrd2 in *Txnrd2*^{-/-} cells). The cell line *Txnrd2*^{-/-}-stop was created using the vector 442-L1-N'TAPe-mito-mTxnrd2-Stop(U524Stop)-IRES-puro (reconstitution of Txnrd2 carrying an inert active site in Txnrd2-knockout cells).

TRANSFORMED CELL LINES

Txnrd2^{+/+} and *Txnrd2*^{-/-} MEFs were transformed by transducing them with lentiviruses encoding the two proto-oncogenes *c-myc* and the mutated *Ha-ras*^{V12} (Val12).

Via soft agar assay, transformed *Txnrd2*^{+/+} and *Txnrd2*^{-/-} single-colony derived cells could be isolated and cultures established.

EMBRYONIC ENDOTHELIAL PROGENITOR CELLS (eEPCs)

At E7.75, eEPCs were isolated from mouse embryos derived from *Txnrd2* heterozygous mice. Txnrd2 wild-type and Txnrd2 knockout cells were identified via genotyping using PCR. To reconstitute Txnrd2 expression, *Txnrd2*^{-/-} cells were stably transfected with pCAG-3SIP-mock and pCAG-NTAPe-mmitoTxnrd2 vectors, yielding *Txnrd2*^{-/-}-mock and *Txnrd2*^{-/-}-add-back cell lines.

HEK 293-T CELLS

The HEK 293-T cells, kindly provided by Dr. Tamara Perisic (Helmholtz Zentrum, München), were used as packaging cells for lentiviral production.

PORCINE AORTIC ENDOTHELIAL CELLS (PAEC)

Endothelial cells from porcine aortas (PAEC) served as controls in the tube formation assay. The cells were kindly provided by Dr. Theres Hennig (Walter Brendel Centre, München).

MOUSE STRAINS

C57BL/6	Charles River Laboratories, Sulzfeld, Germany
Hemizygous <i>Txnrd2</i> mice (<i>Txnrd2</i> ^{+/-})	Dr. Marcus Conrad (Helmholtz Zentrum, München, Germany)
VE-Cadherin-CreER mice	Prof. Dr. Ralf Adams (Max Planck Institute for Molecular Biomedicine, Münster, Germany)

EQUIPMENT AND TOOLSCOMPANY

Cell Counter, Coulter AcT8	Beckman Coulter GmbH, Krefeld, Germany
Confocal laser scanning microscope Leica TCS SP5	Leica Microsystems, Wetzlar, Germany
Cooling centrifuge – for microtubes Biofuge Primo R	Heraeus Instruments, Fisher Scientific, Schwerte, Germany
Cooling centrifuge – for falcon tubes Megafuge 1.0R	Heraeus Instruments, Fisher Scientific, Schwerte, Germany
Coulter® ZZ Particle Count	Beckman Coulter GmbH, Krefeld, Germany
Cryotome HM 560	Microm, Walldorf, Germany
Cytoperm 2	Heraeus Instruments, Fisher Scientific, Schwerte, Germany
Digital camera IXUS55	Canon, Krefeld, Germany
Electrophoresis chamber	Peqlab Biotechnologie GmbH, Erlangen, Germany
ELISA plate reader, Infinite F200	Tecan, Crailsheim, Germany
Flow Cytometer FACSort	BD Biosciences, Heidelberg, Germany
Fluorescence microscope Axiophot equipped with a AxioCam MRm	Carl Zeiss AG, Jena, Germany
Gel Doc 1000	Bio-Rad Laboratoires, Munich, Germany
GenePulser II	BioRad Laboratories GmbH, Munich, Germany
Imaging system for western blot analysis Digital CCD Camera (ORCA-ER)	Hamamatsu Photonics, Herrsching/Ammersee, Germany
Lightmicroscope Olympus IX50	Olympus, Hamburg, Germany
Lumat LB 9507	Berthold Technologies GmbH & Co KG, Bad Wildbad, Germany
Mastercyclerrep gradient for PCR	Eppendorf GmbH, Hamburg, Germany

Multichannel pipette	Eppendorf GmbH, Hamburg, Germany
Oxygraph-2k	Oroboros® Instrumenst GmbH, Innsbruckl, Austria
PHM 82 Standard pH Meter	Radiometer GmbH, Willich, Germany
Spectrophotometer	Eppendorf, Hamburg, Germany
Thermocycler for real-time PCR	Roche Diagnostics GmbH, Mannheim, Germany
Light Cycler 1.5	
Table centrifuge, EBA 12	Hettich Zentrifugen, Tuttlingen, Germany
Ultra-Turrax® X 120 CAT	Bochem Instrumente GmbH, Weilburg, Germany
UV-Star 96-well plate	Greiner Bio-One GmbH, Frickenhausen, Germany
Varioklav® steam steriliser	H+P Labortechnik AG, Oberschleißheim, Germany
xCELLigence RTCA SP system	Roche Diagnostics GmbH, Mannheim, Germany

2.2. Methods

2.2.1. Cell culture techniques and related assays

Cell culture work was performed under sterile conditions using an air flow work bench (Steril compact VBH 48C2, Grandi, Milan, Italy). All cell culture reagents and instruments were autoclaved with a steam steriliser (Varioklav®). Cells were cultured in an incubator at 37°C with water-saturated atmosphere, aerated with 5% CO₂. Depending on the cell line, oxygen levels were kept at 20% or adjusted to 5% by regulating the nitrogen supply. Cell behaviour and appearance was observed using a light microscope (Olympus IX50, 10 x objectives).

2.2.1.1. Cell culture

BACTERIAL CELLS

The bacterial strains TOP10 were cultured over night, either on Luria-Bertani (LB) agar plates or in liquid LB medium in an incubator at 37°C. Transformed bacteria were selected using the antibiotic ampicillin at a final concentration of 25µM.

<u>LB medium</u>		<u>LB agar</u>	
20 mM	MgSO ₄	20 mM	MgSO ₄
10 mM	KCl	10 mM	KCl
1% (w/v)	Tryptone	1% (w/v)	Tryptone
0.5% (w/v)	Bacto yeast extracts	0.5% (w/v)	Bacto yeast extracts
0.5% (w/v)	NaCl	0.5% (w/v)	NaCl
		1.2% (w/v)	Bacto-agar

MURINE EMBRYONIC FIBROBLASTS (MEFs)

Hemizygous *Txnrd2*^{+/-} mice⁶¹ were mated and females were checked daily for vaginal mucous plugs. A vaginal mucous plug is detectable at E0.5. At E12.5 pregnant mice were sacrificed by cervical dislocation. Uterine horns were dissected and placed into sterile PBS. Embryos were separated from the placenta and the surrounding tissue removed. The body trunk was separated from the head, limbs and organs. It was rinsed several times with PBS to wash out blood and loose tissue. Single embryo trunks were minced by two forceps and incubated with Trypsin/EDTA at 37°C for 15 min. By vigorous pipetting, the body trunks were homogenised and the cell suspension was plated in 6 cm dishes and was referred to as passage number 0 (p0). The cells were cultured in standard DMEM at 37°C, 5% CO₂ and 5% O₂. When the cells reached confluence they were split at a ratio of 1:3 and plated on a larger

sized tissue plate. At early passage numbers (p1, p2, p3) part of the cells were cryo-conserved in liquid nitrogen. Only fibroblasts cultured until they reached the passage number 10 were referred to as 'primary'. Primary fibroblasts cultured in standard DMEM and at 37°C, 5% CO₂ and 5% O₂ were routinely split by trypsinisation at a ratio of 1:3 every 3rd or 4th day. Cells with passage numbers >10 (immortalised) were routinely split at a ratio of 1:6 every 3rd or 4th day.

To determine the genotype of the cells, genomic DNA from either mouse embryo tails or cultured cells (p1) was isolated and analysed by PCR with the following primer pairs TR2_Del_for/TR2_Del_rev and TR2_Flox_for/TR2_Flox_rev. The distance between TR2_Del_for and TR2_Del_rev binding site is small enough to be amplified only when the floxed allele is deleted by Cre recombinase. The primer pair TR2_Flox_for/TR2_Flox_rev was used to detect the wild-type allele⁶¹. Only cells with the wild-type (*Txnrd2*^{+/+}, control) and knockout (*Txnrd2*^{-/-}) genotype were used for subsequent experiments.

<i>PBS (-)</i>		<i>standard DMEM</i>	
137 mM	<i>NaCl</i>	500 ml	<i>DMEM (high glucose) 1x</i>
2.68 mM	<i>KCl</i>	10%	<i>FCS</i>
8.10 mM	<i>Na₂HPO₄</i>	1%	<i>L-Glutamine (200 mM)</i>
1.47 mM	<i>KH₂PO₄</i>	1%	<i>Penicillin-Streptomycin</i>
in 1l H ₂ O			
pH 7.4			

EMBRYONIC ENDOTHELIAL PROGENITOR CELLS (eEPCs)

For the isolation and characterisation of embryonic EPCs¹³⁴, hemizygous *Txnrd2* mice were mated and females were monitored daily for mucous plugs. At day E7.75, pregnant females were sacrificed and the uterus was dissected. The egg cylinders with adjacent yolk sacs were washed several times in PBS and the body trunk dissected. The trunk was incubated in Trypsin/EDTA at 37°C for 15-20 min. Dissociated cells were plated in 96-well plates on γ -irradiated, non-proliferating murine fibroblasts serving as feeder layer. The cells were grown in eEPC-DMEM at 37°C, 5% CO₂ and 5% O₂ until cell colonies with cobblestone like cell morphology emerged on the fibroblast layer. When the cells reached confluence they were cultured on larger sized plates covered with γ -irradiated fibroblasts. Finally after two passages on 10 cm dishes, the cells were transferred to 0.1% gelatine-coated plates in the absence of a fibroblast layer and several aliquots were prepared for cryo-conservation. The genotype of the cells was determined as already described for MEFs, and *Txnrd2*^{+/+} (wild-type, control) and *Txnrd2*^{-/-} (knockout) eEPCs were used for subsequent experiments. eEPCs were further grown on 0.1% gelatine pre-coated culture dishes and routinely split at a ratio of 1:6 every 3rd day.

eEPC-DMEM

500 ml	DMEM (high glucose) 1x
15%	FCS
1%	L-Glutamine (200 mM)
1%	Penicillin-Streptomycin
1%	non-essential amino acids 100x
2%	HEPES (1 M)
0.03%	β -Mercaptoethanol (50 mM)

HEK293 T CELLS (HUMAN EMBRYONIC KIDNEY CELLS)

HEK293 T cells were cultured at 37°C in a humidified incubator with 5% CO₂ and 5% O₂. Every 3rd or 4th day the cells were split at a ratio of 1:6 and cultured in standard DMEM.

PORCINE AORTIC ENDOTHELIAL CELLS (PAEC)

The cells were grown in standard DMEM in a humidified incubator at 37°C, 5% CO₂ and 20% O₂. Every 3rd or 4th day the cells were split at a ratio of 1:3.

2.2.1.2. Cell harvesting and passaging

Cells were subcultured to 80-90% confluence. Cells were washed with PBS(-) and incubated in Trypsin/EDTA-solution (1 ml per 10 cm plate) for 5 min at 37°C. During this time, adherent cells detached from the plates due to the proteolytic activity of trypsin and the ability of EDTA to capture bivalent cations as a chelating agent. This process was checked by means of light microscopy and, finally the activity of trypsin was stopped by adding FCS-containing standard DMEM. Depending on the experiment, different splitting rates were chosen, ranging from 1:3 to 1:6 (see for each cell line). Finally, the cells were cultured in medium as indicated above.

Trypsin/EDTA

0.5%	trypsin
0.2%	EDTA

2.2.1.3. Cryo-conservation and thawing

For long-time storage, aliquots of all cell lines were frozen and stored in liquid nitrogen. Cells were grown on 10 or 15 cm diameter culture dishes to 90% confluence. After trypsin treatment, cells were collected by centrifugation (5 min, 1200xg) and the pellet was

resuspended in freezing medium. Aliquots were frozen at -80°C over night and subsequently transferred to a liquid nitrogen tank.

When needed, cells were quickly defrosted at 37°C in a waterbath, added to a falcon tube containing standard DMEM and collected by centrifugation (5 min, 1200xg). The pellet was resolved in standard DMEM, the cells added to a 10 cm diameter culture dish and cultured at 37°C . After 24 h, cells were checked by means of light microscopy and the medium was refreshed.

Freezing medium

10% DMSO
in FCS

2.2.1.4. Determination of cell number

NEUBAUER HAEMOCYTOMETER

Cells were collected from culture dishes via trypsinisation and suspended in an appropriate amount of medium. Subsequently, 30 μl of the cell suspension was mixed with an equal amount of 0.4% trypan blue solution and cells were counted in a Neubauer haemocytometer. Trypan blue can pass the membrane of dead cells, thereby allowing these cells to be excluded during counting (see chapter 2.2.1.6. first subitem).

CELL COUNTER COULTER®

Cells were collected from culture dishes via trypsinisation and suspended in an appropriate amount of medium. Subsequently, 100 μl of the cell suspension was diluted in 10 ml of a NaCl solution and analysed by a Coulter® AcT8. Cell numbers are expressed as cells/ml.

2.2.1.5. Cell stimulation and inhibition

TREATMENT WITH L-BUTHIONINE SULFOXIMINE (BSO)

BSO is known to specifically inhibit the enzyme γ -glutamyl-cysteine-synthase (competitive inhibition) that is necessary to synthesise glutathione. *Txnrd2*^{-/-} cells lack one major redox-regulating enzyme, which is located in the mitochondria. It has been shown that treatment of primary *Txnrd2*^{-/-} cells with BSO leads to reduced proliferation and finally causes cell death⁶¹. In the present study BSO was used as a stressor to further investigate functions of Txnrd2.

Therefore the cells were treated with 10 μ M BSO for several hours or over night in different experimental settings.

BSO solution

150 mM in ethanol	BSO
----------------------	-----

STARVATION

Cells were stressed by depletion of essential nutrients and growth factors. Therefore, cells were grown on 6 cm or 10 cm diameter culture dishes until 80% confluence in standard-DMEM. The culture medium was replaced by DMEM-starvation and cells were incubated for 4 h or over night.

DMEM-starvation

500 ml 1%	DMEM (low glucose) 1x Penicillin-Streptomycin
--------------	--

GALACTOSE-SUPPLEMENTATION

Cells were stressed by deprivation of glucose and replacement by galactose. Therefore, equal numbers of cells were placed on 6-well culture plates and cultured with DMEM-galactose over a period of 5 days. Number of cells was analysed every day (see chapter 2.2.1.4., first subitem and 2.2.1.6. first subitem).

DMEM-galactose

500 ml 10% 1% 1% 1% 1% 1%	DMEM (no glucose) 1x FCS L-Glutamine (200 mM) Penicillin-Streptomycin HEPES (1 M) Sodium Pyruvate (100 mM) D-Galactose (1 M)
---	--

2.2.1.6. Viability and proliferation

TRYPAN BLUE DYE EXCLUSION METHOD

Equal numbers of cells were plated in 6-well dishes in triplicate and cultured in different media (DMEM-low glucose, DMEM-galactose) or treated with several compounds over 5 days. Every 24 h cells were counted using the trypan blue exclusion method. Trypan blue is

excluded from viable cells whereas dead cells are stained blue due to disrupted membranes. Cells were collected in 1 ml standard-DMEM after incubation with trypsin. 30 μ l of the cell suspension was mixed with 30 μ l of 0.4% trypan blue solution (Sigma-Aldrich GmbH) and cells were counted in a Neubauer haemocytometer. Only viable cells were counted.

<u>DMEM-low glucose</u>		<u>DMEM-galactose</u>	
1x	DMEM (low glucose)	1x	DMEM (no glucose)
10%	FCS	10%	FCS
1%	Penicillin-Streptomycin	1%	Penicillin-Streptomycin
1%	L-Glutamin	1%	L-Glutamin
		10 mM	D-Galactose
		10 mM	HEPES
		1 mM	Sodium pyruvate

MTT ASSAY

MTT assay was performed to measure the viability of primary eEPCs ²¹⁸. 96-well culture plates were coated with 0.1%-gelatine and 15,000 cells were plated in triplicate. Cells were cultured in 200 μ l of eEPC-DMEM over 5 days and the cell number was estimated via MTT every 24 h. Therefore, 20 μ l of MTT (50 μ g) was added to the medium and incubated for 4 h at 37°C in the incubator. The medium was aspirated and the formazan crystals were dissolved by adding 200 μ l of isopropanol. Absorbance was measured at 570 nm (620 nm reference wavelength) in a Tecan spectrophotometer. The data were acquired by Magellan software (version 6.4, Tecan).

Thiazolyl blue reagent (MTT)
 stock solution 5 mg/ml in PBS,
 steril filtered, stored at 4 °C protected from light

xCELLigence RTCA SP system

The xCELLigence system (Roche) monitors cellular events in real-time without the incorporation of labels by measuring electrical impedance across interdigitated micro-electrodes integrated in the bottom of its special tissue culture plates. The impedance measurement provides quantitative information about the biological status of the cells, including cell number. The RTCA SP (single-plate) Instrument consists of a RTCA Analyser, a RTCA SP Station, as well as a RTCA Control Unit, and is designed for the use of one E-Plate 96 (a specialised 96-well plate used with the RTCA Instrument). The RTCA SP Station together with the E-Plate 96 is placed into a regular cell culture incubator. The RTCA

Control Unit receives the data measured by the RTCA Analyser and uses the RTCA Software 1.0 for set-up, real-time display, and analysis of each experiment.

The actual variable being measured is derived from the change in electrical impedance as the living cells interact with the biocompatible microelectrode surface in the E-Plate well. The signal is converted to the parameter called cell index. The cell index correlates with the number of viable cells on the 96 E-plate. The experiment was performed in triplicate and 2,500 cells were plated in a final volume of 50 μ l culture medium each well. Cells were allowed to settle for four hours and afterwards incubated with several stimuli (e.g. 10 μ M BSO) or left untreated. Proliferation of cells was monitored and cell index data were acquired throughout a course of 70 h.

2.2.1.7. Soft agarose assay

The anchorage-independent growth of *c-myc/Ha-ras*-transformed fibroblasts was investigated using the soft agarose assay. Each well of a 6-well culture plate was precoated with 2 ml base agar matrix and allowed to cool at 4°C for 30 min. Cells were harvested by adding trypsin/EDTA-solution. 500 cells per well were plated in agar matrix on top of the base agar matrix layer. The matrix was allowed to cool at 4°C for 30 min, covered with standard DMEM and the plate was returned to the incubator. The single cell-derived colonies appeared after three to four days. After seven days the colonies were fixed with methanol and stained with crystal violet. Plates were washed with aqua ad iniectabilia several times and allowed to dry before numbers of colonies were counted visually.

<i>Base agar matrix</i>		<i>Agar matrix</i>	
1%	<i>Agarose, TopVision™ LMGQ</i>	0.5%	<i>Agarose, TopVision™ LMGQ</i>
<i>in PBS(-)</i>		<i>in PBS(-)</i>	

2.2.1.8. Isolation of single-colony derived cell lines

For *in vitro* and *in vivo* investigations concerning tumour growth and progression, transformed cell lines were generated by single-cell cloning. At day 7 of growth multiple colonies derived from *Txnrd2^{+/+}* and *Txnrd2^{-/-}* *c-myc/Ha-ras*-transformed fibroblasts were picked from the soft agar assay and transferred to a 96-well plate. Colonies were cultured in standard-DMEM over night and cells were released from the colony spheroid by incubation with trypsin/ETDA-solution and plated in fresh standard DMEM on a 96-well plate on the next day. When the cells reached confluence they were split on larger sized plates. DNA was isolated and protein lysates were prepared in order to check the genotype and the

expression of *c-myc* and *Ha-ras*. Transformation was also verified by monitoring VENUS expression using FACS analysis.

2.2.1.9. Matrigel® tube formation assay

In vitro angiogenesis assays are important tools for studying the mechanisms of angiogenesis. In the present work the Matrigel® tube formation assay was used to study angiogenesis. Matrigel® is an extracellular matrix derived from murine tumours containing essential growth factors. BD Matrigel® (Becton Dickinson) was thawed on ice at 4°C 24 h before the assay was started. 24-well culture plates and sterile tips were pre-cooled at 4°C. Every well was coated with 100 µl Matrigel® avoiding air bubbles. The plate was incubated for 30 min at 37°C allowing the Matrigel® to polymerise. Cells were harvested from 80% confluent 10 cm plates by trypsin/EDTA. 30,000 cells were dispensed in 1 ml eEPC-DMEM and added per well. Plates were incubated at 37°C for 30 min, gently shaken every 10 min. Sprouting was observed over 24 h every 4 h. Pictures were taken from each well using a microscope (Olympus IX50, 10 x objective) and a digital camera (Canon IXUS 55). PAEC were plated as positive control and observed in parallel. Number of branching points were estimated at several time points.

2.2.2. Flow cytometry

Flow cytometry is an already approved method for quantitative and functional analysis of cells addicted to cell size, granularity and fluorescence intensity. A wide range of applications can be achieved by using flow cytometry (e.g. cell cycle analysis, apoptosis, membrane potential, etc.). In the present study flow cytometry was used for the quantitative analysis of intracellular ROS accumulation as well as determination of mitochondrial mass. All measurements were performed using the BD FACSort (Becton Dickinson). Fluorescence was measured using the appropriate filters for the respective fluorochromes. Data were analysed by the CellQuest software (Becton Dickinson) and WinMDI software (version 2.9). Suitable solutions, like sheath fluid (BD FACSTFlow™), cleaning (BD FACSClean) and rinsing solution (BD FACSRinse), were purchased from Becton Dickinson.

2.2.2.1. Determination of cellular ROS

DICHLOROFLUORESCIN DIACETATE

2',7'-Dichlorofluorescein diacetate (DCFH-DA), a derivative of fluorescein, is a cell-permeant indicator for free intracellular reactive oxygen species (ROS). The reduced and acetylated form (DCFH-DA) is non-fluorescent and able to pass the cell membrane. Cleavage of the acetate group by intracellular esterase yields a non-fluorescent charged form that is much better retained in the cell (DCFH). This compound is trapped inside the cells and oxidised to the fluorescent compound DCF depending on the cellular oxidation status. 300,000 cells were plated on 6 cm culture plates the day before the experiment. Cells were incubated with 2 μ M DCFH-DA in DMEM without FCS for 45 min at 37°C in the incubator protected from light. Cells were harvested, resolved in 300 μ l PBS(-) and transferred to round bottom polypropylene tubes (Greiner Bio-One GmbH). Fluorescence intensity was measured at an excitation wavelength of 488 nm and emission wavelength of 530 nm (FL-1). A number of approximately 10,000 cells was analysed for each sample. Mean fluorescence intensity (MFI) was measured for at least three independent experiments.

DCFH-DA solution
2 mM DCFH-DA
in ethanol

MITOSOX™ RED SUPEROXIDE INDICATOR

To investigate the production of cellular ROS in the *c-myc/Ha-ras*-transformed fibroblasts the MitoSox™ Red superoxide indicator was used. After transfection with the lentivirus for *c-myc* and *Ha-ras* the transformed cells express VENUS. The strong fluorescence of VENUS makes it impossible to use DCFH-DA for the detection of cellular ROS. The non-fluorescent MitoSox™ Red is cell-permeant and rapidly targeted to the mitochondria. There it becomes oxidised by superoxide and exhibits a red fluorescence. 300,000 cells were plated on 6 cm culture plates the day before the experiment. Cells were protected from light and incubated with 5 μ M MitoSox™ Red in DMEM without FCS for 30 min at 37°C. Cells were harvested, resolved in 300 μ l PBS(-) and transferred to round bottom polypropylene tubes (Greiner Bio-One GmbH). Fluorescence intensity was measured at an excitation wavelength of 488 nm and emission wavelength of 580 nm (FL-2). A number of approximately 10,000 cells was analysed for each sample. MFI was measured for at least three independent experiments.

<u>MitoSox™ Red solution</u>	
5 mM	MitoSox™ Red
in DMSO	

2.2.2.2. Quantification of mitochondria in cells

MITOTRACKER® GREEN AND RED

The Mitotracker® Probes contain a mildly thiol-reactive chloromethyl moiety and selectively label mitochondria in living cells. It is predicted that Mitotracker® Green and Mitotracker® Red can be used to measure mitochondrial mass independent of mitochondrial membrane potential (MMP)²⁴². In the present study both agents were used to determine the mitochondrial mass in non-transformed and *c-myc/Ha-ras*-transformed fibroblasts. Since the transformed cells exert strong fluorescence due to VENUS expression, Mitotracker® Red was chosen. 300,000 cells were plated on 6 cm culture plates the day before the experiment. Cells were protected from light and incubated with 20 nM Mitotracker® Green or with 100 nM Mitotracker® Red in DMEM without FCS for 25 min at 37°C. Cells were harvested, resolved in 300 µl PBS(-) and transferred to round bottom polypropylene tubes (Greiner Bio-One GmbH). Mitotracker® Green fluorescence intensity was measured at an excitation wavelength of 448 nm and an emission wavelength of 516 nm (FL-1). Mitotracker® Red fluorescence intensity was measured at an excitation wavelength of 488 nm and an emission wavelength of 599 nm (FL-2). A number of approximately 10,000 cells was analysed for each sample. MFI was measured for at least three independent experiments.

<u>Mitotracker® Green solution</u>		<u>Mitotracker® Red solution</u>	
1 mM	Mitotracker® Green	1 mM	Mitotracker® Red
in DMSO		in DMSO	

NONYL ACRIDINE ORANGE

Alternatively, mitochondrial mass was measured using a second experimental setting by staining cells with nonyl acridine orange (NAO). NAO is well retained in the mitochondria and its uptake is reported to be independent from mitochondrial membrane potential (MMP)²⁸⁷. 300,000 cells were plated on 6 cm culture plates the day before the experiment. Cells were protected from light and incubated with 10 nM NAO in PBS(+) without FCS for 20 min at 37°C. Cells were harvested, resolved in 300 µl PBS(+) and transferred to round bottom polypropylene tubes (Greiner Bio-One GmbH). Fluorescence intensity was measured at an excitation wavelength of 448 nm and an emission wavelength of 519 nm (FL-1).

Mitochondrial mass was normalised to the content of endoplasmic reticulum (ER). Therefore cells were stained with the ER-specific dye ER-Tracker™ Red. The stain consists of the green fluorescent BODIPY® TR dye and glibenclamide. Glibenclamide binds to the receptors of ATP-sensitive K⁺-channels which are prominent on the ER. Cells were protected from light and incubated with 1 µM ER-Tracker™ in PBS(+) with 5% FCS for 20 min at 37°C. Fluorescence intensity was measured at an excitation wavelength of 448 nm and an emission wavelength of 511 nm (FL-1). A number of approximately 10,000 cells was analysed for each sample. MFI for NAO and ER-Tracker™ was measured for at least three independent experiments. The estimated MFI for NAO was normalised to the MFI for ER-Tracker™.

<i>NAO-solution</i>		<i>ER-Tracker™</i>	
<i>1 µM</i>	<i>Acridine Orange 10-NONYL</i>	<i>1 mM</i>	<i>ER-Tracker™</i>
<i>in ethanol</i>		<i>in DMSO</i>	

2.2.3. High-resolution respirometry

High-resolution respirometry (HRR) provides an important tool to study changes in mitochondrial respiratory chain function and mitochondrial ATP production in living cells and isolated mitochondria. We used the Oxygraph-2k (Oroboros®) (Figure 2-1) to determine endogenous oxygen consumption and activity of respiratory chain complexes in living fibroblasts, as described recently²¹⁶.



Figure 2-1: Oxygraph-2k

The Oxygraph-2k provides the instrumental basis for the high-resolution respirometry and offers the opportunity to measure low respiratory activities, fast kinetic transitions and low oxygen levels in living cells, isolated mitochondria from cells or biopsies. The picture is taken from the official Oroboros® homepage.

Mitochondrial respiration was studied at 30°C in respiration medium B¹⁷³. Approximately 1.2 Mio cells were resuspended in 120 µl respiration medium B and applied to the Oxygraph-2k chamber. The experiment was performed with constant stirring of cells. Permeabilisation of cell membranes was achieved by adding 10 µg digitonin per 10⁶ cells. Endogenous oxygen consumption was observed over at least 10 min. Complex I respiration was measured in the presence of glutamate/malate (10 mM/ 5 mM) and ADP (1 mM) and inhibited with rotenone (0.5 µM). Complex II/III were measured after addition of succinate (10 mM) and inhibited with antimycin A (2.5 µM). Finally Complex IV was assessed in the presence of ascorbate/TMPD (2 mM/ 0.5 mM) and inhibited with KCN (1 µM). The software DatLab (Oroboros®) was used for data acquisition and analysis (Figure 2-2). Respiratory flux was calculated as the time derivative of oxygen concentration measured at 1 s sampling intervals and expressed in O₂ flux per cells [pmol/s*Mio]. Values were corrected for instrumental and chemical background.

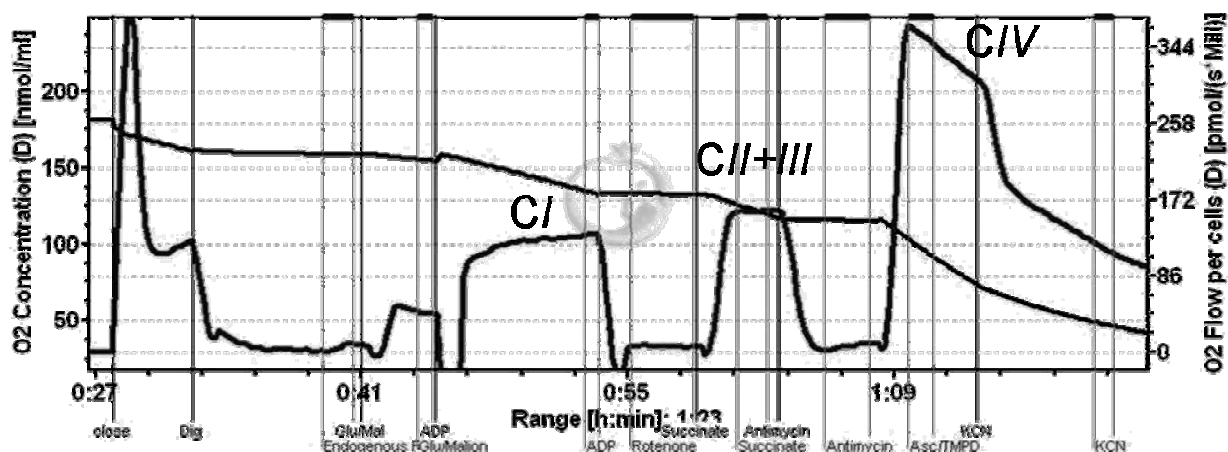


Figure 2-2: High-resolution respirometry in permeabilised murine fibroblasts

The graph depicts Oxygraph-2k recording of the respiratory activities in murine fibroblasts. Upper line represents the oxygen concentration and the lower line the oxygen flux. The vertical lines represent times of addition of stimulants or inhibitors. (CI = activity of Complex I. CII+III = activity of Complex II and III, CIV = activity of Complex IV, Dig = digitonin, Glu/Mal = glutamate/malate, Asc/TMPD = ascorbate/Tetramethylphenylendiamin)

Respiration medium B

0.5 M	EGTA
3 mM	MgCl ₂ xH ₂ O
60 mM	K-lactobionate
20 mM	Taurine
10 mM	KH ₂ PO ₄
20 mM	HEPES
110 mM	Mannitol
1g/l	BSA
pH 7.1	

2.2.4. Molecular biology techniques

2.2.4.1. Isolation of genomic DNA

Cell pellets and tissue samples were lysed in DNA lysis buffer supplemented with 50 µg/ml proteinase K. Samples were incubated over night at 55°C with constant shaking at 550xg. DNA was isolated using phenol/chlorophorm/isoamyl alcohol extraction. Therefore an equal volume of phenol/chloroform/isoamyl was added, samples were vortexed for 20 s and centrifuged 6 min at 10,000xg. The upper aqueous phase was recovered and again mixed with an equal volume of phenol/chloroform/isoamyl. After 6 min of centrifugation at 10,000xg the aqueous phase was separated and precipitated by adding 2.5x volume of ethanol containing 50 mM NaCl. After centrifugation for 10 min at 10,000xg and 4°C the pellet was washed two times in ice-cold 70% ethanol, centrifuged as indicated above and air-dried. The DNA was dissolved in 100 µl 1xTE-buffer and stored at -20°C or used for genotyping of animals or cells and for further expression analysis.

<i>DNA lysis buffer</i>		<i>1x TE-buffer</i>	
10 mM	<i>Tris pH 7.6</i>	1 M	<i>Tris pH 7.6</i>
10 mM	<i>EDTA</i>	0.5 M	<i>EDTA pH 8.0</i>
0.5%	<i>SDS</i>		
10 mM	<i>NaCl</i>		

2.2.4.2. Isolation of total RNA

Total RNA from tissue samples and cells was isolated using the RNeasy Mini Kit (Qiagen) according to the manufacturer's instructions. Maximum 30 mg of frozen or fresh tissue and approximately 1×10^6 cells were lysed in an appropriate amount of RLT buffer (denaturing guanidine-thiocyanate containing buffer) supplemented with 10 µl/ml β-mercaptoethanol. Samples were homogenised using QIAshredder columns (Qiagen) centrifuging 2 min at maximum speed. Ethanol was added to provide proper binding conditions and the sample was applied onto RNeasy Mini spin columns. During centrifugation at 10,000xg the total RNA binds to the column and contaminants can be removed. On-column DNase digestion with RNase-free DNase Set (Qiagen) was performed to reduce DNA contamination. With an appropriate amount of 30 to 50 µl of RNase-free water total RNA was eluted. Aliquots were stored at -80°C after determination of concentration at 260 nm using a spectrophotometer (Eppendorf).

2.2.4.3. Synthesis of cDNA

For cDNA synthesis an amount of 1 µg RNA was used. Reverse transcription was performed using the Reverse Transcription System (Promega) according to manufacturer's instructions. In a final volume of 20 µl cDNA was synthesised at 42°C using random primers. Incubation time was extended to 60 min to obtain more abundant transcripts. At 95°C enzyme activity was stopped and samples were placed on ice. The cDNA was stored at -20°C and used for semi-quantitative PCR and quantitative Real-time PCR.

2.2.4.4. Polymerase chain reaction (PCR)

The standard PCR was performed in a Mastercycler ep gradient (Eppendorf) (Table 2-1). The individual PCR steps were optimised for each template and primer pair combination. For all amplification reactions the *Taq polymerase* (Qiagen) was used. Primers were designed with the software Primer3 v 0.4.0²⁷⁵ and obtained from Eurofins MWG GmbH (Ebersberg). 1-20 ng of DNA and cDNA to be amplified was mixed with *DNA polymerase* (2.5 units), oligonucleotide primers (0.3 µM each), dNTPs (200 µM each, Fermentas), 1x PCR buffer and MgCl₂ (3 mM) in a final volume of 25 µl in water. After PCR amplification the size of the product was analysed by gel electrophoresis.

Table 2-1: PCR standard protocol

Step	Time	Temperature	Cycles
Initial denaturation	3 min	94°C	
Denaturation	1 min	94°C	30-35
Annealing	1 min	55-65°C according to primer pairs	
Elongation	1 min	72°C	
Prolonged elongation	7 min	72°C	

2.2.4.5. Real-time PCR

For quantitative expression analysis the LightCycler FastStart DNA MasterPLUS SYBR Green I Kit (Roche) was used and PCR was performed with the LightCycler 1.5 System (Roche) (Table 2-2). According to the manufacturer's instructions (Roche) each RT-PCR reaction contained cDNA, respective oligonucleotide primers, the LightCycler Master Mix (*Taq DNA polymerase* and SYBR Green I dye) in a final volume of 10 µl. RT-PCR primer were designed with an optimal melting temperature (TM) of approximately 58°C and a

product size between 200 and 300 bp using the Primer3 software V 0.4.0²⁷⁵. To minimise unspecific amplification of possible genomic DNA contaminations, primer pairs were designed that hybridise on different exons. Further formation of non-specific products is minimised by the hot start effect of the FastStart *Taq DNA polymerase*. The amplification is detected by measurement of the fluorescence signal at 530 nm of SYBR Green I that binds to the double-stranded DNA. Relative to the amount of double-stranded DNA the fluorescence signal increases during PCR. The specificity of the amplified product was observed by melting curve analysis which should reveal only one peak at a characteristic melting temperature depending on the GC-content and amplicon length. The expression levels of the gene of interests were normalised to the expression levels of *18S rRNA*, *β -actin* or *aldolase*. At least three independent experiments were performed for statistical evaluation.

Table 2-2: Real-time PCR standard protocol

Step	Time	Temperature	Cycles
Pre-Incubation	10 min	95°C	1
Amplification			
Denaturation	10 s	95°C	35-40
Annealing	10-45 s	according to primer pairs	
Elongation	30 s	72°C	
Melting Curve			
Denaturation	1 s	95°C	1
Annealing	60 s	65°C	
Melting	1 s	95°C	
Cooling	30 s	40°C	1

2.2.4.6. Agarose gel electrophoresis

A 1% agarose gel in TBE buffer containing ethidium bromide (0.05 µg/ml) was prepared and allowed to polymerise. The appropriate DNA marker and samples containing loading buffer at a ratio of 1:6 were poured into the gel pockets. Separation was performed in an electrophoresis chamber (Peqlab Biotechnologie GmbH) at 80 to 100 Volts (power supply Phero-Stab 0310, Biotec-Fischer). Fluorescence of PCR products was documented and analysed with a Gel Doc 1000 station (Bio-Rad).

<i>TBE buffer</i>		<i>Loading buffer 6x</i>	
89 mM	<i>Tris</i>	10 mM	<i>Tris pH 7.6</i>
89 mM	<i>Boric acid</i>	0.03%	<i>Bromphenol blue</i>
2.5 mM	<i>EDTA</i>	0.03%	<i>Xylene cyanol</i>
pH 8.3		60%	<i>Glycerol</i>
		60 mM	<i>EDTA</i>

2.2.4.7. Cloning techniques

PREPARATION OF COMPETENT BACTERIA

Chemically competent *E.coli* TOP10 were produced by a modified rubidium chloride method²⁷⁴. *E.coli* TOP 10 were cultured on an agar plate at 37°C over night. A single colony was inoculated in 2.5 ml of LB medium without antibiotic in a loose-capped falcon and incubated at 37°C with constant shaking over night. The over night culture was diluted 1:100 in 250 ml LB medium containing KCl (100 mM) and MgCl₂ (200 mM) and bacteria were grown until the absorbance at a wavelength of 600 nm reaches 0.4 to 0.6. Bacteria cells were pellet at 4,500xg for 5 min at 4°C and gently resuspended in 0.4x of the original volume of ice-cold standard transformation buffer 1 (TFB1). The remaining steps were carried out on ice. Finally the cells were concentrated in 0.04x of the original volume of ice-cold TFB2, aliquots of 100 µl were snap-frozen in liquid nitrogen and stored at -80°C until further use.

<i>TFB1</i>		<i>TFB2</i>	
30 mM	<i>potassium acetate</i>	10 mM	<i>MOPS (pH 6.5)</i>
10 mM	<i>CaCl₂</i>	75 mM	<i>CaCl₂</i>
50 mM	<i>MgCl₂</i>	10 mM	<i>RbCl</i>
100 mM	<i>RbCl</i>	15%	<i>glycerol</i>
15%	<i>glycerol</i>	pH 6.5	
pH 5.8			
filter-sterilise (0.45 µm)		filter-sterilise (0.45 µm)	

TRANSFORMATION OF BACTERIA BY HEAT SHOCK

For transformation of bacteria 100 µl aliquots from -80°C stocks were thawed on ice, gently mixed with 1-10 pg plasmid DNA or 10 µl ligation preparation and incubated on ice for up to 20 min. Cells were heated for 1-2 min at 42°C and placed on ice for 10 min. 1 ml of pre-warmed LB medium without antibiotic was added and cells were incubated at 37°C for 45 min with constant shaking. After centrifugation for 5 min at 3,500xg LB medium excess was discarded and the pellet was dissolved in 200 µl LB medium. All plasmids in the present study expressed *β-lactamase* for selection and thus the resolved cells were plated on a LB

agar plate containing 50 µg/ml ampicillin and incubated at 37°C for approximately 16 h until single cell colonies became visible.

PREPARATION OF PLASMID DNA

Plasmid DNA was purified using the Plasmid Purification System Jetstar (Genomed) following the manufacturer's instructions. The volume of solutions described here corresponds to a maxi prep and yields an amount of 50 to 500 µg plasmid DNA. After transformation of bacteria single colonies were inoculated in 5 ml of LB medium containing 50 µg/ml ampicillin. Bacteria were vigorously shaken for 16 h at 37°C. After centrifugation at 4000xg and 4°C for 15 min the cell pellet was resuspended in 10 ml of E1 resuspending buffer containing *RNase* (100 µg/ml). 10 ml of E2 lysis buffer were added, mixed carefully and incubated for 5 min at room temperature. After addition of 10 ml E3 neutralising buffer centrifugation was performed at 12,000xg and 4°C for 10 min. Supernatant was applied to the pre-treated columns and allowed to pass through. After washing with 60 ml of E5 washing buffer the column was transferred to a fresh 50 ml falcon and plasmid DNA was eluted with 15 ml of E6 elution buffer. DNA was precipitated with 0.7 volume (10.5 ml) of ice-cold isopropanol and after centrifugation (30 min, 12,000xg, 4°C) the pellet was washed with 70% ethanol. The pelletised plasmid DNA was dried and resuspended in 200-500 µl TE-buffer and stored at -20°C. The concentration of the plasmid DNA was determined by measuring the absorbance at 260 nm in a spectrophotometer (Eppendorf).

<u>Buffer E1</u>	<u>Buffer E2</u>	<u>Buffer E3</u>
50 mM Tris	200 mM NaOH	3.1 M potassium acetate
10 mM EDTA	1.0% SDS	pH 5.5
pH 8.0		
<u>Buffer E4</u>	<u>Buffer E5</u>	<u>Buffer E6</u>
600 mM NaCl	800 mM NaCl	1250 mM NaCl
100 mM sodium acetate	100 mM sodium acetate	100 mM Tris
0.15% TritonX-100	pH 5.0	pH 8.5
pH 5.0		

All buffers E1 – E6 were constituents of the Plasmid Purification System Jetstar and purchased from Genomed.

Mini preps were performed using a similar protocol from Qiagen (QIAprep MiniPrep Kit) following the manufacturer's instructions yielding 20-30 µg of plasmid DNA.

RESTRICTION DIGESTION OF PLASMID DNA

Restriction digestion was performed using corresponding endonucleases and appropriate buffers from NEB (New England Biolabs). Restriction mixture was prepared according to the

manufacturer's instructions and incubated for an adequate time (4 h or 16 h) and a suitable temperature. Plasmid DNA was loaded on a 1% low melting point agarose gel stained with ethidium bromide and separated at 80 to 100 V. Using a scalpel the fragment of desired size was excised and DNA was removed from the agarose by the Qiagen Gel Extraction Kit (Qiagen) according to the instruction manual.

DEPHOSPHORYLATION OF LINEARISED VECTOR DNA

To avoid religation, the vector DNA was treated with the *Antarctic Phosphatase* (New England Biolabs). The *Antarctic Phosphatase* catalyses the removal of 5' phosphate groups and thus the vector DNA can not self-ligate. According to the instruction manual the dephosphorylation protocol was performed in appropriate buffers at 37°C. Finally enzyme activity was inhibited at 65°C for 5 min. The vector DNA was then used for ligation.

LIGATION OF PLASMID DNA

T4 DNA Ligase purified from *E.coli* was used for ligation of the desired insert with the appropriate plasmid back-bone according to the instruction manual (New England Biolabs). *T4 DNA Ligase* catalyses the formation of phosphodiester bonds between juxtaposed 5' phosphate and 3' hydroxyl termini in duplex DNA and is able to join blunt end and cohesive end termini. A common ligation mixture in a final volume of 20 µl consisted of:

2 µl	10x <i>T4 ligase</i> buffer
1 µl	<i>T4 DNA Ligase</i> (stock 400,000 units/ml)
2 µl	dephosphorylated vector (~50 ng)
4 µl	insert (~150 ng)
11 µl	aqua ad iniectabilia

The ligation was carried out at 16°C over night. Afterwards the ligation mixture was used for transformation of competent bacteria. Successful integration of the desired insert into the vector was monitored after transformation. Therefore plasmid DNA from over night cultures of single colonies was exposed to restriction digestion with specifically selected endonucleases. Restriction pattern after electrophoretic separation was aligned with the plasmid map using the pDRAW32 program version 1.0 (AcaClone software).

2.2.4.8. Cloning of Txnrd2 in the pCAG-3SIP system

To generate the expression vector 141pCAG-3SIP-N'TAPe-mito-mTxnrd2-puro (Figure 2-4) the lentiviral vector 442-PL1-N'TAPe-mito-mTxnrd2-IRES-puro (not depicted) was digested with *EcoRI* and *PmlI*. The Txnrd2 fragment was isolated and cloned into the backbone of the plasmid 141pCAG-3SIP-mXCT (Figure 2-3) after digestion with *EcoRI* and *PmlI*. Successful transfection of cells was observed by using an anti-Txnrd2 antibody.

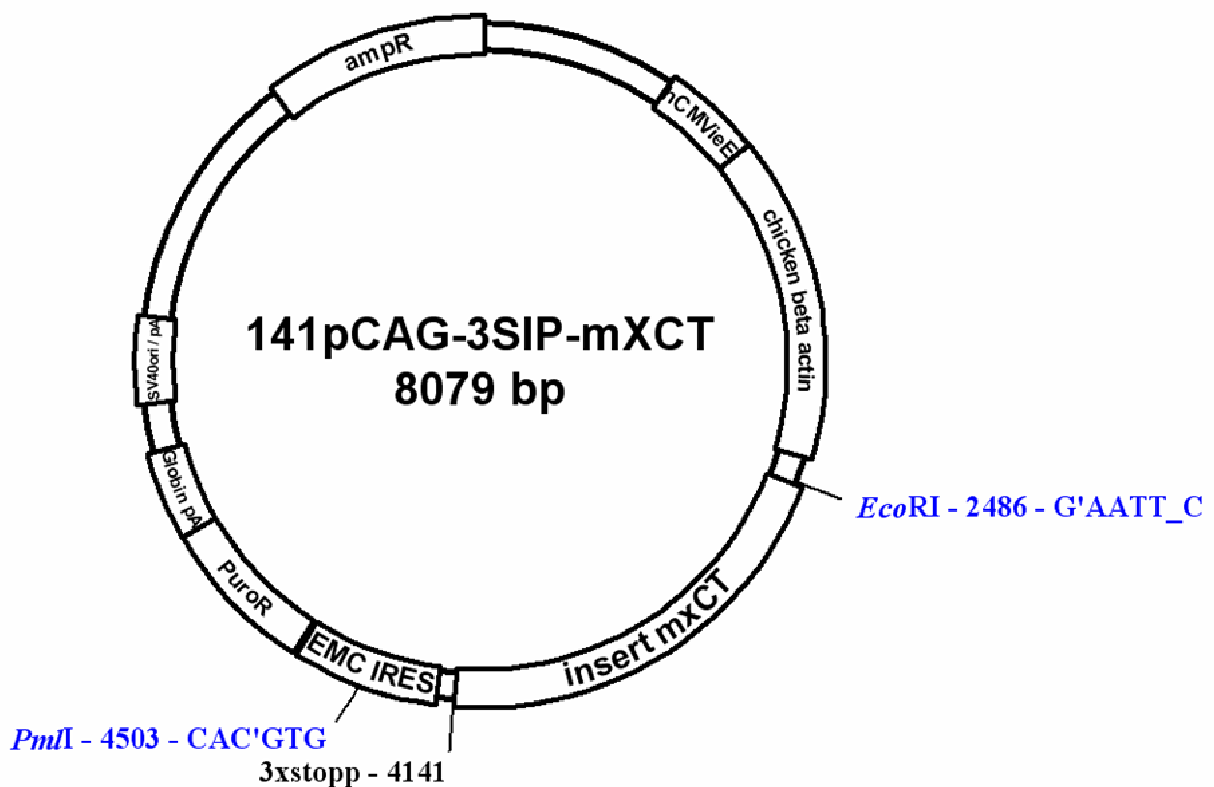


Figure 2-3: Map of the intermediate vector 141pCAG-3SIP-mXCT

Abbreviations: ampR (*β-lactamase*: ampicillin resistance gene), hCMVieE (human cytomegalovirus immediate early-enhancer modified chicken β-actin promoter), mxCT (encoding mouse xCT light chain, the substrate-specific subunit of the cystine transporter, system x_c-), EMC IRES (internal ribosome entry site), PuroR (*puromycin N-acetyltransferase* gene), globin pA (globin poly A signal), SV40 ori pA (simian virus 40 origin of replication), 3xstopp (three stop codons in all three open reading frames). *EcoRI* and *PmlI* depict unique restriction sites used for cloning.

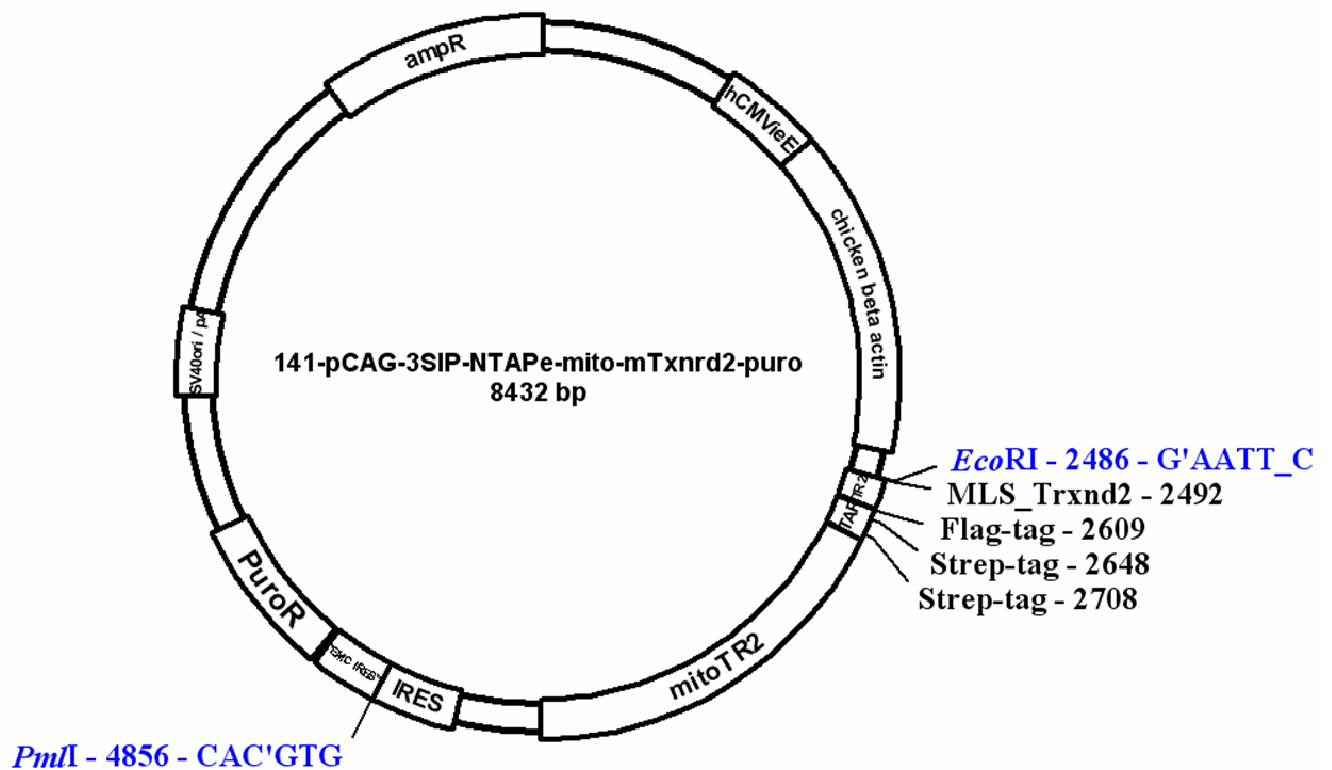


Figure 2-4: Map of the expression vector 141pCAG-3SIP-N'TAPe-mito-mTxnrd2-puro

Abbreviations: ampR (*β -lactamase*: ampicillin resistance gene), hCMVieE (human cytomegalovirus immediate early-enhancer modified chicken β -actin promoter), MLS TR2 (mitochondrial leader sequence for Txnrd2), Flag-tag (polypeptide protein tag), Strep-tag (synthetic peptide sequence towards *Strep*-Tactin), mitoTR2 (gene of interest: *mitochondrial Txnrd*), EMC IRES (internal ribosome entry site), PuroR (puromycin *N-acetyltransferase* gene), globin pA (globin poly A signal), SV40 ori pA (simian virus 40 origin of replication), 3xstopp (three stop codons in all three open reading frames). *EcoRI* and *PmlI* depict unique restriction sites used for cloning.

2.2.5. Gene transfer methods

2.2.5.1. Generation of lentiviral vectors and transduction of target cells

Lentiviruses are able to deliver a significant amount of genetic information into the DNA of the host cell and have the ability to replicate in non-dividing cells. Thus they are one of the most efficient systems of gene delivery. In the present work the HIV-based 3rd generation ecotropic lentiviral vector system was used to transduce murine fibroblasts. To avoid any recombinant events, all necessary proteins for the lentivirus production including Env, Gag, Pol, Rev are encoded by three different plasmids. In this system the natural promoter is replaced by promoters from other viruses (e.g. Rous sarcoma virus) to ensure maximum biosafety. Further the 5' and 3'-LTRs are truncated, all accessory genes are removed and the virus is pseudotyped with glycoproteins from other viruses.

For the virus production HEK 293-T cells were used as packaging cell line. Cells were grown in 10 cm culture plates to 70% confluence and transfected simultaneously with four plasmids via the calcium phosphate method. For each 10 cm plate a transfection plasmid mix was added consisting of:

2 µg pEcoEnv-IRES-puro

5 µg pMDLg_pRRE

10 µg pRSV_Rev

5 µg transfer vector (gene of interest).

The transfection plasmid mix was mixed up with 50 µl of 2.5 M calcium chloride in water to a final volume of 500 µl. While air was bubbled through this mixture, 500 µl of 2x HEPES-buffered saline was added, agitated for several minutes and then kept for 20 min at room temperature. 20 ml of transfection medium were added to the cell monolayer and 1 ml of the above prepared transfection mixture was dispensed drop by drop in each culture plate. Cells were incubated for 8 to 12 h and then the medium was replaced by fresh transfection medium without chloroquine. The cells were incubated for further 36 h at 37°C in a humidified incubator. Supernatants containing virus particles were collected, filtered through a 0.22 µm sterile filter and concentrated by ultracentrifugation at 8000xg at 4°C for nearly 16 h. The supernatant was discarded and virus particles were resuspended in 200 µl of cell culture medium. Aliquots were stored at -80°C until use.

For transduction of mammalian cells the virus containing solution was thawed on ice shortly before use. The day before, cells were seeded on 6-well culture plates and grown to 60% confluence. The medium was replaced by fresh culture medium and 10-20 µl of virus containing solution was added to each well. Incubation time varied between 24 to 48 h, subsequently the medium was replaced by fresh culture medium.

The transduction efficiency was analysed by flow cytometry after 72 h by monitoring VENUS expression in the case of the two lentiviral vectors 441 L1 Ha-rasV12 IRES golgi VENUS and 443 L1 c-myc IRES mito VENUS.

Stable cell lines displaying a *Txnrd2*-mutation (U524Stop) were generated by transducing the cells with 442-L1-N'TAPe-mito-mTxnrd2-Stop(U524Stop)-IRES-puro and 442-L1-N'TAPe-IRES-puro for control, both carrying the puromycin resistance gene. After incubation with virus particles the cells were selected with puromycin, starting from 0.5 µg/ml to a final concentration of 1 µg/ml.

<i>2x HEPES-buffered saline</i>		<i>Transfection medium</i>	
50 mM	HEPES	1x	DMEM (high glucose)
280 mM	NaCl	10%	FCS
1.5 mM	Na ₂ HPO ₄	1%	L-Glutamine
pH 7.05		1%	Penicillin-Streptomycin
		2%	HEPES
		25 µM	Chloroquine

2.2.5.2. Electroporation

Due to an externally applied electrical field the electrical conductivity and permeability of the cell plasma membrane significantly increases. The so called electroporation method is widely used as a way of introducing substances into a cell (e.g. molecular probes, drugs or pieces of coding DNA). Therefore cells were plated on 10 cm culture plates and grown to 80% confluence. Cells were harvested via trypsin/EDTA and washed with PBS(-). Approximately three to five x10⁶ cells in 500 µl PBS(-) were used and mixed with 20 to 30 µg plasmid. Electroporation was performed in 0.4 cm cuvettes using the GenePulser II apparatus (BioRad) with standard settings of 240 V and 950 µF capacitance. The transfected cells were plated on a 10 cm culture plate containing standard medium with 10% FCS and cultured over night. Not later than 24 h after electroporation selection with appropriate antibiotic should be initiated at low concentration.

Stable transfected cells were achieved using the plasmids 141pCAG-3SIP-mock-puro and 141pCAG-3SIP-N'TAPe-mito-mTxnrd2-puro. 24 h after electroporation selection with 0.5 µg/ml puromycin was initiated and over a period of 2 weeks increased to a final concentration of 2 µg/ml puromycin.

2.2.6. Protein biochemistry

2.2.6.1. Preparation of protein lysates

Cells were harvested, lysed in an appropriate volume of protein lysis buffer and incubated for 10 min on ice. The lysed cells were minced and dissolved using an insulin syringe. By centrifugation at 10,000xg at 4°C for 20 min cell debris were separated from the soluble proteins. The protein lysates were stored at -20°C or directly used for protein quantification and further investigations. For analysis of protein expression in tumour samples or mouse organs, frozen or fresh tissue was covered with an appropriate amount of protein lysis buffer (50 mg tissue in 1 ml protein lysis buffer). After incubation of 10 min on ice the tissue was minced and homogenised using the Ultra-Turrax® X120 CAT (Bochem Instrumente GmbH). Non-soluble fragments were removed by centrifugation at 2500xg and 4°C for 10 min. Subsequent the supernatant was again centrifuged at 10,000xg and 4°C for 20 min and the collected supernatant was stored at -20°C or directly used for further analysis.

Protein lysis buffer

20 mM	Tris
137 mM	NaCl
2 mM	EDTA
10%	Glycerol
0.1%	Sodium deoxycholate (freshly added)
pH 7.4	

Protease-inhibitors were added shortly before use (Protease-Inhibitor-Cocktail, Roche) according to the instruction manual. For investigation of protein phosphorylation the phosphatase inhibitors sodium fluoride (0.5 mM) and Na₃VO₄ (0.5 mM) were freshly added to the lysis buffer.

2.2.6.2. Protein quantification

Quantification of protein amount was performed using the bicinchoninic assay BCATM Protein Assay Reagent A/B (Perbio, Fisher-Scientific) according to the instruction manual. The calibration curve was established using a 2 mg/ml bovine serum albumin solution. Protein standard and samples in the appropriate dilution were incubated for 30 min at 37°C with BCA reagents (A/B=50/1) in 96 well plates. Protein standard was measured in duplicate and samples in triplicate. Absorbance of the accumulating BCA-complex was estimated at 550 nm in a spectrophotometer (Tecan). Concentration of protein was calculated by linear regression and expressed in µg/µl.

2.2.6.3. Immunoblotting

Proteins were separated using the SDS-Page electrophoresis depending on their molecular weight in an electric field. Equal amounts of protein (15-20 μg) were mixed with 4x loading buffer and exposed to 95°C for 10 min. Samples for the detection of HIF-1 α protein (~120kDa) were incubated at 37°C for 10 min to avoid formation of large protein clusters that could disrupt electrophoretic separation. Depending on the molecular weight of the protein of interest the samples were separated on gels containing different amounts of acrylamid (low kDa - 12%, high kDa - 8%) (Table 2-3). Separation was performed in electrophoresis running buffer at constant voltage (300 V) in a Mighty Small II SE 250/SE 260 mini vertical unit (Amersham).

Table 2-3: Composition of acrylamid stacking and separating gel

Stacking gel	4%	Separating gel	8%	12%
Acrylamide/Bis-Acrylamide 30%/0.8%	13%	Acrylamide/Bis-Acrylamide 30%/0.8%	26%	40%
Tris pH 6.8	125 mM	Tris pH 8.8	375 mM	375 mM
SDS	0.1%	SDS	0.1%	0.1%
APS	0.05%	APS	0.05%	0.05%
TEMED	0.1%	TEMED	0.1%	0.1%

After electrophoretic separation proteins were transferred to a nitrocellulose membrane (Amersham). Semi-dry blotting was performed in transfer buffer using a self-made blotting unit at constant voltage (300 V) and ~0.8 mA per 1 cm² of membrane for 1 h. Efficiency of the transfer was observed by short incubation of the membrane in 2% PonceauS solution. Unspecific protein bonds were blocked with 5% skim milk in 1x washing buffer for 2 h at room temperature with constant shaking. Primary antibodies were dissolved in 5% skim milk or BSA in 1x washing buffer and hybridisation was performed over night at 4°C with constant shaking (Table 2-4). After 3 times washing in 1x washing buffer, the membrane was incubated with an HRP-conjugated secondary antibody in 3% skim milk for at least 1 h at room temperature (Table 2-5). Visualisation was achieved by incubation with ECL reagent (Amersham) or SuperSignal® West Femto Maximum Sensitivity Substrate (Thermo Scientific) and the Digital CCD Camera from Hamamatsu Photonics. Analysis was performed using a Wasabi imaging software (Hamamatsu Photonics). For re-probing, the membranes were incubated for 10 min in stripping buffer. Prior to incubation with a new primary antibody the membrane was blocked with 5% skim milk or BSA in 1x washing buffer for 60 min.

<i>4x loading buffer</i>		<i>Electrophoresis running buffer</i>		<i>Transfer buffer</i>
250 mM	Tris (pH 6.8)	124 mM	Tris	39 mM Glycin
8%	SDS	960 mM	Glycin	48 mM Tris
40%	Glycin	0.5%	SDS	0.037% SDS
400 mM	β -Mercaptoethanol			10% Methanol
0.02%	Bromophenol blue			

<i>2% PonceauS</i>		<i>1x washing buffer (TBS-T)</i>		<i>Stripping buffer</i>
2%	PonceauS	50 mM	Tris	0.4 M NaOH
30%	TCA	150 mM	NaCl	in dh_2O
		0.1%	Tween20	

Table 2-4: Primary antibodies for immunoblotting

Antigen	Isotype	MW (kDa)	Dilution	Order Number
β -Actin	rabbit polyclonal, IgG	42	1:1000	A 2066
Akt	rabbit polyclonal, IgG	60	1:1000	#9272
c-Myc	rabbit polyclonal, IgG	67	1:200	sc-764
FLAG	mouse-monoclonal, IgG ₁	10	1:2000	F3165
GAPDH	mouse monoclonal, IgG ₁	36	1:1000	MAB374
Glutathione reductase	rabbit polyclonal, IgG	65	1:500	sc-32886
Hif-1 α	rabbit polyclonal, IgG	115	1:500	NB100-479
PHD2	rabbit polyclonal, IgG	43	1:500	NB100-2219
Prx 3	rabbit polyclonal, IgG	20-30	1:1000	LF-PA0030
Phospho-Akt (Ser473)	rabbit polyclonal, IgG	60	1:1000	#9271
Ras	rabbit polyclonal, IgG	21	1:1000	#3965
Trx2	rabbit polyclonal, IgG	12	1:2000	AF3254
β -Tubulin	mouse monoclonal, IgG ₁	55	1:1000	T4026
Txnrd1	rabbit polyclonal, IgG	56	1:1000	-
Txnrd2 (#1C4)	rat monoclonal	56	undiluted	-
Txnrd2	rabbit polyclonal	56	1:1000	-
VEGF-A	rabbit polyclonal, IgG	45	1:500	PA1080

Table 2-5: Secondary antibodies for immunoblotting

Antigen	Dilution	Order Number
Goat anti-mouse IgG HRP conjugate	1:5000	401253
Goat anti-rabbit IgG HRP conjugate	1:5000	401353
Goat anti-rat IgG HRP conjugate	1:5000	112-035-062
Rabbit anti-goat IgG HRP conjugate	1:5000	401515

2.2.6.4. Immunohistochemistry

HEMATOXYLIN-EOSIN HISTOLOGY

To study tumour morphology tissue was fixed in 4% paraformaldehyde in PBS(-) over night at 4°C and embedded in paraffin. Five-micrometer sections were treated with Mayer's hematoxylin and 2% eosin to stain cell nuclei and cytoplasm, kindly performed by the group of Dr. Irene Esposito (Institute of Pathology, Helmholtz Zentrum, München).

IMMUNOSTAINING OF CRYO- AND PARAFFIN-SECTIONS FROM TUMOUR TISSUE

For cryo-sections tissues were frozen in OCT embedding medium (Sakura) and stored at -20°C. Ten-micrometer frozen sections were prepared using a cryotome (HM 560, Microm), mounted on poly-L-lysine-coated glass slides Superfrost® Plus (Thermo Scientific) and fixed in acetone at -20°C for 10 min. Paraffin-sections were prepared as mentioned above (see chapter 2.2.6.4. first subitem). Before staining sections were deparaffinised with xylene and rehydrated through graded alcohol into distilled water. Antigen retrieval was achieved by microwave pre-treatment in sodium citrate buffer (10 mM). For both, cryo- and paraffin-sections, endogenous peroxidase activity was quenched by incubating the sections in methanol containing 1% H₂O₂. Non-specific binding sites were blocked by incubation in PBS(-) containing 5% BSA for 1 h at room temperature. Hybridisation with primary antibody was performed at 4°C over night with 5% BSA in PBS(-) in a humidified chamber. Omission of the primary antibody served as a control. After three times washing with PBS(-) sections were incubated with the peroxidase-conjugated secondary antibody in 5% BSA with PBS(-) for 1 h at room temperature. Immunoperoxidase staining was performed using the Vector ABC Kit and Vector DAB or AEC Kit (Vector Laboratories Inc). Immunostaining was analysed using the Olympus BX41 microscope in combination with the digital camera CAMEDIA C-5050 and the software Olympus DP-Soft v3.2 (Olympus, Tokio, Japan). Analysis of proliferation using Ki67 (Dianova, diluted 1:200) as marker and quantification of apoptotic-necrotic areas by means of cleaved-caspase 3 (Cell Signaling, diluted 1:200) staining were kindly performed and analysed by the group of Dr. Irene Esposito (Institute of Pathology, Helmholtz Zentrum, München). Quantification of tumour vascularisation was achieved by PECAM-1/CD31 (Acris, diluted 1:150) staining. Three representative sections were analysed per animal and five random micrographs were taken from each region of interest from all three sections. Total blood vessels were determined by counting the number of blood

vessels in fifteen random microscopic visual fields using a 20x objective. All analyses were done in a blinded fashion by two researchers.

2.2.6.5. Enzyme-linked immunosorbant assay

To measure mouse VEGF in cell culture supernatants and tissue homogenates, the Quantikine Mouse VEGF Immunoassay (R&D) was used following the instruction manual. In brief, a 96-well microplate was pre-coated with a polyclonal antibody specific for mouse VEGF. For calibration a recombinant mouse VEGF (500 pg/ml) solution was used. To analyse cell culture supernatants, cells were seeded in 24-well culture plates and cultured in 500 µl of standard DMEM or exposed to starvation until 80% confluence. Supernatants were collected and stored at -20°C until analysis was performed. To prepare tissue homogenates, tumours were washed once in ice-cold PBS(-) and homogenised in an appropriate amount of protein lysis buffer containing protease inhibitor (Roche) using the Ultra-Turrax® X 120 CAT (Bochem). The homogenates were centrifuged at 5,000xg for 10 min, non-soluble material was discarded and supernatants were centrifuged again at 10,000xg and 4°C for 20 min. Samples were stored at -20°C until further use. Standards and assay controls were loaded in duplicate, samples with equal amount of protein in triplicate to the pre-coated 96-well microplate. Mouse VEGF binds to the immobilised antibody and any unbound substances are removed by washing steps. Afterwards an enzyme-linked polyclonal antibody specific for mouse VEGF was added to each well. Following incubation, unbound antibody-enzyme reagent is removed by washing and a substrate solution is added. The enzymatic reaction yields a blue product that turns yellow after adding the stop solution. Absorbance of the yellow substrate was measured at 450 nm in a spectrophotometer (Tecan). The intensity of the colour is in proportion to the amount of mouse VEGF bound in the initial step. Sample values were read of the standard curve and expressed in pg/mg protein.

2.2.7. Biochemical assays

2.2.7.1. Estimation of glutathione reductase activity in cells

The activity of the glutathione reductase (GR) in cells was analysed by measuring the decrease of absorbance at 340 nm due to oxidation of NADPH to NADP⁺, co-factor of the reduction of oxidised glutathione (GSSG) (Figure 2-5).

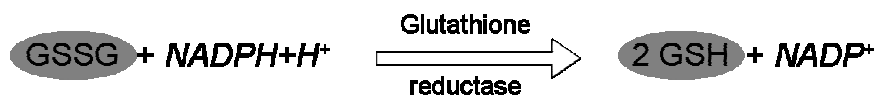


Figure 2-5: Reduction of glutathione

Together with its co-factor NADPH/H⁺, glutathione reductase (GR) catalyses the reduction of oxidised glutathione (GSSG) to the reduced form of glutathione (GSH).

Cells were plated on 10 cm dishes and cultured in standard DMEM to 80% confluence. Cells were harvested and resolved in 10x of volume in cell extraction buffer and incubated on ice for 30 min. After centrifugation the supernatant was stored at -20°C or directly analysed for protein amount and GR activity. GR activity was measured using 25 µg protein of samples and glutathione reductase from yeast, containing 0.3-0.6 U/ml (Sigma), was used for calibration. Standard, positive control (lysate of mouse liver) and samples were estimated in triplicate using a UV-perivious 96-well plate. After intense shaking, decrease of absorbance was monitored over 10 min and reading was taken every 2 min at 340 nm in a Tecan spectrophotometer with UV filter. The change in absorbance/min from the standard was used to calculate the GR activity in the samples and expressed as U/mg protein.

<i>Cell extraction buffer</i>		<i>Solution A</i>	
200 mM	<i>potassium phosphate buffer</i>	200 mM	<i>potassium phosphate</i>
100 µM	<i>PMSF</i>	10 mM	<i>EDTA</i>
20%	<i>Triton X-100</i>	pH 7.2	
<i>Solution B</i>		<i>Solution C</i>	
30 mM	<i>GSSG</i>	0.8 mM	<i>NADPH</i>
<i>in water</i>		<i>in solution A</i>	
<i>Solution D</i>			
1%		<i>BSA</i>	
		<i>in solution A</i>	

2.2.7.2. Determination of total glutathione in cells

Total glutathione content (GSH + GSSG) in cells was determined by performing a modified assay based on a method first described by Tietze (Figure 2-6) ³⁰⁹.

Therefore cells were plated on 10 cm culture dishes and harvested at 80% confluence. For further analysis 1x10⁶ cells were used. After washing with PBS(-) cells were resolved in 5% TCA, incubated on ice for 30 min and pelleted by centrifugation at 10,000xg and 4°C for 10 min. The cell pellet was resuspended in 0.5 M NaOH and samples were analysed for protein amount and after that stored at -20°C. By performing an ether extraction (0.01 M HCl-ether), interfering proteins as well as metabolising enzymes were removed from the samples and glutathione was released from the cells. The aqueous phase was collected and incubated at 37°C for 15 min to remove all ether residues. A 30 mM GSSG solution (Sigma) was used for calibration. All reagents were prepared freshly and 50 µl of sample, blank or

standard were loaded to a 96-well plate in triplicate. Solution A was added and absorbance was estimated at 405 nm in a Tecan spectrophotometer. Finally, solution B was added and absorbance was measured after 30 s, 2 min and 5 min. Concentration of total glutathione in samples was calculated using the standard absorbance values and expressed in $\mu\text{M}/\text{mg}$ protein.

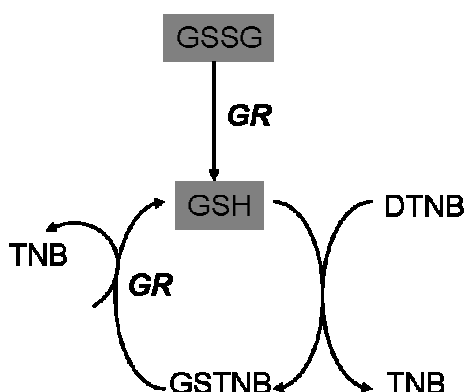


Figure 2-6: GSH recycling mechanism by Tietze ³⁰⁹

The general thiol reagent DTNB reacts with GSH to form the 412 nm chromophore TNB and GSTNB. The GSTNB is subsequently reduced by GR and NADPH, releasing a second TNB molecule and recycling the GSH; thus amplifying the response. Any oxidised glutathione (GSSG) initially present in the reaction mixture or formed from the mixed disulfide reaction of GSH with GSTNB is rapidly reduced to GSH.

<i>Solution A</i>		<i>Solution B</i>	
177 mM	potassium-phosphate buffer	1.3 U/ml	glutathione reductase
0.74 mM	DTNB	in water	
0.15 mM	NADPH		

2.2.7.3. Measurement of GSH concentration in tumour samples by HPLC

The isocratic high-performance liquid chromatography (HPLC) was used for the measurement of total glutathione (GSH+GSSG), reduced (GSH) and oxidised (GSSG) glutathione based on the estimation of total homocysteine with some modifications ⁹⁰. In brief, the measurement is based on the derivatisation of thiol groups with a thiol-specific fluorogenic marker (7-fluoro-benzo-2-oxa-1,3-diazole-4-sulphonate), which can be separated isocratically by reverse-phase HPLC using a Superspher 100 RP-18 column as stationary phase. Tumours were collected following six or 10 days of tumour growth and snap-frozen. Sample preparation and processing as well as HPLC measurement was kindly performed by Dipl.Ing. Pirkko Koelle (Group PD. Dr. Peter Kuhlencordt, Medizinische Poliklinik, Klinikum der Universität München)

2.2.7.4. Quantification of lactate in cell culture and tumour tissue

Lactate is a major intermediate of anaerobic metabolism and plays important roles in many biological processes. Abnormal changes in concentration of lactate have been related to several diseases (diabetes, lactic acidosis, tumours). To estimate lactate in cell culture supernatants and tumour tissue the Lactate Assay Kit II (BioCat) was performed according to the instruction manual. In brief, lactate is oxidised by lactate dehydrogenase to generate a product which interacts with a probe to produce a colour ($\lambda_{\max}=450$ nm). The kit detects L(+)-lactate. Supernatants were collected from cells cultured over night in 24-well plates with standard-DMEM exposed to stimuli or left untreated and stored at -20°C until the assay was performed. For quantitative evaluation, the amount of protein in each well was determined using the bicinchoninic acid assay (see chapter 2.2.6.2.). Tumour tissue was dissected and homogenised using the Ultra-Turrax® X 120 CAT (Bochem) in an appropriate amount of lactate assay buffer (BioCat). After centrifugation at $10,000\times g$ and 4°C for 20 min the clear homogenate was collected and stored at -20°C until protein quantification or the lactate assay was performed. Supernatants and tissue samples were prepared in an appropriate dilution and analysed in triplicates. For calibration a 1 mM lactate solution (BioCat) was used. Absorbance of standard and samples was measured in a spectrophotometer (Tecan) at 450 nm. Sample readings were applied to the calibration curve and results were expressed in nmol/mg protein.

2.2.7.5. Measurement of ATP in cells and tumour tissue

Adenosine 5'triphosphate (ATP) transports chemical energy within cells for metabolism and is a key indicator for cellular activity. To analyse the amount of ATP in cells and tumour tissue, the EnzyLight™ ATP Assay Kit (BioAssay Systems) was performed. The kit provides rapid bioluminescent determination of ATP (Figure 2-7). ATP was extracted from cells by adding equal volume of ATP-extraction buffer to protein lysates and stored at -80°C until analysis. Extraction of ATP from tumour tissue was performed by homogenising the samples in an appropriate amount of 6% ice-cold perchloric acid. After centrifugation at $10,000\times g$ and 4°C for 10 min, the pH of the supernatant was adjusted to 7 by adding 2 M K_2CO_3 . The samples were stored at -80°C . Before estimation of ATP the amount of protein was quantified. The EnzyLight™ assay was performed according to the manufacturer's instructions. For calibration a 30 mM ATP solution (BioAssay Systems) was used. Standard and samples were measured in duplicate using a Lumat LB 9507 (Berthold technologies GmbH & Co KG). Sample readings were applied to the calibration curve and results were expressed in $\mu\text{M}/\text{mg}$ protein.



Figure 2-7: Bioluminescent determination of ATP

The released ATP reacts with the substrate *D*-luciferin in the presence of luciferase and produces light. The light intensity is a direct measure of intracellular ATP concentration.

ATP-extraction buffer

4 mM	EDTA
0.2%	Triton X-100

2.2.8. Tumour transplantation protocols

Animals were kept under standard conditions with food and water ad libitum (ssniff, Soest, Germany). All animal experiments were performed in compliance with the German Animal Welfare Law and been approved by the institutional committee on animal experimentation and the government of Upper Bavaria.

2.2.8.1. Subcutaneous xenograft model

Cells were harvested from 80% confluent 10 cm culture dishes. Mice were anesthetised by a spontaneous inhalation of isoflurane (Forene®, Abbott GmbH & Co KG). The inhalation gas contained a mixture of 30-40% oxygen, 60-70% nitrogen, $2.2 \pm 0.2\%$ isoflurane and was administered continuously through a breathing mask. 4×10^6 single cell-derived transformed cells in a final volume of 200 μl were injected subcutaneously into the flank of C57BL/6 mice. Tumours were allowed to develop and grow for a maximum period of 11 days. At days two, three, four, six, seven, eight, 10 and 11 mice were sacrificed and the tumours were collected. Tumour volume was determined using a sliding calliper and the tumour mass was weighted. Tumour tissue was snap-frozen in liquid nitrogen and stored at -80°C in several aliquots for isolation of DNA, RNA or protein. For immunohistochemistry tumour tissue was fixed with 4% paraformaldehyde and embedded in paraffin or snap frozen in liquid nitrogen, embedded in OCT embedding medium (Sakura) and stored at -20°C .

2.2.8.2. Treatment of Txnrd2-deficient tumour-bearing mice with BSO

Txnrd2-deficient single-cell derived transformed cells (4×10^6) in a final volume of 200 μl were injected subcutaneously into the flank of C57BL/6 mice. Tumours were allowed to grow for three days before the therapy started. BSO (20 mM) was provided in the drinking water for seven days. As a control a second group of Txnrd2-deficient tumour-bearing mice were

provided with drinking water containing no BSO. The drinking water was refreshed every 3rd day. The animals were sacrificed and tumour mass was weighed and volume was determined using a sliding calliper. For immunohistochemistry tumour tissue was snap frozen in liquid nitrogen, embedded in OCT embedding medium (Sakura) and stored at -20°C.

2.2.8.3. Dorsal skinfold chamber

The dorsal skinfold chamber is a well established *in vivo* model to study early processes of angiogenesis in tumours and to investigate functional parameters of tumour vascular network (Figure 2-8). Experiments were performed using C57BL/6 mice. The dorsal skinfold chamber was implanted under anesthesia (75 mg ketamine hydrochloride/25 mg xylazine per kg body weight) as already described ¹⁸². Before tumour cells were inoculated into the skinfold chamber animals were allowed to recover from the surgery for two or three days. Vessel formation and functionality was observed at days three, five and 11 following tumour cell inoculation. Therefore animals were placed in a polycarbonate tube and were injected intravenously with Fluorescein isothiocyanate (FITC)-dextran solution. Tumour vascularisation was observed by using 2.5x, 10x and 20x objectives (LD acroplan). Epi-illumination was achieved using a 100 W mercury lamp with a fluorescence filter for FITC (excitation: 450-490 nm, emission: 515-525 nm). Images of microvessels were acquired using a CCD camera (AVD D7). Representative images and movies were taken from the tumour edge and centre. These experiments were kindly performed and analysed by Siiri Lüdemann (Surgical Clinic and Policlinic, LMU, München).



Figure 2-8: Dorsal skinfold chamber implanted on a nude mouse ²⁸

FITC-labeled dextran solution
5% Fluorescein isothiocyanate-dextran
in 0.9% NaCl

2.3. Statistics

All experiments were performed at least three times. Results are expressed as mean values \pm SD. One-way statistical analysis was performed with SigmaStat© 2.0 for Windows (Jandel GmbH, Erkrath, Germany). Statistical comparisons of two samples were made by Student's t-test. For non-normal data the Rank sum test was used. The corresponding tests are indicated in the figure legends. *P* values <0.05 were considered as statistically significant.

3. RESULTS

3.1. Long-term effects of Txnrd2-deletion in murine fibroblasts

Previous work in our laboratory demonstrated that deletion of Txnrd2 in freshly isolated murine fibroblasts restricts in vitro proliferation, disturbs redox balance and impacts on mitochondrial redox-regulating enzymes^{61, 245}. Hence, the first part of the present study aimed to investigate the long-term effects of Txnrd2 deletion on cellular function and metabolism.

3.1.1. Characterisation of immortalised fibroblasts lacking Txnrd2

Embryonic fibroblasts were isolated from pregnant mice at E12.5 and immortalised by serial passages. Cells with a passage number less than 10 were considered as 'primary' cells and cells with a passage number above 10 were considered as 'immortalised'. The deletion of Txnrd2 was verified by semi-quantitative PCR, real-time PCR as well as immunoblotting (Figure 3-1 A - C). To analyse the proliferation rate of primary *versus* immortalised Txnrd2-deficient fibroblasts, equal numbers of cells were plated on 6-well culture plates and proliferation was monitored over at least 96 h. Surprisingly, immortalised fibroblasts lacking Txnrd2 showed an increased proliferation rate compared to their wild-type counterparts. This effect was at variance to the previous observations using primary fibroblasts⁶¹ (Figure 3-2 A). Primary Txnrd2-deficient fibroblasts showed reduced proliferation which could be rescued by antioxidants (GSH, NAC, α -Tocopherol, NaSe)^{61, 245}. The cells revealed increased levels of intracellular ROS and were highly susceptible to oxidising agents (H_2O_2 , PEITC, antimycin A) and genotoxic agents²⁴⁵. Expression of mitochondrial specific H_2O_2 -scavenging enzymes, Prx3 and Prx5, was increased and cells were highly sensitive to inhibition of the intracellular de novo synthesis of GSH²⁴⁵. This sensitivity to GSH-depletion was also observed in immortalised Txnrd2-knockout fibroblasts (Figure 3-2 B). Therefore, we were interested in the redox status of immortalised Txnrd2-deficient cells and their sensitivity to oxidising agents.

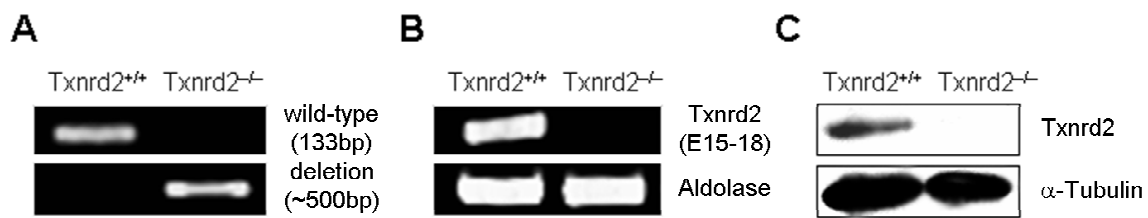


Figure 3-1: Analysis of *Txnrd2* expression in immortalised murine fibroblasts

Expression of *Txnrd2* was analysed on the (A) genomic level or (B) on the mRNA level using adequate primers spanning the exons 15 to 18 coding for Sec and SECIS. Equal loading was confirmed by *aldolase* expression. (C) *Txnrd2*-deletion was additionally confirmed by immunoblotting. The expected signal at a molecular weight of 55 kDa was only detectable in *Txnrd2*^{+/+} fibroblasts. Equal loading was confirmed by analysis of α -Tubulin expression.

3.1.2. GSH-depletion is associated with increased ROS levels in *Txnrd2*-deficient cells

To investigate, whether immortalised *Txnrd2*-deficient cells accumulate more intracellular ROS, cells were cultured overnight in the presence or absence of L-buthionine sulphoximine (BSO). BSO is an irreversible inhibitor of γ -glutamylcysteine synthetase (γ -GCS), the enzyme catalysing the first and rate-limiting step in the de novo synthesis of GSH. Cells were stained with DCFH-DA (a marker used for ROS detection) and afterwards analysed by flow cytometry. Surprisingly, and in contrast to primary fibroblasts, immortalised *Txnrd2*-deficient fibroblasts showed even slightly reduced ROS levels compared to wild-type cells under baseline conditions. However, treatment with 10 μ M BSO for 16 h revealed a much stronger increase of soluble ROS in fibroblasts lacking *Txnrd2* (Figure 3-2 C).

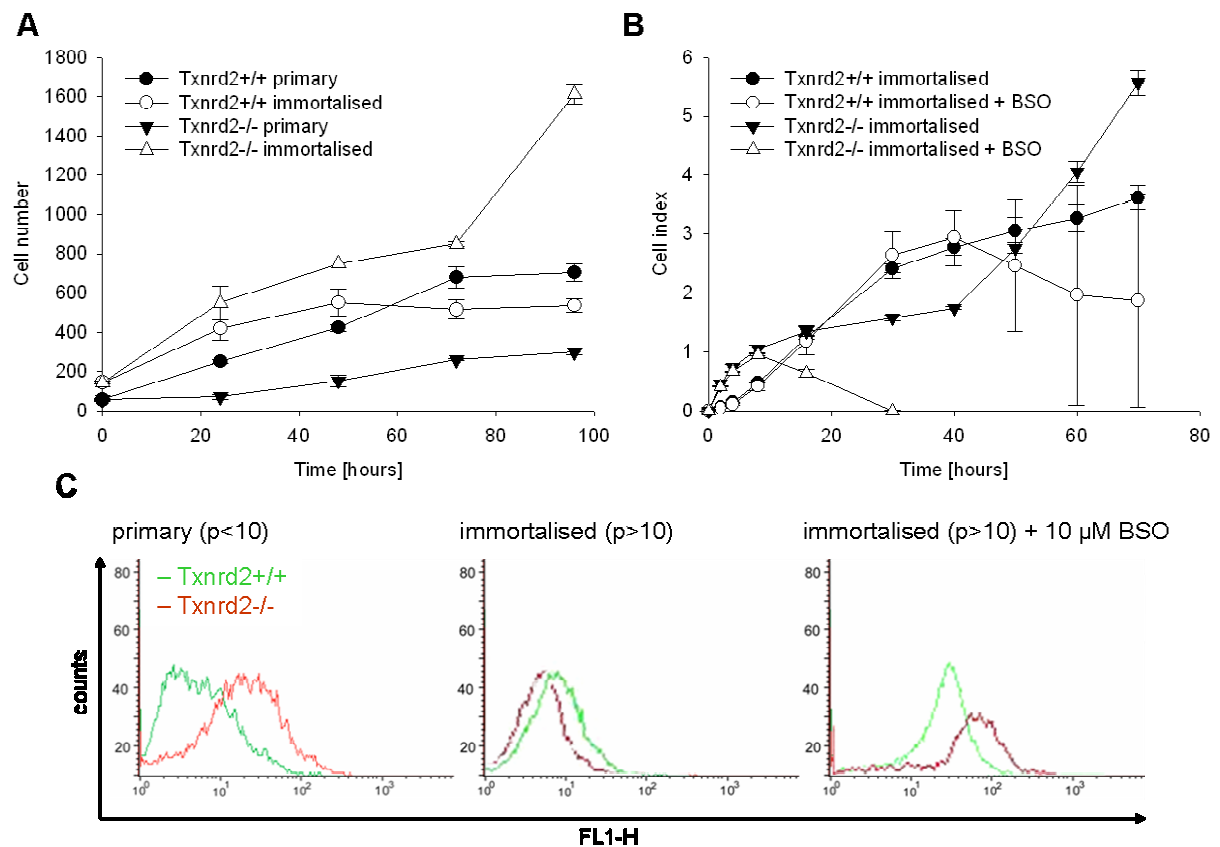


Figure 3-2: Proliferation and intracellular ROS level of Txnrd2-deficient fibroblasts

(A) Primary *Txnrd2*^{-/-} fibroblasts show decreased proliferation rates compared to *Txnrd2*^{+/+} cells. Analysis of immortalised fibroblasts yielded a different picture. *Txnrd2*^{-/-} fibroblasts showed increased proliferation under baseline cell culture conditions. Depicted is one representative experiment out of four. (B) Yet immortalised *Txnrd2*-deficient fibroblasts were still more sensitive towards GSH-depletion induced by BSO (10 μM) than wild-type cells. The line chart depicts one of three independent experiments. Depicted are mean values ± SD. The number of cells is expressed as cell index (explanation see chapter 2.2.1.6.). (C) Primary and immortalised *Txnrd2*^{+/+} and *Txnrd2*^{-/-} fibroblasts were stained with DCFH-DA. Primary (left panel) and immortalised (middle panel) *Txnrd2*^{+/+} and *Txnrd2*^{-/-} cells were analysed under baseline cell culture conditions. Soluble ROS were further measured in immortalised fibroblasts following BSO treatment (10 μM) (right panel). Green curves: *Txnrd2*^{+/+}, red curves: *Txnrd2*^{-/-}. Representative graphs of three independent experiments are shown.

3.1.3. Cells respond to Txnrd2 deletion by upregulating other redox enzymes

Under baseline cell culture conditions primary *Txnrd2*-deficient fibroblasts showed elevated ROS levels, whereas immortalised *Txnrd2*-deficient fibroblasts had ROS levels which were under baseline culture conditions comparable to those of wild-type cells (Figure 3-2 C, left and middle panel). Thus, the question raised whether compensatory upregulation of other redox-related enzymes may occur in the response to *Txnrd2*-deletion. Along the same line, treatment with BSO revealed a strong susceptibility of *Txnrd2* knockout cells to GSH deprivation, indicating that one or several GSH metabolising enzymes may rescue *Txnrd2*-deficiency (Figure 3-2 C, right panel). Therefore, the activity and expression of the GSH

recycling enzyme, glutathione reductase (GR), was investigated. Indeed, immortalised *Txnrd2*-deficient fibroblasts showed increased GR activity compared to wild-type cells under baseline cell culture conditions (Figure 3-3 A). In cells lacking *Txnrd2*, GR activity was indeed 3-fold higher (14.9 ± 3.9 mU/mg protein) compared to the wild-type counterparts (5.2 ± 1.2 mU/mg protein) (Figure 3-3 B), which was paralleled by an increased GR protein expression (Figure 3-3 D). On the other hand, the amount of total glutathione was comparable in wild-type and *Txnrd2*-knockout cells (216 ± 132 μ M/mg protein in *Txnrd2*^{+/+} cells vs. 204 ± 138 μ M/mg protein in *Txnrd2*^{-/-} cells) (Figure 3-3 C). Interestingly, the expression level of *Txnrd1* was elevated in *Txnrd2*-deficient fibroblasts (Figure 3-3 E). The expression of the mitochondria-specific H₂O₂-scavenging enzymes *Prx3* and *Prx5* were comparable in immortalised wild-type and *Txnrd2*-null cells at mRNA and protein level under baseline culture conditions as well as following starvation (Figure 3-3 F - G). These data were in contrast to previous observations in our laboratory using primary fibroblasts. Expression of *Prx3* and *Prx5* mRNA were found to be increased in primary *Txnrd2*-deficient fibroblasts under baseline culture conditions and protein expression of *Prx3* strongly increased after stimulation with H₂O₂ in primary *Txnrd2*-deficient cells²⁴⁵.

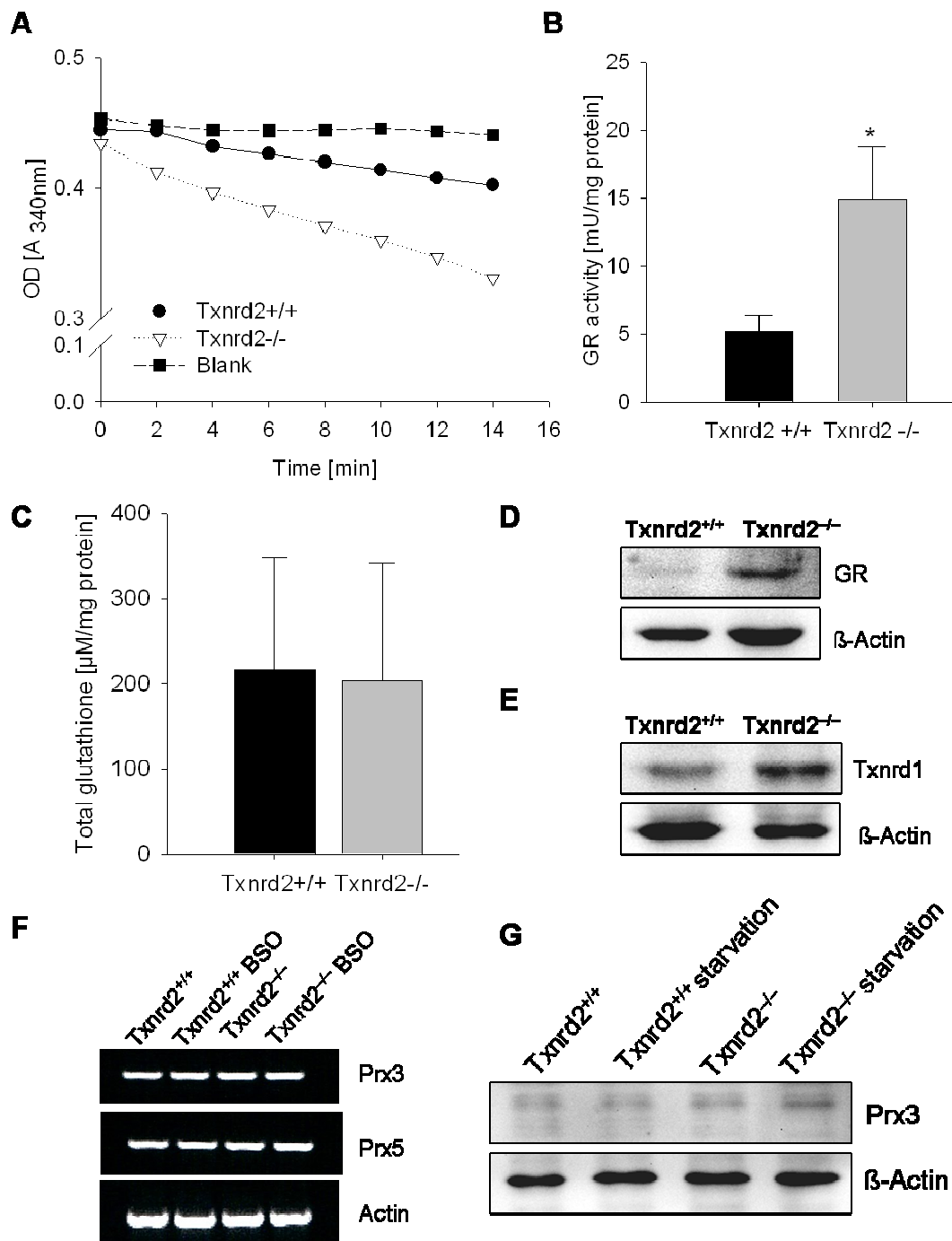


Figure 3-3: Activity and expression of redox-regulating enzymes

(A) The activity of the GR was analysed in supernatants from cell lysates by measuring the decrease of absorbance at 340 nm due to oxidation of NADPH to NADP⁺ at the indicated time points. (B) GR activity is expressed in mU/mg protein and was compared between *Txnrd2*^{+/+} and *Txnrd2*^{-/-} cells. Depicted are the mean values ± SD from seven independent experiments. * p<0.05 (Student's t-test) (C) Total glutathione was measured after TCA-extraction from cells and is expressed in μmol/mg protein. The graph shows the mean values ± SD from three independent measurements. Expression of GR (D) and Txnrd1 (E) was analysed by immunoblotting. One representative blot from three independent experiments is depicted. For equal loading expression of β-actin was analysed. (F) mRNA expression of *Prx3* and *Prx5* in immortalised fibroblasts was analysed using semi-quantitative PCR under baseline culture conditions and following treatment with 10 μM BSO. *Actin* served as control. (G) Expression level of *Prx3* under baseline culture conditions and after starvation was verified in immortalised fibroblasts using immunoblotting. β-actin served as loading control. One representative blot of three independent experiments is depicted.

3.1.4. Structure and functionality of mitochondria in *Txnrd2*-deficient cells

Mitochondrial metabolism is essential for energy production in form of ATP in cells and tissues. The Trx2/*Txnrd2*/Prx3-system is considered to play a pivotal role in scavenging mitochondrial ROS, thereby contributing to proper mitochondrial function. To investigate the impact of the *Txnrd2*-deletion on mitochondria, morphological and functional analyses were performed. Structural and intracellular organisation of mitochondria were analysed using the organelle-specific probe Mitotracker Green®. Mitotracker Green® is considered to specifically accumulate in mitochondria, independent of mitochondrial membrane potential²⁴². Mitochondria of primary wild-type and knockout fibroblasts appeared similar in shape (Figure 3-4, upper panel). Interestingly, immortalised *Txnrd2*-deficient cells showed reduced accumulation of Mitotracker Green® and in contrast to the tubular-shaped mitochondria of wild-type cells they appeared more punctate (Figure 3-4, lower panel).

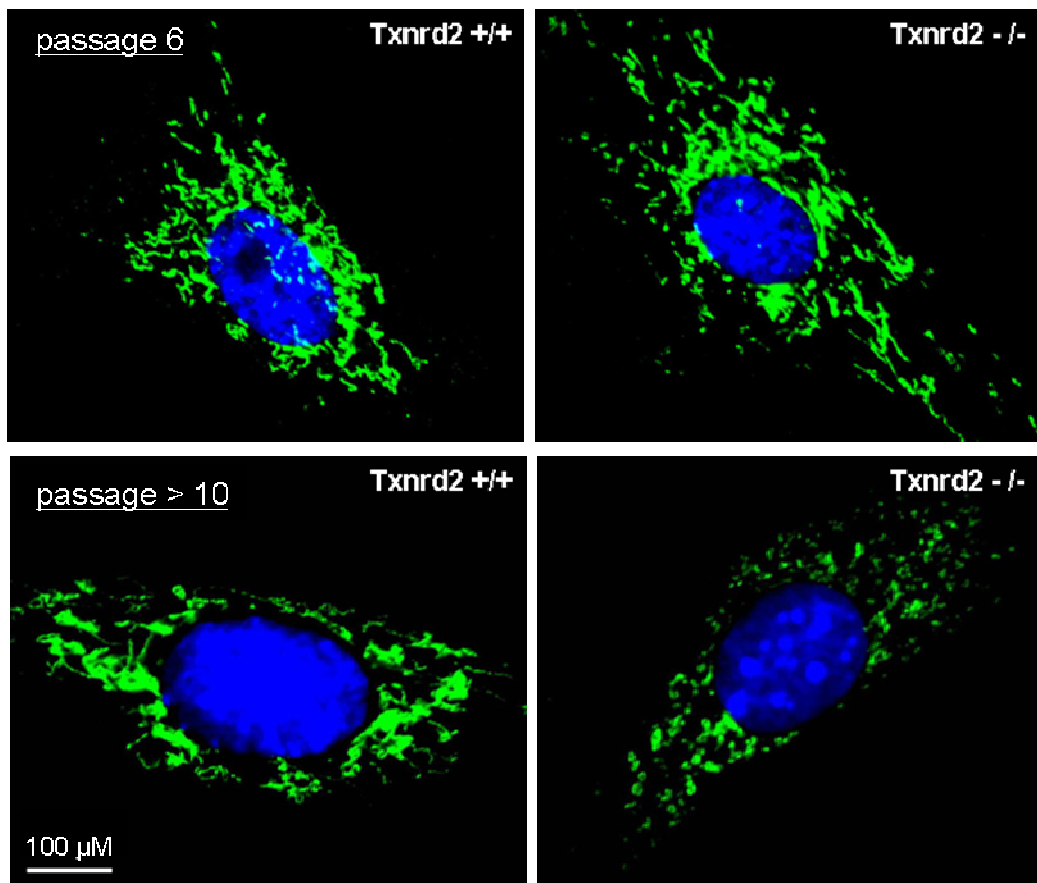


Figure 3-4: Structural analysis of mitochondria in *Txnrd2*-deficient fibroblasts

Intracellular organisation of mitochondria in *Txnrd2*^{+/+} and *Txnrd2*^{-/-} cells was analysed by confocal microscopy using the mitochondrial selective probe Mitotracker Green® (20 nM). The upper panel compares primary fibroblasts (passage number 6) and the lower panel compares immortalised fibroblasts (passage number >10). Depicted are representative images of one cell chosen from three independent stainings.

To quantify numbers of mitochondria in the cells, staining with Mitotracker Green® was performed and analysed using flow cytometry. Wild-type and knockout cells of different passage numbers were analysed for the mean fluorescence intensity (MFI) of Mitotracker Green®, which, in turn, is linear correlated to mitochondrial mass^{142, 172, 242} (Figure 3-5 A). As expected, primary fibroblasts (p4) showed no differences in mitochondrial mass with an MFI of $92\pm 13.4\%$ for Txnrd2-deficient cells compared to 100% of control wild-type cells. However, immortalised Txnrd2-deficient fibroblasts (p>10) revealed significantly reduced MFI with $61.9\pm 14.9\%$ compared to 100% of control (Figure 3-5 B).

Since the validity of mitochondrial mass estimation using Mitotracker Green® is controversially discussed due to its possible dependence on the membrane potential^{155, 209, 242}, a second fluorescent probe was used for quantitative analysis of mitochondrial mass. Nonyl acridine orange (NAO) interacts with non-oxidised cardiolipin which is located in the inner mitochondrial membrane and is incorporated independently of the mitochondrial membrane potential²⁰⁹. Cells were stained for 20 min with 10 nM NAO at 37°C in the dark and analysed by flow cytometry. For normalisation, MFI for NAO was corrected for the endoplasmic reticulum (ER) tracker fluorescence intensity. Primary wild-type and knockout cells showed approximately equal mitochondrial mass with 23.4 ± 10.7 compared to 22.9 ± 8.4 . In contrast to the findings obtained with Mitotracker Green®, immortalised Txnrd2-lacking cells (21.9 ± 3.8) showed no significantly reduced mitochondrial mass compared to wild-type cells (24.8 ± 2.5) (Figure 3-5 C).

Another widely-used method to quantify the amount of mitochondria is the analysis of mitochondrial DNA. We therefore analysed the mRNA expression level of *16S rRNA* using semi-quantitative (Figure 3-5 D) and real-time PCR in immortalised fibroblasts. The expression of the mitochondria-specific mRNA was normalised to the expression of *hexokinase* mRNA (nuclear encoded). Mitochondrial DNA was comparable between wild-type and Txnrd2-deficient immortalised cells (data not shown). These observations were in accordance with the results obtained from the NAO-staining and confirmed that there were no differences in the amount of mitochondria between primary as well as immortalised wild-type and Txnrd2-knockout cells.

However, previous studies were performed in our laboratory using transmission electron microscopy in order to analyse mitochondria in Txnrd2-deficient cardiomyocytes derived from heart-specific Txnrd2-knockout mice. Here, mitochondria revealed severe malformation and swelling with destruction or loss of cristae⁶¹.

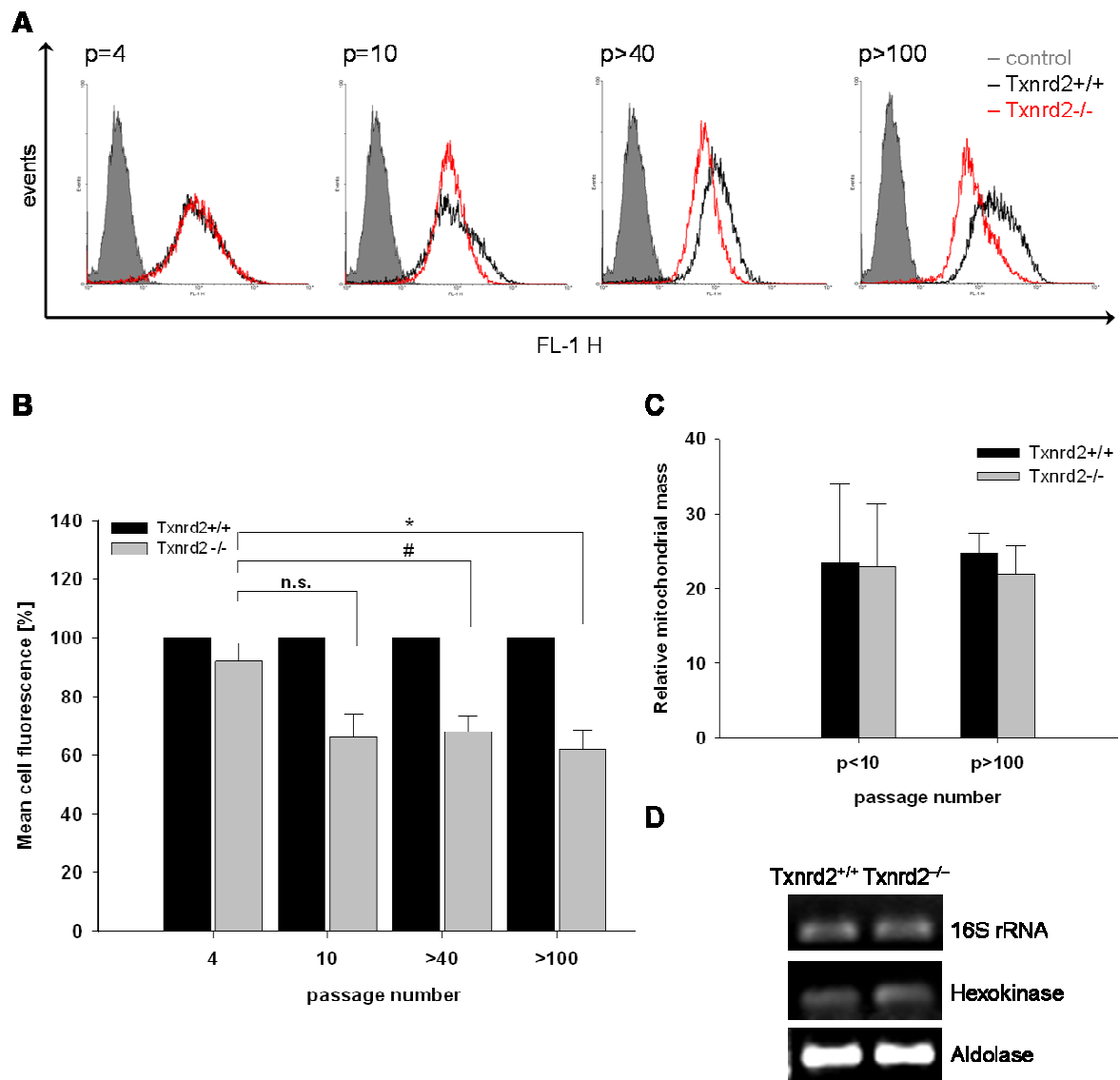


Figure 3-5: Quantitative evaluation of mitochondria in Txnrd2-deficient fibroblasts

(A) Cells were stained with Mitotracker Green® for 25 min. Afterwards mitochondria were analysed using flow cytometry. *Txnrd2*^{+/+} (black curve) and *Txnrd2*^{-/-} (red curve) fibroblasts were compared at different number of passages (4, 10, >40 and >100). Unstained *Txnrd2*^{+/+} and *Txnrd2*^{-/-} cells showed equal auto-fluorescence and served as control (filled grey curve). Histogram of one out of three representative experiments is shown. (B) Quantitative analysis of the mean fluorescence representing mitochondrial mass in *Txnrd2*^{-/-} cells at different passage numbers (4, 10, >40 and >100). Depicted are mean values ± SD. *Txnrd2*^{+/+} cells were considered as 100% for each passage and compared to *Txnrd2*^{-/-} cells. Passage number 4 of *Txnrd2*^{-/-} was compared to passage number 10, >40 and >100 with * p<0.05, # p<0.1 and n.s. = not significant (Student's t-test). (C) Quantitative analysis of the mean fluorescence of NAO representing mitochondrial mass. For normalisation, mean fluorescence intensity of NAO was correlated to those of the ER tracker. Mean values ± SD are expressed as relative mitochondrial mass of three independent experiments. (D) Mitochondrial DNA was quantified using semi-quantitative PCR in immortalised fibroblasts. The expression of the mitochondrial-specific *16S rRNA* was normalised to the expression of the nuclear-encoded *hexokinase*. *Aldolase* expression served as control.

3.1.5. Respiratory capacity of Txnrd2-deficient cells

The potential impact of the Txnrd2-deletion on mitochondria raised further questions concerning mitochondrial functionality, including respiration. Therefore, the individual respiratory capacity of the mitochondrial respiratory chain complexes was analysed. Using high-resolution respirometry (HRR) the cellular basal O₂-consumption and the highest inducible activity of the individual complexes was studied. Primary and immortalised cells of both genotypes were included in the studies (Figure 3-6 A-D).

Primary Txnrd2-deficient cells showed slightly reduced levels of cellular basal O₂-consumption with an O₂-flow per cell of 5.1 ± 2.6 pmol/s*10⁶ compared to the wild-type cells (6.2 ± 1.9 pmol/s*10⁶) (Figure 3-7 A). The maximum achievable activity of complex I and II/III of the respiratory chain after stimulation was slightly decreased in primary Txnrd2-deficient cells (O₂ flow per cells: *Txnrd2*^{+/+} vs. *Txnrd2*^{-/-}; complex I: 146 ± 34 vs. 101 ± 47 ; complex II/III: 178 ± 42 vs. 126 ± 72 , pmol/s*10⁶) and similar for complex IV (O₂ flow per cells: *Txnrd2*^{+/+} vs. *Txnrd2*^{-/-}, complex IV: 243 ± 4 vs. 219 ± 43 pmol/s*10⁶) (Figure 3-7 B). Interestingly, immortalised Txnrd2-deficient cells showed a slightly elevated cellular basal O₂-consumption with an O₂-flow per cell of 4.9 ± 3.0 pmol/s*10⁶ compared to the wild-type cells (3.0 ± 0.9 pmol/s*10⁶) (Figure 3-7 C). Furthermore, particularly complex I and complex IV of immortalised Txnrd2-deficient cells achieved much higher activities after stimulation with the corresponding substrates (O₂ flow per cells: *Txnrd2*^{+/+} vs. *Txnrd2*^{-/-}; complex I: 69 ± 32 vs. 135 ± 18 ; complex II/III: 111 ± 11 vs. 123 ± 19 , complex IV: 185 ± 35 vs. 221 ± 16 , pmol/s*10⁶) (Figure 3-7 D). Provided there is any impairment of mitochondrial morphology in immortalised Txnrd2-deficient fibroblasts, these results document that the cells have a fully active respiratory chain.

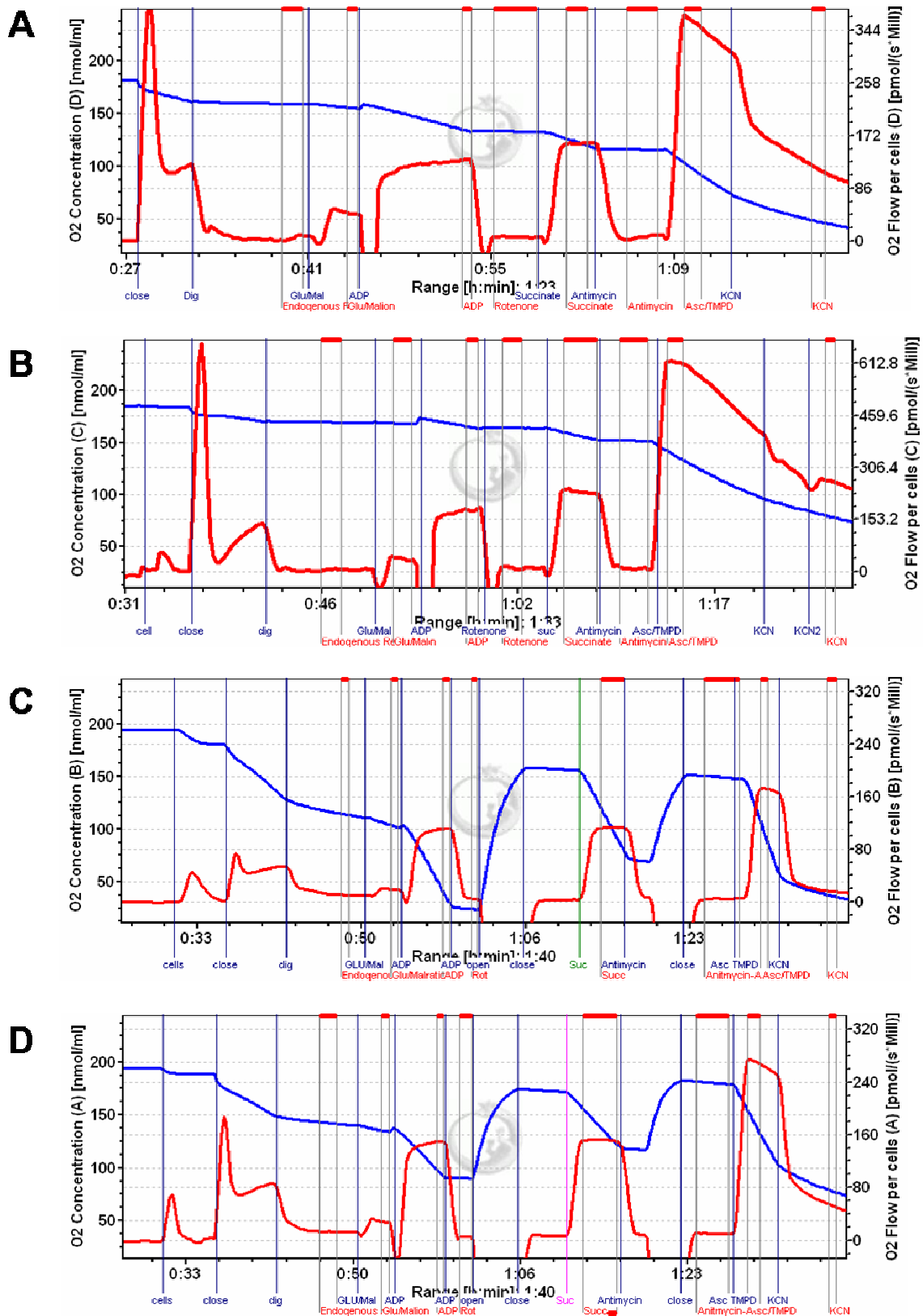


Figure 3-6: Functional analysis of respiratory chain complexes

Recordings of the O₂-flow in primary wild-type (A) and knockout (B) fibroblasts as well as immortalised wild-type (C) and knockout (D) fibroblasts were taken with an oxymeter. The blue curve represents changes in the oxygen concentration and the red curve depicts the oxygen flux of the cells. (See figure 2-2 for detailed informations about the diagrams.)

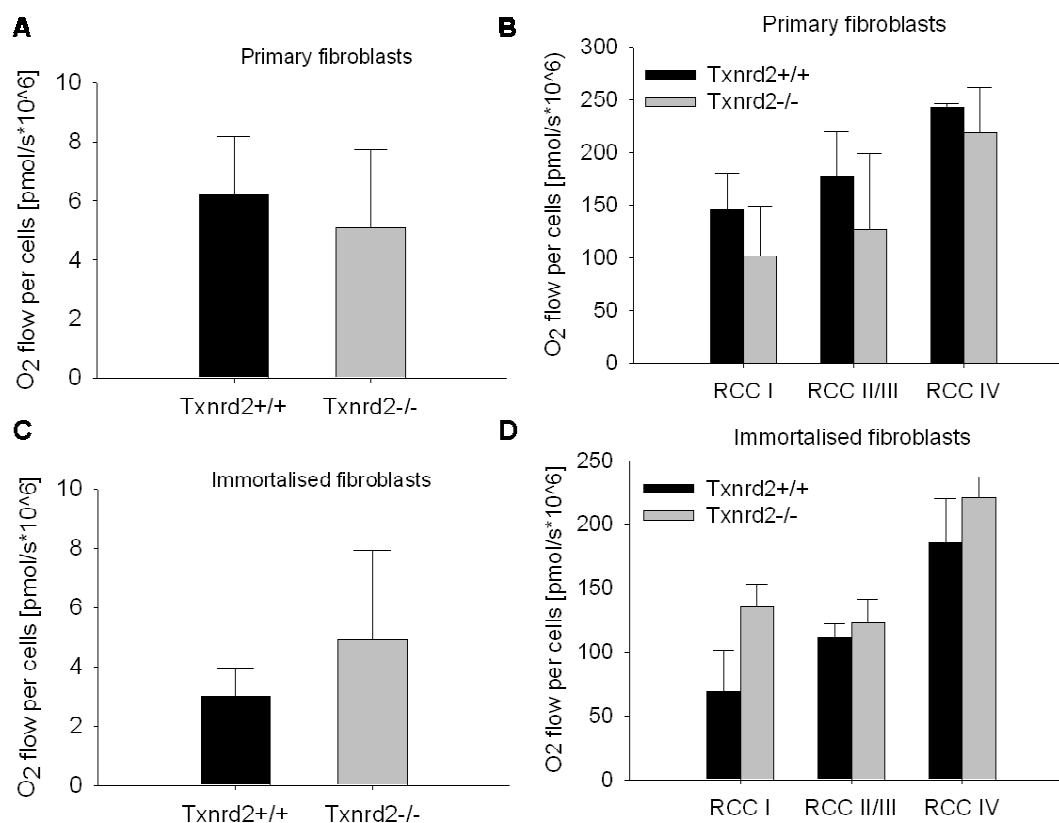


Figure 3-7: Quantification of respiratory capacity in Txnrd2-deficient fibroblasts

Endogenous O₂-consumption, representing the cellular basal activity of respiratory chain enzyme complexes, was observed at least over a period of 10 min in primary (A) and immortalised fibroblasts (C) with no significant differences detectable. Maximum capacity of the individual complexes was measured after stimulation with glutamate/malate/ADP (complex I), succinate (complex II + III) and ascorbate/TMPD (complex III) in primary (B) and immortalised fibroblasts (D). Depicted are the mean values \pm SD from three independent experiments. No significant differences between the activities of the single complexes could be observed.

3.1.6. Metabolic changes due to Txnrd2-deletion

A striking feature of immortalised Txnrd2 knockout cells was that the colour of the cell culture medium changed faster from red to yellow (= more acidic) than in wild-type cells. Therefore it was hypothesised that Txnrd2-knockout cells might increase their energy production via anaerobic glycolysis possibly resulting in a higher release of lactate into the cell culture.

To analyse this, cells were seeded and the amount of lactate release was analysed in the supernatant after 16 h. Under baseline cell culture conditions primary Txnrd2-deficient fibroblasts produced similar amounts of lactate (9 ± 1 nmol/mg protein) compared to wild-type cells (12 ± 0.6 nmol/mg protein) (Figure 3-8 A). In contrast, immortalised Txnrd2-deficient cells showed a much higher lactate release into the cell culture medium (25 ± 2 nmol/mg protein) compared to their wild-type counterparts (8 ± 0.4 nmol/mg protein) (Figure 3-8 B). These results pointed towards a change of cellular metabolism particularly in knockout cells during the process of immortalisation.

To proof these initial observations, *Txnrd2*-deficient as well as wild-type cells were again freshly isolated from wild-type and *Txnrd2*-knockout embryos at E12.5. Changes of lactate release were studied in six individual cell lines derived from six individual embryos (three knockout and three wild-type cell lines were pooled in each case) in a longitudinal fashion for more than 20 passages. Indeed, we observed in each of the knockout clones an increasing lactate release over time in contrast to wild-type cells (*Txnrd2*^{+/+}: p3-6 112±17, p9-12 114±7, p>20 96±52, nmol/mg protein) (*Txnrd2*^{-/-}: p3-6 88±13, p9-12 89±15, p>20 168±126, nmol/mg protein) (Figure 3-8 C).

As immortalised *Txnrd2*-deficient cells are highly susceptible to depletion of intracellular GSH-synthesis causing increased levels of intracellular ROS, we further stressed the cells by treatment with BSO (10 µM). Both cell types showed an increase of lactate level in the cell culture supernatants, but this increase appeared much stronger in wild-type than in *Txnrd2*-deficient cells (*Txnrd2*^{+/+}: control 100±0% vs. BSO 186±26%) (*Txnrd2*^{-/-}: control 100±0% vs. BSO 123±15%) (Figure 3-8 D).

In a second experimental setting the sensitivity of the cells to glucose-depletion was analysed by supplementing glucose-free-medium with galactose. When glucose is no longer available, as it can occur in solid tumours⁷³, cancer cells are forced to use other substrates like galactose^{264, 272}. Metabolising galactose requires oxidative phosphorylation for ATP production. Observation of cell growth over 96 h revealed reduced proliferation of *Txnrd2*-deficient primary cells compared to control cells. In contrast, immortalised *Txnrd2*-deficient cells showed similar or even enhanced proliferation rate compared to the wild-type control cells (Figure 3-8 E – F).

Additionally, the expression of several receptors and signalling molecules involved in energy metabolism were investigated. Since glycolysis generates approximately 19-fold less ATP per mole of glucose, the metabolic reprogramming of *Txnrd2* deficient cells during the process of immortalisation might be compensated by an upregulation of genes encoding glucose transporters. Using semi-quantitative PCR and real-time PCR mRNA levels of the glucose transporter *GLUT-1* (Figure 3-9 A) was analysed. No difference between immortalised *Txnrd2*-deficient and wild-type fibroblasts could be observed for *GLUT-1*. The transporters *GLUT-3* and *GLUT-4* were also investigated by semi-quantitative PCR, but the expression levels were too low to provide robust quantitative analysis (data not shown). Unexpectedly, the transcriptional co-activator PGC1α, an important regulator of energy metabolism, was found to be highly expressed in immortalised *Txnrd2*-deficient cells. Compared to the wild-type control cells (arbitrarily defined as 1), cells that lack *Txnrd2* expressed 4-fold elevated levels of PGC1α (5±2.4) (Figure 3-9 B). PGC1α promotes oxidative metabolism by stimulating processes such as mitochondrial biogenesis and cellular respiration.

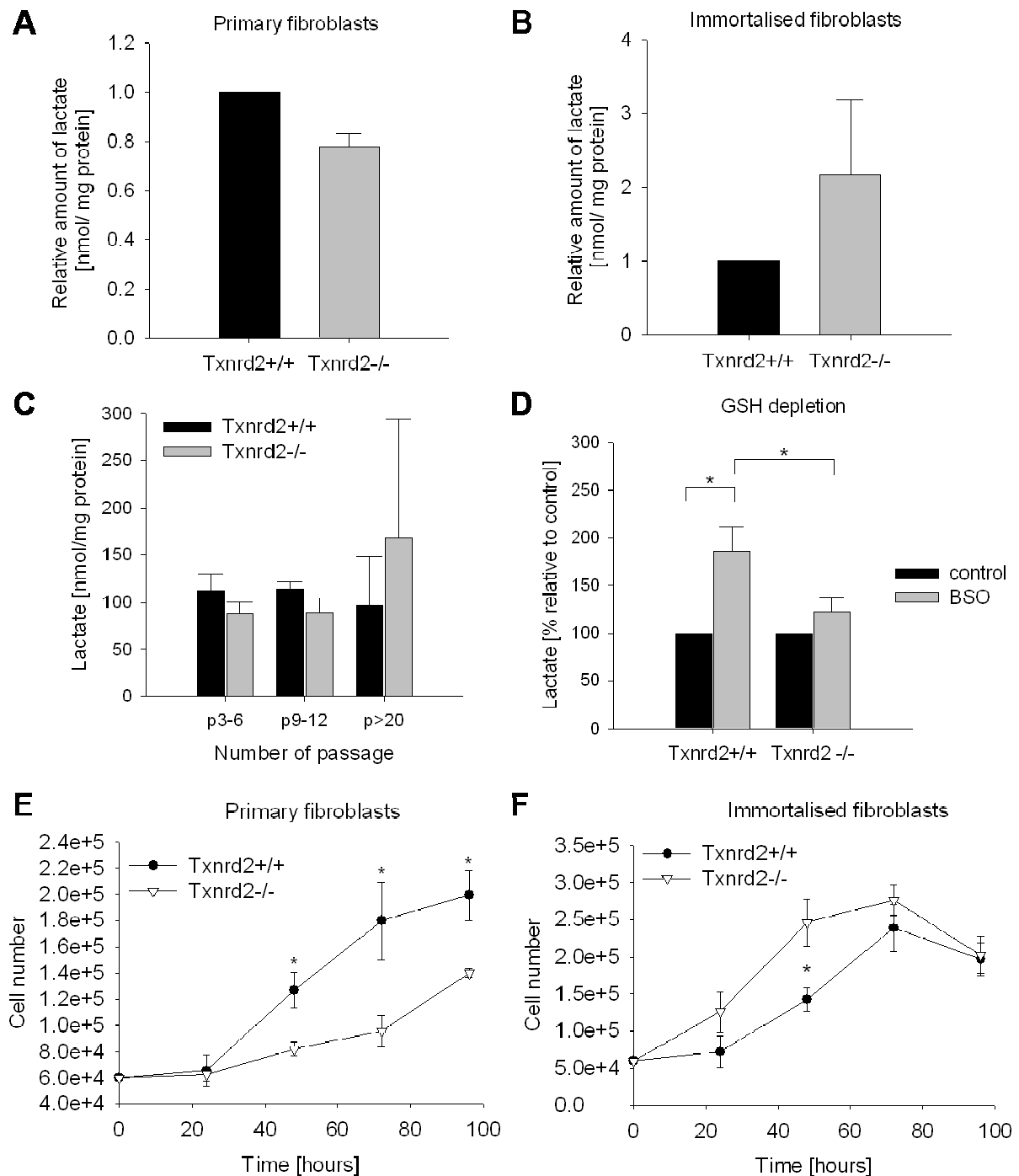
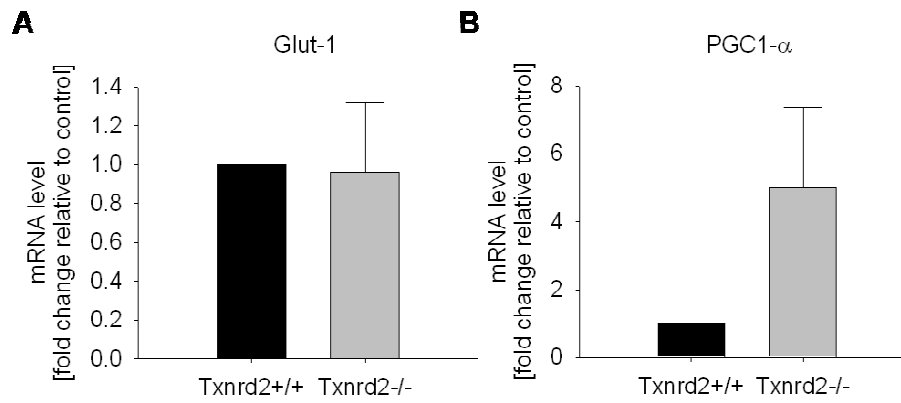


Figure 3-8: Changes in energy metabolism due to Txnrd2-deletion

Lactate release into the cell culture medium was analysed in preliminary experiments for primary (A) and immortalised (B) fibroblasts under baseline cell culture conditions. Mean values \pm SD from two independent experiments performed in duplicates are depicted. P values > 0.05 . (C) Release of lactate into the cell culture medium was observed for cells of different passage numbers during spontaneous immortalisation. Bars represent mean values \pm SD from three independent cell lines. P values > 0.05 . (D) Lactate in cell culture supernatant after treatment with BSO (10 μ M) was observed for immortalised fibroblasts. Lactate under baseline cell culture conditions was considered as 100% for each cell line. Mean values \pm SD from three independent experiments are depicted. * $p < 0.05$ (Student's t -test). Proliferation of primary (E) and immortalised (F) fibroblasts was observed in glucose-free-galactose-medium for 96 h. Depicted are mean values \pm SD from three independent measurements. * $p < 0.05$ (Student's t -test)

**Figure 3-9: Expression of *GLUT-1* and *PGC1 α***

To analyse *GLUT-1* and *PGC1 α* quantitative real-time PCR was performed. The expression levels of *GLUT-1* (A) and *PGC1 α* (B) were normalised to the expression level of *18S rRNA*. Depicted are mean values \pm SD from three independent experiments. *Txnrd2*^{-/-} cells were compared with *Txnrd2*^{+/+} cells, the latter defined as 100%. *P* values > 0.05.

3.2. Studies of the impact of Txnrd2-deletion in transformed cells *in vitro*

3.2.1. Generation of transformed Txnrd2-knockout cells

The basis of neoplastic cell transformation are genetic and epigenetic changes¹³¹. These changes mainly affect genes that are involved in the regulation of cell cycle progression and proliferation, such as proto-oncogenes and tumour suppressor genes. Rodent cells require at least two oncogenic alterations before they retain tumourigenic competence¹²⁹. The two proto-oncogenes *c-myc* and the mutated *Ha-ras*^{V12} are known to synergise in the process of transformation¹⁷⁴. To establish a transformed Txnrd2-deficient cell line, along with the appropriate control cell line, immortalised *Txnrd2*^{-/-} and *Txnrd2*^{+/+} fibroblasts were transduced with lentiviruses expressing the *c-myc* and *Ha-ras*^{V12} oncogenes. As expected expression of one oncogene alone was not sufficient to promote transformation of the immortalised fibroblasts (Figure 3-10 A, left and middle panel), while simultaneous expression of both oncogenes resulted in efficient transformation of the cells (Figure 3-10 A, right panel). When transformed wild-type cells were plated on normal cell culture dishes they grew as multilayers and were only loosely attached to the culture dish, a characteristic sign of transformed cells. On the contrary, transformed Txnrd2-deficient cells still preferentially grew in a monolayer and remained tightly attached to the culture dish (Figure 3-10 B).

Tumourigenic competence is characterised by unlimited growth potential, loss of contact inhibition and anchorage independent growth. Compared to the primary and immortalised fibroblasts the transformed cells showed a higher proliferation rate (data not shown) and formed single cell colonies in agar matrix (Figure 3-10 B). The lentiviral vector is coupled with VENUS, thus the efficiency of transformation could be assessed using flow cytometry. For both, wild-type and Txnrd2-deficient cells, the transduction with *c-myc* and *Ha-ras*^{V12} was comparable (*Txnrd2*^{+/+}: 84±6% vs. *Txnrd2*^{-/-}: 94±1% cells expressing VENUS following transformation). The expression of *c-myc* and *Ha-ras*^{V12} was also analysed by immunoblotting. Unlike immortalised fibroblasts, the transformed cells showed highly increased expression of both proto-oncogenes (Figure 3-10 C).

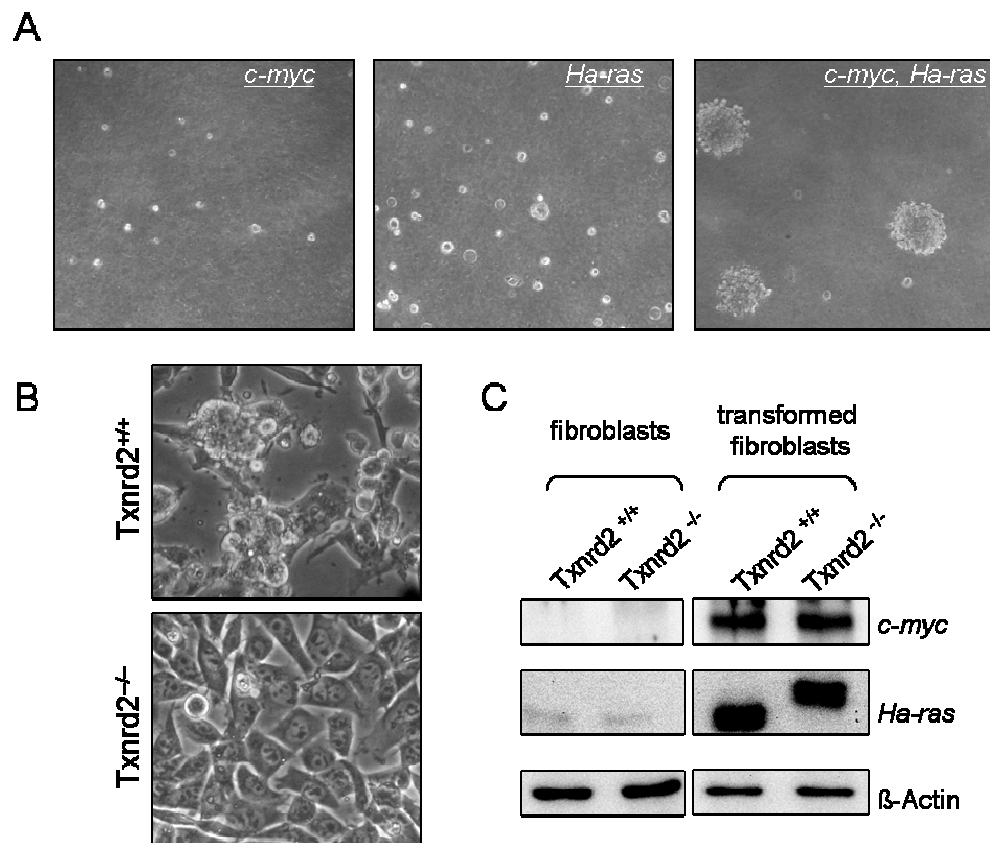


Figure 3-10: Transformation of *Txnrd2* wild-type and knockout fibroblasts with *c-myc* and *Ha-ras*^{V12}

(A) Transduction of fibroblasts with *c-myc* (left panel) or *Ha-ras*^{V12} (middle panel) alone or both oncogenes together (right panel) using lentiviral vectors. (B) Growth behaviour of transformed *Txnrd2*^{+/+} and *Txnrd2*^{-/-} cells under baseline cell culture conditions. (C) To monitor expression of both oncogenes in transformed cells, immunoblotting was performed in immortalised fibroblasts (left panel) and after transformation (right panel). β -actin served as control.

3.2.2. Deletion of *Txnrd2* impairs colony formation capacity of tumour cells

To investigate the effects of *Txnrd2* on the tumourigenic potential, clonal tumour cell lines were established. After transformation with *c-myc* and *Ha-ras*^{V12} cells were placed in soft agar. After seven days, individual single cell colonies were picked and expanded to establish transformed cell lines. Surprisingly, *Txnrd2*-deficient cells showed strongly reduced colony formation capacity (Figure 3-11 A). Compared to wild-type cells (set as 100%), the *Txnrd2*-deficient cells revealed a five-fold decrease in the numbers of colonies per well (20±13 %) (Figure 3-11 B). To proof that this was due to the lack of *Txnrd2*, *Txnrd2*-deficient cells were stably transfected via electroporation with a plasmid carrying the N-terminally FLAG-tagged full length *Txnrd2* (add-back) and an empty vector for control (mock) (Figure 3-11 C). Formation of colonies was observed over seven days. After reconstitution of *Txnrd2* expression, the formation of colonies was significantly increased (Figure 3-11 D). Compared

to the add-back cells (set as 100%) empty vector transfected cells (= mock) formed only 36 ± 22 % colonies per well (Figure 3-11 E).

As described above, immortalised *Txnrd2*-deficient cells showed increased ROS levels, particularly under oxidative stress-inducing conditions (Figure 3-2 C). To proof, whether the reduced number of colonies is due to increased ROS-levels, soft agar assay was performed in the presence of the antioxidant N-acetyl-L-cysteine (NAC). Previous work in our laboratory demonstrated that treatment with NAC was able to reduce the elevated ROS-level in primary *Txnrd2*-deficient cells to the level of primary wild-type cells under baseline cell culture conditions²⁴⁵. Both, *Txnrd2* wild-type and *Txnrd2*-deficient cells were observed over seven days in soft agar containing 5 mM NAC (Figure 3-12 A - B). Interestingly, the numbers of colonies derived from wild-type cells were reduced (100 ± 0 % vs. 67 ± 18 %), whereas the numbers of colonies derived from *Txnrd2*-deficient cells were not affected by NAC treatment (16 ± 10 % vs. 19 ± 10 %) (Figure 3-12 C). To further investigate if the redox-regulating function of the *Txnrd2* is crucial for the formation of colonies, *Txnrd2*-deficient cells were stably transfected with lentiviral vectors carrying the full-length *Txnrd2* (add-back), a mutated *Txnrd2* sequence (stop) and an empty vector for control (mock) (Figure 3-12 D). The mutation comprises a real STOP codon (UAA) instead of UGA coding for Sec at the amino acid U524 of the C-terminal part of *Txnrd2*. Thus, the mutated *Txnrd2* carries an inert active site due to the lack of the essential amino acid for the redox-regulating functions carried out by the C-terminal active site. *Txnrd2*^{-/-}-add-back, *Txnrd2*^{-/-}-stop and *Txnrd2*^{-/-}-mock fibroblasts were grown in soft agar over a period of seven days (Figure 3-12 E) and the numbers of colonies were counted (Figure 3-12 F). The number of colonies derived from *Txnrd2*^{-/-}-add-back cells was considered as 100%. Interestingly, *Txnrd2*^{-/-}-stop expressing fibroblasts also formed significantly more colonies (46 ± 18 % of *Txnrd2*^{-/-}-add-back cells) than cells infected with the empty control vector (15 ± 4 % of *Txnrd2*^{-/-}-add-back cells). Compared to the *Txnrd2*^{-/-}-add-back cells, incorporation of a mutated *Txnrd2* carrying a sequence coding for a real STOP instead of the redox-active Sec, could only partially (50%) rescue the impaired colonogenic competence of *Txnrd2*-deficient cells.

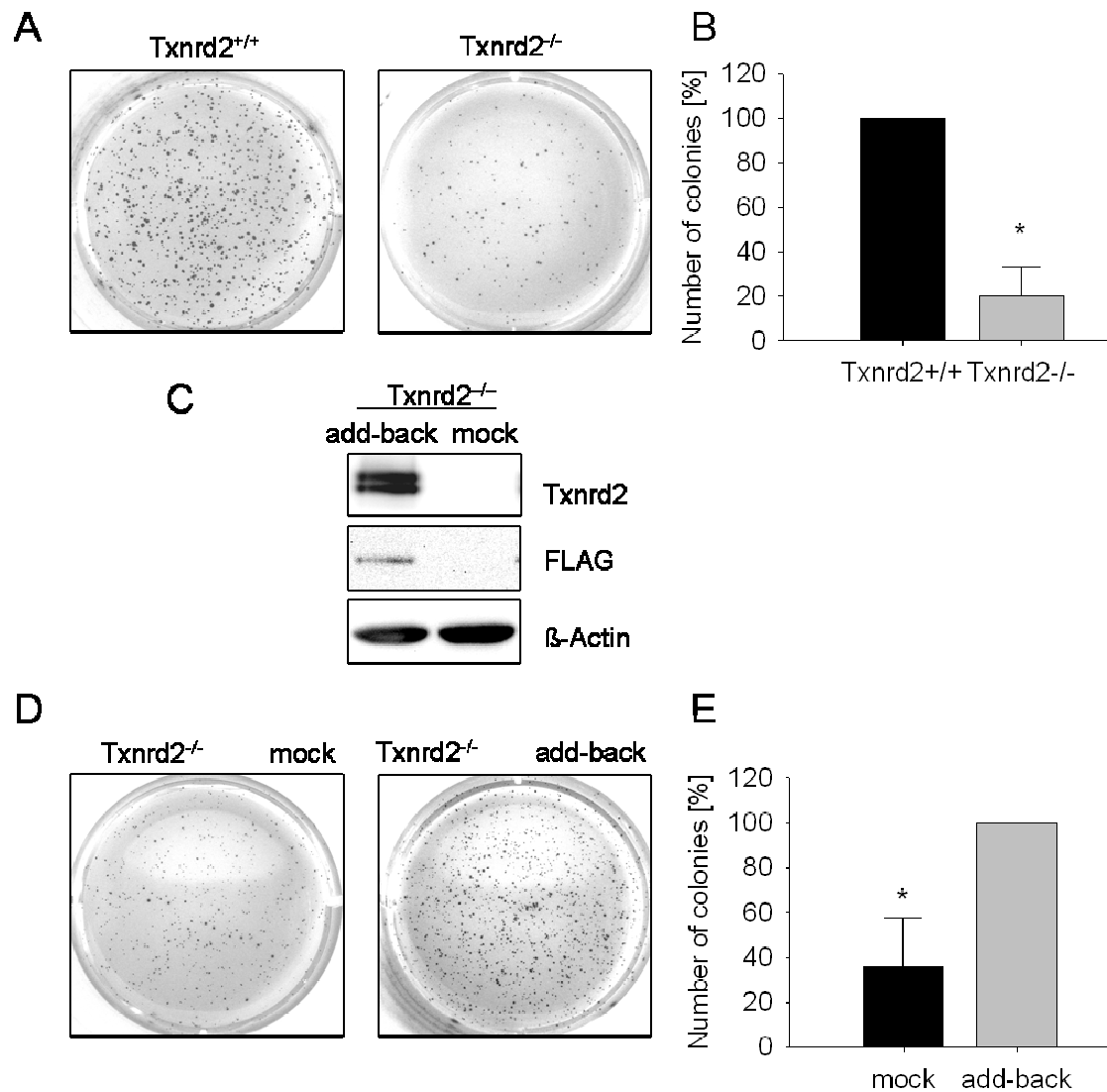


Figure 3-11: Txnrd2-deletion impairs colony formation capacity

The colonogenic potential of transformed fibroblasts was studied using the soft agar assay. (A) Transformed wild-type and Txnrd2-deficient cells were grown for seven days in agar matrix. (B) Number of colonies per well from transformed wild-type and Txnrd2-deficient cells were compared. Mean values \pm SD from three independent experiments are depicted. Wild-type cells were considered as 100%. * $p < 0.05$ (Student's t-test) (C) Expression of Txnrd2 was confirmed by immunoblotting following reconstitution of the enzyme with the FLAG-tagged full-length *Txnrd2*. β -actin served as a control. (D) Txnrd2-deficient transformed cells were stably transfected with full-length Txnrd2 (add-back) and an empty vector control (mock). Formation of colonies was observed after seven days in soft agar. (E) Number of colonies per well from mock and add-back cells were compared. Add-back was considered as 100%. Mean values \pm SD from three independent experiments are depicted. * $p < 0.05$ (Student's t-test)

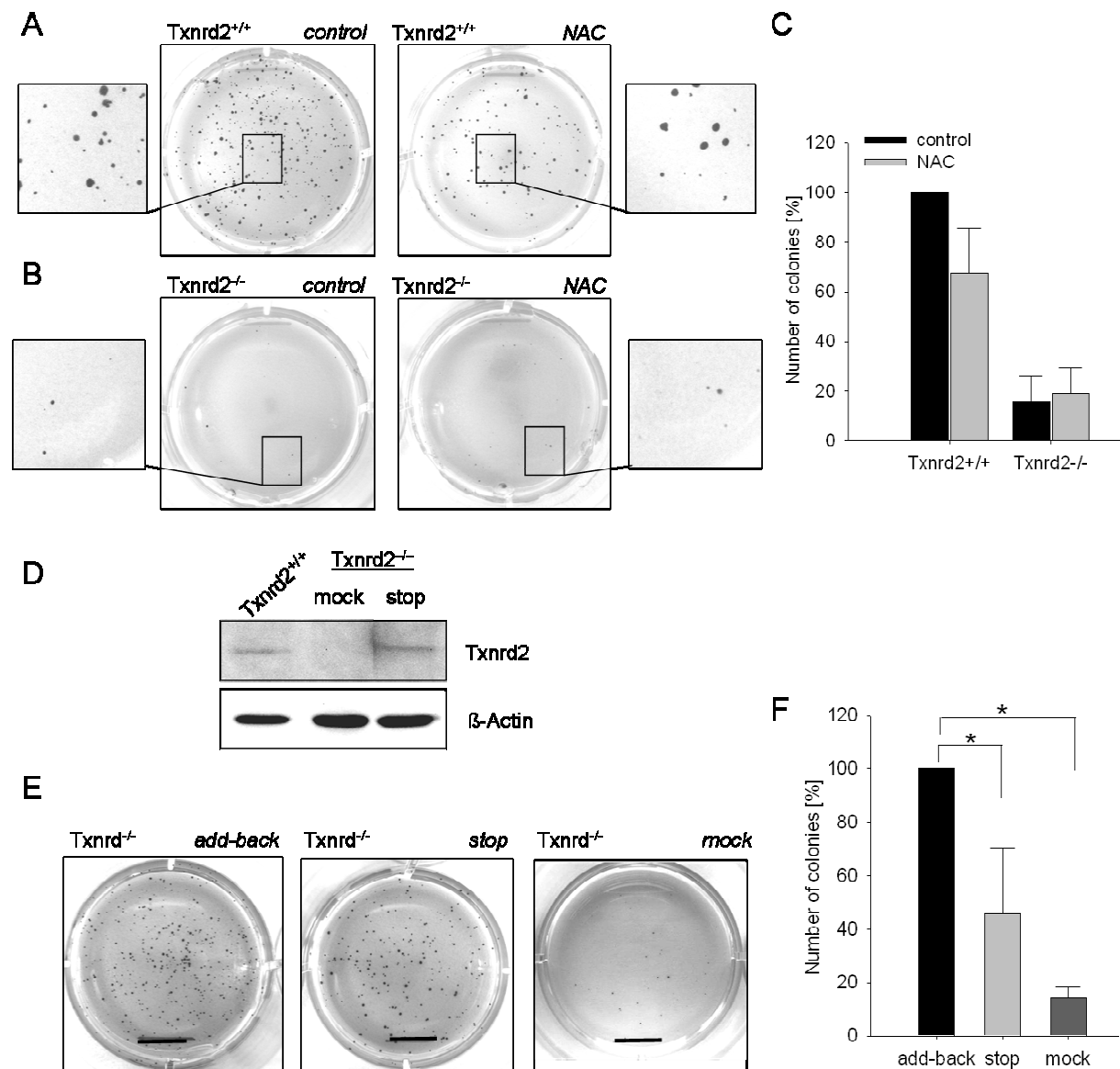


Figure 3-12: Influence of NAC and restoration of a redox-inactive Txnrd2 on colonogenic capacity

The impact of the antioxidant NAC on the colony growth in soft agar matrix was analysed for transformed (A) wild-type fibroblasts and (B) Txnrd2-deficient fibroblasts. Soft agar assay was performed with 5 mM NAC over a period of seven days. Numbers of colonies per well were counted and compared with wild-type cells without NAC considered as 100%. (C) Mean values \pm SD of three independent experiments are depicted. P values > 0.05 for Txnrd2^{+/+} control versus NAC and Txnrd2^{-/-} control versus NAC. (D) Txnrd2-deficient cells were stable transfected with Txnrd2 (add-back) and Txnrd2 carrying a real STOP codon instead of Sec at the amino acid U524 (stop) and an empty vector for control (mock). Expression of mutated Txnrd2 was confirmed using immunoblotting. β -actin served as a control. (E) Formation of colonies in soft agar was observed over a period of seven days and counted. (F). The add-back was considered as 100% and mean values \pm SD of five independent experiments are depicted. * $p < 0.05$ (Student's t-test)

3.2.3. Generation and characterisation of clonal single-cell lines

To further investigate the impact of Txnrd2-deficiency on tumour cell proliferation and functionality, wild-type and Txnrd2-deficient clonal single-cell lines were established from the transformed cell lines after growth in soft agar assay. Therefore, single cell-derived colonies were isolated from soft agar, expanded to clonal single-cell lines and characterised and analysed *in vitro*. The absence of Txnrd2 was confirmed by semi-quantitative PCR and immunoblotting (Figure 3-13 A – B). The colonigenic potential of the established clonal tumour cell lines was confirmed by soft agar assay (Figure 3-13 C). Quantification revealed no difference between wild-type (100%) and Txnrd2-deficient cells (93±23%) (Figure 3-13 D). *In vitro* proliferation under baseline cell culture conditions revealed also no differences (Figure 3-13 E, left panel). However, GSH-depletion induced by BSO caused cell death of transformed Txnrd2-deficient cells (Figure 3-13 E, right panel) but not of wild-type cells in a manner similar to that already observed in immortalised Txnrd2-deficient fibroblasts (chapter 3.1.2.). It was shown (chapter 3.1.3) that immortalised Txnrd2-deficient cells compensate for the lack of Txnrd2 by e.g. inducing the expression and activity of GR and by increasing Txnrd1 expression (Figure 3-3). Apparently, a similar trend was observed for transformed MEFs (Figure 3-14 A – B), but not for the isolated clonal single-cell lines (Figure 3-14 C – D). Quantitative analysis of intracellular ROS in wild-type and Txnrd2-null clonal single-cell lines, which was performed using MitoSox RedTM (a marker used for detection of superoxide anions) and flow cytometry, revealed no difference in ROS level under baseline cell culture conditions (Figure 3-14 E) as well as following GSH-depletion (Figure 3-14 F). Investigation of GR activity and total amount of GSH revealed no appreciable difference between wild-type and Txnrd2-deficient clonal single cell-derived cells (Figure 3-14 C – D). This was also true for protein amount of GR (Figure 3-14 G) and Txnrd1 (Figure 3-14 H). Accordingly, the isolated transformed clonal cell lines showed comparable behaviour under baseline cell culture conditions, no eminent differences in ROS level and tumourigenic competence. Therefore, the small proportion of Txnrd2-deficient cells that were able to form colonies in soft agar assay probably bypass Txnrd2 –deficiency by a yet-unknown mechanism. Nevertheless, clonal single cell-derived Txnrd2-deficient cells were still susceptible to GSH-depletion induced cell death.

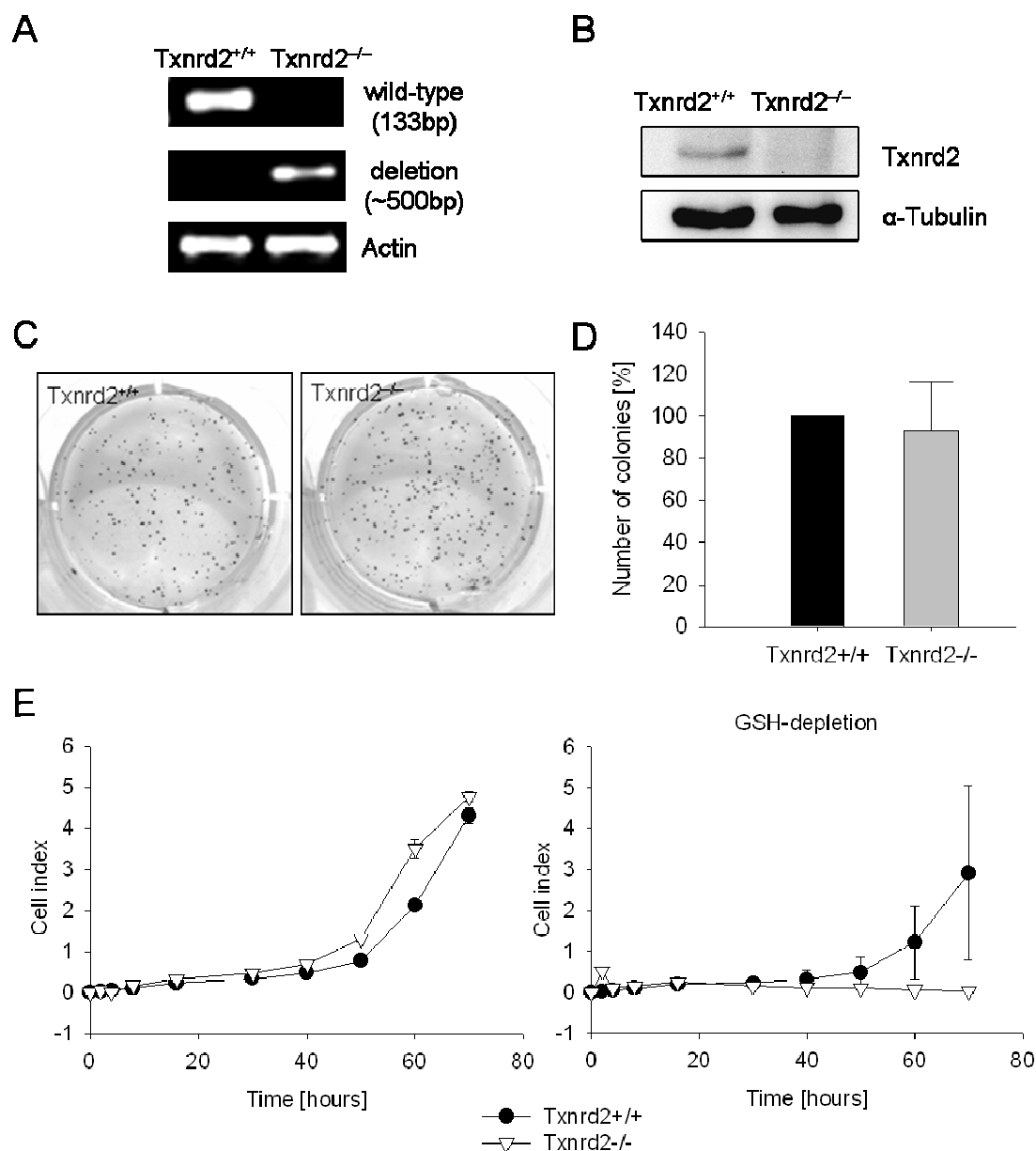


Figure 3-13: Proliferation and colonigenic potential of single-cell clones

Expression of *Txnrd2* in isolated single-cell clones was studied by semi-quantitative PCR and immunoblotting. (A) Genotyping of wild-type and knockout *Txnrd2* alleles is shown. *Actin* served as control. (B) Immunoblotting showed that *Txnrd2* was only detectable in transformed *Txnrd2*^{+/+} fibroblasts. Equal loading was assessed by α -Tubulin expression. (C) Colonigenic potential of *Txnrd2* wild-type and *Txnrd2*-deficient single-cell clones was studied over a period of seven days in soft agar assay. The number of colonies of *Txnrd2* wild-type cells was considered as 100% (D). Mean values \pm SD of three independent experiments are depicted. (E) Proliferation of single-colony-derived cells was studied over a period of three days using the xCELLigence RTCA SP instrument (Roche) and the amount of cells is expressed as cell index (for detailed information see chapter 2.2.1.6.). Wild-type cells and *Txnrd2*-deficient cells were compared under baseline cell culture conditions (left panel) and after treatment with BSO (10 μ M) (right panel). The experiment was performed in triplicates and mean values \pm SD are depicted. The analysis of proliferation of single-colony derived cell lines was performed in three independent experiments using three different methods, trypan blue exclusion method, MTT assay and xCELLigence system (depicted). All three methods produced comparable results.

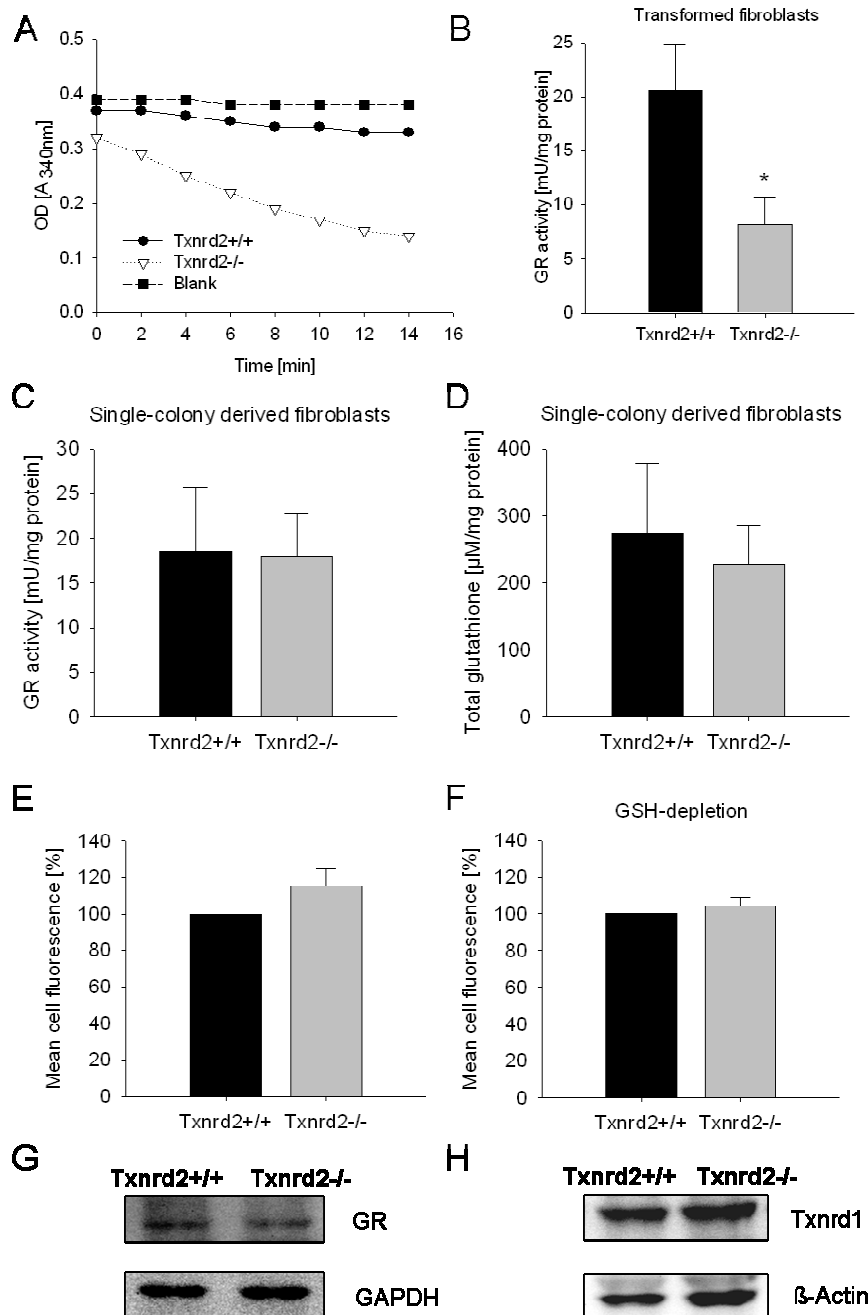


Figure 3-14: Analysis of ROS and redox-regulating systems following transformation

(A) GR-activity was measured in supernatants from transformed cell lysates at 340 nm every 2 min for at least 14 min. (B) Activity is expressed in mU/mg protein and compared for *Txnrd2^{+/+}* and *Txnrd2^{-/-}* cells. Depicted are mean values \pm SD from five independent experiments. * $p < 0.05$ (Student's t-test). Single-colony-derived cells were treated with MitoSoxTM Red superoxide indicator and analysed using flow cytometry. (C) GR-activity of single-colony-derived cells is expressed in mU/mg protein and was compared for *Txnrd2* wild-type and *Txnrd2*-deficient cells. Depicted are mean values \pm SD from seven independent experiments. (D) Total GSH was measured after TCA-extraction from single-colony-derived cells and is expressed in $\mu\text{mol/mg}$ protein. The graph shows mean values \pm SD from three independent measurements. (E) Level of soluble ROS was quantified under baseline cell culture conditions and (F) following GSH-depletion with 10 μM BSO. Mean fluorescence intensities \pm SD of three independent experiments are depicted. *Txnrd2*-deficient cells were compared with *Txnrd2* wild-type cells (set as 100%). Expression of GR (G) and *Txnrd1* (H) in single-colony-derived cells was analysed by immunoblotting. One representative blot from three independent experiments is shown. Equal loading was confirmed by analysis of GAPDH or β -actin expression.

3.2.4. Analysis of mitochondrial parameters and cellular metabolism following transformation of Txnrd2-knockout cells

Immortalised Txnrd2-deficient fibroblasts showed structural changes of mitochondria and alterations in cellular metabolism (Figure 3-4, 3-5, 3-8). To analyse if these changes could also be found in single-colony-derived cells lacking Txnrd2, staining with a mitochondrial-specific dye and analysis of metabolic markers as well as proliferation under supply of different energy substrates was investigated. Staining with the mitochondria-selective probe Mitotracker Green® and analysis by confocal microscopy revealed no apparent differences in the overall morphology of mitochondria (data not shown). However, quantification of mitochondria following Mitotracker Red® staining using flow cytometry disclosed significantly reduced fluorescence intensity in single-colony-derived Txnrd2-deficient fibroblasts (Figure 3-15 A). We also analysed the mitochondrial DNA using real-time PCR, as already described for immortalised fibroblasts (see chapter 3.1.4.). Mitochondrial DNA was comparable between wild-type and Txnrd2-deficient single-colony derived cells (data not shown).

To investigate if the deletion of Txnrd2 also has consequences on cell metabolism in single colony-derived fibroblasts, the concentration of lactate in cell culture supernatants was determined. In fact, there were significantly increased lactate concentrations in the supernatant of Txnrd2-deficient cells (392 ± 57 nmol/mg protein) as compared to wild-type cells (298 ± 31 nmol/mg protein) (Figure 3-15 B) suggesting that these cells produce more energy via anaerobic glycolysis.

In the *in vivo* situation, the growing tumour lacks sufficient supply of oxygen and energy substrates due to inadequate vascularisation starting at a size of approximately 1mm^3 . Thus, cancer cells are often forced to use alternative substrates like glutamine or galactose for their energy production²⁶⁴. The effects of such changes in substrate availability were studied *in vitro* over a period of at least four days. Restriction of glucose availability (1 g/l culture medium) did not cause any differences in the proliferation of Txnrd2-deficient and wild-type cells (Figure 3-15 C). In contrast, complete withdrawal of glucose and supplementation with glutamine and galactose revealed differences between wild-type and knockout single colony-derived fibroblasts. Interestingly, wild-type cells showed increased cell death starting around 24 h following incubation, whereas transformed single colony-derived Txnrd2-deficient cells tolerated the alternative energy sources much better (Figure 3-15 D).

Glutamine/glutamate metabolism goes via α -ketoglutarate, TCA and thus requires oxidative phosphorylation. Thus, we investigated the activity of the respiratory chain of single-colony derived wild-type and Txnrd2-knockout cells. Using high-resolution respirometry, the basal O_2 -consumption of the cells was analysed (Figure 3-16 A). However, no difference in

endogenous O₂-flow was detectable. In contrast, when comparing the maximum activity of each complex, after stimulation with the appropriate substrate, Txnrd2-deficient cells showed slightly increased activity at each complex and in particular at complex IV (Figure 3-16 B). These observations were accompanied with a similar or even slightly elevated concentration of intracellular ATP in the Txnrd2-deficient cells under baseline cell culture conditions (*Txnrd2*^{+/+}: 1.3±1.0 vs. *Txnrd2*^{-/-}: 2.2±0.5 μM/mg protein) (Figure 3-16 C).

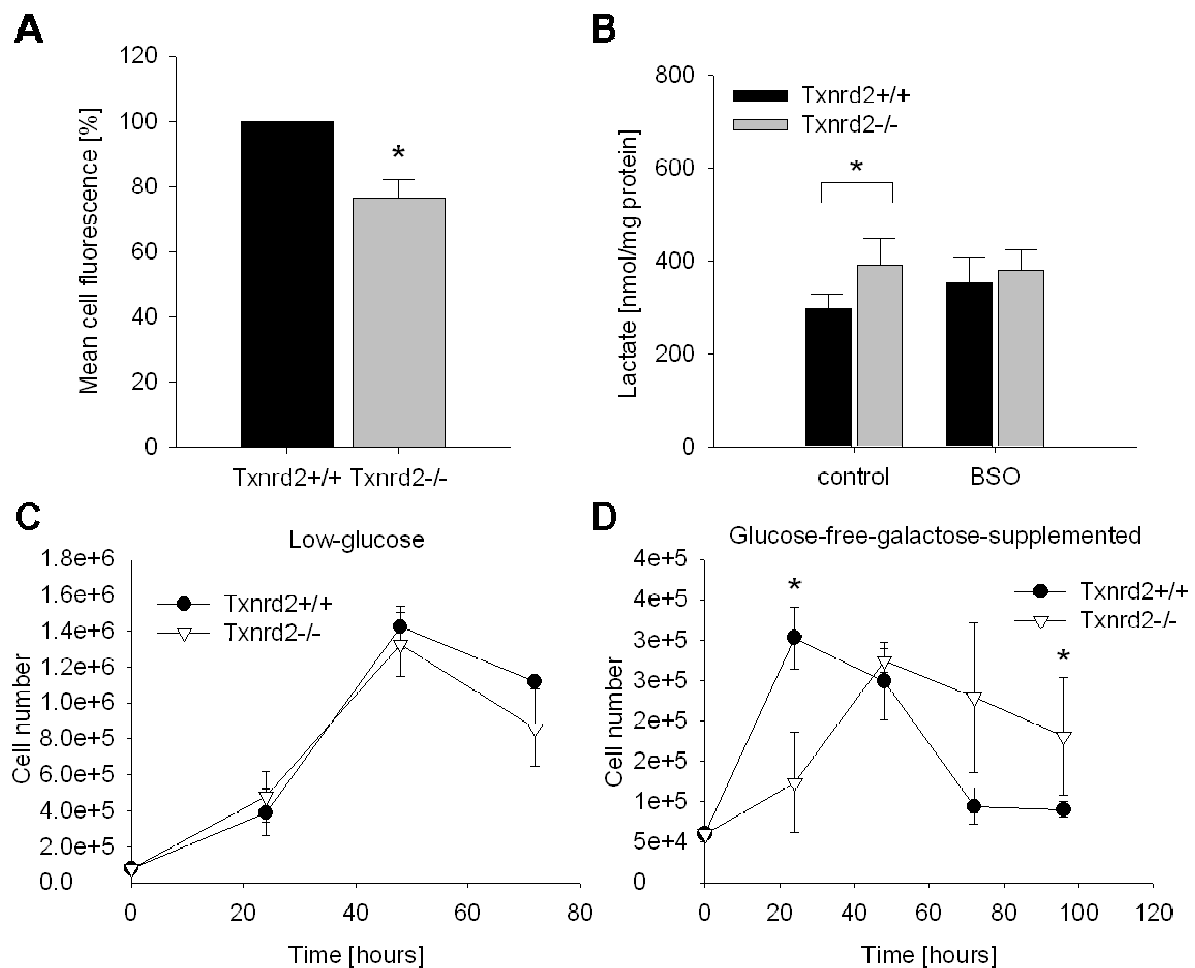


Figure 3-15: Mitochondria shape and energy metabolism of transformed fibroblasts

(A) To quantify mitochondria, single-colony derived cells were stained with Mitotracker Red® and mean cell fluorescence was analysed using flow cytometry. Values for wild-type cells were considered as 100% and compared to *Txnrd2*-deficient fibroblasts. Depicted are mean values ± SD of five independent experiments. **p* < 0.05 (Mann-Whitney Rank sum test). (B) Release of lactate by transformed cells was analysed as lactate concentrations in the corresponding cell culture supernatants without further treatment or after incubation with 10 μM BSO. Mean values ± SD of three independent experiments are shown. **p* < 0.05 (Paired t-test) (C) Proliferation of transformed fibroblasts was observed over four days in low glucose-medium and (D) five days in glucose-free-galactose medium. Mean values ± SD from (C) two and (D) three independent experiments performed in triplicate are depicted. **p* < 0.05 (Student's t-test)

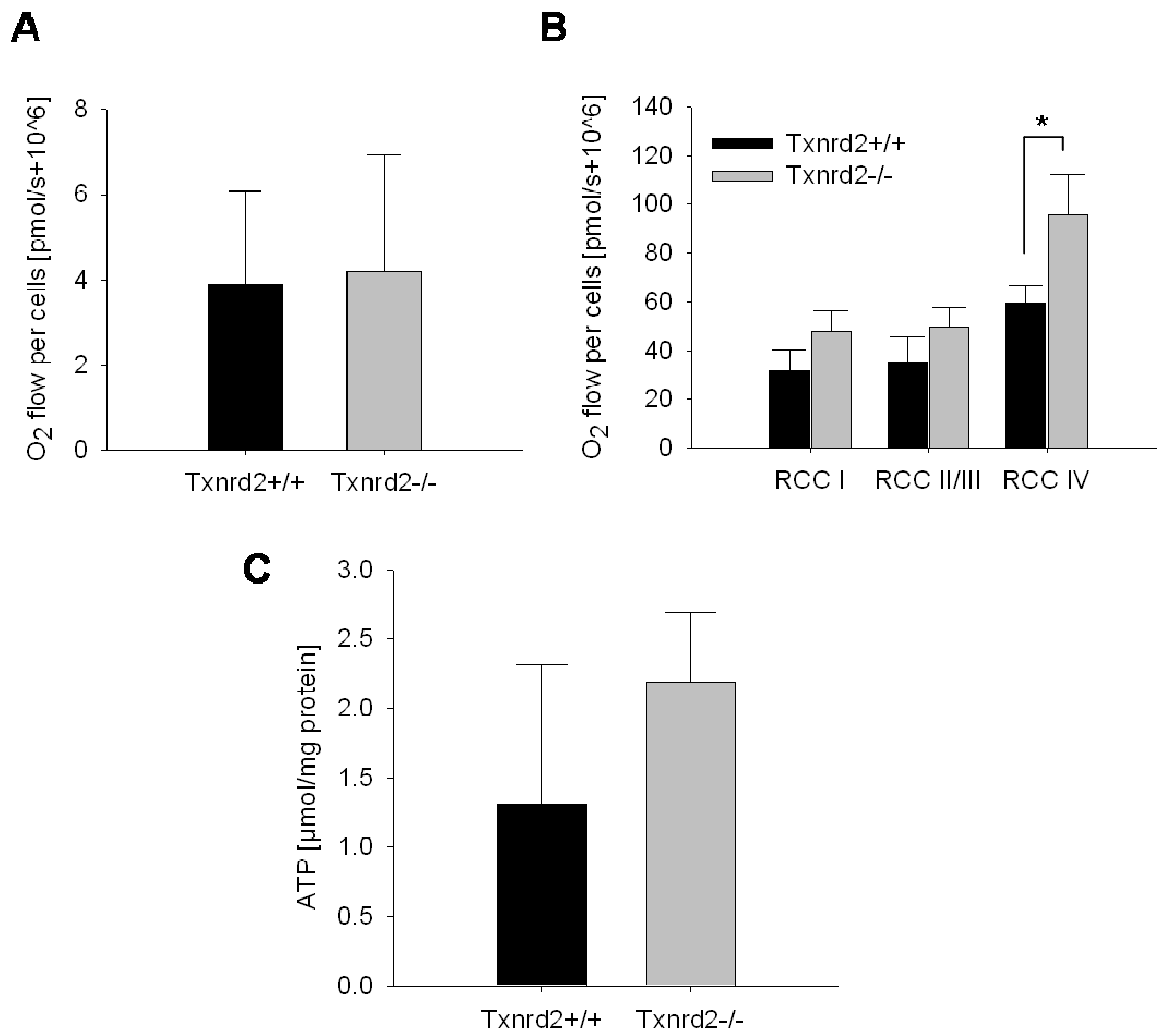


Figure 3-16: Activity of the respiratory chain in transformed fibroblasts

Mitochondrial respiratory chain activity was analysed using high-resolution respirometry (HRR). Approximately 1.2 Mio cells were collected in respiration medium B and O₂ flow per cells was observed. (A) Endogenous O₂ consumption, representing the cellular basal activity of respiratory chain enzyme complexes, was observed over at least 10 min. (B) Maximum capacity of the individual complexes was measured after stimulation with glutamate/malate/ADP (complex I), succinate (complex II + III) and ascorbate/TMPD (complex III). Depicted are mean values \pm SD from three independent experiments. * $p < 0.05$ (Student's t-test) (C) The intracellular amount of ATP in cells was estimated using bioluminescent determination. Mean values \pm SD of four independent experiments are compared between wild-type and Txnrd2-deficient fibroblasts. P value > 0.05 .

3.3. Relevance of Txnrd2 for *in vivo* tumour growth

Extensive research has been carried out to investigate the controversial impact of Txnrd1 on tumour development and progression. On the one hand the enzyme is described as a cancer preventing protein as it is believed to account for the putative chemo-preventive effects of selenium against cancer, at least in parts^{39, 101, 170}. On the other hand many studies observed elevated levels of Txnrd1 in several types of cancer and demonstrated that Txnrd1 is involved in tumour progression, implying that Txnrd1 may represent a potential target for cancer therapy^{133, 192, 350-351}. Indeed, inhibition of Txnrd1 sensitises tumour cells to oxidative stress inducing agents and triggers apoptosis of these cells¹³⁵. It is considered that this impact of the Txnrd1 is associated with its role in cell proliferation, transcription, DNA repair and angiogenesis. Surprisingly much less is known about Txnrd2 and its relevance for tumour development and progression. Only one study demonstrated elevated expression of Txnrd2 in hepatocellular carcinomas⁵⁹. Further evidence for a potential impact of Txnrd2 on tumour growth was provided by the above reported *in vitro* experiments using transformed wild-type and Txnrd2-deficient cell lines (chapter 3.2.). Therefore the following experiments focused on the potential impact of Txnrd2 on tumour development and tumour-associated angiogenesis *in vivo*. We used the above described and characterised single colony-derived transformed Txnrd2-deficient fibroblasts in an ectopic, subcutaneous *in vivo* tumour model.

3.3.1. Loss of Txnrd2 limits tumour growth

To study the impact of the Txnrd2 on tumour development and progression, 4×10^6 transformed single-colony derived wild-type and Txnrd2-deficient cells were transplanted subcutaneously into the retral flank of C57BL/6 mice (Figure 3-17 A - B). Tumour size and volume was analysed on days two, three, four, six, eight, ten and 11. Though single cell-derived transformed fibroblasts showed no difference in their proliferation rate under baseline cell culture conditions (Figure 3-13 E), tumour mass of Txnrd2-deficient tumours revealed a 50% reduction (0.8 ± 0.6 g) compared to wild-type tumours (1.7 ± 0.8 g) on day 11 of tumour growth (Figure 3-17 C). The same holds true also for tumour volume (Txnrd2^{+/+}: 11.9 ± 4.5 vs. Txnrd2^{-/-} 3.8 ± 1.6 mm³) (Figure 3-17 D). Observations of tumour mass at different time points during tumour growth (Figure 3-17 E) indicated that the variation between both groups started to emerge around day four and six, becoming highly significant on day 11 ($p < 0.001$). Expression of Txnrd2 in tumours of both groups was checked on day three (Figure 3-17 F) and day 11 (Figure 3-17 G). These results show that loss of Txnrd2 had a clear influence on the progression of tumour growth. To adress how Txnrd2 affected tumour growth, further experiments were conducted. Therefore tumour tissue was collected and prepared for immunohistological stainings and immunoblot analysis.

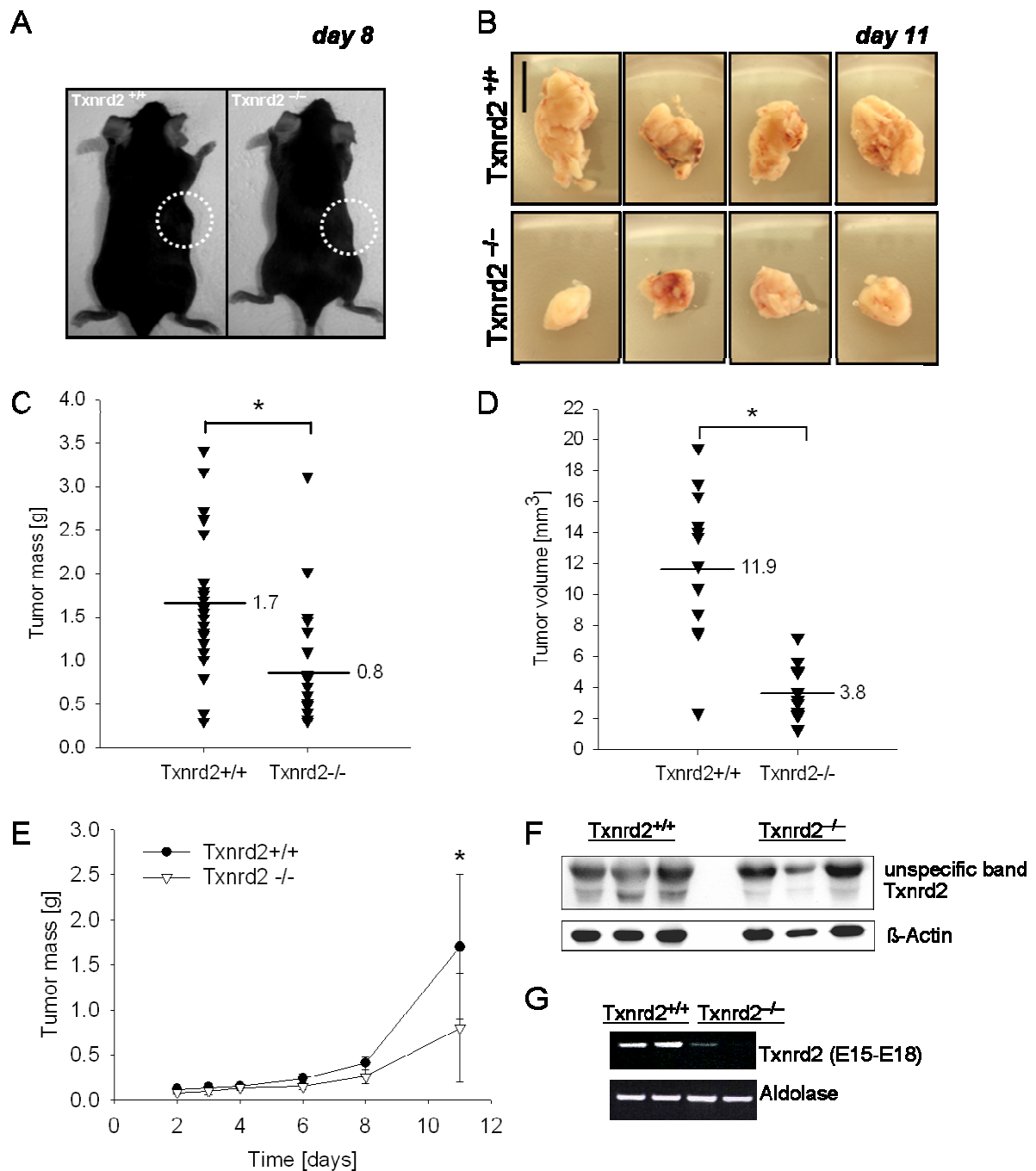


Figure 3-17: Observation of tumour growth *in vivo*

(A) 4×10^6 single-colony derived wild-type and Txnrd2 knockout cells were subcutaneously injected into the retrol flank of C57BL/6 mice and formation of tumours was observed over a period of 11 days and tumours were dissected. (C) Exact tumour mass and (D) volume were analysed. For determination of tumour mass 24 and for tumour volume 13 individual samples are displayed. Lines and numbers assign mean values. * $p < 0.001$ (Mann-Whitney Rank Sum Test) (E) Observation of development of tumour size is shown. Depicted are mean values \pm SD. * $p < 0.001$ (Mann-Whitney Rank Sum Test) (number of samples at each single time point: day2=3, day3=20, day4=3, day6=9, day8=3 and day11=24). (F) Txnrd2 expression was analysed in tumour sections by immunoblotting at day three and (G) semi-quantitative PCR at day 11. Equal loading was confirmed by β -actin or *aldolase* expression, respectively.

3.3.2. Histological analysis of *Txnrd2*-deficient tumours

Sections from day 11 tumours were analysed for morphological characteristics using H&E staining. Both groups consisted of poorly differentiated tumours with infiltration of skeletal muscle and sporadically subcutaneous adipose tissue (Figure 3-18 A). Cells appeared mainly in a less organised or diffuse growth pattern (Figure 3-18 B, right panel). However, some tumour cells were arranged in a fascicular pattern, comparable to a draught of fish, which is typical of fibrosarcomas.

At higher magnification tumours of both groups frequently showed mitotic and apoptotic cells (quantification see chapters 3.3.3 and 3.3.4). Necrotic areas were frequently detectable in both groups, but appeared more extensive in *Txnrd2*-deficient tumours (Figure 3-18 A, asterisk). In wild-type tumours a slightly 'nodular' architecture was distinguishable at low magnification (Figure 3-18 B, left panel, arrows). The 'nodules' consisted of highly pleomorphic, large cells with prominent nucleoli, probably representing less differentiated cells, surrounded of smaller spindle cells with dark nuclei. These two cell populations were not clearly detectable in *Txnrd2*-deficient tumours (Figure 3-18 B, right panel). Taken together, no characteristic or quantifiable differences in the morphology of wild-type and *Txnrd2*-deficient tumours were detectable.

3.3.3. Quantification of apoptotic cells and necrotic area in tumour sections

For the precise quantification of apoptotic cells in tumour tissue a staining for cleaved-caspase 3 was performed. The number of apoptotic cells (Figure 3-19 A – B) as well as the total necrotic area was investigated (Figure 3-19 B – C). Quantification of single apoptotic cells per field of view, expressed as apoptotic index, revealed no difference between wild-type and *Txnrd2*-deficient tumours at day 11 ($n=12$ each group; *Txnrd2*^{+/+} 0.08 ± 0.1 vs. *Txnrd2*^{-/-} 0.07 ± 0.05 , apoptotic index). Furthermore the entire necrotic area of the whole tumour section, was estimated and expressed as % necrotic area. In *Txnrd2*-deficient tumours slightly larger necrotic areas were observed (3.8 ± 1.0 %) compared to wild-type tumours (1.8 ± 1.7 %). However, this difference was not significant. Comparable results were obtained analysing tumour sections of day 11 using the ApopTag® Peroxidase in situ Apoptosis Detection Kit (Millipore GmbH, Schwalbach/Ts., Germany). *Txnrd2*-deficient tumours showed similar or even slightly reduced numbers of apoptotic cells per visual field compared to wild-type tumours (data not shown).

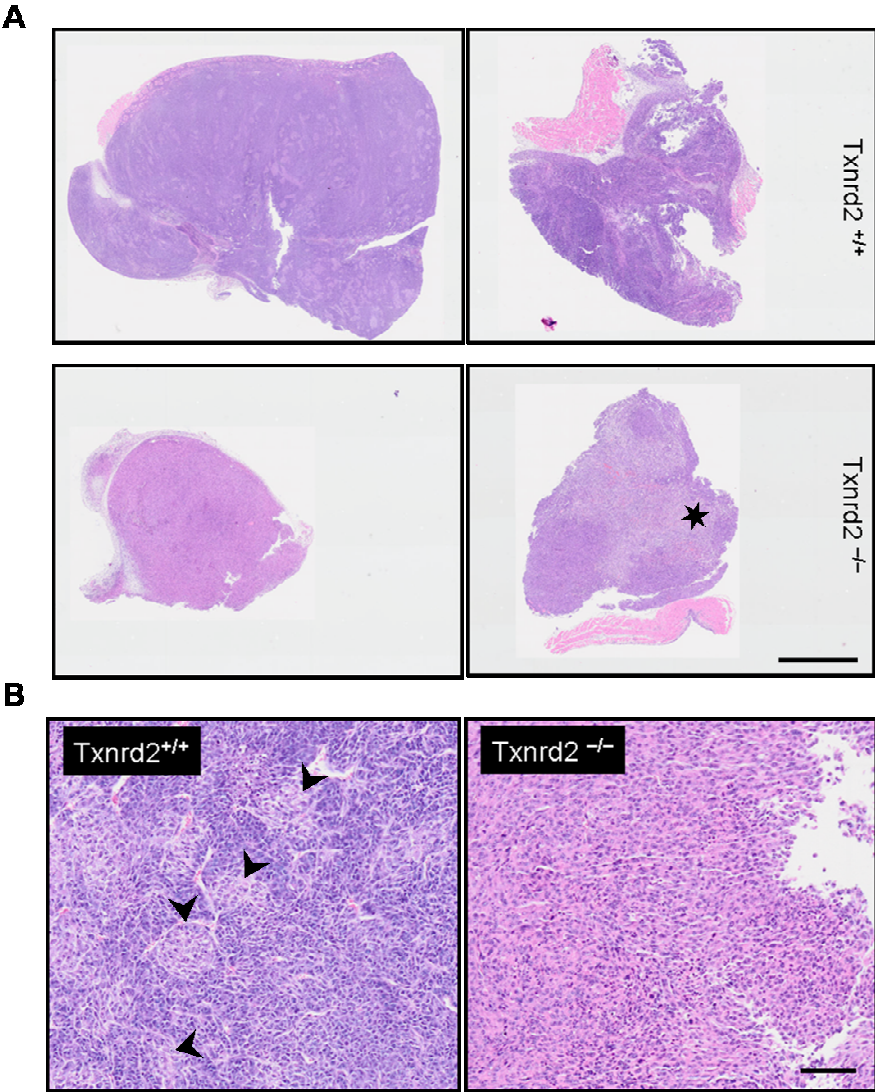


Figure 3-18: Morphological analysis of tumour sections

To investigate the morphological phenotype of tumours derived from wild-type cells and Txnrd2-deficient cells, tumour sections were stained with H&E and pictures of different magnifications (A - B) were taken (n=12 per group). Two representative images of Txnrd2 wild-type tumour sections (A, upper panel) and of Txnrd2-deficient tumour sections (A, lower panel) are displayed (scale bar = 2 mm). (B) High magnification images show different cellular organisation in the tumour tissue (scale bar = 100 µm). ★ necrotic area, ▼ nodular architecture

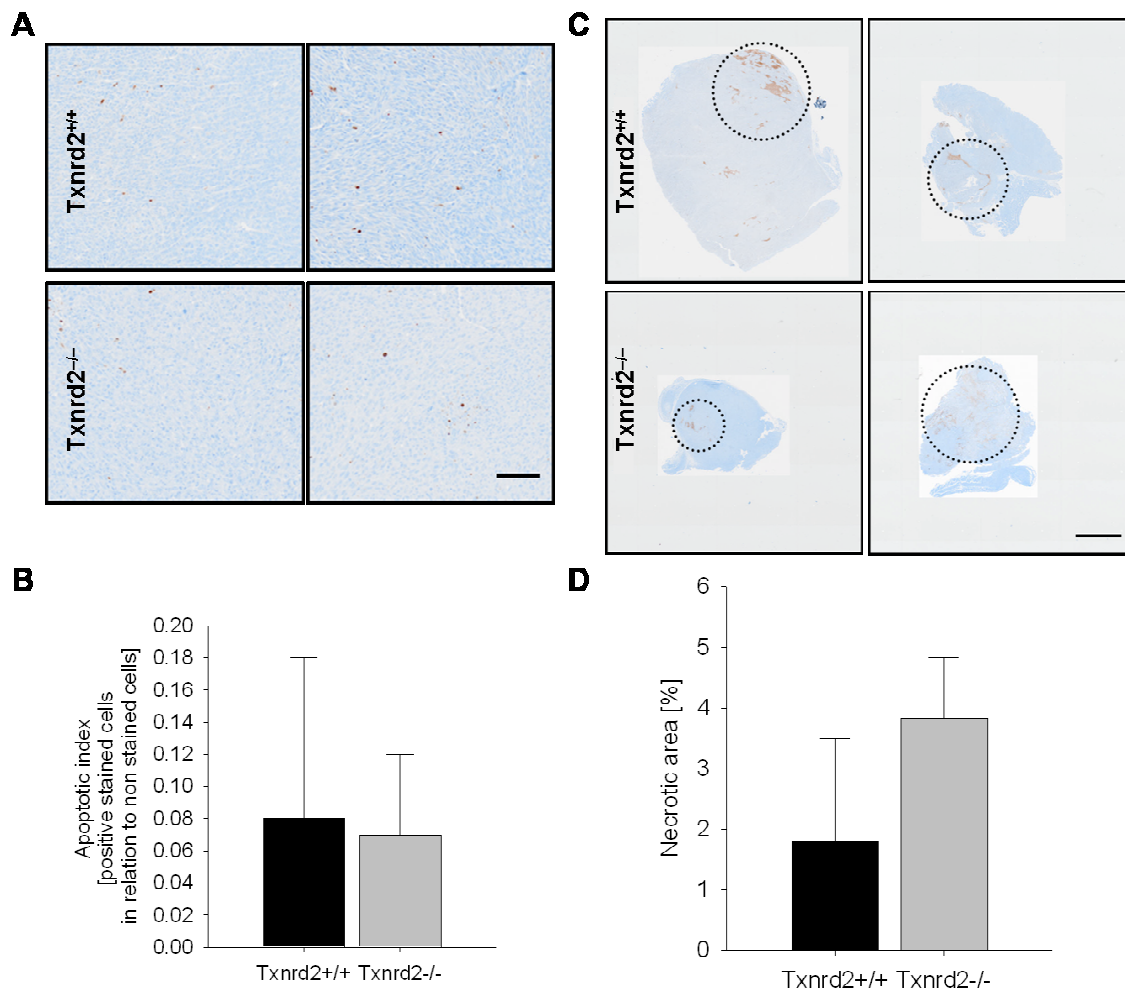


Figure 3-19: Number of cleaved-caspase 3 positive cells in tumour sections

To analyse the number of apoptotic cells and the ratio of apoptotic-necrotic area, paraffin sections of tumours were stained with an appropriate antibody for cleaved-caspase 3. (A) Number of cleaved-caspase 3 positive cells were analysed per visual field (scale bar = 100 μ m). (B) The apoptotic index was analysed from 12 tumour sections and mean \pm SD was pooled. (C) Size of necrotic area was determined and quantified in relation to the total tumour area (scale bar = 2 mm). (D) The necrotic area was analysed from 12 tumour sections and mean \pm SD are depicted.

3.3.4. Impaired tumour growth due to restricted proliferation of tumour cells

To analyse the number of proliferating tumour cells in the whole tumour tissue, sections from day 11 of tumour growth were stained for the proliferation marker Ki67 (Figure 3-20 A). Ki67-positive cells were counted per field and the ratio of proliferative and non-proliferative cells was expressed as proliferation index. With a proliferation index of 0.39 ± 0.2 Txnr2-deficient tumours showed a significant lower proliferation index than wild-type tumours with an index of 0.68 ± 0.2 (Figure 3-20 B). Investigation of the proliferation index in tumour sections on earlier time points did not reveal any difference between both groups (*Txnr2*^{+/+} 0.7 ± 0.1 vs. *Txnr2*^{-/-} 0.6 ± 0.2 ; images of day seven not shown), indicating that initial tumour

growth was not hampered by Txnrd2 deficiency. These results show that loss of Txnrd2 goes along with an impaired proliferation of tumour cells, in particular when tumours have reached a certain size (see also Figure 3-17 E).

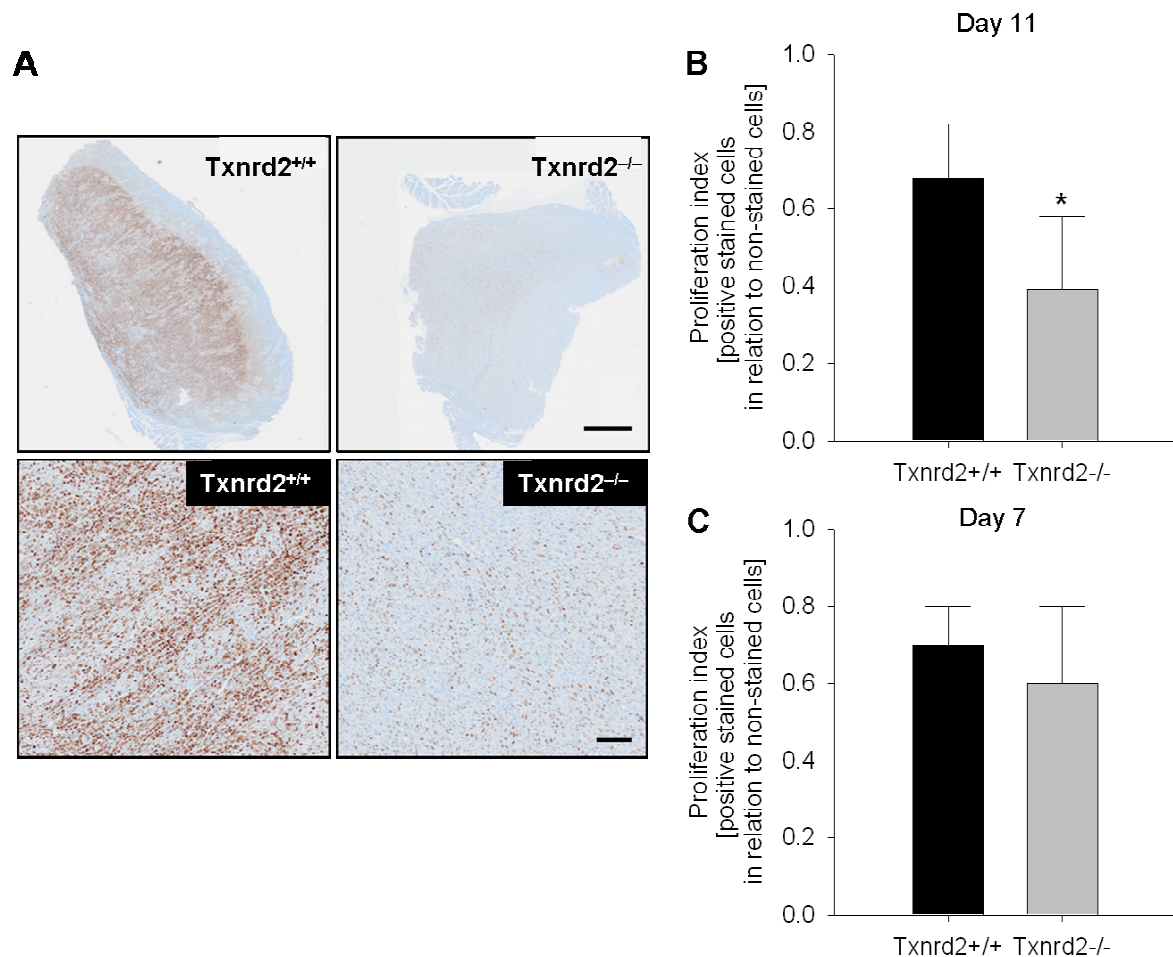


Figure 3-20: Analysis of proliferation in tumour sections

(A) To quantify proliferation in tumours paraffin sections were stained with Ki67-specific antibody. (A, upper panel, scale bar = 1 mm) Ki67-positive cells (brown) were analysed in relation to non-stained (blue) cells and quantified per visual field (A, lower panel, scale bar= 100 μ m). (B) Proliferation index was observed in 12 tumour sections of day 11 and mean \pm SD are depicted. * $p < 0.001$ (Student's t-test). (C) Proliferation index was observed in three tumour sections of day seven and mean \pm SD are depicted.

3.3.5. Loss of Txnrd2 delays the angiogenic switch

As rapid expansion of tumours beyond a given size requires a steady supply with sufficient amounts of oxygen, nutrients and growth factors, we next asked whether tumour vascularisation might be perturbed in Txnrd2 knockout tumours. During dissection of tumours at early time points after implantation, a macroscopically different appearance of the vascular network of tumours was detectable. Figure 3-21 A illustrates the vessel recruitment from the host towards the tumour tissue. Interestingly, in most cases vessels surrounding Txnrd2-

deficient tumours appeared less prominent compared to wild-type tumours at day three (Figure 3-21 A). Quantification of tumour vessels at day 11 of tumour growth using CD31-staining, however, revealed no difference in the vessel density (*Txnrd2*^{+/+} 345±18 vs. *Txnrd2*^{-/-} 329±8 vessels/mm²). Since growing tumours beyond a certain size supposedly trigger tumour angiogenesis, tumour sections from both groups were analysed for CD31 staining at the time point of same tumour size (Figure 3-21 B). Indeed, *Txnrd2*-deficient tumours revealed reduced vessel density per tumour (155±10) compared to wild-type tumours (219±29). The observed difference remained significant (n=3 per group). These data provided first evidence that the *Txnrd2* is essential for tumour cell proliferation and an important factor for tumour-associated angiogenesis.

To further complete these findings, the functionality of tumour vessels was studied using skinfold chambers in combination with intravital microscopy. Therefore, tumour cells were transplanted into the skinfold chamber of C57BL/6 mice and the progression of the vascular network was studied after injection of a FITC-dextran solution on days three, five, seven and 11. At early times (day three and five) the shape of the developing vascular network revealed already differences between wild-type and knockout tumours. Both groups of tumours recruited host vessels at the edges of the tumours. However, in *Txnrd2*-deficient tumours the first arising vessels appeared randomly distributed at the tumour surface, whereas in wild-type tumours the formation of a more organised vessel network was clearly detectable (Figure 3-22 A – B). Analysis of tumour vessels on day 11 revealed a dense vascular network with smaller and larger capillaries in wild-type tumours, which appeared less prominent in *Txnrd2*-deficient tumours (Figure 3-22 C).

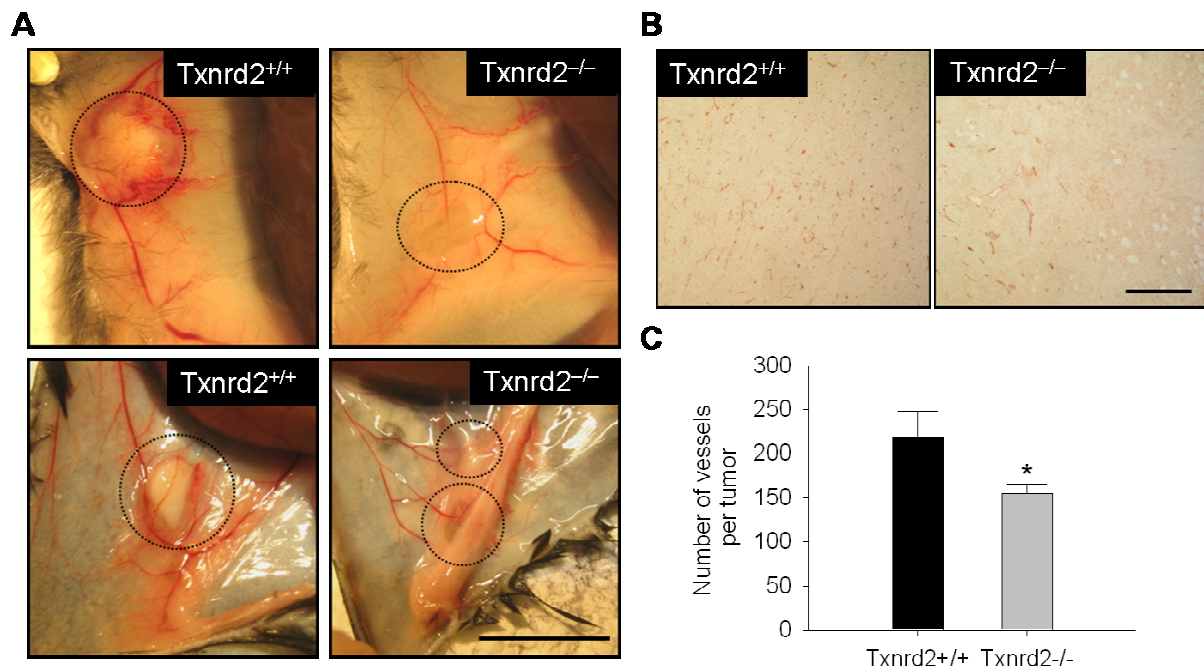


Figure 3-21: Analysis of tumour vascularisation

(A) During dissection of tumour samples at day three, a distinct vascular network surrounding the tumours was observed. Depicted are two images of representative tumour sections of each genotype from two independent experiments (B) Number of vessels per tumour were analysed using paraffin sections of tumours of equal size (*Txnrd2*^{+/+} day 7: 0.41 ± 0.04 g; *Txnrd2*^{-/-} day 10: 0.39 ± 0.11g). Vessels were stained with an antibody against CD31 and (C) the number of vessels were quantified in three tumour samples from each genotype. Mean values ± SD are depicted. *p<0.05 (Student's t-test)

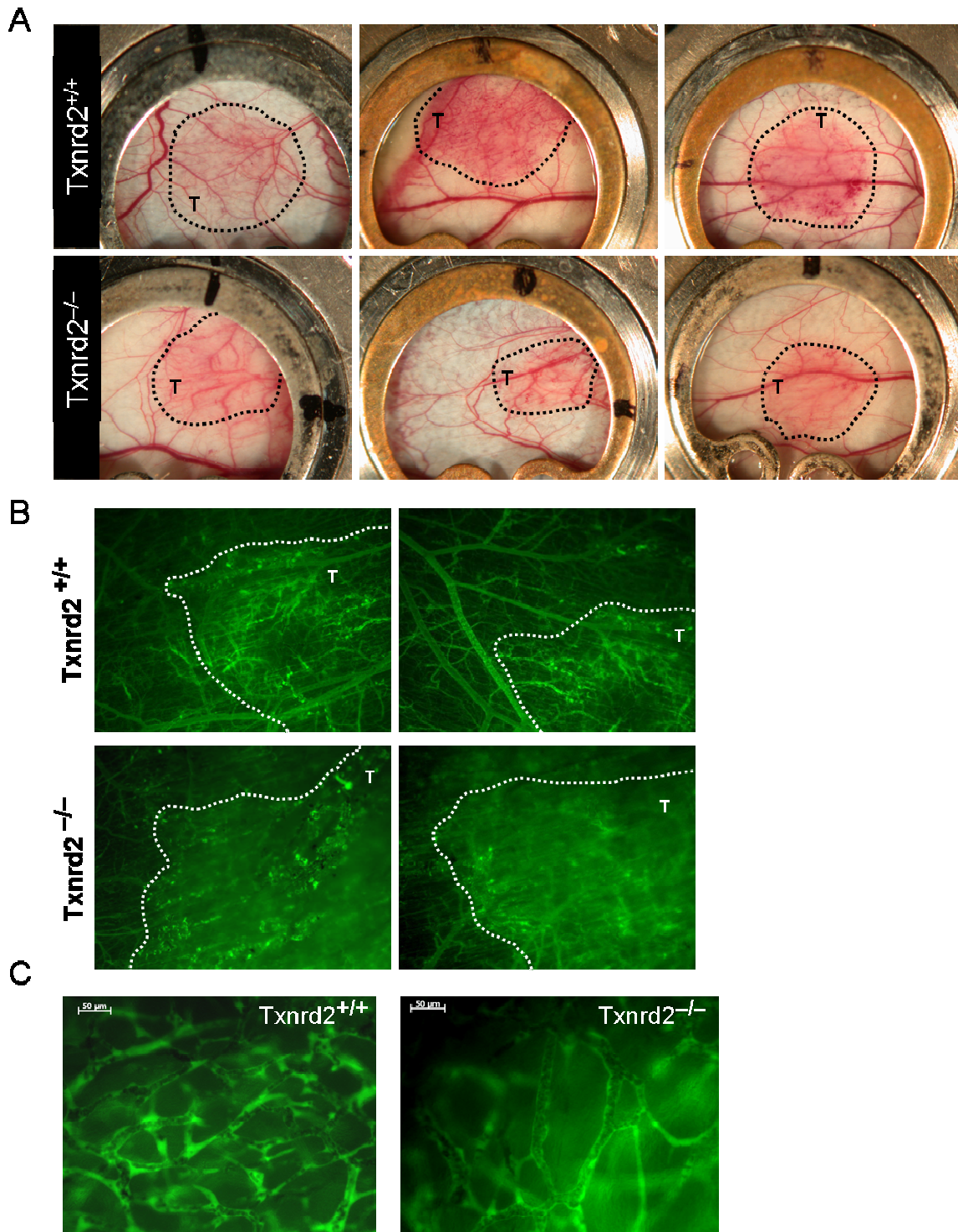


Figure 3-22: Intravital microscopy of tumor vessel network

Single-colony derived transformed fibroblasts were implanted into dorsal skinfold chambers and formation and functionality of developing vessels were studied over a period of 11 days every third day. (A) Images of the whole chamber windows are depicted from three representative tumours derived from wild-type cells (n=6) and Txnrd2-deficient cells (n=7) at day three. (B) Vessels were visualised by tail vein injection of FITC-dextran solution. Images are depicted from two representative wild-type (n=6) and Txnrd2-deficient (n=7) tumours at day three following implantation. (C) Final observations of tumour vascularisation at day 11 revealed different impressions of wild-type and Txnrd2-deficient tumours. One representative image is depicted (n=4). Scale bars = 50 μm . Dashed line defines tumour tissue, T = tumour

3.3.6. Investigation of angiogenic key players in Txnrd2-deficient tumours

To further investigate the underlying mechanisms that led to the altered vascularisation of Txnrd2-deficient tumours, the expression of key-players of the angiogenic cascade was analysed. It is well known that growing tumours, when they reach a size of more than one mm³, have to overcome hypoxic conditions and the deprivation of nutrients as well as the lack of disposal of waste products. An important and extensively studied crucial molecule, which is upregulated following hypoxia and starvation, is Hif-1 α . Tumour tissues of early (day three) and later (day six) time points of tumour growth were analysed for the expression of Hif-1 α by immunoblotting (Figure 3-23 A). Interestingly, a significant lower expression of Hif-1 α protein could be observed in Txnrd2-deficient tumours (day three: 0.4 \pm 0.0; day six: 0.4 \pm 0.1) as compared to tumours expressing Txnrd2 (day three: 1.0 \pm 0.0; day six: 1.0 \pm 0.0) at both points time (Figure 3-23 B).

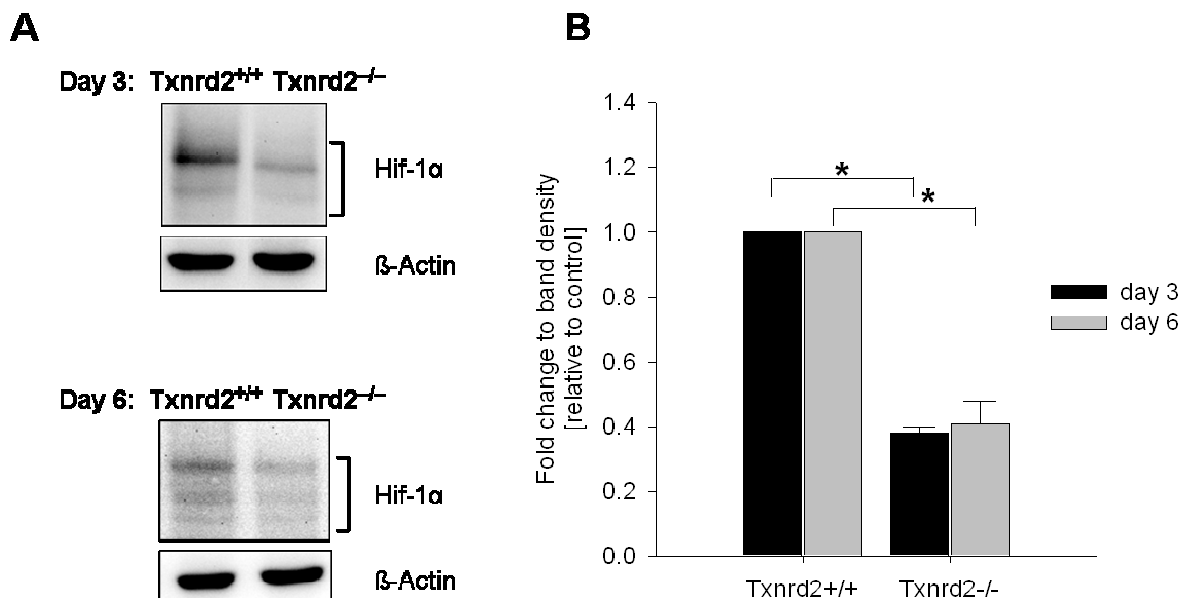


Figure 3-23: Analysis of Hif-1 α in tumour tissue

(A) Protein expression of Hif-1 α in tumours was observed using immunoblotting on day three and day six of tumour growth. Equal loading was confirmed by β -actin immunoblotting. (B) Quantification was done by analysis of three tumours derived from wild-type cells (control) compared to Txnrd2-deficient cells. Depicted are mean values \pm SD. * p <0.01 (Paired t-test).

Hif-1 α is described as a transcription factor that regulates energy metabolism of cells by activating a multitude of downstream target genes which are important for cellular adaptation to restricted oxygen and nutrient availability. The vascular endothelial growth factor (VEGF) is one of the most extensively studied and well known target genes of Hif-1 α . As VEGF is crucial for vasculogenesis, angiogenesis and in particular required for tumour vessel development, it was interesting to study the expression of VEGF in wild-type and Txnrd2-

knockout tumours. Therefore, tumour tissue of day three and six was analysed using immunoblotting. Consistent with the lowered Hif-1 α expression, VEGF was significantly reduced in *Txnrd2*-deficient tumours at day three (0.2 ± 0.2) compared to wild-type tumours (1.0 ± 0.0) (Figure 3-24 A). On day six of tumour growth *Txnrd2*-deficient tumours showed even slightly reduced expression of VEGF compared to wild-type tumours (*Txnrd2*^{+/+}: 1.0 ± 0.0 vs. *Txnrd2*^{-/-}: 0.6 ± 0.2). These data were confirmed by an additional assay using VEGF ELISA on the same days (Figure 3-24 B). Again, *Txnrd2*-deficient tumours showed decreased levels of VEGF (day three: 0.19 ± 0.06 pg/ μ g protein; day six: 0.09 ± 0.05 pg/ μ g protein) compared to wild-type tumours (day three: 0.48 ± 0.24 pg/ μ g protein, day six: 0.12 ± 0.05 pg/ μ g protein). However, the differences were not significant.

In summary, loss of *Txnrd2* in tumour cells is associated with a reduced expression of the transcription factor Hif-1 α and its target gene VEGF. Lack of VEGF is considered as an important cause for a delayed angiogenic switch as well as a reduced tumour vascularisation.

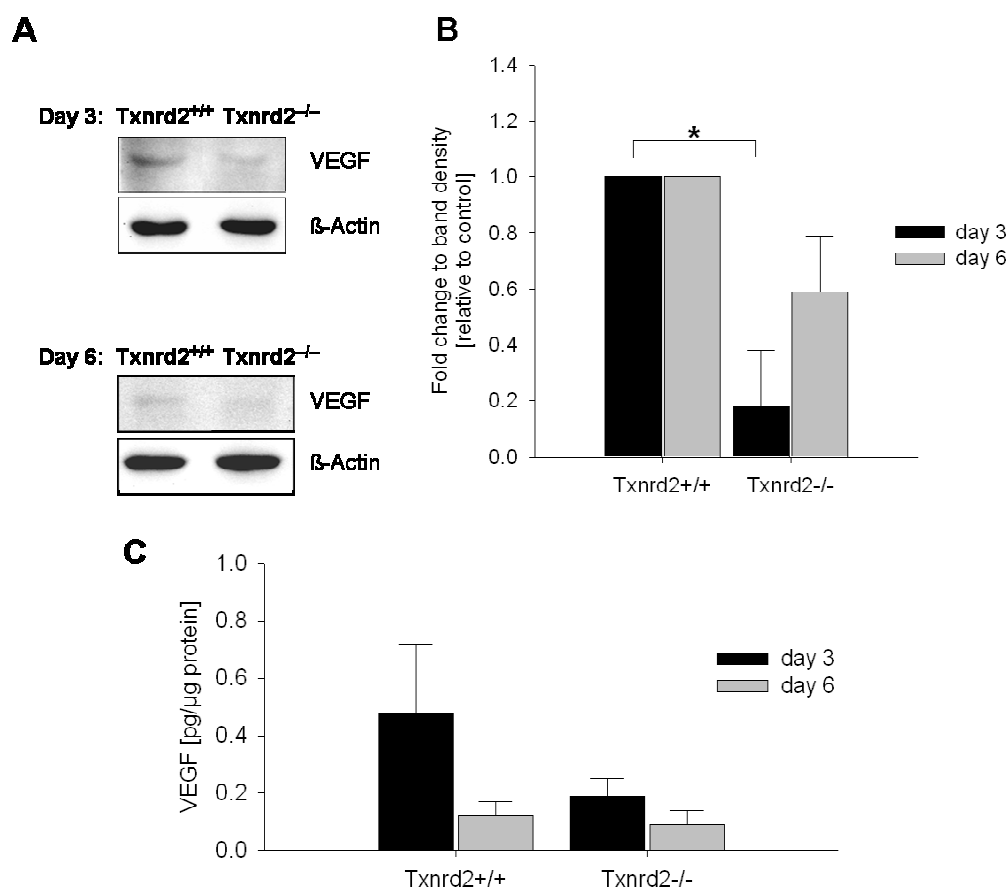


Figure 3-24: Quantification of VEGF in tumour samples

(A) VEGF expression in whole tumours was studied using immunoblotting on day three and day six of tumour growth. β -actin served as loading control. (B) Quantification was done with analysis of three tumours per group. Depicted are mean values \pm SD. * $p < 0.01$ (Paired t-test). (C) The amount of VEGF was further analysed by mouse VEGF immunoassay (ELISA) using whole tumour tissue lysates. Quantification was performed using three different tumour samples of each genotype at day three and at day six. Depicted are mean values \pm SD.

The regulation of the transcription factor Hif-1 α is highly complex and far from being understood. Indeed, the increase in Hif-1 α levels may occur either on the transcriptional, translational or posttranslational level. It is well known that a group of enzymes regulate the stabilisation of Hif-1 α protein. Mainly depending on the availability of oxygen prolyl hydroxylases (PHDs) hydroxylate Hif-1 α , thereby marking the protein for proteasomal degradation. To investigate whether the reduced amounts of Hif-1 α protein in *Txnrd2*-deficient tumours might be due to increased hydroxylation and thus proteasomal degradation, the expression of the three PHDs (PHD1-3) was investigated in tumour tissues by semi-quantitative PCR and immunoblotting (Figure 3-25). While *PHD1* was not detectable by semi-quantitative PCR (data not shown), semi-quantitative PCR did not show differences in the expression levels of *PHD2* and *PHD3* (Figure 3-25 A). Since PHD2 is considered to be the main regulator of Hif-1 α levels, and thus of great importance in tumour vessel recruitment, PHD2 expression was additionally investigated on protein level (Figure 3-25 B). Yet, no differences in PHD2 protein levels were detectable between wild-type (1.0 \pm 0.0) and *Txnrd2*-deficient tumours (1.1 \pm 0.4).

While these observations suggest that the reduced Hif-1 α protein levels in *Txnrd2*-deficient tumours might not be due to changes in hydroxylation by PHDs, the enzymatic activity of PHD2 remains to be investigated.

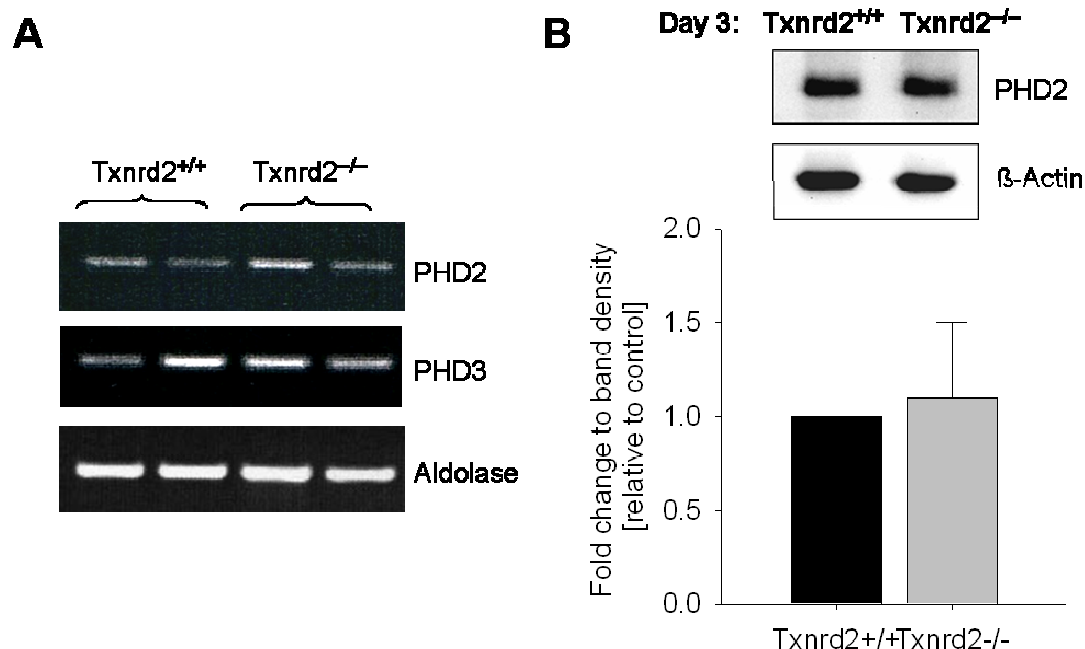


Figure 3-25: Quantification of PHD2 in tumours on day three and 11

(A) Expression of *PHD2* and *PHD3* was analysed by semi-quantitative PCR. *Aldolase* served as control. (B) Protein expression of PHD2 in tumour tissue was analysed by immunoblotting on day three of tumour growth. Equal loading was confirmed by β -actin expression. Quantification was performed by analysis of three tumours derived from wild-type cells compared to *Txnrd2*-deficient cells. Depicted are mean values \pm SD.

3.3.7. Starved Txnrd2-deficient cells express decreased Hif-1 α levels

To further investigate the underlying mechanisms of reduced Hif-1 α protein levels in Txnrd2-deficient tumours, *in vitro* experiments were performed using transformed single-cell colony derived wild-type and Txnrd2-deficient fibroblasts. Cells were exposed to starvation, as this condition appears typically in tumours at a size of more than one mm³, when diffusion is not sufficient to supply enough energy substrates. The amount of Hif-1 α was analysed using immunoblotting. Under baseline cell culture conditions Hif-1 α was barely detectable in both cell lines (*Txnrd2*^{+/+}:1.0 \pm 0.0 vs. *Txnrd2*^{-/-}:0.8 \pm 0.2) (Figure 3-26). Following starvation Hif-1 α expression strongly increased in wild-type cells, but not in Txnrd2-deficient cells (*Txnrd2*^{+/+}:71 \pm 68 vs. *Txnrd2*^{-/-}:1 \pm 0). These findings support our hypothesis that the loss of Txnrd2 impairs Hif-1 α signalling.

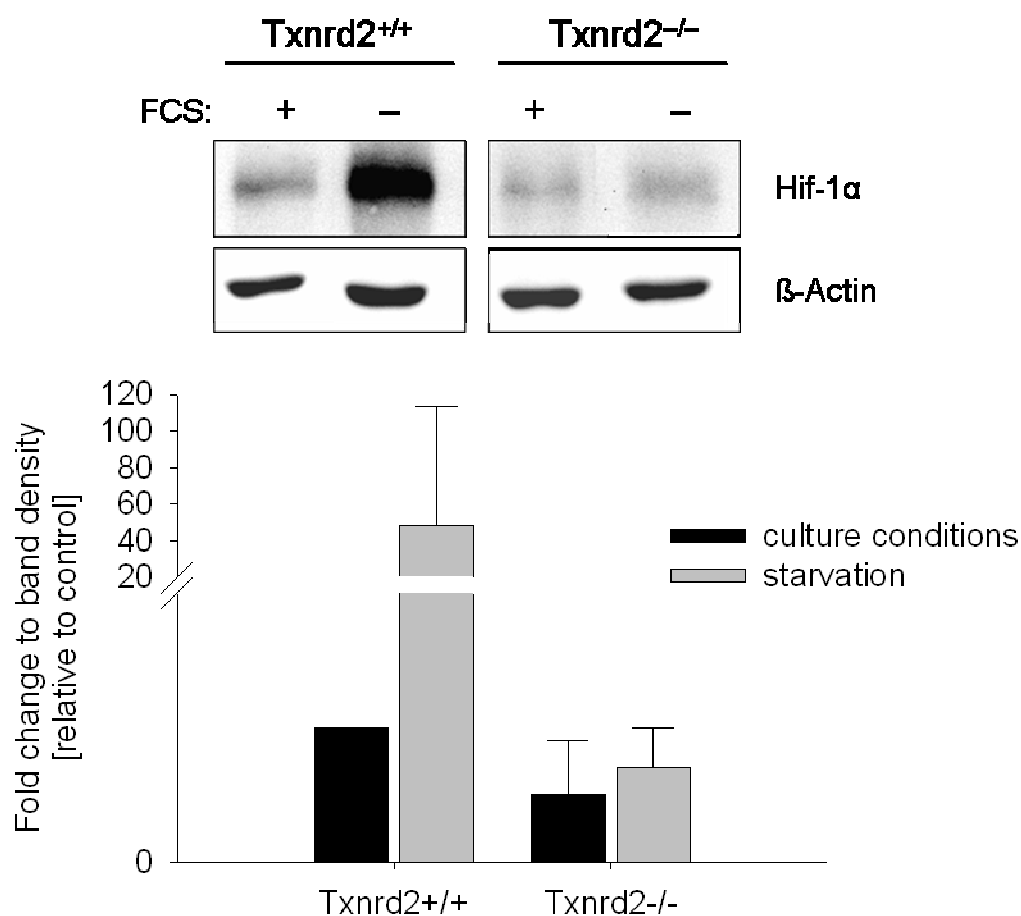


Figure 3-26: Expression of Hif-1 α in Txnrd2-deficient tumour cells

Wild-type and Txnrd2 knockout transformed single-cell derived fibroblasts were cultured under baseline cell culture conditions and exposed to starvation for 4 h. Total cell lysates were analysed for Hif-1 α by immunoblotting. β -actin served as loading control. Txnrd2 wild-type cells under control conditions were considered as one and change of band density was analysed relative to control. The image depicts one representative immunoblot. Bars represent mean values \pm SD from three independent experiments. *P* values > 0.05.

Next, *Hif-1α* expression was analysed on the mRNA level under baseline cell culture conditions as well as under starvation (Figure 3-27). Interestingly, under baseline cell culture conditions *Hif-1α* mRNA levels of both cell lines were similar (*Txnrd2*^{+/+}: 1.0±0.0 vs. *Txnrd2*^{-/-}: 1.1±0.3), whereas *Txnrd2*-deficient cells failed to induce *Hif-1α* mRNA levels under starvation conditions (*Txnrd2*^{+/+}: 1.9±0.8 vs. *Txnrd2*^{-/-}: 0.9±0.3). Investigation of PHD2 expression by immunoblotting did not reveal major differences between both cell lines, neither under baseline cell culture conditions (*Txnrd2*^{+/+}: 1.0±0.0 vs. *Txnrd2*^{-/-}: 2.0±1.1) nor under starvation conditions (*Txnrd2*^{+/+}: 1.6±0.9 vs. *Txnrd2*^{-/-}: 1.7±0.6) (Figure 3-28).

These findings tentatively support the idea that the reduced *Hif-1α* levels in response to *Txnrd2* deletion are caused by changes on transcriptional level with subsequent alterations in protein stabilisation.

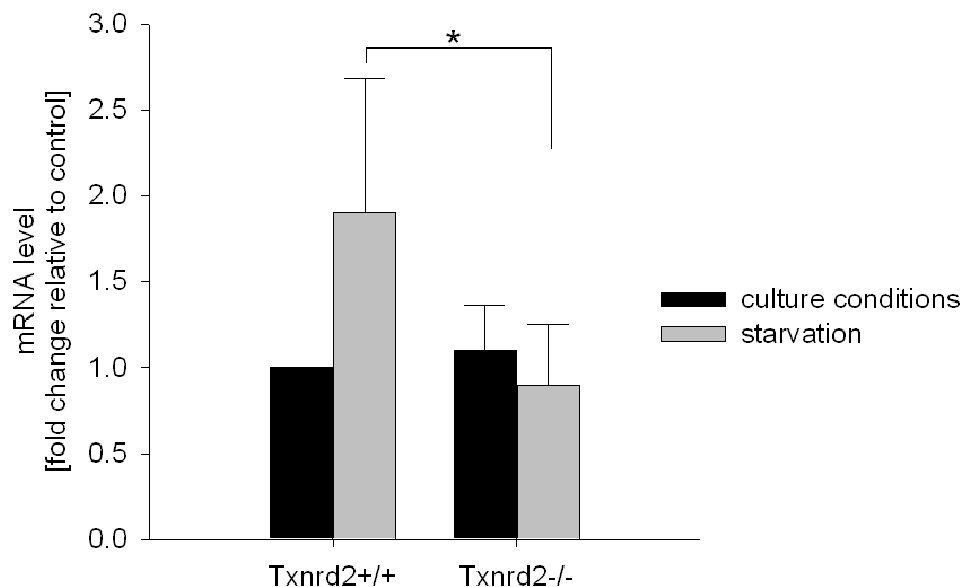


Figure 3-27: Quantitative analysis of *Hif-1α* mRNA-level

Transformed single-cell derived fibroblasts of both genotypes were cultured under baseline cell culture conditions and exposed to starvation for 4 h. *Hif-1α* expression was analysed using quantitative real-time PCR. The image summarises five independent measurements. Data are shown as mean values ± SD. Wild-type cells were considered as control and defined as one. Normalisation was performed using primers specific for *actin*. *p<0.05 (Student's t-test)

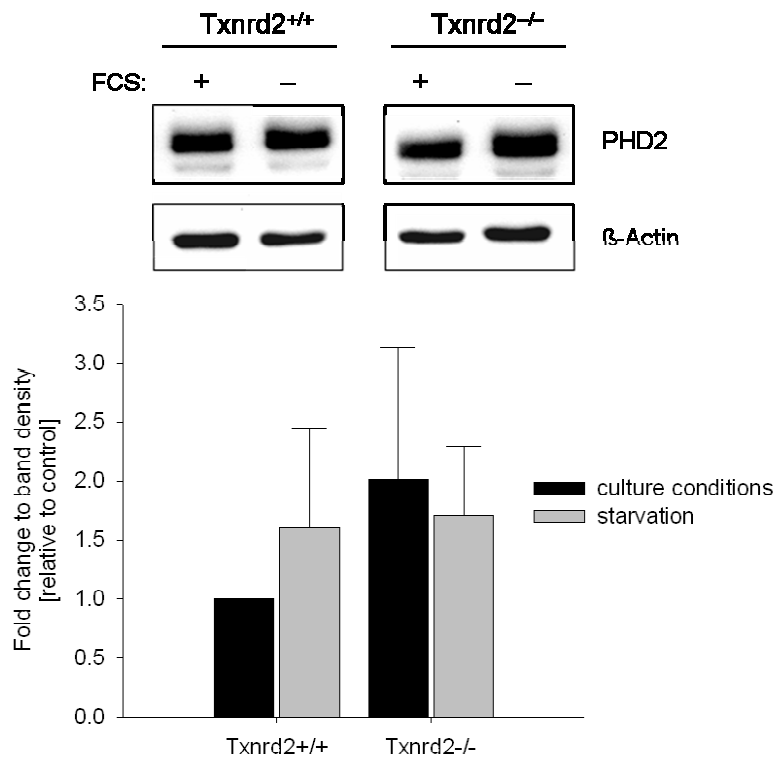


Figure 3-28: Analysis of PHD2 in transformed cells

Expression of PHD2 in transformed fibroblasts under baseline cell culture conditions and under starvation was analysed by immunoblotting. Depicted is one representative blot of three independent experiments. Bars represent pooled mean values \pm SD. β -actin served as control.

3.3.8. Hif-1 α translation is altered in Txnrd2-deficient cells

Another possible reason for the altered Hif-1 α expression might be changes in translation. A previous study demonstrated that the thioredoxin-dependent system exerts an influence on the cap-dependent translation of Hif-1 α ³⁵⁹. In light of the findings of Zhou *et al.* we aimed to investigate the possible pathways that are involved in the regulation of Hif-1 α translation. The PI3K/Akt-dependent signalling pathway is involved in the phosphorylation of components required for cap-dependent translation thereby enhancing Hif-1 α accumulation.

Therefore, the phosphorylation of the serine/threonine protein kinase Akt was investigated in immortalised fibroblasts by immunoblotting (Figure 3-29). Indeed, there was a difference in the phosphorylation of Akt at Ser473 between wild-type and Txnrd2-deficient cells. Even under baseline cell culture conditions the phosphorylation of Akt was decreased in Txnrd2-deficient fibroblasts (*Txnrd2*^{+/+}: 1.0 \pm 0.0 vs. *Txnrd2*^{-/-} 0.6 \pm 0.2). This impairment appeared much stronger under starvation (*Txnrd2*^{+/+}: 0.7 \pm 0.1 vs. *Txnrd2*^{-/-} 0.2 \pm 0.2).

These findings show that the decreased amount of Hif-1 α in Txnrd2-deficient cells and tumours might be due to effects on Hif-1 α transcription as well as translation and subsequent protein stabilisation.

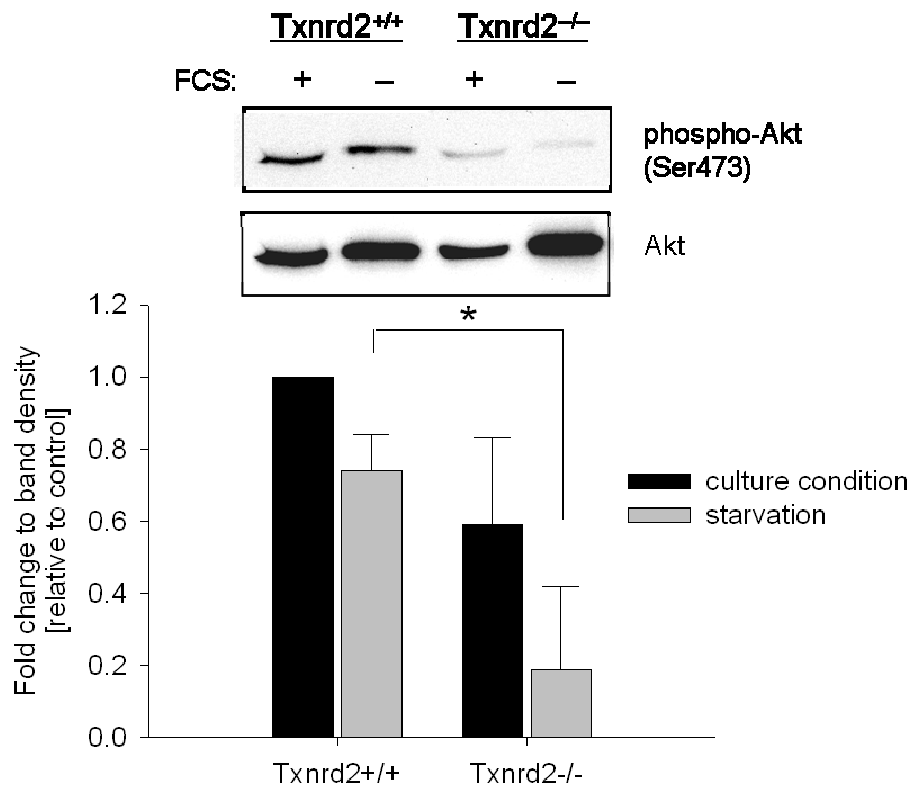


Figure 3-29: Phosphorylation of Akt

Immortalised wild-type and Txnrd2-deficient cells were exposed to starvation for 2 h. Phosphorylation of Akt at Ser473 was investigated by immunoblotting. Equal loading was confirmed by immunoblotting total Akt. One representative blot is depicted and mean values \pm SD from three independent experiments are shown. Phosphorylation of Akt in wild-type cells under baseline cell culture condition severed as control and was considered as one. * $p < 0.05$ (Student's t-test)

3.3.9. Txnrd2-null tumours are susceptible to pharmacological GSH-inhibition

Immortalised Txnrd2-deficient fibroblasts showed higher GR activity and were susceptible to BSO-mediated GSH-depletion. Further *in vitro* experiments had indicated that also transformed single-colony derived Txnrd2-deficient cells were highly susceptible to BSO-mediated cell death. Previous work in our laboratory demonstrated that growth of Txnrd1-deficient tumours was dependent on an intact GSH-dependent pathway¹⁹⁷. Although, Txnrd1-deficient tumour cells showed higher GSH content and GR activity, they were highly sensitive to GSH-depletion induced cell death. Txnrd1-null tumours showed no differences in progression and sizes compared to control tumours, but were highly susceptible to pharmacological inhibition of GSH whereas wild-type tumours were not. Thus the question raised if additional pharmacological intervention of the GSH-dependent pathway in Txnrd2-null tumours might be a further therapeutically efficient way to treat cancer.

To test GSH-dependency *in vivo*, 4×10^6 transformed single-colony derived Txnrd2-deficient cells were implanted subcutaneously into the flanks of C57BL/6 mice (n=8 per group). Tumour cells were allowed to settle until small tumours were palpable around day three. Starting at day three the tumour-bearing mice were treated with BSO (20 mM) via drinking water until day 10 of tumour growth. Mice were then sacrificed and tumours were collected (Figure 3-30 A). Analysis of tumour mass revealed a significant difference between the control group (0.84 ± 0.27 g) and the BSO treated group (0.52 ± 0.14 g) (Figure 3-30 B – C). Notably, this reduction in tumour size was about 38% in addition to the already observed reduction of tumour size due to Txnrd2-deletion.

To proof, whether the application of BSO via drinking water efficiently inhibits GSH de novo synthesis reduced (GSH) and oxidised (GSSG) was estimated by HPLC in tumour tissue (Figure 3-30 D – E). We observed only a marginal difference between wild-type and Txnrd2-null tumors for GSH (0.011 ± 0.004 $\mu\text{mol}/\mu\text{g}$ protein vs. 0.015 ± 0.003 $\mu\text{mol}/\mu\text{g}$ protein, Figure 3-30 D) as well as GSSG (0.002 ± 0.001 $\mu\text{mol}/\mu\text{g}$ protein vs. 0.003 ± 0.001 $\mu\text{mol}/\mu\text{g}$ protein, Figure 30 E). However, Txnrd2-deficient tumours treated with BSO showed a significant reduction in GSH (0.0007 ± 0.0002 $\mu\text{mol}/\mu\text{g}$ protein, Figure 3-30 D) and GSSG levels (0.0008 ± 0.0003 $\mu\text{mol}/\mu\text{g}$ protein, Figure 3-30 E) compared to the two other groups. These results confirm that BSO treatment efficiently depletes glutathione *in vivo*. Previous data from our laboratory have demonstrated that BSO treatment in wild-type tumour-bearing mice had no effect on tumour size¹⁹⁷.

In summary, the inhibition of the mitochondrial Txnrd in combination with depletion of glutathione had a profound additive effect on tumour growth inhibition.

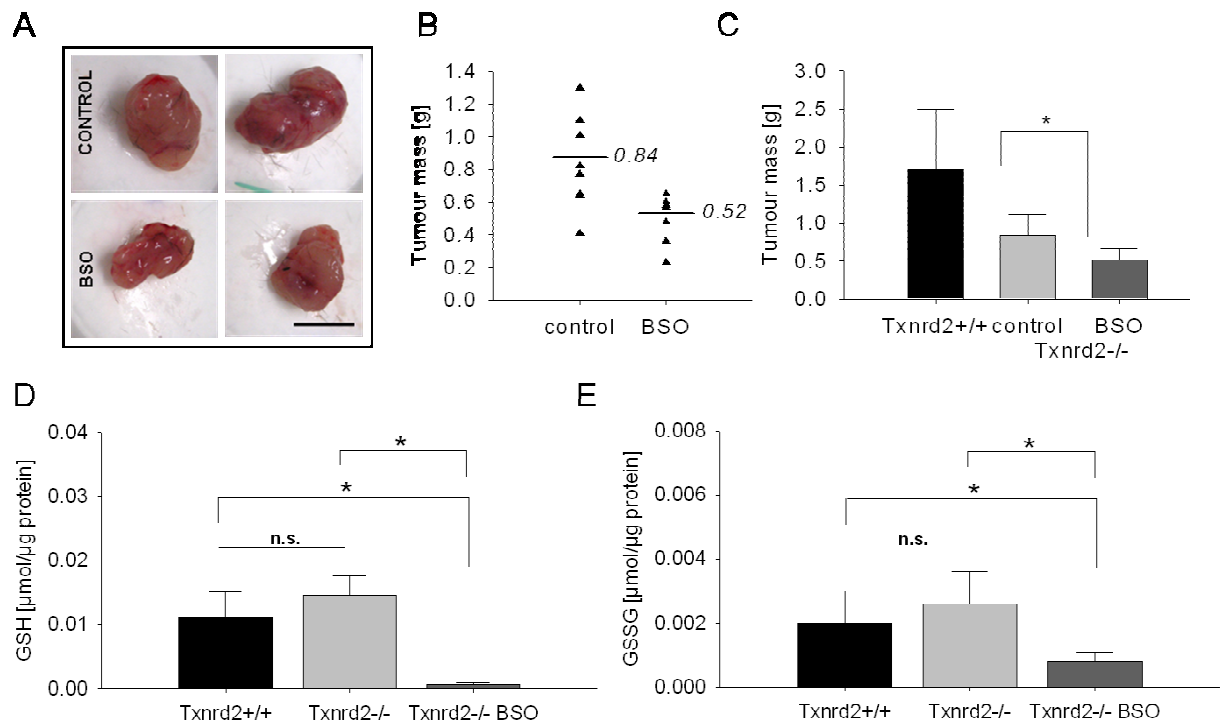


Figure 3-30: Inhibition of GSH synthesis further limits tumour growth of Txnrd2-null tumours

(A) Txnrd2-deficient tumour cells were implanted subcutaneously in C57BL/6 mice and allowed to settle for three days. Starting at day three, mice received drinking water containing BSO (20 mM). At day 10 of tumour growth mice were sacrificed and tumour mass and volume were analysed. (B) Txnrd2-deficient tumours were susceptible to the depletion of GSH synthesis compared to the untreated control group. Line and numbers represent mean values of each group. (C) Mean values \pm SD are shown in the bar chart ($n=8$ tumours each group). (D) Reduced glutathione (GSH) and (E) oxidised glutathione (GSSG) was estimated in tumours collected at day six by HPLC. The bar charts represent mean values \pm SD ($n=8$ tumours). * $p<0.05$ (Student's t-test)

3.4. Txnrd2-deficiency modifies function of endothelial cells

The findings of the present work support the assumption that Txnrd2 may be directly or indirectly involved in Hif-1 α signalling in tumour cells. Several studies already demonstrated that Trx2 and Txnrd2 are of importance for endothelial cell function^{65, 68, 212, 354}. Hence, the last part of the present work aimed to investigate whether Txnrd2 has an impact on endothelial cell function.

3.4.1. Generation and characterisation of Txnrd2-deficient eEPCs

To investigate the impact of Txnrd2 on endothelial cell proliferation which is considered essential for angiogenesis, we established wild-type and Txnrd2-deficient endothelial cell lines. Therefore, embryonic endothelial progenitor cells (eEPCs) were chosen as an *in vitro* model and isolated from pregnant *Txnrd2*^{+/-} mice at embryonic day E7.75, as described by Hatzopoulos¹³⁴ (Figure 3-31 A). The deletion of *Txnrd2* was confirmed by semi-quantitative PCR (Figure 3-31 B). Then, it was analysed whether impaired proliferation, as already observed for primary Txnrd2-deficient fibroblasts, may also occur in Txnrd2-deficient eEPCs. We observed just a slightly decreased proliferation rate of Txnrd2-deficient eEPCs compared to the wild-type cells (Figure 3-31 C).

Endothelial progenitor cells are known to have the capacity to form capillary like structures in extra-cellular matrix *in vitro*^{154, 220, 265}. Therefore, we studied the angiogenic competence of our isolated eEPCs in the tube formation assay using Matrigel®^{7, 12, 205, 348}. Cells were embedded in Matrigel® and the formation of sprouts was monitored over 24 h. Indeed, we observed a partially impaired sprouting of Txnrd2-deficient eEPCs when comparing the number of branching points per visual field between the groups (*Txnrd2*^{+/+} 16 \pm 6 vs. *Txnrd2*^{-/-} 3 \pm 3) (Figure 3-32 A, D). Stable re-expression of an N-terminally FLAG-tagged full-length Txnrd2 in Txnrd2-deficient eEPCs by electroporation (add-back) (Figure 3-32 B), was able to rescue the impaired sprouting capacity compared to control cells carrying an empty vector (mock) (mock: 6 \pm 3 vs. add-back: 14 \pm 5) (Figure 3-32 C, E). These findings suggest, that Txnrd2 deficiency has an adverse effect on angiogenic function of endothelial progenitor cells *in vitro*, evidenced by marginally reduced proliferation and limited angiogenic capacity of Txnrd2-deficient eEPCs.

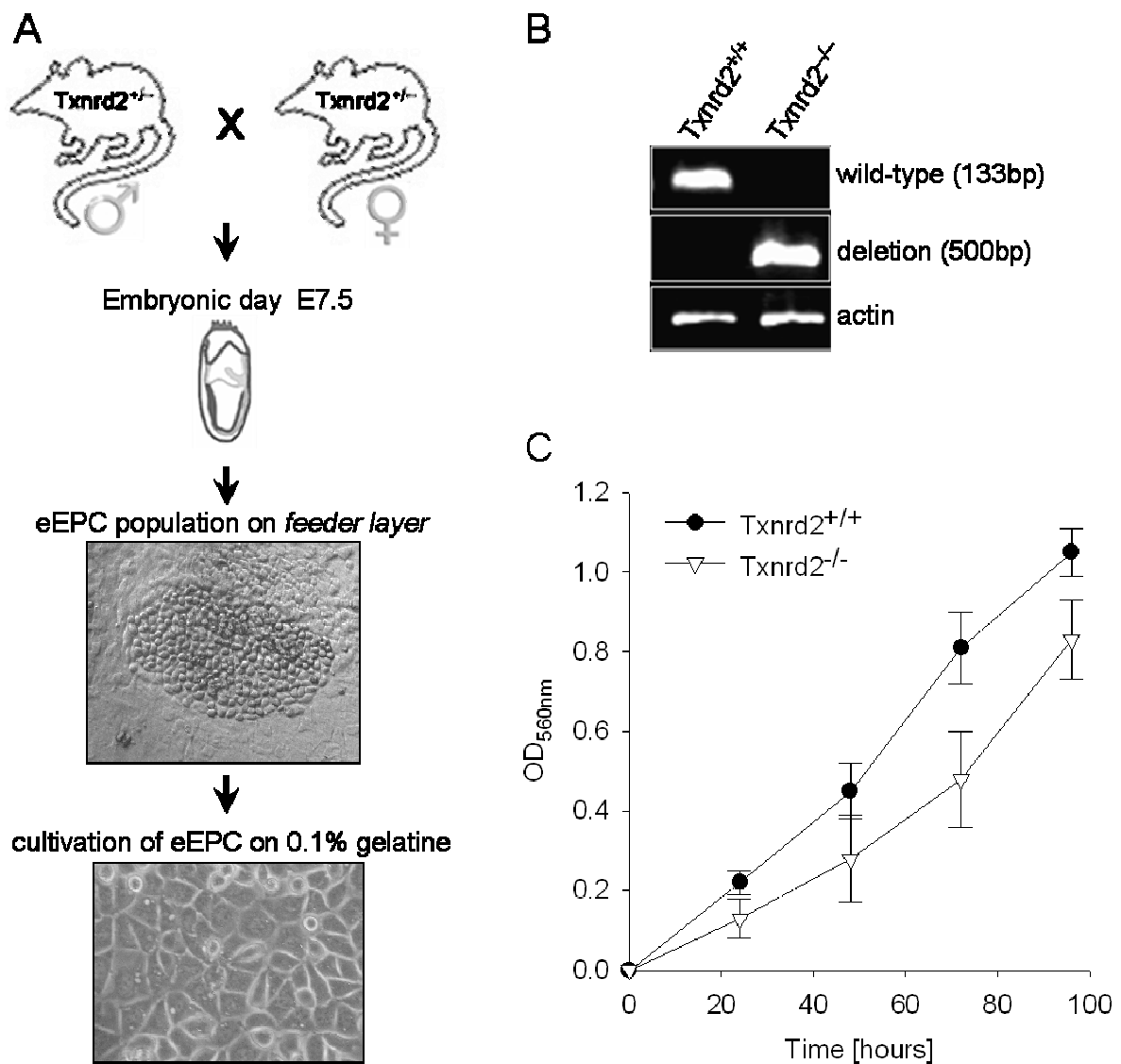


Figure 3-31: Generation of eEPC Txnrd2 wild-type and Txnrd2-deficient cell lines

(A) The isolation of eEPCs from heterozygous Txnrd2 breedings was performed according to Hatzopoulos and as described in chapter 2.2.1.1. (B) Expression of *Txnrd2* was analysed on the genome level using semi-quantitative PCR. *Actin* served as control. (C) Proliferation of wild-type and Txnrd2-deficient eEPCs was determined by the MTT assay carried out in 96-well plates. The chart shows pooled mean values \pm SD from three independent experiments. *P* values > 0.05.

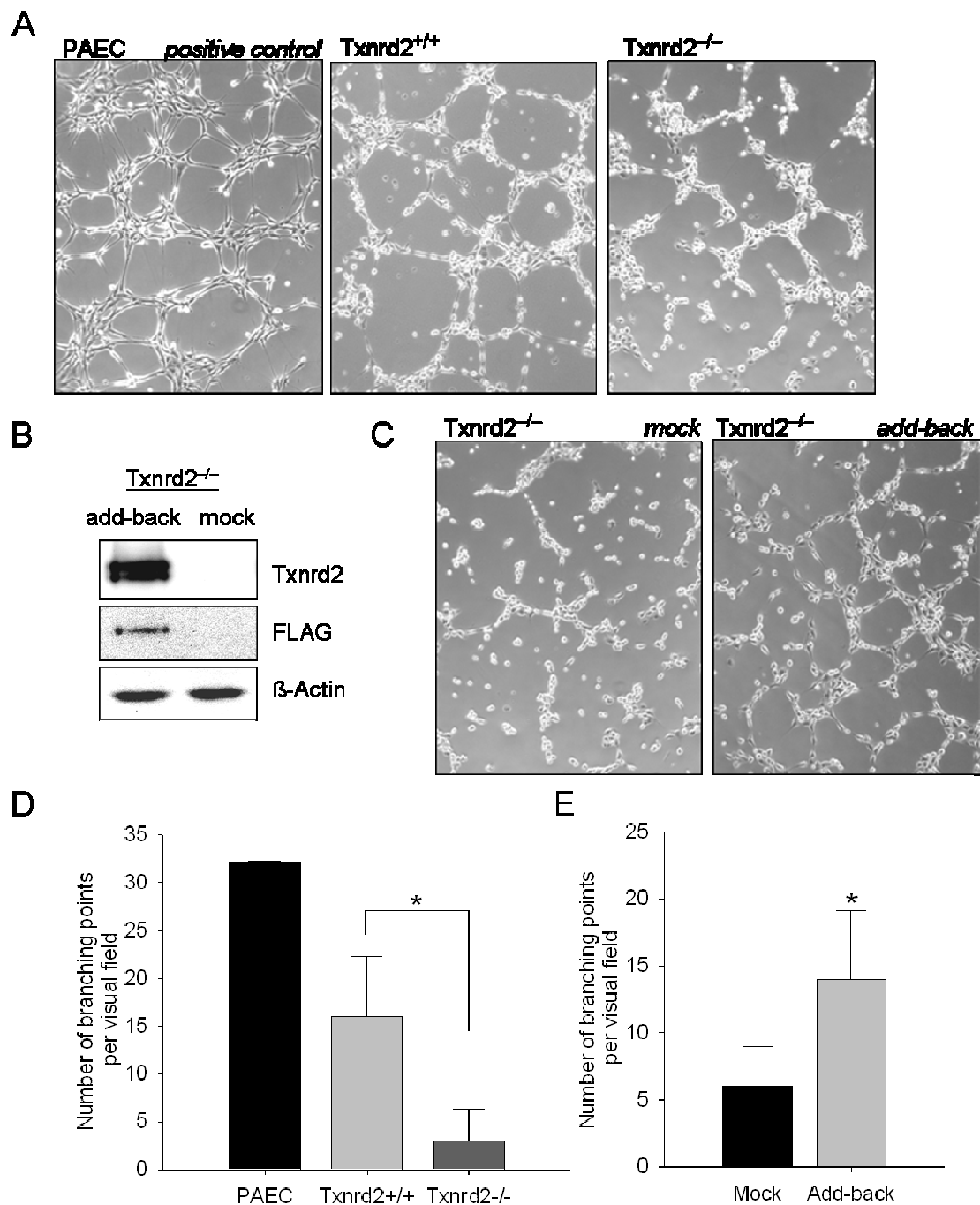


Figure 3-32: Limited pro-angiogenic potential of Txnrd2-deficient eEPCs

To investigate the ability of eEPCs to form three-dimensional vessels (sprouting), the *in vitro* tube formation assay was performed using the extracellular matrix Matrigel®. (A) Txnrd2 wild-type and Txnrd2-deficient eEPCs as well as PAEC (positive control) were plated on the extracellular matrix and allowed to settle for 30 min. Sprouting was observed over 24 h and pictures were taken every 4 hours. The images were taken after 24 h and are representative for four independent experiments. (B) To investigate if the observed phenotype is indeed due to Txnrd2-deficiency, Txnrd2-null cells were stably transfected with a vector carrying full-length Txnrd2 (add-back) and an empty vector (Mock). Txnrd2 expression was confirmed by immunoblotting and β -actin served as control. (C) The tube formation assay was performed as described above. (D) Quantitative analysis of branching points revealed that the sprouting of Txnrd2-deficient eEPCs is highly impaired. Depicted are mean values \pm SD from four independent experiments with $*p < 0.05$ (Student's t-test). (E) Reconstitution of Txnrd2 expression in Txnrd2-deficient eEPCs restored the capacity of the cells to form sprouts. Depicted are mean values \pm SD from four independent experiments with $*p < 0.05$ (paired t-test).

3.4.2. Tamoxifen-inducible endothelial-specific *Txnrd2* knockout mice

We could show that *Txnrd2* is crucial for the progression of tumour growth and the development of a fully functional tumour vascular network. Furthermore, *Txnrd2* seemed to play a pivotal autocrine role for endothelial cell angiogenic function. To investigate the biological significance of *Txnrd2* expression by vascular endothelial cells *in vivo*, tamoxifen-inducible VE-cadherin-Cre (Cre-VE-CadherinER) transgenic mice (a kind gift of Prof. Dr. Ralf Adams, Max Planck Institute for Molecular Biomedicine, Münster, Germany) were crossed to *Txnrd2*^{fl/fl} mice to generate *Txnrd2*^{wt/fl-Tg[Cre-VE-CadherinER]} mice. These were further crossed with *Txnrd2*^{fl/fl} mice to obtain *Txnrd2*^{fl/fl-Tg[Cre-VE-CadherinER]} mice (Figure 3-33). The Cre-estrogen receptor fusion protein (CreERT2) is sequestered in the cytoplasm by heat shock protein 90 (Hsp90). Only upon application of tamoxifen Cre protein is liberated from the complex and translocates to the nucleus where Cre-mediated recombination leads to endothelium-specific deletion of the *Txnrd2*. Tamoxifen application was performed orally by gavage at four consecutive days followed by a final fifth oral application one week later. Following eight weeks from the last tamoxifen application both control groups (*Txnrd2*^{wt/fl-Tg[Cre-VE-CadherinER]} and *Txnrd2*^{fl/fl}) and the endothelial-specific *Txnrd2*-knockout mice (*Txnrd2*^{fl/fl-Tg[Cre-VE-CadherinER]}) were viable. The latter showed no pathological phenotype or macroscopical noticeable alterations in all observed organs (data not shown) compared to animals of the control groups.

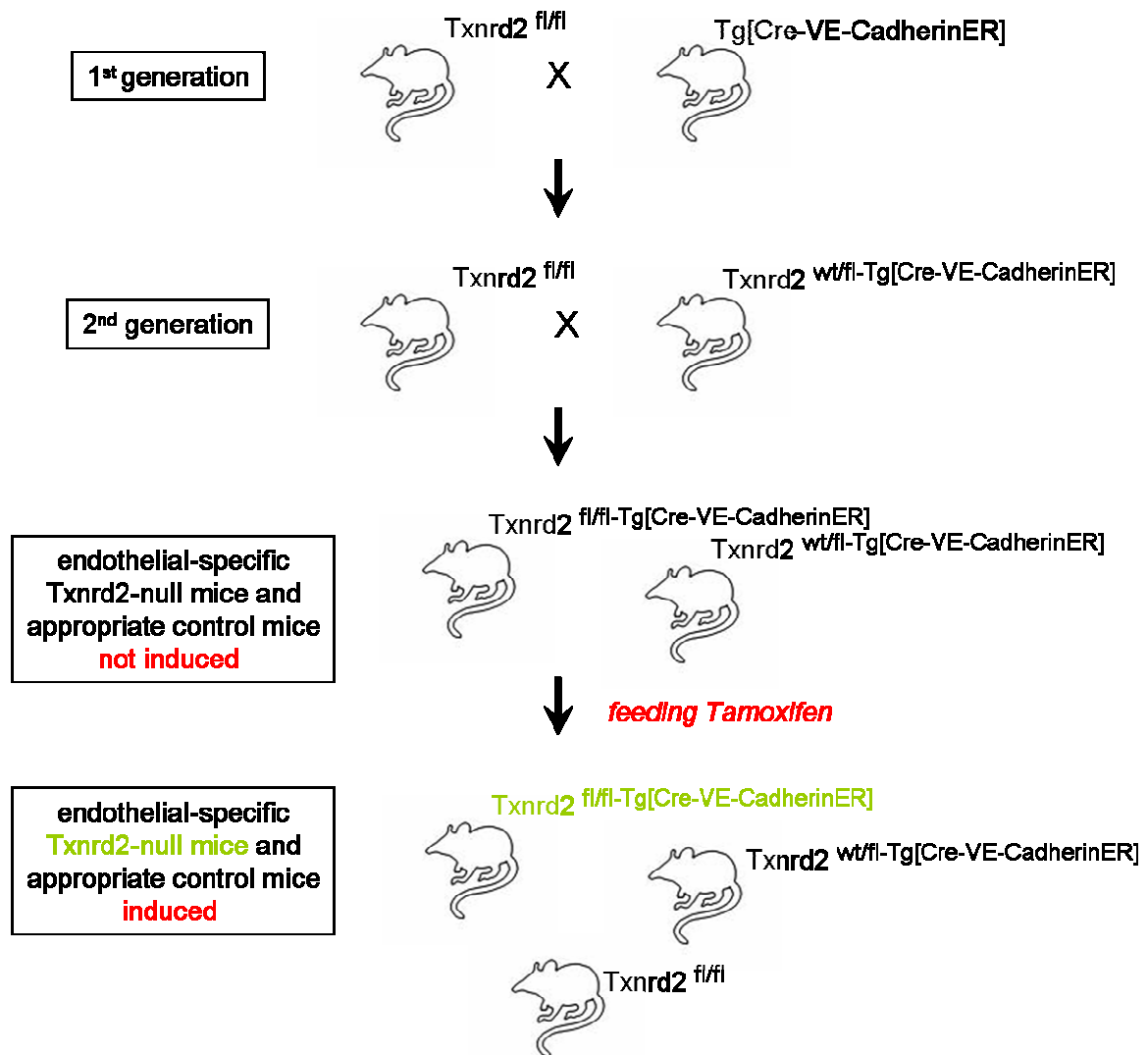


Figure 3-33: Breeding scheme for endothelial-specific *Txnrd2*-null mice

Txnrd2^{fl/fl} mice were bred with a mouse line expressing tamoxifen-inducible Cre-recombinase under the regulation of the vascular endothelial cadherin promoter (*Tg[Cre-VE-CadherinER]*).

4. DISCUSSION

Growing evidence indicates that cellular redox status regulates various aspects of cellular function. Dependent on the dosage, oxidative stress can elicit cellular proliferation or growth inhibition, cell activation as well as cell death^{224, 254}. During the last decades the thioredoxin-dependent system has been identified as one major player regulating cellular redox homeostasis^{8, 167}. Substantial data document the implication of Txnrd1 not only in processes like antioxidant defence, proliferation and apoptosis but also in cellular transformation and tumour growth^{9, 16, 123, 221}. However, much less is known about Txnrd2. Previous work demonstrated that Txnrd2 is not only indispensable for embryogenesis (especially heart development and fetal hematopoiesis) but also affects proliferation, proper mitochondrial function and antioxidant defence of myocardial tissue^{61, 245}. Recently, it has been shown that Txnrd2 is much higher expressed in hepatocellular carcinoma compared to adjacent healthy tissue⁵⁹.

The present work aimed to clarify functions of Txnrd2 in cellular signalling and tumour growth. Using the *Cre-loxP* technology, a conditional Txnrd2 knockout mouse line was previously generated in our laboratory⁶¹. We isolated fibroblasts from wild-type and Txnrd2-null embryos and established primary, immortalised and transformed cell lines to investigate the role of Txnrd2 in several aspects of cell metabolism and proliferation, tumour growth and angiogenesis. Indeed, we could show that disruption of the *Txnrd2* gene significantly impaired tumour growth mainly due to altered tumour angiogenesis and altered cell metabolism.

4.1. Immortalised MEFs compensate Txnrd2-deficiency by induction of other redox-regulating enzymes

Data regarding the role of Txnrd2 in the regulation of cell proliferation are conflicting. Overexpression of a dominant negative mutant of Txnrd2 in HeLa cells in a tetracycline-regulable manner resulted in increased production of H₂O₂, proliferation and progression of G1 to S phase in the cell cycle¹⁶¹. On the other hand previous findings from our laboratory revealed that the full knockout of Txnrd2 in freshly isolated MEFs resulted in increased cell death which was accompanied with increased levels of intracellular ROS^{61, 245}. In the present study we could show that immortalised Txnrd2-deficient MEFs show increased proliferation compared to the wild-type cells. Furthermore, immortalised Txnrd2-knockout fibroblasts showed comparable amounts of intracellular ROS with wild-type cells in contrast to freshly isolated (primary) knockout fibroblasts. These findings were surprising and prompted us to further characterise the immortalised Txnrd2-deficient cells. As reported previously, primary

Txnrd2-null fibroblasts were highly susceptible to depletion of the GSH de-novo synthesis by treatment with BSO and showed massive cell death⁶¹. BSO is known as a potent and specific inhibitor of γ -glutamylcysteine synthetase, catalysing the first and rate-limiting step in GSH biosynthesis¹²². Immortalised Txnrd2-deficient and wild-type fibroblasts were treated with BSO and cell numbers as well as soluble intracellular ROS were analysed. Indeed, the immortalised fibroblasts lacking Txnrd2 were still highly susceptible to intracellular GSH-depletion. The cells showed augmented cell death and a strong increase in intracellular ROS compared to the wild-type cells.

Mitochondria are considered to be a major physiological source of ROS in the cell and thus it seems logic that a set of antioxidant defence systems is localised in this organelle²⁹⁰. Therefore, it was hypothesised that other mitochondrial redox-regulating systems might compensate for the impaired mitochondrial thioredoxin-dependent system in immortalised cells. Previous findings revealed that in freshly isolated MEFs the mitochondria-specific peroxiredoxins, Prx3 and Prx5, were upregulated under baseline cell culture conditions²⁴⁵. mRNA and protein levels were elevated in Txnrd2-knockout cells and could be further increased by various triggers of oxidative stress. This was not the case for immortalised Txnrd2-deficient fibroblasts. mRNA levels of *Prx3* and *Prx5* were comparable between *Txnrd2*^{+/+} and *Txnrd2*^{-/-} cells and remained unchanged after BSO treatment.

The high susceptibility of the Txnrd2-deficient cells towards GSH-depletion prompted us to investigate whether parts of the GSH-dependent pathway might be upregulated in our cells. Analysis of the activity of glutathione reductase, the enzyme that restores oxidised glutathione (GSSG), revealed increased activity in Txnrd2-null fibroblasts. Enhanced enzyme activity was accompanied by elevated protein expression. Yet, the total intracellular amount of the glutathione (oxidised and reduced) remained unchanged. At the same time studies in our laboratory concerning the role of Txnrd1 in tumourigenesis revealed similar effects in Txnrd1-deficient fibroblasts. Namely, Txnrd1-null cells showed elevated enzyme activity and increased amounts of glutathione reductase¹⁹⁷, supporting the assumption that deletion of one redox-regulating system might be compensated by upregulation of other redox-regulating enzymes. A related phenomenon has been observed for the different forms of glutathione peroxidases and was described as hierarchy of selenoproteins^{38, 344}. While GPx1 (cytosolic GPx) and GPx3 (plasmatic GPx) were highly susceptible to selenium deficiency by showing decreased protein expression and activity, GPx2 (gastrointestinal GPx) and GPx4 (phospholipid hydroperoxide GPx) remained stable, indicating that the latter enzymes might compensate for the reduced activity of GPx1 and GPx3.

We also investigated whether Txnrd1 might be affected in response to Txnrd2 deletion. Indeed, immunoblot analysis of Txnrd1 revealed elevated protein levels in immortalised Txnrd2-deficient cells. In which way the cytosolic located Txnrd1 might be able to

compensate for the loss of the mitochondrial located Txnrd2 remains to be clarified. Primary Txnrd2-knockout cells and GSH-depleted immortalised Txnrd2-knockout cells showed intracellular accumulation of H₂O₂. H₂O₂ is able to pass membranes and therefore could accumulate in the cytosol and interact with cytosolic Trx1 or Trx2 if not scavenged and detoxified in the mitochondria. In this case, Txnrd1 might be able to compensate for the lack of Txnrd2. Furthermore *in vitro* studies by Turanov *et al.*, identifying two distinct isoforms of Txnrd2 that are located extramitochondrially, did not show catalytic preferences for Trx2 versus Trx1³¹⁵. In fact both, Txnrd2 and also Txnrd1, were equally active with Trx1 or Trx2. These data support our findings that Txnrd1 might be upregulated in Txnrd2-deficient cells to partially achieve reduction of intracellular ROS by reducing Trx2 instead of missing Txnrd2. The present findings indicate that Txnrd2-knockout cells change their expression pattern during immortalisation and upregulate some components of the GSH-dependent system to compensate consequences of Txnrd2 deletion. This allows Txnrd2-knockout cells to proliferate normally, which, however, makes them highly susceptible to cellular GSH-depletion. Studying the expression pattern on a genome-wide scale before and after immortalisation remains to be carried out and would certainly identify more enzymes which are altered in Txnrd2-knockout cells. Furthermore, it might be interesting to study the expression pattern of redox-regulating systems following full depletion of both, Txnrd2 and Txnrd1.

4.2. Txnrd2-deficient fibroblasts switch their energy metabolism from oxidative phosphorylation to anaerobic glycolysis

The predicted function of Txnrd2 is to control mitochondrial ROS level as well as the redox state of mitochondrial proteins, thereby ensuring proper mitochondrial function^{56, 159, 246, 267}. Mitochondrial ROS are known to participate in the apoptotic pathway as well as in the regulation of the mitochondrial permeability transition pore (PT) and Ca²⁺-signalling^{307, 362}. Therefore, we were interested to study how mitochondria and particularly mitochondrial function are influenced if one major ROS detoxifying system is inactivated.

First of all, structural and intracellular organisation of mitochondria were analysed using the organelle-specific probe Mitotracker Green®. Confocal microscopy revealed that mitochondria of primary Txnrd2 wild-type and Txnrd2-deficient fibroblasts appeared equal in shape and intracellular organisation. Surprisingly, mitochondria of immortalised Txnrd2-deficient cells appeared in distinct shape and accumulated much less of the mitochondria-specific dye. Quantification of mitochondrial mass by flow cytometry using two different mitochondria-selective dyes revealed conflicting results. Analysis of mitochondria in primary

cells showed similar accumulation of Mitotracker Green® and NAO in mitochondria of wild-type and Txnrd2-deficient fibroblasts. Whereas in immortalised cells, quantitative evaluation of Mitotracker Green® enrichment in mitochondria revealed reduced accumulation in Txnrd2-deficient cells, this was not the case using NAO, a fluorescent dye that binds in a manner independent of mitochondrial membrane potential to non-oxidised cardiolipin in the inner mitochondrial membrane. Measurements with this dye are hampered by the effect that cardiolipin binds NAO differently dependent on its grade of oxidation, which due to deletion of Txnrd2, might have changed^{105, 148, 155}. As estimation of mitochondrial mass by use of fluorescent dyes is controversially discussed^{155, 209, 242} the obtained results had to be clarified by further analysis. Thus, we performed another independent and commonly used method, the analysis of mitochondrial DNA by quantitative Real-time PCR. Quantification of the gene encoding mitochondria-specific *16S rRNA* normalised to the expression of nuclear encoded *hexokinase* of primary and immortalised fibroblasts revealed no differences between wild-type and Txnrd2-deficient cells. Taken together, these experiments suggest that there was no impact of the Txnrd2-deletion on the number of mitochondria per cell. In view of the conflicting data using mitochondrial-specific dyes and the potential impact of the mitochondrial membrane potential we have already started to further analyse mitochondrial membrane potential using the cationic dye JC-1 and flow cytometry, which could not be included in the present work due to time limitations.

Dysfunction of mitochondria is well known to be involved in several metabolic and degenerative (Parkinson's disease) diseases, aging and cancer^{185, 322}. It has been reported that altered mitochondrial function can be associated with changes in morphology of these organelles³²⁰. Several observations indicate that mitochondrial energy production may be controlled by structural rearrangements of the organelle including the remodelling of cristae morphology and elongation of fragmentation of the tubular network organisation^{20, 183}. Furthermore signalling molecules, e.g. ROS and Ca²⁺, have been shown to induce opening of megachannels of mitochondrial membranes resulting in swelling and structural changes of the organelles as a crucial step in the apoptotic signalling of cells³¹⁹. Electron microscopy may therefore provide new insights into the internal organisation of mitochondria⁹⁷. It is therefore conceivable that in immortalised Txnrd2-deficient cells mitochondrial function was impaired in spite of an unaltered number of mitochondria. It has been already reported that elevated generation of ROS induces mitochondrial dysfunction and increases mitochondrial autophagy²⁶⁰. Previous studies in our laboratory using transmission electron microscopy revealed severe malformation of mitochondria and swelling with destruction or loss of cristae in Txnrd2-deficient myocardial cells of newborn mice⁶¹. Therefore, it would be interesting to see what the impact of Txnrd2-deletion on intracellular and structural organisation of

mitochondria is by using transmission electron microscopy in primary and immortalised fibroblasts.

To extent these investigations, we also studied the functionality of mitochondria of Txnrd2-deficient cells. Thus further experiments were performed to test the activity of the respiratory chain complexes using high-resolution respirometry (HRR). The basal cellular O₂-consumption and maximum achievable activity of each complex was slightly decreased in primary Txnrd2-deficient fibroblasts. Surprisingly, this was not the case for immortalised Txnrd2-deficient cells. Compared to wild-type cells Txnrd2-knockout cells showed an even slightly elevated basal O₂-consumption and particularly a higher activity of complex I and IV after stimulation. These results were unexpected as it is obvious that any structural impairment of mitochondria should also impair the functionality of the respiratory chain and other mitochondria-specific functions. The redox balance in the mitochondrial matrix, where the particular complexes are located, is indispensable for proper function of the respiratory chain. Furthermore, it has already been reported that the ATPase F₀-F₁ complex and the cytochrom-c-oxidase are indeed regulated by redox mechanisms³⁴⁶⁻³⁴⁷. In primary Txnrd2-deficient cells the elevated production of ROS under baseline conditions was accompanied with a slightly impaired function of the respiratory chain. On the other hand immortalised Txnrd2-null fibroblasts showed no increase in the production of ROS under baseline conditions and similar activity of the respiratory chain compared to wild-type cells. Thus, the earlier described compensatory mechanisms (e.g. elevated GR activity and expression) may stabilise a proper redox balance in the mitochondria despite the deletion of Txnrd2 and therefore allow proper mitochondrial respiratory chain function. Thus, the obtained results indicate that there are no alterations in the number of mitochondria per cell in primary and immortalised wild-type and Txnrd2-knockout cells. If there are any structural changes or any impairments of mitochondria functions due to deletion of Txnrd2 can not be fully excluded by now and needs to be further investigated.

Mitochondria are the major site of ATP production in a cell, yet electron flow through the mitochondrial respiratory chain is inevitably linked to mitochondrial ROS generation. The 'cellular powerhouses' provide energy much more efficiently than anaerobic glycolysis. Primary Txnrd2-deficient fibroblasts showed increased ROS level and increased cell death^{61, 245}. Following immortalisation this phenotype was no longer detectable. Cells were able to compensate for the loss of Txnrd2, balance their ROS level and recover to normal proliferation rates. These phenomenons were accompanied by a quick decrease in pH of the cell culture medium of cultured immortalised Txnrd2-deficient cells. Thus, the question was raised whether the observed phenotype may be due to changes in cell metabolism. A switch from oxidative phosphorylation to anaerobic glycolysis might have several advantages for

cells lacking a major mitochondrial redox-regulating system. Since ROS are a by-product of mitochondrial respiration, a metabolic shift from oxidative phosphorylation to anaerobic glycolysis, by regeneration of NADH/H⁺ to NAD⁺ through lactate dehydrogenase, may allow cells to produce ATP only via anaerobic glycolysis and thus to reduce the overall ROS burden. The multienzyme pyruvate dehydrogenase (PDH) catalyses the conversion of pyruvate, CoA and NAD⁺ into acetyl-CoA, NADH and CO₂²⁶³. This several-step process of oxidative decarboxylation of pyruvate occupies a central position in cellular metabolism, linking glycolysis with the TCA and lipid biosynthesis. In eukaryotic cells the PDH complex is located in the mitochondrial matrix^{321, 342}. The mechanisms that control PDH complex activity include its phosphorylation by a family of pyruvate dehydrogenase kinases (PDKs) and dephosphorylation by phosphopyruvate dehydrogenase phosphatases (PDPs), the first inactivating and the latter activating the PDH complex^{239-240, 298-299}. Phosphatases are known to be regulated through reversible oxidation of the active-site cysteine and previous studies have implied intracellular ROS, e.g. H₂O₂, as the mediators of phosphatase oxidation^{58, 63}. Thus, elevated levels of intracellular ROS, as we observed in primary Txnrd2-deficient fibroblasts, might induce oxidation of phosphatases thereby reducing their activity. This in turn might lead to an hyperphosphorylation and inactivation of the PDH complex, constraining the cell to switch to anaerobic glycolysis for ATP production.

Therefore, we measured the amount of lactate released into the cell culture medium. Indeed we found elevated lactate levels in the supernatant of immortalised Txnrd2-deficient cells but not of primary Txnrd2-null cells. To further proof these results, freshly isolated cells were immortalised over multiple numbers of passages and lactate level were measured every few passages. We could actually observe increasing levels of lactate in the cell culture supernatant of Txnrd2-null cells during subsequent passaging of cells for immortalisation, which was not the case for wild-type cells. Since immortalised Txnrd2-deficient cells upregulate other redox-systems (e.g. GR) and thus were highly susceptible to GSH-depletion, we wondered if the stressing conditions due to BSO treatment might further influence the cellular energy metabolism. Both, wild-type and Txnrd2-deficient immortalised fibroblasts demonstrated an increase of lactate in the cell culture supernatant following BSO treatment. Interestingly, this increase appeared much stronger in wild-type cells. The observed phenomenon is not unknown and is already subject of research since it was first mentioned in the 1930s. The so-called 'Warburg-effect' describes the switch of energy metabolism in cancer cells from oxidative phosphorylation to anaerobic glycolysis³²⁶⁻³²⁷. Warburg postulated, that malignant cells have dysfunctional mitochondria and therefore rely on anaerobic glycolysis even in the presence of sufficient level of oxygen. Later, this view has been challenged and research revealed that mitochondria of tumour cells are not dysfunctional and are able to produce ATP¹¹⁹. However, many cancer cell lines do exhibit a

higher rate of anaerobic glycolysis and this shift appears to be relevant for the malignant process and offers growth advantages^{69, 326-327}. It allows cells to use the most abundant extracellular nutrient glucose. If the glycolytic flux is high enough, the percentage of cellular ATP produced from glycolysis can indeed exceed that produced from oxidative phosphorylation^{125, 248, 327}. Furthermore, glucose degradation provides intermediates needed for biosynthetic pathways (ribose sugars, glycerol, non-essential amino acids, NADPH)⁶⁹.

Cells were also exposed to glucose-depletion and instead cell culture medium was supplemented with galactose and glutamine. When glucose is no longer available, cells are forced to use other substrates for energy production. Metabolising these substrates (galactose and glutamine) requires functional mitochondria and oxidative phosphorylation for production of ATP²⁶⁴. Whereas primary Txnrd2-deficient cells were susceptible to glucose-depletion and showed decreased proliferation, immortalised Txnrd2-null cells easily coped with the change of energy source and showed enhanced proliferation compared to wild-type cells. These data further support the assumption that the Txnrd2-deficient cells have indeed functional mitochondria and compensate for the loss of Txnrd2 by upregulating other mitochondrial redox-systems, e.g. GR^{110, 147}, or cytosolic redox-systems, e.g. Txnrd1³⁰⁶.

The proposed metabolic reprogramming of immortalised Txnrd2-deficient cells was not paralleled with an upregulation of genes participating in glucose metabolism. Using semi-quantitative and quantitative Real-time PCR the expression of mRNA of the glucose transporters *GLUT-1, 3* and *4* were analysed. Though it is reported that *GLUT-1, 3*, and *4* are the isoforms that are upregulated in several types of cancer²⁰⁶, we could not find any change of expression level of all three isoforms.

Surprisingly we observed increased mRNA level of *PGC1 α* in immortalised Txnrd2-deficient fibroblasts. The transcriptional co-activator PGC1 α is known as an important regulator of energy metabolism and mitochondrial oxygen metabolism. As a regulator of mitochondrial biogenesis it increases the expression of most if not all mitochondrial proteins^{261, 260, 294}. This means PGC1 α increases proteins that increase ROS (enzymes of electron transport chain) and on the other hand PGC1 α also upregulates proteins that suppress ROS. Indeed PGC1 α exhibits dual activities: stimulation of mitochondrial electron transport while suppressing ROS by upregulation of ROS detoxifying proteins. Recent data support this assumption by showing that PGC1 α regulates ROS-defense systems and protects cells from oxidative stress²⁹⁵. Knockdown of PGC1 α by siRNA technique revealed decreasing expression of several ROS-defense systems, e.g. SOD1, SOD2, GPx1 and catalase²⁹⁵. Furthermore PGC1 α -null cells showed increased levels of ROS and decreased expression of antioxidant systems²⁹⁵. Thus, it might be possible that immortalised Txnrd2-null cells upregulate PGC1 α , both, to stimulate mitochondrial respiration and to balance excessive ROS levels.

Taken together, immortalised Txnrd2-deficient cells employed several mechanisms to compensate for the loss of one major mitochondrial redox-regulating system. These compensatory mechanisms comprise upregulation of several other redox-pathways to cope with elevated ROS level and adjustment of proliferation. These results are also in accordance with the fact that the activities of the respiratory chain enzymes are not affected and the mitochondria are still functional. The proposed switch of energy production from oxidative phosphorylation to anaerobic glycolysis represents an additional way to protect mitochondria of increasing ROS production. However, if the cells really switch their metabolism and in which way this adjustment takes place (regulation of PDH complex activity), needs to be fully clarified.

4.3. Txnrd2 is necessary for colonigenic potential of transformed MEFs

Trx1 and its reductase Txnrd1 are reported to be augmented in various types of cancer, and its expression correlates with invasiveness, metastasis and poor survival rate^{9, 16, 221}. Previous reports further demonstrated that Txnrd1 is important for proliferation and tumourigenesis. Reduction of Txnrd1 in cancer cells reversed the malignant phenotype and emerged to be critical for self-sufficiency in growth signals.^{101, 192, 350-351} These and other data provided the rationale to develop many cancer drugs targeting the thioredoxin-dependent system, however, without discriminating between the cytosolic and mitochondrial forms^{123, 192, 255}. Contrary to the aforementioned reports recent work in our laboratory demonstrated that Txnrd1-deficiency in *c-myc* and *Ha-ras*^{V12} transformed cells had no effects on proliferation nor on cell cycle distribution. Likewise, tumour growth was comparable between Txnrd1-deficient and wild-type tumours¹⁹⁷. Therefore, we speculated that Txnrd2 might be the more relevant part of the thioredoxin-system in the process of cancer progression. Indeed, little is known about the function of Txnrd2 in the development or growth of cancer. Therefore wild-type and Txnrd2-deficient MEFs were transformed by co-transducing them with the two proto-oncogenes *c-myc* and *Ha-ras*^{V12} expressing lentiviruses. Wild-type cells grew in multilayer and loosely attached to the culture dish, which is characteristic for malignant cells. Interestingly, transformed Txnrd2-deficient cells preferentially grew in monolayer and tightly attached to the culture dish. A feature of many cancer cells is that they have the ability of an anchorage-independent growth when plated in soft agar, while most untransformed cells do not proliferate under these conditions⁹⁶. Up to now, multiple genetic factors for anchorage independence have been identified, but the molecular basis is still largely unknown^{60, 281, 337}. Previously, one study could demonstrate that the anchorage-independent phenotype is associated with increased mitochondrial biogenesis using genome-wide DNA microarray studies²¹⁷. To test whether deletion of

Txnrd2 has an influence on the anchorage-independent growth of transformed wild-type and Txnrd2-deficient MEFs, cells were plated in soft agar and numbers of growing colonies were counted. Interestingly, Txnrd2-deficient cells showed strongly reduced colony formation capacity compared to wild-type cells. Reconstitution of Txnrd2 in Txnrd2-null cells by electroporation with a plasmid carrying the full length enzyme (add-back) was able to reverse this phenotype. This shows that the observed effects were solely due to Txnrd2 inactivation and not due to possible clonal effects or differences in transformation efficiency. Similar observations have been reported for Txnrd1: loss of *Txnrd1* function by siRNA knock-down led to impairment of tumorigenicity and metastatic properties of Lewis Lung Cancer Cells (LLC1) ³⁵⁰. Later it was also demonstrated that due to Txnrd1 knockdown LLC1 cells lost their ability to form colonies in soft agar ³⁵¹. These data support the assumption that thioredoxin reductases may act as pro-cancer proteins. Nevertheless, at the same time as the present study indicated that full genetic deletion of *Txnrd2* impairs colonogenicity of tumour cells, investigations in our laboratory could show that this is not the case for *Txnrd1* ¹⁹⁷. Opposing effects of Txnrd1 on tumour development were already reported. On the one hand it was shown that Txnrd1 supports p53 function and thereby may induce apoptosis in tumour cells, while on the other hand upregulation of Txnrd1 in various cancers suggests a cancer promoting influence and is furthermore accompanied with metastasis, invasiveness and resistance to chemotherapy ⁹. One has to keep in mind that the discrepancies of the published reports may be due to different cellular systems and deletion strategies. Furthermore, it is challenging to distinguish between contributions of the individual components of the thioredoxin-dependent system to the malignant processes, thioredoxin and its related reductase, as both are reported to be upregulated in various types of cancer. However, the present results provide first evidence that Txnrd2 might be essential for anchorage-independent growth in tumour cells *in vitro*.

In the present work, full genetic deletion of *Txnrd2* was able to impair proliferation of transformed cells in soft agar, and we asked the question, whether its redox-regulating function might be involved. Lentiviral reconstitution of a mutated *Txnrd2* in Txnrd2-null cells carrying a inert active site due to a real STOP codon instead of UGA coding for Sec, was able to only partly recover the formation of colonies. However, one has to keep in mind the C-terminal Cys located in front of Sec and also the N-terminal Cys-containing active site. Even though it is reported that Sec is required for the catalytic activities of the enzyme ^{301, 357}, removal of Sec and incorporation of Cys and Ser revealed interesting results ³⁵⁸. Whereas the Ser-mutant did not show any catalytical activity, mutation of Sec to Cys showed catalytic activity in the reduction of thioredoxin with a 100-fold decreased catalytic constant (k_{cat}) and 10-fold reduced Michaelis constant (K_m) but not in reduction of H₂O₂. Thus, it is possible that at least a residual redox-function may be achieved with the above mentioned Cys.

Since restoration of an modified redox-active Txnrd2 only partially rescued colony formation we conclude that Txnrd2 in its function as a redox-regulating enzyme might influence the colonogenicity and tumorigenicity of tumour cells.

Previous work in our laboratory demonstrated that treatment of primary Txnrd2-deficient cells with the thiol-containing antioxidant NAC was able to restore proliferation to levels of untreated wild-type cells by reducing the elevated ROS level ²⁴⁵. To further proof if the reduced formation of colonies is related to elevated oxidative stress, cells were embedded in soft agar containing NAC. However, NAC did not rescue the colonogenic potential of transformed Txnrd2-deficient cells. Interestingly, for wild-type cells the formation of colonies was slightly decreased due to NAC. This complies with the observation that low levels of ROS have a stimulatory effect on proliferation due to the transient oxidation and thus inactivation of protein tyrosine phosphatases, which counteract receptor tyrosine kinase signalling ⁹⁵. Previous work in our laboratory revealed that Txnrd2-deficient cells have elevated levels of intracellular ROS (e.g. H₂O₂) and lipid peroxides ²⁴⁵. We assume that a combination of antioxidants (water-soluble and lipophilic) might fully or even partly rescue colony formation. The accordant experiments are already in progress but could not be included in the present work due to time limitations.

4.4. Transformed Txnrd2-deficient single cell-derived cells were still sensitive towards GSH-depletion

To further study the impact of Txnrd2 on tumour growth *in vivo*, wild-type and Txnrd2-null single-colony derived cell lines were established from the *c-myc* and *Ha-ras*^{V12} transformed cell lines. The batch cell lines shortly after transformation represent a mixed cell population of efficiently transformed and still several non-transformed cells, which might influence the experimental outcome. Only efficiently transformed cells are able to grow in soft agar and therefore isolated single-colony derived cell lines possess a comparable efficiency of transformation. The established single-colony derived cell lines were characterised *in vitro* prior to studying tumour growth *in vivo*. Wild-type and Txnrd2-deficient single-colony derived cell lines showed no differences in proliferation under baseline culture conditions. Colony formation capacity was also identical, in contrast to batch cell lines. Under normal culture conditions Txnrd2-deficient single-colony derived cells showed slightly increased amounts of ROS, which did not further increase after depletion of GSH. However, *in vitro* proliferation rate was impaired following GSH depletion. Interestingly, Txnrd2-deficient cells had no alterations in the GSH-dependent pathway as observed for the immortalised Txnrd2-deficient fibroblasts. Txnrd2-deficient cells showed comparable activity of GR and similar levels of total glutathione (GSH + GSSG). Thus, the compensatory mechanisms as seen for

immortalised Txnrd2-deficient cells were not upregulated under normal culture conditions. These observations in single-colony derived cell lines were at the first sight surprising and the question arises what may be the advantage of the transformed Txnrd2-deficient cells compared to immortalised Txnrd2-deficient cells. One explanation might be the transformation itself. Both proto-oncogenes, *c-myc* and *Ha-ras*, are well known to perfectly synergise in the process of transforming murine fibroblasts¹⁷⁴, and are overexpressed (*c-myc*)^{131, 230} or mutated (*ras*)^{34, 144, 341} in most human tumours. The ras protein plays a central role in the regulation of diverse cellular processes in invertebrates and vertebrates, controlling processes like differentiation, cell survival and proliferation²⁷¹. Also *c-myc* is known to coordinate many of the cellular programmes necessary for the growth and expansion of cancer cells^{276, 291}. Thus, under normal culture conditions transformed single-colony derived Txnrd2-deficient cells may benefit from the induction of *c-myc* and mutation of *Ha-ras*^{V12}. However, the observed persisting sensitivity to GSH-depletion indicates that Txnrd2-deficiency also seems to play a role in transformed cells. Even though GR and Txnrd1 were not upregulated in transformed single-colony derived Txnrd2-null cells, one can not exclude alternative compensatory mechanisms that have not been investigated yet. The selenoproteins glutathione peroxidase 4 (GPx4)³¹⁷ and glutathione peroxidase 1 (GPx1)²¹¹ are known to be also located in mitochondria^{77, 187, 211}. Both redox enzymes are able to scavenge H₂O₂ and use glutathione as a substrate^{92, 189, 195, 273, 317}.

We further characterised the established single-colony derived cell lines with regard to their mitochondrial morphology, energy metabolism and respiratory capacity. Microscopical observations of mitochondrial morphology using the organelle-specific dye Mitotracker Green® revealed no detectable variations between wild-type and Txnrd2-null single-cell clones. Quantification of Mitotracker Red® accumulation in mitochondria using FACS revealed reduced accumulation of mitochondria-selective dye in Txnrd2-null cells when compared to wild-type cells. As already mentioned and discussed in chapter 4.2. staining with mitochondria-selective dyes, used in the present study, is discussed controversially^{155, 209, 242}. Mitotracker Green® and Mitotracker Red® is discussed to be membrane potential dependent, and we were not able to exclude changes in the mitochondrial membrane potential due to Txnrd2-deletion up to now. We furthermore analysed mitochondrial DNA of single-colony derived cells using quantitative Real-time PCR, which revealed similar amounts for wild-type and Txnrd2-knockout cells. Thus, we conclude that morphology and number of mitochondria is not altered in Txnrd2-deficient transformed cells. To fully elucidate a possible effect of Txnrd2-deficiency on mitochondria in transformed cells it seems essential to perform electron transmission microscopy, as already discussed for primary and immortalised fibroblasts (chapter 4.2.)⁹⁷.

Investigations of energy metabolism were performed by analysis of lactate release and proliferation in glucose-free-galactose-supplemented cell culture medium. Txnrd2-deficient cells released increased amounts of lactate into the culture medium under normal culture conditions compared to wild-type cells proposing a switch of energy production from oxidative phosphorylation to anaerobic glycolysis. GSH-depletion did slightly increase lactate levels in the cell culture supernatants of wild-type cells but not of Txnrd2-null cells, which was in line with the observations in immortalised Txnrd2-null cells (see chapter 4.2.). Single-cell clones showed similar proliferative activity when exposed to low-glucose culture medium. Furthermore, Txnrd2-null cells had no difficulties with the change of energy substrate when cultured under conditions of glucose deprivation and galactose supplementation. The cells showed enhanced or even similar proliferation compared to wild-type cells, indicating active oxidative phosphorylation and thus functional mitochondria as it was already discussed for immortalised Txnrd2-deficient cells in chapter 4.2.^{73, 264, 272}. The activity of the respiratory chain was analysed using HRR. Whereas basal O₂-consumption remained comparable between wild-type and Txnrd2-null cells, maximum activity of the single respiratory complexes following stimulation was increased in Txnrd2-deficient cells. This effect was most prominent for complex IV. In accordance with the observations of the respiratory chain activity the Txnrd2-null cells produced similar amounts of ATP under baseline cell culture conditions. The results indicate that Txnrd2-deficient cells show no alterations in mitochondrial morphology and no impaired function of the respiratory chain. These findings are in accordance with the observations of the last decade, showing that tumour cells do have functional mitochondria and perform active oxidative phosphorylation¹¹⁹. Nevertheless, transformed single-colony derived Txnrd2-deficient cells seem to preferentially produce ATP using anaerobic glycolysis instead of oxidative phosphorylation, indicated by elevated release of lactate. Thus, it still needs to be elucidated for what reason Txnrd2-deficient cells preferentially rely on anaerobic glycolysis although they have functional mitochondria.

In summary, these observations demonstrate that at first sight Txnrd2 appears to be dispensable for transformed cells under baseline cell culture conditions *in vitro*. But, GSH-depletion or deprivation of adequate energy substrates disclosed that Txnrd2-deficient tumour cells are indeed more susceptible to stress conditions and have several disadvantages and impairments due to the deletion of Txnrd2. Furthermore these data support the assumption that the limitations due to the Txnrd2-deletion are only partially caused by elevated oxidative stress and redox-dependent processes. Though, there must be an yet unknown additional impact of Txnrd2 that influences cellular metabolism of tumour cells.

4.5. Loss of Txnrd2 impairs tumour growth due to limited proliferation and diminished tumour vascularisation

The thioredoxin-dependent system is reported to be involved at several if not all stages of the multi-step process of tumour development. However, most reports refer to Trx1 and Txnrd1^{9, 16, 103, 192, 221, 350-351}. Literature reporting about the involvement of the mitochondrial Txnrd in malignant processes is scarce. Nevertheless, Txnrd2 was found to be highly expressed in malignant hepatocellular tissue compared to healthy tissue⁵⁹. The distinct feature of Txnrd2 is its localisation in mitochondria. Mitochondria are not only the powerhouses of the cells but are also centrally involved in multiple cellular processes, e.g. Ca²⁺ homeostasis, cell death signalling, ROS signalling, as well as cell growth and survival. All these functions are crucial for tumour cell growth and thus mitochondria are discussed as major parts of the malignant processes and potential target for cancer therapy^{116, 203, 335}. Since Txnrd2 controls mitochondrial redox-balance it was considered as an attractive target to investigate. Insofar the *in vitro* findings of the present study indicated that Txnrd2 impacts anchorage-independent growth and proliferation of transformed cells under stressing conditions. However, number of mitochondria per cell, morphology and respiratory chain activity were not impaired due to deletion of Txnrd2 in transformed cells. Therefore we were curious to see what impact Txnrd2-deletion exerts on tumour growth *in vivo*.

Using single-colony derived wild-type and Txnrd2-knockout cells for *in vivo* studies of tumour growth, we were able to show that loss of Txnrd2 strongly affects tumour growth *in vivo* even though Txnrd2-deficiency did not affect proliferation and colonogenicity of single-colony derived tumour cells *in vitro*. Initial growth of Txnrd2-deficient and wild-type tumours was comparable but between four to six days post implantation tumour growth of wild-type cells was much stronger than that of Txnrd2-knockout cells. The impaired tumour growth was associated with clearly decreased proliferation of Txnrd2-deficient tumour cells. Previously, it was shown that HeLa cells overexpressing a catalytically inactive dominant-negative form of Txnrd2 show increased progression from G₁ to S-phase in cell cycle and increased proliferation¹⁶¹. Overexpression of an alternative splicing variant of Txnrd2, comprising three independent point deletions in the coding region and an insertion of 1228 bp in the 3'UTR between the stop codon and the SECIS element, caused increased apoptosis in HeLa cells⁵⁴. Both studies investigated the impact of a catalytically inactive Txnrd2 on cell cycle and proliferation of tumour cells *in vitro*. We now show that the overall deletion of the Txnrd2 impairs tumour growth *in vivo* which was at first sight mainly due to decreased tumour cell proliferation.

Tumour growth beyond a certain size is dependent on an adequate supply of tumour cells with nutrients and oxygen as well as an effective removal of waste products. Therefore

tumour growth requires the induction of a tumour vasculature, termed the 'angiogenic switch'. It was reported that decreased activity of *Txnrd1* is associated with increased VEGF expression, increased migration and proliferation of endothelial cells as well as enhanced vessel growth²⁹⁷. Previous work demonstrated that siRNA-mediated knockdown of *Txnrd1* and *Txnrd2* suppressed VEGF-induced NO production and also blocked eNOS activity in bovine aortic endothelial cells (BAEC)³⁰⁰. To more precisely elucidate the mechanism by which deletion of *Txnrd2* impairs tumour growth, we analysed tumour vascularisation. Macroscopical observations of tumours revealed a less developed vessel network surrounding *Txnrd2*-deficient tumours, concluding that the recruitment of host vessels towards newly growing tumour tissue is impaired. Quantitative analysis of CD31-positive cells in tumours of comparable size revealed decreased vascularisation of *Txnrd2*-null tumours, whereas vascular structures at day 11 of tumour growth did not reveal any difference. Yet, immunohistochemical staining of tumour sections does not provide any information regarding the functionality of vessels. Therefore, the development and functionality of tumour vasculature was investigated using skinfold chambers in combination with intravital microscopy. At early time points (day three) vessels of *Txnrd2*-deficient tumours appeared in an unorganised pattern and seemed to be leaky in contrast to a well organised developing vessel network in wild-type tumours. On day 11 of tumour growth wild-type tumours showed a typical dense and irregular tumour vessel network in contrast to *Txnrd2*-null tumours showing a less prominent developed but continuous vascular network. Without an adequate vascular supply, solid tumours can grow only to a critical size of 1-2 mm³ due to lack of oxygen and nutrients^{22, 43}. Folkman hypothesised in 1971, that tumour blood vessel formation was dependent on a tumour angiogenic factor, and that its blockade during the period when a tumour is most vulnerable (e.g. prior to angiogenesis) may restrict tumour growth⁹³. Later VEGF was identified as one of the most potent tumour angiogenic molecules⁸³. The differences in tumour vascularisation at early time points indicates that there might be an impairment of the angiogenic signalling at the above mentioned critical time point of tumour growth, e.g. due to reduced production of VEGF, in *Txnrd2*-deficient tumours (see following chapter 4.6.). However, at day 11, the *Txnrd2*-knockout tumours showed a functional vascular network, suggesting that the angiogenic signalling is not fully disturbed but only postponed. Thus, we concluded that loss of *Txnrd2* impairs tumour growth due to early severe defects in vessel recruitment thereby limiting tumour angiogenesis and as a consequence tumour growth. Several studies already revealed that *Trx2* and also *Txnrd2* may play a critical role for endothelial cell function^{65, 68, 212, 354}. Hence, we asked the question if *Txnrd2* might effect angiogenic signalling of tumour cells.

4.6. Angiogenic signalling is impaired in Txnrd2-deficient tumours and tumour cells

The 'angiogenic switch' is often described as the conversion of an avascular tumour to an angiogenic phenotype during the process of tumour progression¹³⁰. This implies that the process of angiogenesis is either switched 'on' or 'off'. But neovascularisation becomes increasingly prevalent during tumour progression and is accompanied by the recruitment of already existing vessels of the host^{22, 48, 126}. The 'angiogenic switch' is the result of changes in the tightly regulated balance between the expressions of pro- and anti-angiogenic molecules. Up to now numerous molecules have been identified that positively or negatively regulate the process of angiogenesis during tumour progression^{48, 332}. To further elucidate the molecular mechanisms underlying Txnrd2 dependent impairment of tumour vascularisation we investigated the expression of several key molecules that regulate angiogenesis. One prominent key-player in the regulation of tumour vascularisation is the transcription factor Hif-1 α . Hif-1 α is mainly regulated by the availability of oxygen, but also by several growth factors and cytokines^{136, 296, 353} as well as ROS^{158, 165, 199}. Once activated, Hif-1 α acts as a master regulator and regulates more than 100 putative genes that are involved in angiogenesis, cell proliferation, cell survival, glucose metabolism and erythropoiesis^{82, 262, 285}. One prominent representative of those genes is *VEGF*, the most potent endothelial cell mitogen and inducer of angiogenesis^{50, 86, 84, 286}. Both molecules, Hif-1 α and *VEGF*, are crucial for the 'angiogenic switch' during the process of tumour progression^{50, 138, 188}. Indeed, we found not only reduced Hif-1 α levels at early and later time points (day three and six) of tumour growth in Txnrd2-deficient tumours, but also a reduced expression of its target gene *VEGF*.

To further analyse the molecular mechanisms underlying the reduced Hif-1 α protein accumulation in Txnrd2-null tumours, we performed several *in vitro* experiments. First of all, tumour cells were exposed to starvation, a situation similar to hypoxia in tumours. We observed reduced Hif-1 α protein accumulation in Txnrd2-deficient tumour cells after starvation. The predominant mode of Hif-1 α regulation occurs at the level of protein stabilisation^{57, 282, 352}, and PHD2 is reported to be the responsible enzyme that sets the low steady-state level of Hif-1 α under normoxic conditions and adequate energy supply²⁶. At protein level, PHD2 is reported to be the most abundant of all three PHDs in all mouse organs³⁰⁴ and cell lines^{5, 26} examined. Therefore, we further analysed PHD2 protein levels. However, no changes in PHD2 protein level between wild-type and Txnrd2-deficient tumour cells could be detected, which was also true for wild-type and Txnrd2-knockout tumours. At this point it is important to mention that the protein expression of an enzyme not urgently correlates with its activity. Hydroxylation of Hif-1 α by PHD2 is not simply dependent on its

expression, though increased PHD2 activity was found to be correlated with increased protein expression²¹, but rather on its enzymatic activity and therefore subject to the availability of its essential substrates, Fe²⁺, 2-oxoglutarate, ascorbate and oxygen^{94, 279} and a number of potential regulators. Also environmental factors (e.g. nickel (II) and cobalt (II)) have been shown to inhibit PHD activity causing Hif-1 α stabilisation²⁷⁹. From our findings we conclude that it is not a compensatory increase of the protein level of PHD2 (and subsequent augmented degradation of Hif-1 α) which would explain the decreased Hif-1 α protein level. However, precise investigation of PHD2 activity remains to be done.

Many studies demonstrated that Hif-1 α is mainly regulated at the post-transcriptional level and that *Hif-1 α* mRNA remains almost unchanged after exposure to hypoxia, starvation or other stimuli^{76, 120, 143, 340}. Nevertheless, several recent *in vivo* studies reported also that a *Hif-1 α* mRNA upregulation occurred following exposure to hypoxia^{18, 57, 117, 284, 343}. Since our present results did not clearly reveal a regulatory role of Txnrd2 in Hif-1 α protein stabilisation, we investigated *Hif-1 α* mRNA levels in tumour cells under basal cell culture conditions and following starvation. Interestingly, we observed slightly increased *Hif-1 α* mRNA levels in wild-type tumour cells due to starvation but not in Txnrd2-deficient tumour cells. These findings support the hypothesis of an interaction of Txnrd2 with Hif-1 α transcription. Previous data hinted towards an involvement of the Akt-dependent signalling pathway in translational Hif-1 α regulation. For example vanadate, a substance which can produce a whole spectrum of ROS and is known as a potent inducer of tumours in humans and animals, has been shown to induce Hif-1 α in a human prostate carcinoma cell line dependent on the PI3K/Akt-pathway¹⁰⁴. Furthermore, it was also reported that the thioredoxin-dependent system exerts an influence on the cap-dependent translation of Hif-1 α via an Akt-dependent signalling pathway³⁵⁹. At the same time it was demonstrated that Hif-1 α is a transcriptional target of NF κ B which is activated via a PIK3/Akt-dependent pathway under hypoxic conditions¹⁸. We first investigated whether the reduced level of Hif-1 α protein might be due to altered Hif-1 α translation. Indeed, we observed an impaired phosphorylation and hence activity of Akt in Txnrd2-deficient cells when exposed to starvation.

In summary, these findings suggest that Txnrd2 is apparently not involved in the stabilisation of Hif-1 α protein, but positively affects Hif-1 α expression via transcription, and probably via Akt, translation.

4.7. Depletion of GSH de novo synthesis in Txnrd2-null tumours further diminishes tumour growth

The present findings illustrate that Txnrd2 is crucial for the colonigenic and tumourigenic potential of tumour cells. Previous work in our laboratory demonstrated that depletion of

Txnrd1 had no effect on colonogenic and tumorigenic potential of tumour cells, but additional depletion of the GSH-pathway efficiently impaired growth of Txnrd1-deficient tumours¹⁹⁶. Similar studies with GSH-depletion by BSO treatment caused increased cell death of Txnrd2-deficient tumour cells *in vitro*. Several studies demonstrated that supply of 20 mM of BSO via the drinking water in mouse models does strongly deplete GSH over a period of 14 days without toxic side effects³³¹. Hence, we were interested whether GSH-depletion by BSO leads to a further reduction in tumour growth in Txnrd2-null tumours. Indeed, growth of knockout tumours was further decreased by about 38%. Measurement of GSH levels in tumour tissue samples by HPLC indicated a massive drop of glutathione levels. Thus we conclude, that the concomitant inhibition of Txnrd2 and GSH system may represent an efficient pharmacological strategy for cancer treatment. Indeed, drugs targeting the thioredoxin-dependent system as well as the GSH-pathway are already in clinical trial phase³¹¹. The cancer drug motexafin gadolinium e.g., is reported to inhibit the thioredoxin-dependent system and GSH-dependent system thereby inducing increased accumulation of ROS^{27, 79, 132}. The present study strongly supports the hypothesis that the concomitant inhibition of both pathways offers an attractive strategy for cancer therapy. Whether this reduction of tumour growth is due to excessive accumulation of ROS or due to impairment of tumour cell proliferation or angiogenesis needs to be fully elucidated.

4.8. Txnrd2 impacts on eEPC proliferation and angiogenic function

Since we observed a strong effect of Txnrd2-deficiency on the recruitment of pre-existing host vessels and on the formation of an adequate tumour vascular network, we were further interested if there is also an important function of Txnrd2 specifically in endothelial cells. We therefore used eEPCs for *in vitro* studies¹³⁴. In line with the studies with primary Txnrd2-deficient MEFs, a slightly diminished proliferation of Txnrd2-deficient eEPCs was detectable. Embryonic endothelial progenitor cells are known to have the capacity to form capillary like structures in Matrigel®¹⁷¹. The tube formation assay is a well known method for studying the angiogenic competence of endothelial cells *in vitro*^{7, 12, 205, 348}. As we observed impaired vessel recruitment and angiogenesis in Txnrd2-deficient tumours, we asked whether Txnrd2 has an impact on the angiogenic capacity of endothelial cells. Indeed, we observed impaired sprouting of Txnrd2-deficient eEPCs in Matrigel®. The diminished sprouting could be rescued by restoration of an active full-length Txnrd2 in Txnrd2-null eEPCs. These findings support the assumption, that Txnrd2 is essential for proper proangiogenic function of eEPCs and thereby pivotal for vessel formation. It was already reported that Trx2 plays a critical role in preserving vascular endothelial cell function³⁵⁴. It increases the capacity of the cells to scavenge ROS and improves cellular function. Further data supported a role of Trx2 in

promoting ischemia-mediated arteriogenesis and angiogenesis by enhancing endothelial cell survival through inhibition of ASK1 activity^{68, 212}. Recent studies also suggest a critical role of Txnrd2 in the antioxidant defense of the endothelium⁶⁵. The present findings show that Txnrd2 appears to be important for endothelial cell proliferation and angiogenic capacity, though the underlying mechanisms remain to be studied.

4.9. Future prospects

Over the last decades extensive research has shown that ROS and antioxidant defence systems play an important role in the process of tumour development and progression. Therefore, inhibition of members of the thioredoxin family may contribute to successful cancer therapy. Numerous effective natural and synthetic Txnrd inhibitors are described to possess anti-tumour potential. The mode of action ranges from induction of oxidative stress to cell cycle arrest and apoptosis. Most of these drugs target the Sec-containing active site of Txnrds, e.g. gold compounds, platinum compounds, arsenic trioxide, motexafin gadolinium, nitrous compounds and various flavonoids, extensively summarised by Urig and Tonissen^{310, 316}. Several studies reported on gold(III)-compounds that specifically inhibit Txnrd2, thereby leading to Ca²⁺-dependent mitochondrial membrane permeability followed by cytochrom C release and induction of apoptosis^{64, 268-269}. Motexafin gadolinium (MGd), a drug that was reported to undergo redox cycling and to generate superoxide and other ROS, has been also shown to inhibit Txnrds and ribonucleotide reductase^{78-79, 132, 193-194, 266}. Currently MGd was tested successfully already in clinical trials (phase I-III) as single drug or in combination with other chemotherapeutic agents and/or radiotherapy for the treatment of different types of cancer^{4, 80, 207, 314}.

Also BSO, a selective inhibitor of intracellular GSH-synthesis, has been shown to effectively enhance the cytotoxicity of cisplatin-resistant tumours and the anti-tumour activity of the alkylating agent melphalan^{55, 277}. Previous work in our laboratory demonstrated, targeting more than one redox-regulating system might be a promising approach for anti-cancer therapy¹⁹⁷.

The outcome of the present study suggests that inhibition of Txnrd2 alone might offer an efficient way to interfere with cancer growth. Depletion of the GSH-dependent system in tumour-bearing mice seems to provide an additional benefit in reducing tumour growth. The *in vitro* data of the present work only partially indicate an impact of Txnrd2 on tumour cell proliferation and colonigenic potential, whereas our *in vivo* data show that genetic deletion of *Txnrd2* affects tumour progression, most likely due to impaired vessel recruitment and tumour vascularisation. However, further research is needed to fully clarify the role of Txnrd2 in proliferation, angiogenesis and endothelial cell function, especially in context of the discrepancies between *in vitro* and *in vivo* findings. Until now most research has been performed to investigate the cellular functions of the cytosolic counterpart in the context of tumour angiogenesis and endothelial cell function^{72, 162, 219, 297}, whereas only some studies implicate the mitochondrial thioredoxin-dependent system in endothelial function^{65, 68, 212, 354}. To further explore the role of Txnrd2 in endothelial function and tumour growth, we

established the tamoxifen-inducible endothelial-specific *Txnrd2*-knockout mice (chapter 3.4.2). The endothelial-specific *Txnrd2*-knockout mice are viable and thus will offer an efficient tool to further investigate the role of *Txnrd2* in endothelial function and tumour angiogenesis *in vivo*. To study the signalling between tumour cells and endothelial cells we are currently also establishing an *in vitro* endothelial sprouting assay^{227, 229, 278}. This model will allow us to study the consequences of genetic deletion of *Txnrd2* in endothelial cells and/or tumour cells in the process of endothelial cell sprouting.

5. SUMMARY

The mitochondria specific thioredoxin-dependent system consists of thioredoxin 2 (Trx2), thioredoxin reductase 2 (Txnrd2) and thioredoxin-dependent peroxidases (Prx3 and Prx5). Along with the glutathione (GSH)-dependent system it is critically involved in the maintenance of an intracellular redox balance.

Previous studies revealed that primary Txnrd2-deficient mouse embryonic fibroblasts (MEFs) show impaired proliferation, produce increased levels of reactive oxygen species (ROS) and are highly susceptible towards several pro-oxidants as well as depletion of the intracellular GSH.

In contrast, Txnrd2-null MEFs which continuously lack Txnrd2 seemed to compensate for Txnrd2-deficiency by upregulation of other redox-regulating systems. Additionally, these cells switched their energy metabolism towards anaerobic glycolysis in favour to oxidative phosphorylation to protect themselves from a potentially increased formation of mitochondrial ROS.

The main objective of the current study was to analyse the impact of Txnrd2 on tumour growth. Indeed we could show that loss of Txnrd2 strongly impairs the colonigenic potential of tumour cells whereas proliferation and ROS level were unaffected. Transformed Txnrd2-null cells were highly susceptible to depletion of intracellular GSH.

In vivo studies revealed that deletion of Txnrd2 resulted in 50% reduction in tumour size which was accompanied by reduced proliferation due to impaired formation of tumour vessels. These phenomena could be attributed to reduced Hif-1 α and VEGF protein expression. In agreement with the *in vitro* data additional therapeutic treatment of mice bearing Txnrd2-null tumours with L-buthionine sulfoximine (BSO), revealed increased susceptibility of the Txnrd2-null tumours towards GSH-depletion and resulted in further reduction in tumour size about 38%. Altogether, our results identify Txnrd2 as a promising drug target for cancer therapy. Furthermore the dual inhibition of Txnrd2 and GSH-dependent system, offers an attractive strategy to combat tumour growth.

The second part of the study investigated, whether Txnrd2 could influence endothelial cell proliferation and angiogenic function directly. Therefore, wild-type and Txnrd2-deficient embryonic endothelial progenitor cells (eEPCs) were isolated and cultivated. *In vitro* proliferation of Txnrd2-null eEPCs was only slightly diminished. In tube formation assays, the cells showed impaired angiogenic capacity, indicating that Txnrd2 might be indeed pivotal for endothelial proangiogenic function.

6. REFERENCES

- (1) Acker, T. and Plate, K.H., (2002) A role for hypoxia and hypoxia-inducible transcription factors in tumor physiology. *J Mol Med* (80) 9, 562-75
- (2) Acker, T., Fandrey, J. and Acker, H., (2006) The good, the bad and the ugly in oxygen-sensing: ROS, cytochromes and prolyl-hydroxylases. *Cardiovasc Res* (71) 2, 195-207
- (3) Airley, R.E. and Mobasheri, A., (2007) Hypoxic regulation of glucose transport, anaerobic metabolism and angiogenesis in cancer: novel pathways and targets for anticancer therapeutics. *Chemotherapy* (53) 4, 233-56
- (4) Amato, R.J., Jac, J. and Hernandez-Mcclain, J., (2008) Motexafin gadolinium for the treatment of metastatic renal cell carcinoma: phase II study results. *Clin Genitourin Cancer* (6) 2, 73-8
- (5) Appelhoff, R.J., Tian, Y.M., Raval, R.R., Turley, H., Harris, A.L., Pugh, C.W., Ratcliffe, P.J. and Gleadle, J.M., (2004) Differential function of the prolyl hydroxylases PHD1, PHD2, and PHD3 in the regulation of hypoxia-inducible factor. *J Biol Chem* (279) 37, 38458-65
- (6) Arbiser, J.L., Petros, J., Klaffer, R., Govindajaran, B., Mclaughlin, E.R., Brown, L.F., Cohen, C., Moses, M., Kilroy, S., Arnold, R.S. and Lambeth, J.D., (2002) Reactive oxygen generated by Nox1 triggers the angiogenic switch. *Proc Natl Acad Sci U S A* (99) 2, 715-20
- (7) Arnaoutova, I., George, J., Kleinman, H.K. and Benton, G., (2009) The endothelial cell tube formation assay on basement membrane turns 20: state of the science and the art. *Angiogenesis* (12) 3, 267-74
- (8) Arner, E.S. and Holmgren, A., (2000) Physiological functions of thioredoxin and thioredoxin reductase. *Eur J Biochem* (267) 20, 6102-9
- (9) Arner, E.S. and Holmgren, A., (2006) The thioredoxin system in cancer. *Semin Cancer Biol* (16) 6, 420-6
- (10) Asano, M., Yukita, A., Matsumoto, T., Kondo, S. and Suzuki, H., (1995) Inhibition of tumor growth and metastasis by an immunoneutralizing monoclonal antibody to human vascular endothelial growth factor/vascular permeability factor121. *Cancer Res* (55) 22, 5296-301
- (11) Baeriswyl, V. and Christofori, G., (2009) The angiogenic switch in carcinogenesis. *Semin Cancer Biol* (19) 5, 329-37

- (12) Bahlmann, F.H., Degroot, K., Duckert, T., Niemczyk, E., Bahlmann, E., Boehm, S.M., Haller, H. and Fliser, D., (2003) Endothelial progenitor cell proliferation and differentiation is regulated by erythropoietin. *Kidney Int* (64) 5, 1648-52
- (13) Bai, J. and Cederbaum, A.I., (2001) Mitochondrial catalase and oxidative injury. *Biol Signals Recept* (10) 3-4, 189-99
- (14) Baker, A., Payne, C.M., Briehl, M.M. and Powis, G., (1997) Thioredoxin, a gene found overexpressed in human cancer, inhibits apoptosis in vitro and in vivo. *Cancer Res* (57) 22, 5162-7
- (15) Baysal, B.E., (2003) On the association of succinate dehydrogenase mutations with hereditary paraganglioma. *Trends Endocrinol Metab* (14) 10, 453-9
- (16) Becker, K., Gromer, S., Schirmer, R.H. and Muller, S., (2000) Thioredoxin reductase as a pathophysiological factor and drug target. *Eur J Biochem* (267) 20, 6118-25
- (17) Becker, N. and Holzmeier, S., (2008)
http://www.dkfz.de/de/krebsatlas/gesamt/mort_2.html
- (18) Belaiba, R.S., Bonello, S., Zahringer, C., Schmidt, S., Hess, J., Kietzmann, T. and Gorlach, A., (2007) Hypoxia up-regulates hypoxia-inducible factor-1alpha transcription by involving phosphatidylinositol 3-kinase and nuclear factor kappaB in pulmonary artery smooth muscle cells. *Mol Biol Cell* (18) 12, 4691-7
- (19) Bell, E.L., Klimova, T.A., Eisenbart, J., Moraes, C.T., Murphy, M.P., Budinger, G.R. and Chandel, N.S., (2007) The Qo site of the mitochondrial complex III is required for the transduction of hypoxic signaling via reactive oxygen species production. *J Cell Biol* (177) 6, 1029-36
- (20) Benard, G. and Rossignol, R., (2008) Ultrastructure of the mitochondrion and its bearing on function and bioenergetics. *Antioxid Redox Signal* (10) 8, 1313-42
- (21) Berchner-Pfannschmidt, U., Tug, S., Trinidad, B., Oehme, F., Yamac, H., Wotzlaw, C., Flamme, I. and Fandrey, J., (2008) Nuclear oxygen sensing: induction of endogenous prolyl-hydroxylase 2 activity by hypoxia and nitric oxide. *J Biol Chem* (283) 46, 31745-53
- (22) Bergers, G. and Benjamin, L.E., (2003) Tumorigenesis and the angiogenic switch. *Nat Rev Cancer* (3) 6, 401-10
- (23) Bergers, G. and Hanahan, D., (2008) Modes of resistance to anti-angiogenic therapy. *Nat Rev Cancer* (8) 8, 592-603

- (24) Berggren, M., Gallegos, A., Gasdaska, J.R., Gasdaska, P.Y., Warneke, J. and Powis, G., (1996) Thioredoxin and thioredoxin reductase gene expression in human tumors and cell lines, and the effects of serum stimulation and hypoxia. *Anticancer Res* (16) 6B, 3459-66
- (25) Berggren, M.M., Mangin, J.F., Gasdaka, J.R. and Powis, G., (1999) Effect of selenium on rat thioredoxin reductase activity: increase by supranutritional selenium and decrease by selenium deficiency. *Biochem Pharmacol* (57) 2, 187-93
- (26) Berra, E., Benizri, E., Ginouves, A., Volmat, V., Roux, D. and Pouyssegur, J., (2003) HIF prolyl-hydroxylase 2 is the key oxygen sensor setting low steady-state levels of HIF-1alpha in normoxia. *EMBO J* (22) 16, 4082-90
- (27) Biaglow, J.E. and Miller, R.A., (2005) The thioredoxin reductase/thioredoxin system: novel redox targets for cancer therapy. *Cancer Biol Ther* (4) 1, 6-13
- (28) Bingle, L., Lewis, C.E., Corke, K.P., Reed, M.W. and Brown, N.J., (2006) Macrophages promote angiogenesis in human breast tumour spheroids in vivo. *Br J Cancer* (94) 1, 101-7
- (29) Biterova, E.I., Turanov, A.A., Gladyshev, V.N. and Barycki, J.J., (2005) Crystal structures of oxidized and reduced mitochondrial thioredoxin reductase provide molecular details of the reaction mechanism. *Proc Natl Acad Sci U S A* (102) 42, 15018-23
- (30) Bjornstedt, M., Hamberg, M., Kumar, S., Xue, J. and Holmgren, A., (1995) Human thioredoxin reductase directly reduces lipid hydroperoxides by NADPH and selenocystine strongly stimulates the reaction via catalytically generated selenols. *J Biol Chem* (270) 20, 11761-4
- (31) Borgstrom, P., Hillan, K.J., Sriramarao, P. and Ferrara, N., (1996) Complete inhibition of angiogenesis and growth of microtumors by anti-vascular endothelial growth factor neutralizing antibody: novel concepts of angiostatic therapy from intravital videomicroscopy. *Cancer Res* (56) 17, 4032-9
- (32) Borgstrom, P., Bourdon, M.A., Hillan, K.J., Sriramarao, P. and Ferrara, N., (1998) Neutralizing anti-vascular endothelial growth factor antibody completely inhibits angiogenesis and growth of human prostate carcinoma micro tumors in vivo. *Prostate* (35) 1, 1-10
- (33) Borgstrom, P., Gold, D.P., Hillan, K.J. and Ferrara, N., (1999) Importance of VEGF for breast cancer angiogenesis in vivo: implications from intravital microscopy of combination treatments with an anti-VEGF neutralizing monoclonal antibody and doxorubicin. *Anticancer Res* (19) 5B, 4203-14

- (34) Bourne, H.R., Wrischnik, L. and Kenyon, C., (1990) Ras proteins. Some signal developments. *Nature* (348) 6303, 678-9
- (35) Brahimi-Horn, C. and Pouyssegur, J., (2006) The role of the hypoxia-inducible factor in tumor metabolism growth and invasion. *Bull Cancer* (93) 8, E73-80
- (36) Brahimi-Horn, M.C., Chiche, J. and Pouyssegur, J., (2007) Hypoxia and cancer. *J Mol Med* (85) 12, 1301-7
- (37) Brauchle, M., Funk, J.O., Kind, P. and Werner, S., (1996) Ultraviolet B and H₂O₂ are potent inducers of vascular endothelial growth factor expression in cultured keratinocytes. *J Biol Chem* (271) 36, 21793-7
- (38) Brigelius-Flohe, R., (1999) Tissue-specific functions of individual glutathione peroxidases. *Free Radic Biol Med* (27) 9-10, 951-65
- (39) Brigelius-Flohe, R., (2008) Selenium compounds and selenoproteins in cancer. *Chem Biodivers* (5) 3, 389-95
- (40) Brown, L.F., Berse, B., Jackman, R.W., Tognazzi, K., Manseau, E.J., Dvorak, H.F. and Senger, D.R., (1993) Increased expression of vascular permeability factor (vascular endothelial growth factor) and its receptors in kidney and bladder carcinomas. *Am J Pathol* (143) 5, 1255-62
- (41) Brown, L.F., Berse, B., Jackman, R.W., Tognazzi, K., Manseau, E.J., Senger, D.R. and Dvorak, H.F., (1993) Expression of vascular permeability factor (vascular endothelial growth factor) and its receptors in adenocarcinomas of the gastrointestinal tract. *Cancer Res* (53) 19, 4727-35
- (42) Brown, L.F., Berse, B., Jackman, R.W., Tognazzi, K., Guidi, A.J., Dvorak, H.F., Senger, D.R., Connolly, J.L. and Schnitt, S.J., (1995) Expression of vascular permeability factor (vascular endothelial growth factor) and its receptors in breast cancer. *Hum Pathol* (26) 1, 86-91
- (43) Brown, L.F., Guidi, A.J., Schnitt, S.J., Van De Water, L., Iruela-Arispe, M.L., Yeo, T.K., Tognazzi, K. and Dvorak, H.F., (1999) Vascular stroma formation in carcinoma in situ, invasive carcinoma, and metastatic carcinoma of the breast. *Clin Cancer Res* (5) 5, 1041-56
- (44) Brunelle, J.K., Bell, E.L., Quesada, N.M., Vercauteren, K., Tiranti, V., Zeviani, M., Scarpulla, R.C. and Chandel, N.S., (2005) Oxygen sensing requires mitochondrial ROS but not oxidative phosphorylation. *Cell Metab* (1) 6, 409-14
- (45) Callapina, M., Zhou, J., Schmid, T., Kohl, R. and Brune, B., (2005) NO restores HIF-1 α hydroxylation during hypoxia: role of reactive oxygen species. *Free Radic Biol Med* (39) 7, 925-36

- (46) Carew, J.S. and Huang, P., (2002) Mitochondrial defects in cancer. *Mol Cancer* (1) 9
- (47) Carmeliet, P., Ferreira, V., Breier, G., Pollefeyt, S., Kieckens, L., Gertsenstein, M., Fahrig, M., Vandenhoek, A., Harpal, K., Eberhardt, C., Declercq, C., Pawling, J., Moons, L., Collen, D., Risau, W. and Nagy, A., (1996) Abnormal blood vessel development and lethality in embryos lacking a single VEGF allele. *Nature* (380) 6573, 435-9
- (48) Carmeliet, P. and Jain, R.K., (2000) Angiogenesis in cancer and other diseases. *Nature* (407) 6801, 249-57
- (49) Carmeliet, P., (2003) Angiogenesis in health and disease. *Nat Med* (9) 6, 653-60
- (50) Carmeliet, P., (2005) VEGF as a key mediator of angiogenesis in cancer. *Oncology* (69 Suppl 3) 4-10
- (51) Chae, H.Z., Chung, S.J. and Rhee, S.G., (1994) Thioredoxin-dependent peroxide reductase from yeast. *J Biol Chem* (269) 44, 27670-8
- (52) Chandel, N.S., Maltepe, E., Goldwasser, E., Mathieu, C.E., Simon, M.C. and Schumacker, P.T., (1998) Mitochondrial reactive oxygen species trigger hypoxia-induced transcription. *Proc Natl Acad Sci U S A* (95) 20, 11715-20
- (53) Chandel, N.S., McClintock, D.S., Feliciano, C.E., Wood, T.M., Melendez, J.A., Rodriguez, A.M. and Schumacker, P.T., (2000) Reactive oxygen species generated at mitochondrial complex III stabilize hypoxia-inducible factor-1 α during hypoxia: a mechanism of O₂ sensing. *J Biol Chem* (275) 33, 25130-8
- (54) Chang, E.Y., Son, S.K., Ko, H.S., Baek, S.H., Kim, J.H. and Kim, J.R., (2005) Induction of apoptosis by the overexpression of an alternative splicing variant of mitochondrial thioredoxin reductase. *Free Radic Biol Med* (39) 12, 1666-75
- (55) Chen, X., Carystinos, G.D. and Batist, G., (1998) Potential for selective modulation of glutathione in cancer chemotherapy. *Chem Biol Interact* (111-112) 263-75
- (56) Chen, Y., Cai, J. and Jones, D.P., (2006) Mitochondrial thioredoxin in regulation of oxidant-induced cell death. *FEBS Lett* (580) 28-29, 6596-602
- (57) Chen, Y.R., Dai, A.G., Hu, R.C. and Jiang, Y.L., (2006) Differential and reciprocal regulation between hypoxia-inducible factor- α subunits and their prolyl hydroxylases in pulmonary arteries of rat with hypoxia-induced hypertension. *Acta Biochim Biophys Sin (Shanghai)* (38) 6, 423-34

- (58) Chiarugi, P. and Cirri, P., (2003) Redox regulation of protein tyrosine phosphatases during receptor tyrosine kinase signal transduction. *Trends Biochem Sci* (28) 9, 509-14
- (59) Choi, J.H., Kim, T.N., Kim, S., Baek, S.H., Kim, J.H., Lee, S.R. and Kim, J.R., (2002) Overexpression of mitochondrial thioredoxin reductase and peroxiredoxin III in hepatocellular carcinomas. *Anticancer Res* (22) 6A, 3331-5
- (60) Cifone, M.A. and Fidler, I.J., (1980) Correlation of patterns of anchorage-independent growth with in vivo behavior of cells from a murine fibrosarcoma. *Proc Natl Acad Sci U S A* (77) 2, 1039-43
- (61) Conrad, M., Jakupoglu, C., Moreno, S.G., Lippl, S., Banjac, A., Schneider, M., Beck, H., Hatzopoulos, A.K., Just, U., Sinowatz, F., Schmahl, W., Chien, K.R., Wurst, W., Bornkamm, G.W. and Brielmeier, M., (2004) Essential role for mitochondrial thioredoxin reductase in hematopoiesis, heart development, and heart function. *Mol Cell Biol* (24) 21, 9414-23
- (62) Conrad, M., (2009) Transgenic mouse models for the vital selenoenzymes cytosolic thioredoxin reductase, mitochondrial thioredoxin reductase and glutathione peroxidase 4. *Biochim Biophys Acta* (1790) 11, 1575-85
- (63) Conrad, M., Sandin, A., Forster, H., Seiler, A., Frijhoff, J., Dagnell, M., Bornkamm, G.W., Radmark, O., Hooft Van Huijsduijnen, R., Aspenstrom, P., Bohmer, F. and Ostman, A., (2010) 12/15-lipoxygenase-derived lipid peroxides control receptor tyrosine kinase signaling through oxidation of protein tyrosine phosphatases. *Proc Natl Acad Sci U S A* (107) 36, 15774-9
- (64) Coronello, M., Mini, E., Caciagli, B., Cinellu, M.A., Bindoli, A., Gabbiani, C. and Messori, L., (2005) Mechanisms of cytotoxicity of selected organogold(III) compounds. *J Med Chem* (48) 21, 6761-5
- (65) Crane, M.S., Howie, A.F., Arthur, J.R., Nicol, F., Crosley, L.K. and Beckett, G.J., (2009) Modulation of thioredoxin reductase-2 expression in EAhy926 cells: implications for endothelial selenoprotein hierarchy. *Biochim Biophys Acta* (1790) 10, 1191-7
- (66) Crawford, Y. and Ferrara, N., (2009) VEGF inhibition: insights from preclinical and clinical studies. *Cell Tissue Res* (335) 1, 261-9
- (67) D'autreaux, B. and Toledano, M.B., (2007) ROS as signalling molecules: mechanisms that generate specificity in ROS homeostasis. *Nat Rev Mol Cell Biol* (8) 10, 813-24

- (68) Dai, S., He, Y., Zhang, H., Yu, L., Wan, T., Xu, Z., Jones, D., Chen, H. and Min, W., (2009) Endothelial-specific expression of mitochondrial thioredoxin promotes ischemia-mediated arteriogenesis and angiogenesis. *Arterioscler Thromb Vasc Biol* (29) 4, 495-502
- (69) Deberardinis, R.J., Lum, J.J., Hatzivassiliou, G. and Thompson, C.B., (2008) The biology of cancer: metabolic reprogramming fuels cell growth and proliferation. *Cell Metab* (7) 1, 11-20
- (70) Dong, J., Grunstein, J., Tejada, M., Peale, F., Frantz, G., Liang, W.C., Bai, W., Yu, L., Kowalski, J., Liang, X., Fuh, G., Gerber, H.P. and Ferrara, N., (2004) VEGF-null cells require PDGFR alpha signaling-mediated stromal fibroblast recruitment for tumorigenesis. *EMBO J* (23) 14, 2800-10
- (71) Duyndam, M.C., Hulscher, T.M., Fontijn, D., Pinedo, H.M. and Boven, E., (2001) Induction of vascular endothelial growth factor expression and hypoxia-inducible factor 1alpha protein by the oxidative stressor arsenite. *J Biol Chem* (276) 51, 48066-76
- (72) Ebrahimian, T. and Touyz, R.M., (2008) Thioredoxin in vascular biology: role in hypertension. *Antioxid Redox Signal* (10) 6, 1127-36
- (73) Eigenbrodt, E., Kallinowski, F., Ott, M., Mazurek, S. and Vaupel, P., (1998) Pyruvate kinase and the interaction of amino acid and carbohydrate metabolism in solid tumors. *Anticancer Res* (18) 5A, 3267-74
- (74) Emerling, B.M., Plataniias, L.C., Black, E., Nebreda, A.R., Davis, R.J. and Chandel, N.S., (2005) Mitochondrial reactive oxygen species activation of p38 mitogen-activated protein kinase is required for hypoxia signaling. *Mol Cell Biol* (25) 12, 4853-62
- (75) Eng, C., Kiuru, M., Fernandez, M.J. and Aaltonen, L.A., (2003) A role for mitochondrial enzymes in inherited neoplasia and beyond. *Nat Rev Cancer* (3) 3, 193-202
- (76) Epstein, A.C., Gleadle, J.M., Mcneill, L.A., Hewitson, K.S., O'rourke, J., Mole, D.R., Mukherji, M., Metzen, E., Wilson, M.I., Dhanda, A., Tian, Y.M., Masson, N., Hamilton, D.L., Jaakkola, P., Barstead, R., Hodgkin, J., Maxwell, P.H., Pugh, C.W., Schofield, C.J. and Ratcliffe, P.J., (2001) *C. elegans* EGL-9 and mammalian homologs define a family of dioxygenases that regulate HIF by prolyl hydroxylation. *Cell* (107) 1, 43-54
- (77) Esworthy, R.S., Doan, K., Doroshov, J.H. and Chu, F.F., (1994) Cloning and sequencing of the cDNA encoding a human testis phospholipid hydroperoxide glutathione peroxidase. *Gene* (144) 2, 317-8

- (78) Evens, A.M., (2004) Motexafin gadolinium: a redox-active tumor selective agent for the treatment of cancer. *Curr Opin Oncol* (16) 6, 576-80
- (79) Evens, A.M., Balasubramanian, L. and Gordon, L.I., (2005) Motexafin gadolinium induces oxidative stress and apoptosis in hematologic malignancies. *Curr Treat Options Oncol* (6) 4, 289-96
- (80) Evens, A.M., Spies, W.G., Helenowski, I.B., Patton, D., Spies, S., Jovanovic, B.D., Miyata, S., Hamilton, E., Variakojis, D., Chen, J., Naumovski, L., Rosen, S.T., Winter, J.N., Miller, R.A. and Gordon, L.I., (2009) The novel expanded porphyrin, motexafin gadolinium, combined with [90Y]ibritumomab tiuxetan for relapsed/refractory non-Hodgkin's lymphoma: preclinical findings and results of a phase I trial. *Clin Cancer Res* (15) 20, 6462-71
- (81) Fandrey, J., Frede, S. and Jelkmann, W., (1994) Role of hydrogen peroxide in hypoxia-induced erythropoietin production. *Biochem J* (303 (Pt 2)) 507-10
- (82) Fandrey, J., (1995) Hypoxia-inducible gene expression. *Respir Physiol* (101) 1, 1-10
- (83) Ferrara, N. and Henzel, W.J., (1989) Pituitary follicular cells secrete a novel heparin-binding growth factor specific for vascular endothelial cells. *Biochem Biophys Res Commun* (161) 2, 851-8
- (84) Ferrara, N., Houck, K., Jakeman, L. and Leung, D.W., (1992) Molecular and biological properties of the vascular endothelial growth factor family of proteins. *Endocr Rev* (13) 1, 18-32
- (85) Ferrara, N., Carver-Moore, K., Chen, H., Dowd, M., Lu, L., O'shea, K.S., Powell-Braxton, L., Hillan, K.J. and Moore, M.W., (1996) Heterozygous embryonic lethality induced by targeted inactivation of the VEGF gene. *Nature* (380) 6573, 439-42
- (86) Ferrara, N. and Davis-Smyth, T., (1997) The biology of vascular endothelial growth factor. *Endocr Rev* (18) 1, 4-25
- (87) Ferrara, N., Gerber, H.P. and Lecouter, J., (2003) The biology of VEGF and its receptors. *Nat Med* (9) 6, 669-76
- (88) Ferrara, N., (2004) Vascular endothelial growth factor: basic science and clinical progress. *Endocr Rev* (25) 4, 581-611
- (89) Ferrara, N., (2009) Vascular endothelial growth factor. *Arterioscler Thromb Vasc Biol* (29) 6, 789-91
- (90) Feussner, A., Rolinski, B., Weiss, N., Deufel, T., Wolfram, G. and Roscher, A.A., (1997) Determination of total homocysteine in human plasma by isocratic high-performance liquid chromatography. *Eur J Clin Chem Clin Biochem* (35) 9, 687-91

- (91) Flamme, I., Krieg, M. and Plate, K.H., (1998) Up-regulation of vascular endothelial growth factor in stromal cells of hemangioblastomas is correlated with up-regulation of the transcription factor HRF/HIF-2alpha. *Am J Pathol* (153) 1, 25-9
- (92) Flohe, L., Gunzler, W.A. and Schock, H.H., (1973) Glutathione peroxidase: a selenoenzyme. *FEBS Lett* (32) 1, 132-4
- (93) Folkman, J., (1971) Tumor angiogenesis: therapeutic implications. *N Engl J Med* (285) 21, 1182-6
- (94) Fong, G.H. and Takeda, K., (2008) Role and regulation of prolyl hydroxylase domain proteins. *Cell Death Differ* (15) 4, 635-41
- (95) Frank, G.D. and Eguchi, S., (2003) Activation of tyrosine kinases by reactive oxygen species in vascular smooth muscle cells: significance and involvement of EGF receptor transactivation by angiotensin II. *Antioxid Redox Signal* (5) 6, 771-80
- (96) Freedman, V.H. and Shin, S.I., (1974) Cellular tumorigenicity in nude mice: correlation with cell growth in semi-solid medium. *Cell* (3) 4, 355-9
- (97) Frey, T.G. and Mannella, C.A., (2000) The internal structure of mitochondria. *Trends Biochem Sci* (25) 7, 319-24
- (98) Fujio, Y. and Walsh, K., (1999) Akt mediates cytoprotection of endothelial cells by vascular endothelial growth factor in an anchorage-dependent manner. *J Biol Chem* (274) 23, 16349-54
- (99) Fukumura, D., Xavier, R., Sugiura, T., Chen, Y., Park, E.C., Lu, N., Selig, M., Nielsen, G., Taksir, T., Jain, R.K. and Seed, B., (1998) Tumor induction of VEGF promoter activity in stromal cells. *Cell* (94) 6, 715-25
- (100) Fyles, A.W., Milosevic, M., Wong, R., Kavanagh, M.C., Pintilie, M., Sun, A., Chapman, W., Levin, W., Manchul, L., Keane, T.J. and Hill, R.P., (1998) Oxygenation predicts radiation response and survival in patients with cervix cancer. *Radiother Oncol* (48) 2, 149-56
- (101) Gallegos, A., Berggren, M., Gasdaska, J.R. and Powis, G., (1997) Mechanisms of the regulation of thioredoxin reductase activity in cancer cells by the chemopreventive agent selenium. *Cancer Res* (57) 21, 4965-70
- (102) Gambhir, S.S., (2002) Molecular imaging of cancer with positron emission tomography. *Nat Rev Cancer* (2) 9, 683-93

- (103) Gan, L., Yang, X.L., Liu, Q. and Xu, H.B., (2005) Inhibitory effects of thioredoxin reductase antisense RNA on the growth of human hepatocellular carcinoma cells. *J Cell Biochem* (96) 3, 653-64
- (104) Gao, N., Ding, M., Zheng, J.Z., Zhang, Z., Leonard, S.S., Liu, K.J., Shi, X. and Jiang, B.H., (2002) Vanadate-induced expression of hypoxia-inducible factor 1 alpha and vascular endothelial growth factor through phosphatidylinositol 3-kinase/Akt pathway and reactive oxygen species. *J Biol Chem* (277) 35, 31963-71
- (105) Garcia Fernandez, M.I., Ceccarelli, D. and Muscatello, U., (2004) Use of the fluorescent dye 10-N-nonyl acridine orange in quantitative and location assays of cardiolipin: a study on different experimental models. *Anal Biochem* (328) 2, 174-80
- (106) Gasdaska, J.R., Berggren, M. and Powis, G., (1995) Cell growth stimulation by the redox protein thioredoxin occurs by a novel helper mechanism. *Cell Growth Differ* (6) 12, 1643-50
- (107) Gasdaska, P.Y., Berggren, M.M., Berry, M.J. and Powis, G., (1999) Cloning, sequencing and functional expression of a novel human thioredoxin reductase. *FEBS Lett* (442) 1, 105-11
- (108) Gatenby, R.A., Kessler, H.B., Rosenblum, J.S., Coia, L.R., Moldofsky, P.J., Hartz, W.H. and Broder, G.J., (1988) Oxygen distribution in squamous cell carcinoma metastases and its relationship to outcome of radiation therapy. *Int J Radiat Oncol Biol Phys* (14) 5, 831-8
- (109) Geisberger, R., Kiermayer, C., Homig, C., Conrad, M., Schmidt, J., Zimmer-Strobl, U. and Brielmeier, M., (2007) B- and T-cell-specific inactivation of thioredoxin reductase 2 does not impair lymphocyte development and maintenance. *Biol Chem* (388) 10, 1083-90
- (110) George, D.L. and Francke, U., (1976) Gene dose effect: regional mapping of human nucleoside phosphorylase on chromosome 14. *Science* (194) 4267, 851-2
- (111) Gerald, D., Berra, E., Frapart, Y.M., Chan, D.A., Giaccia, A.J., Mansuy, D., Pouyssegur, J., Yaniv, M. and Mechta-Grigoriou, F., (2004) JunD reduces tumor angiogenesis by protecting cells from oxidative stress. *Cell* (118) 6, 781-94
- (112) Gerber, H.P., Dixit, V. and Ferrara, N., (1998) Vascular endothelial growth factor induces expression of the antiapoptotic proteins Bcl-2 and A1 in vascular endothelial cells. *J Biol Chem* (273) 21, 13313-6
- (113) Gerber, H.P., Mcmurtrey, A., Kowalski, J., Yan, M., Keyt, B.A., Dixit, V. and Ferrara, N., (1998) Vascular endothelial growth factor regulates endothelial cell survival through the phosphatidylinositol 3'-kinase/Akt signal transduction pathway. Requirement for Flk-1/KDR activation. *J Biol Chem* (273) 46, 30336-43

- (114) Gerber, H.P., Hillan, K.J., Ryan, A.M., Kowalski, J., Keller, G.A., Rangell, L., Wright, B.D., Radtke, F., Aguet, M. and Ferrara, N., (1999) VEGF is required for growth and survival in neonatal mice. *Development* (126) 6, 1149-59
- (115) Gladyshev, V.N., Jeang, K.T. and Stadtman, T.C., (1996) Selenocysteine, identified as the penultimate C-terminal residue in human T-cell thioredoxin reductase, corresponds to TGA in the human placental gene. *Proc Natl Acad Sci U S A* (93) 12, 6146-51
- (116) Gogvadze, V., Orrenius, S. and Zhivotovsky, B., (2008) Mitochondria in cancer cells: what is so special about them? *Trends Cell Biol* (18) 4, 165-73
- (117) Gorlach, A., (2009) Regulation of HIF-1alpha at the transcriptional level. *Curr Pharm Des* (15) 33, 3844-52
- (118) Gorlatov, S.N. and Stadtman, T.C., (1999) Human selenium-dependent thioredoxin reductase from HeLa cells: properties of forms with differing heparin affinities. *Arch Biochem Biophys* (369) 1, 133-42
- (119) Gottlieb, E. and Tomlinson, I.P., (2005) Mitochondrial tumour suppressors: a genetic and biochemical update. *Nat Rev Cancer* (5) 11, 857-66
- (120) Gradin, K., Mcguire, J., Wenger, R.H., Kvietikova, I., Fhitelaw, M.L., Toftgard, R., Tora, L., Gassmann, M. and Poellinger, L., (1996) Functional interference between hypoxia and dioxin signal transduction pathways: competition for recruitment of the Arnt transcription factor. *Mol Cell Biol* (16) 10, 5221-31
- (121) Greijer, A.E., Van Der Groep, P., Kemming, D., Shvarts, A., Semenza, G.L., Meijer, G.A., Van De Wiel, M.A., Belien, J.A., Van Diest, P.J. and Van Der Wall, E., (2005) Up-regulation of gene expression by hypoxia is mediated predominantly by hypoxia-inducible factor 1 (HIF-1). *J Pathol* (206) 3, 291-304
- (122) Griffith, O.W., (1982) Mechanism of action, metabolism, and toxicity of buthionine sulfoximine and its higher homologs, potent inhibitors of glutathione synthesis. *J Biol Chem* (257) 22, 13704-12
- (123) Gromer, S., Urig, S. and Becker, K., (2004) The thioredoxin system--from science to clinic. *Med Res Rev* (24) 1, 40-89
- (124) Guidi, A.J., Schnitt, S.J., Fischer, L., Tognazzi, K., Harris, J.R., Dvorak, H.F. and Brown, L.F., (1997) Vascular permeability factor (vascular endothelial growth factor) expression and angiogenesis in patients with ductal carcinoma in situ of the breast. *Cancer* (80) 10, 1945-53

- (125) Guppy, M., Greiner, E. and Brand, K., (1993) The role of the Crabtree effect and an endogenous fuel in the energy metabolism of resting and proliferating thymocytes. *Eur J Biochem* (212) 1, 95-9
- (126) Gupta, M.K. and Qin, R.Y., (2003) Mechanism and its regulation of tumor-induced angiogenesis. *World J Gastroenterol* (9) 6, 1144-55
- (127) Guzy, R.D., Hoyos, B., Robin, E., Chen, H., Liu, L., Mansfield, K.D., Simon, M.C., Hammerling, U. and Schumacker, P.T., (2005) Mitochondrial complex III is required for hypoxia-induced ROS production and cellular oxygen sensing. *Cell Metab* (1) 6, 401-8
- (128) Haddad, J.J. and Land, S.C., (2001) A non-hypoxic, ROS-sensitive pathway mediates TNF-alpha-dependent regulation of HIF-1alpha. *FEBS Lett* (505) 2, 269-74
- (129) Hahn, W.C., Counter, C.M., Lundberg, A.S., Beijersbergen, R.L., Brooks, M.W. and Weinberg, R.A., (1999) Creation of human tumour cells with defined genetic elements. *Nature* (400) 6743, 464-8
- (130) Hanahan, D. and Folkman, J., (1996) Patterns and emerging mechanisms of the angiogenic switch during tumorigenesis. *Cell* (86) 3, 353-64
- (131) Hanahan, D. and Weinberg, R.A., (2000) The hallmarks of cancer. *Cell* (100) 1, 57-70
- (132) Hashemy, S.I., Ungerstedt, J.S., Zahedi Avval, F. and Holmgren, A., (2006) Motexafin gadolinium, a tumor-selective drug targeting thioredoxin reductase and ribonucleotide reductase. *J Biol Chem* (281) 16, 10691-7
- (133) Hatfield, D.L., Yoo, M.H., Carlson, B.A. and Gladyshev, V.N., (2009) Selenoproteins that function in cancer prevention and promotion. *Biochim Biophys Acta* (1790) 11, 1541-5
- (134) Hatzopoulos, A.K., Folkman, J., Vasile, E., Eiselen, G.K. and Rosenberg, R.D., (1998) Isolation and characterization of endothelial progenitor cells from mouse embryos. *Development* (125) 8, 1457-68
- (135) Hedstrom, E., Eriksson, S., Zawacka-Pankau, J., Arner, E.S. and Selivanova, G., (2009) p53-dependent inhibition of TrxR1 contributes to the tumor-specific induction of apoptosis by RITA. *Cell Cycle* (8) 21, 3576-83
- (136) Hellwig-Burgel, T., Rutkowski, K., Metzen, E., Fandrey, J. and Jelkmann, W., (1999) Interleukin-1beta and tumor necrosis factor-alpha stimulate DNA binding of hypoxia-inducible factor-1. *Blood* (94) 5, 1561-7
- (137) Henze, K. and Martin, W., (2003) Evolutionary biology: essence of mitochondria. *Nature* (426) 6963, 127-8

- (138) Hirota, K. and Semenza, G.L., (2006) Regulation of angiogenesis by hypoxia-inducible factor 1. *Crit Rev Oncol Hematol* (59) 1, 15-26
- (139) Hlatky, L., Tsiou, C., Hahnfeldt, P. and Coleman, C.N., (1994) Mammary fibroblasts may influence breast tumor angiogenesis via hypoxia-induced vascular endothelial growth factor up-regulation and protein expression. *Cancer Res* (54) 23, 6083-6
- (140) Hockel, M., Schlenger, K., Aral, B., Mitze, M., Schaffer, U. and Vaupel, P., (1996) Association between tumor hypoxia and malignant progression in advanced cancer of the uterine cervix. *Cancer Res* (56) 19, 4509-15
- (141) Holash, J., Davis, S., Papadopoulos, N., Croll, S.D., Ho, L., Russell, M., Boland, P., Leidich, R., Hylton, D., Burova, E., Ioffe, E., Huang, T., Radziejewski, C., Bailey, K., Fandl, J.P., Daly, T., Wiegand, S.J., Yancopoulos, G.D. and Rudge, J.S., (2002) VEGF-Trap: a VEGF blocker with potent antitumor effects. *Proc Natl Acad Sci U S A* (99) 17, 11393-8
- (142) Hoth, M., Fanger, C.M. and Lewis, R.S., (1997) Mitochondrial regulation of store-operated calcium signaling in T lymphocytes. *J Cell Biol* (137) 3, 633-48
- (143) Huang, L.E., Arany, Z., Livingston, D.M. and Bunn, H.F., (1996) Activation of hypoxia-inducible transcription factor depends primarily upon redox-sensitive stabilization of its alpha subunit. *J Biol Chem* (271) 50, 32253-9
- (144) Hunter, T., (1997) Oncoprotein networks. *Cell* (88) 3, 333-46
- (145) Ide, A.G., Baker, N.H. and Warren, S.L., (1939) Vascularization of the Brown Pearce rabbit epithelioma transplant as seen in the transparent ear chamber. *Am J Roentgenol.* (42) 891-899
- (146) Inoue, M., Hager, J.H., Ferrara, N., Gerber, H.P. and Hanahan, D., (2002) VEGF-A has a critical, nonredundant role in angiogenic switching and pancreatic beta cell carcinogenesis. *Cancer Cell* (1) 2, 193-202
- (147) Iozef, R., Becker, K., Boehme, C.C., Schirmer, R.H. and Werner, D., (2000) Assembly and functional expression of murine glutathione reductase cDNA: a sequence missing in expressed sequence tag libraries. *Biochim Biophys Acta* (1500) 1, 137-41
- (148) Jacobson, J., Duchon, M.R. and Heales, S.J., (2002) Intracellular distribution of the fluorescent dye nonyl acridine orange responds to the mitochondrial membrane potential: implications for assays of cardiolipin and mitochondrial mass. *J Neurochem* (82) 2, 224-33
- (149) Jain, R.K., (2001) Normalizing tumor vasculature with anti-angiogenic therapy: a new paradigm for combination therapy. *Nat Med* (7) 9, 987-9

- (150) Jain, R.K., (2003) Molecular regulation of vessel maturation. *Nat Med* (9) 6, 685-93
- (151) Jakupoglu, C., Przemeck, G.K., Schneider, M., Moreno, S.G., Mayr, N., Hatzopoulos, A.K., De Angelis, M.H., Wurst, W., Bornkamm, G.W., Brielmeier, M. and Conrad, M., (2005) Cytoplasmic thioredoxin reductase is essential for embryogenesis but dispensable for cardiac development. *Mol Cell Biol* (25) 5, 1980-8
- (152) Kaelin, W.G., Jr., (2005) ROS: really involved in oxygen sensing. *Cell Metab* (1) 6, 357-8
- (153) Kalluri, R. and Zeisberg, M., (2006) Fibroblasts in cancer. *Nat Rev Cancer* (6) 5, 392-401
- (154) Kaushal, S., Amiel, G.E., Guleserian, K.J., Shapira, O.M., Perry, T., Sutherland, F.W., Rabkin, E., Moran, A.M., Schoen, F.J., Atala, A., Soker, S., Bischoff, J. and Mayer, J.E., Jr., (2001) Functional small-diameter neovessels created using endothelial progenitor cells expanded ex vivo. *Nat Med* (7) 9, 1035-40
- (155) Keij, J.F., Bell-Prince, C. and Steinkamp, J.A., (2000) Staining of mitochondrial membranes with 10-nonyl acridine orange, MitoFluor Green, and MitoTracker Green is affected by mitochondrial membrane potential altering drugs. *Cytometry* (39) 3, 203-10
- (156) Keith, B. and Simon, M.C., (2007) Hypoxia-inducible factors, stem cells, and cancer. *Cell* (129) 3, 465-72
- (157) Kiermayer, C., Conrad, M., Schneider, M., Schmidt, J. and Brielmeier, M., (2007) Optimization of spatiotemporal gene inactivation in mouse heart by oral application of tamoxifen citrate. *Genesis* (45) 1, 11-6
- (158) Kietzmann, T. and Gorch, A., (2005) Reactive oxygen species in the control of hypoxia-inducible factor-mediated gene expression. *Semin Cell Dev Biol* (16) 4-5, 474-86
- (159) Kim, J.R., Lee, S.M., Cho, S.H., Kim, J.H., Kim, B.H., Kwon, J., Choi, C.Y., Kim, Y.D. and Lee, S.R., (2004) Oxidation of thioredoxin reductase in HeLa cells stimulated with tumor necrosis factor-alpha. *FEBS Lett* (567) 2-3, 189-96
- (160) Kim, K.J., Li, B., Winer, J., Armanini, M., Gillett, N., Phillips, H.S. and Ferrara, N., (1993) Inhibition of vascular endothelial growth factor-induced angiogenesis suppresses tumour growth in vivo. *Nature* (362) 6423, 841-4
- (161) Kim, M.R., Chang, H.S., Kim, B.H., Kim, S., Baek, S.H., Kim, J.H., Lee, S.R. and Kim, J.R., (2003) Involvements of mitochondrial thioredoxin reductase (TrxR2) in cell proliferation. *Biochem Biophys Res Commun* (304) 1, 119-24

- (162) Kim, W.J., Cho, H., Lee, S.W., Kim, Y.J. and Kim, K.W., (2005) Antisense-thioredoxin inhibits angiogenesis via pVHL-mediated hypoxia-inducible factor-1alpha degradation. *Int J Oncol* (26) 4, 1049-52
- (163) Kishimoto, C., Shioji, K., Nakamura, H., Nakayama, Y., Yodoi, J. and Sasayama, S., (2001) Serum thioredoxin (TRX) levels in patients with heart failure. *Jpn Circ J* (65) 6, 491-4
- (164) Klement, G., Baruchel, S., Rak, J., Man, S., Clark, K., Hicklin, D.J., Bohlen, P. and Kerbel, R.S., (2000) Continuous low-dose therapy with vinblastine and VEGF receptor-2 antibody induces sustained tumor regression without overt toxicity. *J Clin Invest* (105) 8, R15-24
- (165) Klimova, T. and Chandel, N.S., (2008) Mitochondrial complex III regulates hypoxic activation of HIF. *Cell Death Differ* (15) 4, 660-6
- (166) Knowles, H.J., Raval, R.R., Harris, A.L. and Ratcliffe, P.J., (2003) Effect of ascorbate on the activity of hypoxia-inducible factor in cancer cells. *Cancer Res* (63) 8, 1764-8
- (167) Kondo, N., Nakamura, H., Masutani, H. and Yodoi, J., (2006) Redox regulation of human thioredoxin network. *Antioxid Redox Signal* (8) 9-10, 1881-90
- (168) Kozin, S.V., Boucher, Y., Hicklin, D.J., Bohlen, P., Jain, R.K. and Suit, H.D., (2001) Vascular endothelial growth factor receptor-2-blocking antibody potentiates radiation-induced long-term control of human tumor xenografts. *Cancer Res* (61) 1, 39-44
- (169) Krieg, M., Haas, R., Brauch, H., Acker, T., Flamme, I. and Plate, K.H., (2000) Up-regulation of hypoxia-inducible factors HIF-1alpha and HIF-2alpha under normoxic conditions in renal carcinoma cells by von Hippel-Lindau tumor suppressor gene loss of function. *Oncogene* (19) 48, 5435-43
- (170) Kumar, S., Bjornstedt, M. and Holmgren, A., (1992) Selenite is a substrate for calf thymus thioredoxin reductase and thioredoxin and elicits a large non-stoichiometric oxidation of NADPH in the presence of oxygen. *Eur J Biochem* (207) 2, 435-39
- (171) Kupatt, C., Horstkotte, J., Vlastos, G.A., Pfosser, A., Lebherz, C., Semisch, M., Thalgott, M., Buttner, K., Browarzyk, C., Mages, J., Hoffmann, R., Deten, A., Lamparter, M., Muller, F., Beck, H., Buning, H., Boekstegers, P. and Hatzopoulos, A.K., (2005) Embryonic endothelial progenitor cells expressing a broad range of proangiogenic and remodeling factors enhance vascularization and tissue recovery in acute and chronic ischemia. *FASEB J* (19) 11, 1576-8
- (172) Kuznetsov, A.V., Mayboroda, O., Kunz, D., Winkler, K., Schubert, W. and Kunz, W.S., (1998) Functional imaging of mitochondria in saponin-permeabilized mice muscle fibers. *J Cell Biol* (140) 5, 1091-9

- (173) Kuznetsov, A.V., Schneeberger, S., Seiler, R., Brandacher, G., Mark, W., Steurer, W., Saks, V., Usson, Y., Margreiter, R. and Gnaiger, E., (2004) Mitochondrial defects and heterogeneous cytochrome c release after cardiac cold ischemia and reperfusion. *Am J Physiol Heart Circ Physiol* (286) 5, H1633-41
- (174) Land, H., Parada, L.F. and Weinberg, R.A., (1983) Tumorigenic conversion of primary embryo fibroblasts requires at least two cooperating oncogenes. *Nature* (304) 5927, 596-602
- (175) Lando, D., Pongratz, I., Poellinger, L. and Whitelaw, M.L., (2000) A redox mechanism controls differential DNA binding activities of hypoxia-inducible factor (HIF) 1 α and the HIF-like factor. *J Biol Chem* (275) 7, 4618-27
- (176) Lara, P.C., Lloret, M., Clavo, B., Apolinario, R.M., Henriquez-Hernandez, L.A., Bordon, E., Fontes, F. and Rey, A., (2009) Severe hypoxia induces chemo-resistance in clinical cervical tumors through MVP over-expression. *Radiat Oncol* (4) 29
- (177) Laurent, T.C., Moore, E.C. and Reichard, P., (1964) Enzymatic Synthesis of Deoxyribonucleotides. Iv. Isolation and Characterization of Thioredoxin, the Hydrogen Donor from Escherichia Coli B. *J Biol Chem* (239) 3436-44
- (178) Lee, C.G., Heijn, M., Di Tomaso, E., Griffon-Etienne, G., Ancukiewicz, M., Koike, C., Park, K.R., Ferrara, N., Jain, R.K., Suit, H.D. and Boucher, Y., (2000) Anti-Vascular endothelial growth factor treatment augments tumor radiation response under normoxic or hypoxic conditions. *Cancer Res* (60) 19, 5565-70
- (179) Lee, J.W., Bae, S.H., Jeong, J.W., Kim, S.H. and Kim, K.W., (2004) Hypoxia-inducible factor (HIF-1) α : its protein stability and biological functions. *Exp Mol Med* (36) 1, 1-12
- (180) Lee, K.A., Roth, R.A. and Lapres, J.J., (2007) Hypoxia, drug therapy and toxicity. *Pharmacol Ther* (113) 2, 229-46
- (181) Lee, S.R., Kim, J.R., Kwon, K.S., Yoon, H.W., Levine, R.L., Ginsburg, A. and Rhee, S.G., (1999) Molecular cloning and characterization of a mitochondrial selenocysteine-containing thioredoxin reductase from rat liver. *J Biol Chem* (274) 8, 4722-34
- (182) Lehr, H.A., Leunig, M., Menger, M.D., Nolte, D. and Messmer, K., (1993) Dorsal skinfold chamber technique for intravital microscopy in nude mice. *Am J Pathol* (143) 4, 1055-62
- (183) Lenaz, G., Baracca, A., Fato, R., Genova, M.L. and Solaini, G., (2006) New insights into structure and function of mitochondria and their role in aging and disease. *Antioxid Redox Signal* (8) 3-4, 417-37

- (184) Lescure, A., Gautheret, D., Carbon, P. and Krol, A., (1999) Novel selenoproteins identified in silico and in vivo by using a conserved RNA structural motif. *J Biol Chem* (274) 53, 38147-54
- (185) Lesnefsky, E.J., Moghaddas, S., Tandler, B., Kerner, J. and Hoppel, C.L., (2001) Mitochondrial dysfunction in cardiac disease: ischemia--reperfusion, aging, and heart failure. *J Mol Cell Cardiol* (33) 6, 1065-89
- (186) Leung, D.W., Cachianes, G., Kuang, W.J., Goeddel, D.V. and Ferrara, N., (1989) Vascular endothelial growth factor is a secreted angiogenic mitogen. *Science* (246) 4935, 1306-9
- (187) Liang, H., Yoo, S.E., Na, R., Walter, C.A., Richardson, A. and Ran, Q., (2009) Short form glutathione peroxidase 4 is the essential isoform required for survival and somatic mitochondrial functions. *J Biol Chem* (284) 45, 30836-44
- (188) Liao, D. and Johnson, R.S., (2007) Hypoxia: a key regulator of angiogenesis in cancer. *Cancer Metastasis Rev* (26) 2, 281-90
- (189) Lindenau, J., Noack, H., Asayama, K. and Wolf, G., (1998) Enhanced cellular glutathione peroxidase immunoreactivity in activated astrocytes and in microglia during excitotoxin induced neurodegeneration. *Glia* (24) 2, 252-6
- (190) Liu, Q., Berchner-Pfannschmidt, U., Moller, U., Brecht, M., Wotzlaw, C., Acker, H., Jungermann, K. and Kietzmann, T., (2004) A Fenton reaction at the endoplasmic reticulum is involved in the redox control of hypoxia-inducible gene expression. *Proc Natl Acad Sci U S A* (101) 12, 4302-7
- (191) Low, S.C. and Berry, M.J., (1996) Knowing when not to stop: selenocysteine incorporation in eukaryotes. *Trends Biochem Sci* (21) 6, 203-8
- (192) Lu, J., Chew, E.H. and Holmgren, A., (2007) Targeting thioredoxin reductase is a basis for cancer therapy by arsenic trioxide. *Proc Natl Acad Sci U S A* (104) 30, 12288-93
- (193) Magda, D., Lepp, C., Gerasimchuk, N., Lee, I., Sessler, J.L., Lin, A., Biaglow, J.E. and Miller, R.A., (2001) Redox cycling by motexafin gadolinium enhances cellular response to ionizing radiation by forming reactive oxygen species. *Int J Radiat Oncol Biol Phys* (51) 4, 1025-36
- (194) Magda, D. and Miller, R.A., (2006) Motexafin gadolinium: a novel redox active drug for cancer therapy. *Semin Cancer Biol* (16) 6, 466-76

- (195) Maiorino, M., Coassin, M., Roveri, A. and Ursini, F., (1989) Microsomal lipid peroxidation: effect of vitamin E and its functional interaction with phospholipid hydroperoxide glutathione peroxidase. *Lipids* (24) 8, 721-6
- (196) Mandal, P.K., (2009) Complex Redundancy between the Mammalian Thioredoxin and Glutathione Systems in Cell Proliferation and Tumorigenesis. Phd thesis, Faculty of Veterinary Medicine of the Ludwig-Maximilians-University, Munich
- (197) Mandal, P.K., Schneider, M., Kolle, P., Kuhlencordt, P., Forster, H., Beck, H., Bornkamm, G.W. and Conrad, M., (2010) Loss of thioredoxin reductase 1 renders tumors highly susceptible to pharmacologic glutathione deprivation. *Cancer Res* (70) 22, 9505-14
- (198) Mansfield, K.D., Guzy, R.D., Pan, Y., Young, R.M., Cash, T.P., Schumacker, P.T. and Simon, M.C., (2005) Mitochondrial dysfunction resulting from loss of cytochrome c impairs cellular oxygen sensing and hypoxic HIF- α activation. *Cell Metab* (1) 6, 393-9
- (199) Martinez-Sanchez, G. and Giuliani, A., (2007) Cellular redox status regulates hypoxia inducible factor-1 activity. Role in tumour development. *J Exp Clin Cancer Res* (26) 1, 39-50
- (200) Matsui, M., Oshima, M., Oshima, H., Takaku, K., Maruyama, T., Yodoi, J. and Taketo, M.M., (1996) Early embryonic lethality caused by targeted disruption of the mouse thioredoxin gene. *Dev Biol* (178) 1, 179-85
- (201) May, J.M., Mendiratta, S., Hill, K.E. and Burk, R.F., (1997) Reduction of dehydroascorbate to ascorbate by the selenoenzyme thioredoxin reductase. *J Biol Chem* (272) 36, 22607-10
- (202) May, J.M., Cobb, C.E., Mendiratta, S., Hill, K.E. and Burk, R.F., (1998) Reduction of the ascorbyl free radical to ascorbate by thioredoxin reductase. *J Biol Chem* (273) 36, 23039-45
- (203) Mayevsky, A., (2009) Mitochondrial function and energy metabolism in cancer cells: past overview and future perspectives. *Mitochondrion* (9) 3, 165-79
- (204) McBride, H.M., Neuspiel, M. and Wasiak, S., (2006) Mitochondria: more than just a powerhouse. *Curr Biol* (16) 14, R551-60
- (205) McCloskey, K.E., Gilroy, M.E. and Nerem, R.M., (2005) Use of embryonic stem cell-derived endothelial cells as a cell source to generate vessel structures in vitro. *Tissue Eng* (11) 3-4, 497-505
- (206) Medina, R.A. and Owen, G.I., (2002) Glucose transporters: expression, regulation and cancer. *Biol Res* (35) 1, 9-26

- (207) Mehta, M.P., Shapiro, W.R., Phan, S.C., Gervais, R., Carrie, C., Chabot, P., Patchell, R.A., Glantz, M.J., Recht, L., Langer, C., Sur, R.K., Roa, W.H., Mahe, M.A., Fortin, A., Nieder, C., Meyers, C.A., Smith, J.A., Miller, R.A. and Renschler, M.F., (2009) Motexafin gadolinium combined with prompt whole brain radiotherapy prolongs time to neurologic progression in non-small-cell lung cancer patients with brain metastases: results of a phase III trial. *Int J Radiat Oncol Biol Phys* (73) 4, 1069-76
- (208) Melnyk, O., Shuman, M.A. and Kim, K.J., (1996) Vascular endothelial growth factor promotes tumor dissemination by a mechanism distinct from its effect on primary tumor growth. *Cancer Res* (56) 4, 921-4
- (209) Metivier, D., Dallaporta, B., Zamzami, N., Larochette, N., Susin, S.A., Marzo, I. and Kroemer, G., (1998) Cytofluorometric detection of mitochondrial alterations in early CD95/Fas/APO-1-triggered apoptosis of Jurkat T lymphoma cells. Comparison of seven mitochondrion-specific fluorochromes. *Immunol Lett* (61) 2-3, 157-63
- (210) Metzen, E., Berchner-Pfannschmidt, U., Stengel, P., Marxsen, J.H., Stolze, I., Klinger, M., Huang, W.Q., Wotzlaw, C., Hellwig-Burgel, T., Jelkmann, W., Acker, H. and Fandrey, J., (2003) Intracellular localisation of human HIF-1 alpha hydroxylases: implications for oxygen sensing. *J Cell Sci* (116) Pt 7, 1319-26
- (211) Mills, G.C., (1957) Hemoglobin catabolism. I. Glutathione peroxidase, an erythrocyte enzyme which protects hemoglobin from oxidative breakdown. *J Biol Chem* (229) 1, 189-97
- (212) Min, W., Xu, L.K., Zhou, H.J., Huang, Q., Zhang, H., He, Y., Zhe, X. and Luo, Y., (2010) Thioredoxin and redox signaling in vasculature-studies using Trx2 endothelium-specific transgenic mice. *Methods Enzymol* (474) 315-24
- (213) Miranda-Vizuete, A., Damdimopoulos, A.E., Pedrajas, J.R., Gustafsson, J.A. and Spyrou, G., (1999) Human mitochondrial thioredoxin reductase cDNA cloning, expression and genomic organization. *Eur J Biochem* (261) 2, 405-12
- (214) Miranda-Vizuete, A., Damdimopoulos, A.E. and Spyrou, G., (1999) cDNA cloning, expression and chromosomal localization of the mouse mitochondrial thioredoxin reductase gene(1). *Biochim Biophys Acta* (1447) 1, 113-8
- (215) Miranda-Vizuete, A., Damdimopoulos, A.E. and Spyrou, G., (2000) The mitochondrial thioredoxin system. *Antioxid Redox Signal* (2) 4, 801-10
- (216) Monge, C., Beraud, N., Kuznetsov, A.V., Rostovtseva, T., Sackett, D., Schlattner, U., Vendelin, M. and Saks, V.A., (2008) Regulation of respiration in brain mitochondria and synaptosomes: restrictions of ADP diffusion in situ, roles of tubulin, and mitochondrial creatine kinase. *Mol Cell Biochem* (318) 1-2, 147-65

- (217) Mori, S., Chang, J.T., Andrechek, E.R., Matsumura, N., Baba, T., Yao, G., Kim, J.W., Gatzka, M., Murphy, S. and Nevins, J.R., (2009) Anchorage-independent cell growth signature identifies tumors with metastatic potential. *Oncogene* (28) 31, 2796-805
- (218) Mosmann, T., (1983) Rapid colorimetric assay for cellular growth and survival: application to proliferation and cytotoxicity assays. *J Immunol Methods* (65) 1-2, 55-63
- (219) Mukherjee, A. and Martin, S.G., (2008) The thioredoxin system: a key target in tumour and endothelial cells. *Br J Radiol* (81 Spec No 1) S57-68
- (220) Murohara, T., Ikeda, H., Duan, J., Shintani, S., Sasaki, K., Eguchi, H., Onitsuka, I., Matsui, K. and Imaizumi, T., (2000) Transplanted cord blood-derived endothelial precursor cells augment postnatal neovascularization. *J Clin Invest* (105) 11, 1527-36
- (221) Mustacich, D. and Powis, G., (2000) Thioredoxin reductase. *Biochem J* (346 Pt 1) 1-8
- (222) Nagy, J.A., Vasile, E., Feng, D., Sundberg, C., Brown, L.F., Detmar, M.J., Lawitts, J.A., Benjamin, L., Tan, X., Manseau, E.J., Dvorak, A.M. and Dvorak, H.F., (2002) Vascular permeability factor/vascular endothelial growth factor induces lymphangiogenesis as well as angiogenesis. *J Exp Med* (196) 11, 1497-506
- (223) Nagy, J.A., Vasile, E., Feng, D., Sundberg, C., Brown, L.F., Manseau, E.J., Dvorak, A.M. and Dvorak, H.F., (2002) VEGF-A induces angiogenesis, arteriogenesis, lymphangiogenesis, and vascular malformations. *Cold Spring Harb Symp Quant Biol* (67) 227-37
- (224) Nakamura, H., Nakamura, K. and Yodoi, J., (1997) Redox regulation of cellular activation. *Annu Rev Immunol* (15) 351-69
- (225) Nakamura, H., De Rosa, S.C., Yodoi, J., Holmgren, A., Ghezzi, P. and Herzenberg, L.A., (2001) Chronic elevation of plasma thioredoxin: inhibition of chemotaxis and curtailment of life expectancy in AIDS. *Proc Natl Acad Sci U S A* (98) 5, 2688-93
- (226) Nakamura, H., (2004) Thioredoxin as a key molecule in redox signaling. *Antioxid Redox Signal* (6) 1, 15-7
- (227) Nakatsu, M.N., Sainson, R.C., Aoto, J.N., Taylor, K.L., Aitkenhead, M., Perez-Del-Pulgar, S., Carpenter, P.M. and Hughes, C.C., (2003) Angiogenic sprouting and capillary lumen formation modeled by human umbilical vein endothelial cells (HUVEC) in fibrin gels: the role of fibroblasts and Angiopoietin-1. *Microvasc Res* (66) 2, 102-12

- (228) Nalvarte, I., Dandimopoulos, A.E., Nystom, C., Nordman, T., Miranda-Vizuete, A., Olsson, J.M., Eriksson, L., Bjornstedt, M., Arner, E.S. and Spyrou, G., (2004) Overexpression of enzymatically active human cytosolic and mitochondrial thioredoxin reductase in HEK-293 cells. Effect on cell growth and differentiation. *J Biol Chem* (279) 52, 54510-7
- (229) Nehls, V. and Drenckhahn, D., (1995) A microcarrier-based cocultivation system for the investigation of factors and cells involved in angiogenesis in three-dimensional fibrin matrices in vitro. *Histochem Cell Biol* (104) 6, 459-66
- (230) Nesbit, C.E., Tersak, J.M. and Prochownik, E.V., (1999) MYC oncogenes and human neoplastic disease. *Oncogene* (18) 19, 3004-16
- (231) Neuzil, J., Dyason, J.C., Freeman, R., Dong, L.F., Prochazka, L., Wang, X.F., Scheffler, I. and Ralph, S.J., (2007) Mitocans as anti-cancer agents targeting mitochondria: lessons from studies with vitamin E analogues, inhibitors of complex II. *J Bioenerg Biomembr* (39) 1, 65-72
- (232) Nicosia, R.F., Nicosia, S.V. and Smith, M., (1994) Vascular endothelial growth factor, platelet-derived growth factor, and insulin-like growth factor-1 promote rat aortic angiogenesis in vitro. *Am J Pathol* (145) 5, 1023-9
- (233) Nonn, L., Williams, R.R., Erickson, R.P. and Powis, G., (2003) The absence of mitochondrial thioredoxin 2 causes massive apoptosis, exencephaly, and early embryonic lethality in homozygous mice. *Mol Cell Biol* (23) 3, 916-22
- (234) Nulton-Persson, A.C. and Szweda, L.I., (2001) Modulation of mitochondrial function by hydrogen peroxide. *J Biol Chem* (276) 26, 23357-61
- (235) Ott, M., Gogvadze, V., Orrenius, S. and Zhivotovsky, B., (2007) Mitochondria, oxidative stress and cell death. *Apoptosis* (12) 5, 913-22
- (236) Paez-Ribes, M., Allen, E., Hudock, J., Takeda, T., Okuyama, H., Vinals, F., Inoue, M., Bergers, G., Hanahan, D. and Casanovas, O., (2009) Antiangiogenic therapy elicits malignant progression of tumors to increased local invasion and distant metastasis. *Cancer Cell* (15) 3, 220-31
- (237) Palade, G.E., (1952) The fine structure of mitochondria. *Anat Rec* (114) 3, 427-51
- (238) Park, J.H., Kim, T.Y., Jong, H.S., Chun, Y.S., Park, J.W., Lee, C.T., Jung, H.C., Kim, N.K. and Bang, Y.J., (2003) Gastric epithelial reactive oxygen species prevent normoxic degradation of hypoxia-inducible factor-1alpha in gastric cancer cells. *Clin Cancer Res* (9) 1, 433-40

- (239) Patel, M.S. and Korotchkina, L.G., (2001) Regulation of mammalian pyruvate dehydrogenase complex by phosphorylation: complexity of multiple phosphorylation sites and kinases. *Exp Mol Med* (33) 4, 191-7
- (240) Patel, M.S. and Korotchkina, L.G., (2006) Regulation of the pyruvate dehydrogenase complex. *Biochem Soc Trans* (34) Pt 2, 217-22
- (241) Pedrajas, J.R., Kosmidou, E., Miranda-Vizuete, A., Gustafsson, J.A., Wright, A.P. and Spyrou, G., (1999) Identification and functional characterization of a novel mitochondrial thioredoxin system in *Saccharomyces cerevisiae*. *J Biol Chem* (274) 10, 6366-73
- (242) Pendergrass, W., Wolf, N. and Poot, M., (2004) Efficacy of MitoTracker Green and CMXrosamine to measure changes in mitochondrial membrane potentials in living cells and tissues. *Cytometry A* (61) 2, 162-9
- (243) Pepper, M.S., Ferrara, N., Orci, L. and Montesano, R., (1992) Potent synergism between vascular endothelial growth factor and basic fibroblast growth factor in the induction of angiogenesis in vitro. *Biochem Biophys Res Commun* (189) 2, 824-31
- (244) Pepper, M.S., Wasi, S., Ferrara, N., Orci, L. and Montesano, R., (1994) In vitro angiogenic and proteolytic properties of bovine lymphatic endothelial cells. *Exp Cell Res* (210) 2, 298-305
- (245) Perisic, T., (2009) Addressing the Role of Mitochondrial Thioredoxin Reductase and xCT in the Maintenance of Redox Homeostasis. Phd thesis, Faculty of Biology at the Ludwig-Maximilians-University, Munich
- (246) Petronilli, V., Costantini, P., Scorrano, L., Colonna, R., Passamonti, S. and Bernardi, P., (1994) The voltage sensor of the mitochondrial permeability transition pore is tuned by the oxidation-reduction state of vicinal thiols. Increase of the gating potential by oxidants and its reversal by reducing agents. *J Biol Chem* (269) 24, 16638-42
- (247) Petros, J.A., Baumann, A.K., Ruiz-Pesini, E., Amin, M.B., Sun, C.Q., Hall, J., Lim, S., Issa, M.M., Flanders, W.D., Hosseini, S.H., Marshall, F.F. and Wallace, D.C., (2005) mtDNA mutations increase tumorigenicity in prostate cancer. *Proc Natl Acad Sci U S A* (102) 3, 719-24
- (248) Pfeiffer, T., Schuster, S. and Bonhoeffer, S., (2001) Cooperation and competition in the evolution of ATP-producing pathways. *Science* (292) 5516, 504-7
- (249) Plate, K.H., Breier, G., Weich, H.A. and Risau, W., (1992) Vascular endothelial growth factor is a potential tumour angiogenesis factor in human gliomas in vivo. *Nature* (359) 6398, 845-8

- (250) Plouet, J., Schilling, J. and Gospodarowicz, D., (1989) Isolation and characterization of a newly identified endothelial cell mitogen produced by AtT-20 cells. *EMBO J* (8) 12, 3801-6
- (251) Pollard, P.J., Wortham, N.C. and Tomlinson, I.P., (2003) The TCA cycle and tumorigenesis: the examples of fumarate hydratase and succinate dehydrogenase. *Ann Med* (35) 8, 632-9
- (252) Polyak, K., Li, Y., Zhu, H., Lengauer, C., Willson, J.K., Markowitz, S.D., Trush, M.A., Kinzler, K.W. and Vogelstein, B., (1998) Somatic mutations of the mitochondrial genome in human colorectal tumours. *Nat Genet* (20) 3, 291-3
- (253) Pouyssegur, J. and Mechta-Grigoriou, F., (2006) Redox regulation of the hypoxia-inducible factor. *Biol Chem* (387) 10-11, 1337-46
- (254) Powis, G., Briehl, M. and Oblong, J., (1995) Redox signalling and the control of cell growth and death. *Pharmacol Ther* (68) 1, 149-73
- (255) Powis, G. and Kirkpatrick, D.L., (2007) Thioredoxin signaling as a target for cancer therapy. *Curr Opin Pharmacol* (7) 4, 392-7
- (256) Presta, L.G., Chen, H., O'connor, S.J., Chisholm, V., Meng, Y.G., Krummen, L., Winkler, M. and Ferrara, N., (1997) Humanization of an anti-vascular endothelial growth factor monoclonal antibody for the therapy of solid tumors and other disorders. *Cancer Res* (57) 20, 4593-9
- (257) Prewett, M., Huber, J., Li, Y., Santiago, A., O'connor, W., King, K., Overholser, J., Hooper, A., Pytowski, B., Witte, L., Bohlen, P. and Hicklin, D.J., (1999) Antivascular endothelial growth factor receptor (fetal liver kinase 1) monoclonal antibody inhibits tumor angiogenesis and growth of several mouse and human tumors. *Cancer Res* (59) 20, 5209-18
- (258) Rabilloud, T., Heller, M., Rigobello, M.P., Bindoli, A., Aebersold, R. and Lunardi, J., (2001) The mitochondrial antioxidant defence system and its response to oxidative stress. *Proteomics* (1) 9, 1105-10
- (259) Radi, R., Sims, S., Cassina, A. and Turrens, J.F., (1993) Roles of catalase and cytochrome c in hydroperoxide-dependent lipid peroxidation and chemiluminescence in rat heart and kidney mitochondria. *Free Radic Biol Med* (15) 6, 653-9
- (260) Rasbach, K.A. and Schnellmann, R.G., (2007) Signaling of mitochondrial biogenesis following oxidant injury. *J Biol Chem* (282) 4, 2355-62
- (261) Rasbach, K.A. and Schnellmann, R.G., (2007) PGC-1alpha over-expression promotes recovery from mitochondrial dysfunction and cell injury. *Biochem Biophys Res Commun* (355) 3, 734-9

- (262) Ratcliffe, P.J., O'Rourke, J.F., Maxwell, P.H. and Pugh, C.W., (1998) Oxygen sensing, hypoxia-inducible factor-1 and the regulation of mammalian gene expression. *J Exp Biol* (201) Pt 8, 1153-62
- (263) Reed, L.J., (2001) A trail of research from lipoic acid to alpha-keto acid dehydrogenase complexes. *J Biol Chem* (276) 42, 38329-36
- (264) Reitzer, L.J., Wice, B.M. and Kennell, D., (1979) Evidence that glutamine, not sugar, is the major energy source for cultured HeLa cells. *J Biol Chem* (254) 8, 2669-76
- (265) Reyes, M., Dudek, A., Jahagirdar, B., Koodie, L., Marker, P.H. and Verfaillie, C.M., (2002) Origin of endothelial progenitors in human postnatal bone marrow. *J Clin Invest* (109) 3, 337-46
- (266) Richards, G.M. and Mehta, M.P., (2007) Motexafin gadolinium in the treatment of brain metastases. *Expert Opin Pharmacother* (8) 3, 351-9
- (267) Rigobello, M.P., Callegaro, M.T., Barzon, E., Benetti, M. and Bindoli, A., (1998) Purification of mitochondrial thioredoxin reductase and its involvement in the redox regulation of membrane permeability. *Free Radic Biol Med* (24) 2, 370-6
- (268) Rigobello, M.P., Scutari, G., Boscolo, R. and Bindoli, A., (2002) Induction of mitochondrial permeability transition by auranofin, a gold(I)-phosphine derivative. *Br J Pharmacol* (136) 8, 1162-8
- (269) Rigobello, M.P., Scutari, G., Folda, A. and Bindoli, A., (2004) Mitochondrial thioredoxin reductase inhibition by gold(I) compounds and concurrent stimulation of permeability transition and release of cytochrome c. *Biochem Pharmacol* (67) 4, 689-96
- (270) Rodriguez, J.A., Nespereira, B., Perez-Illarbe, M., Eguinoa, E. and Paramo, J.A., (2005) Vitamins C and E prevent endothelial VEGF and VEGFR-2 overexpression induced by porcine hypercholesterolemic LDL. *Cardiovasc Res* (65) 3, 665-73
- (271) Rommel, C. and Hafen, E., (1998) Ras--a versatile cellular switch. *Curr Opin Genet Dev* (8) 4, 412-8
- (272) Rossignol, R., Gilkerson, R., Aggeler, R., Yamagata, K., Remington, S.J. and Capaldi, R.A., (2004) Energy substrate modulates mitochondrial structure and oxidative capacity in cancer cells. *Cancer Res* (64) 3, 985-93
- (273) Rotruck, J.T., Pope, A.L., Ganther, H.E., Swanson, A.B., Hafeman, D.G. and Hoekstra, W.G., (1973) Selenium: biochemical role as a component of glutathione peroxidase. *Science* (179) 73, 588-90

- (274) Roychoudhury, A., Basu, S. and Sengupta, D.N., (2009) Analysis of comparative efficiencies of different transformation methods of *E. coli* using two common plasmid vectors. *Indian J Biochem Biophys* (46) 5, 395-400
- (275) Rozen, S. and Skaletsky, H., (2000) Primer3 on the WWW for general users and for biologist programmers. *Methods Mol Biol* (132) 365-86
- (276) Ruggero, D., (2009) The role of Myc-induced protein synthesis in cancer. *Cancer Res* (69) 23, 8839-43
- (277) Russo, A., Degraff, W., Friedman, N. and Mitchell, J.B., (1986) Selective modulation of glutathione levels in human normal versus tumor cells and subsequent differential response to chemotherapy drugs. *Cancer Res* (46) 6, 2845-8
- (278) Sainson, R.C., Aoto, J., Nakatsu, M.N., Holderfield, M., Conn, E., Koller, E. and Hughes, C.C., (2005) Cell-autonomous notch signaling regulates endothelial cell branching and proliferation during vascular tubulogenesis. *FASEB J* (19) 8, 1027-9
- (279) Salnikow, K., Donald, S.P., Bruick, R.K., Zhitkovich, A., Phang, J.M. and Kasprzak, K.S., (2004) Depletion of intracellular ascorbate by the carcinogenic metals nickel and cobalt results in the induction of hypoxic stress. *J Biol Chem* (279) 39, 40337-44
- (280) Sanjuan-Pla, A., Cervera, A.M., Apostolova, N., Garcia-Bou, R., Victor, V.M., Murphy, M.P. and McCreath, K.J., (2005) A targeted antioxidant reveals the importance of mitochondrial reactive oxygen species in the hypoxic signaling of HIF-1alpha. *FEBS Lett* (579) 12, 2669-74
- (281) Scheel, C., Onder, T., Karnoub, A. and Weinberg, R.A., (2007) Adaptation versus selection: the origins of metastatic behavior. *Cancer Res* (67) 24, 11476-9; discussion 11479-80
- (282) Schofield, C.J. and Ratcliffe, P.J., (2004) Oxygen sensing by HIF hydroxylases. *Nat Rev Mol Cell Biol* (5) 5, 343-54
- (283) Semenza, G.L. and Wang, G.L., (1992) A nuclear factor induced by hypoxia via de novo protein synthesis binds to the human erythropoietin gene enhancer at a site required for transcriptional activation. *Mol Cell Biol* (12) 12, 5447-54
- (284) Semenza, G.L., Agani, F., Booth, G., Forsythe, J., Iyer, N., Jiang, B.H., Leung, S., Roe, R., Wiener, C. and Yu, A., (1997) Structural and functional analysis of hypoxia-inducible factor 1. *Kidney Int* (51) 2, 553-5
- (285) Semenza, G.L., (1998) Hypoxia-inducible factor 1: master regulator of O₂ homeostasis. *Curr Opin Genet Dev* (8) 5, 588-94

- (286) Senger, D.R., Galli, S.J., Dvorak, A.M., Perruzzi, C.A., Harvey, V.S. and Dvorak, H.F., (1983) Tumor cells secrete a vascular permeability factor that promotes accumulation of ascites fluid. *Science* (219) 4587, 983-5
- (287) Septinus, M., Berthold, T., Naujok, A. and Zimmermann, H.W., (1985) [Hydrophobic acridine dyes for fluorescent staining of mitochondria in living cells. 3. Specific accumulation of the fluorescent dye NAO on the mitochondrial membranes in HeLa cells by hydrophobic interaction. Depression of respiratory activity, changes in the ultrastructure of mitochondria due to NAO. Increase of fluorescence in vital stained mitochondria in situ by irradiation]. *Histochemistry* (82) 1, 51-66
- (288) Shatrov, V.A., Sumbayev, V.V., Zhou, J. and Brune, B., (2003) Oxidized low-density lipoprotein (oxLDL) triggers hypoxia-inducible factor-1alpha (HIF-1alpha) accumulation via redox-dependent mechanisms. *Blood* (101) 12, 4847-9
- (289) Shidara, Y., Yamagata, K., Kanamori, T., Nakano, K., Kwong, J.Q., Manfredi, G., Oda, H. and Ohta, S., (2005) Positive contribution of pathogenic mutations in the mitochondrial genome to the promotion of cancer by prevention from apoptosis. *Cancer Res* (65) 5, 1655-63
- (290) Shigenaga, M.K., Hagen, T.M. and Ames, B.N., (1994) Oxidative damage and mitochondrial decay in aging. *Proc Natl Acad Sci U S A* (91) 23, 10771-8
- (291) Singh, A.M. and Dalton, S., (2009) The cell cycle and Myc intersect with mechanisms that regulate pluripotency and reprogramming. *Cell Stem Cell* (5) 2, 141-9
- (292) Soerensen, J., Jakupoglu, C., Beck, H., Forster, H., Schmidt, J., Schmahl, W., Schweizer, U., Conrad, M. and Brielmeier, M., (2008) The role of thioredoxin reductases in brain development. *PLoS One* (3) 3, e1813
- (293) Spyrou, G., Enmark, E., Miranda-Vizuetes, A. and Gustafsson, J., (1997) Cloning and expression of a novel mammalian thioredoxin. *J Biol Chem* (272) 5, 2936-41
- (294) Srivastava, S., Diaz, F., Iommarini, L., Aure, K., Lombes, A. and Moraes, C.T., (2009) PGC-1alpha/beta induced expression partially compensates for respiratory chain defects in cells from patients with mitochondrial disorders. *Hum Mol Genet* (18) 10, 1805-12
- (295) St-Pierre, J., Drori, S., Uldry, M., Silvaggi, J.M., Rhee, J., Jager, S., Handschin, C., Zheng, K., Lin, J., Yang, W., Simon, D.K., Bachoo, R. and Spiegelman, B.M., (2006) Suppression of reactive oxygen species and neurodegeneration by the PGC-1 transcriptional coactivators. *Cell* (127) 2, 397-408
- (296) Stiehl, D.P., Jelkmann, W., Wenger, R.H. and Hellwig-Burgel, T., (2002) Normoxic induction of the hypoxia-inducible factor 1alpha by insulin and interleukin-1beta involves the phosphatidylinositol 3-kinase pathway. *FEBS Lett* (512) 1-3, 157-62

- (297) Streicher, K.L., Sylte, M.J., Johnson, S.E. and Sordillo, L.M., (2004) Thioredoxin reductase regulates angiogenesis by increasing endothelial cell-derived vascular endothelial growth factor. *Nutr Cancer* (50) 2, 221-31
- (298) Strumilo, S., (2005) Short-term regulation of the mammalian pyruvate dehydrogenase complex. *Acta Biochim Pol* (52) 4, 759-64
- (299) Sugden, M.C. and Holness, M.J., (2006) Mechanisms underlying regulation of the expression and activities of the mammalian pyruvate dehydrogenase kinases. *Arch Physiol Biochem* (112) 3, 139-49
- (300) Sugiyama, T. and Michel, T., (2010) Thiol-metabolizing proteins and endothelial redox state: differential modulation of eNOS and biopterin pathways. *Am J Physiol Heart Circ Physiol* (298) 1, H194-201
- (301) Sun, Q.A., Wu, Y., Zappacosta, F., Jeang, K.T., Lee, B.J., Hatfield, D.L. and Gladyshev, V.N., (1999) Redox regulation of cell signaling by selenocysteine in mammalian thioredoxin reductases. *J Biol Chem* (274) 35, 24522-30
- (302) Sun, Q.A., Kirnarsky, L., Sherman, S. and Gladyshev, V.N., (2001) Selenoprotein oxidoreductase with specificity for thioredoxin and glutathione systems. *Proc Natl Acad Sci U S A* (98) 7, 3673-8
- (303) Sun, Q.A., Zappacosta, F., Factor, V.M., Wirth, P.J., Hatfield, D.L. and Gladyshev, V.N., (2001) Heterogeneity within animal thioredoxin reductases. Evidence for alternative first exon splicing. *J Biol Chem* (276) 5, 3106-14
- (304) Takeda, K., Aguila, H.L., Parikh, N.S., Li, X., Lamothe, K., Duan, L.J., Takeda, H., Lee, F.S. and Fong, G.H., (2008) Regulation of adult erythropoiesis by prolyl hydroxylase domain proteins. *Blood* (111) 6, 3229-35
- (305) Talks, K.L., Turley, H., Gatter, K.C., Maxwell, P.H., Pugh, C.W., Ratcliffe, P.J. and Harris, A.L., (2000) The expression and distribution of the hypoxia-inducible factors HIF-1alpha and HIF-2alpha in normal human tissues, cancers, and tumor-associated macrophages. *Am J Pathol* (157) 2, 411-21
- (306) Tamura, T. and Stadtman, T.C., (1996) A new selenoprotein from human lung adenocarcinoma cells: purification, properties, and thioredoxin reductase activity. *Proc Natl Acad Sci U S A* (93) 3, 1006-11
- (307) Tan, S., Sagara, Y., Liu, Y., Maher, P. and Schubert, D., (1998) The regulation of reactive oxygen species production during programmed cell death. *J Cell Biol* (141) 6, 1423-32

- (308) Thews, O., Wolloscheck, T., Dillenburg, W., Kraus, S., Kelleher, D.K., Konerding, M.A. and Vaupel, P., (2004) Microenvironmental adaptation of experimental tumours to chronic vs acute hypoxia. *Br J Cancer* (91) 6, 1181-9
- (309) Tietze, F., (1969) Enzymic method for quantitative determination of nanogram amounts of total and oxidized glutathione: applications to mammalian blood and other tissues. *Anal Biochem* (27) 3, 502-22
- (310) Tonissen, K.F. and Di Trapani, G., (2009) Thioredoxin system inhibitors as mediators of apoptosis for cancer therapy. *Mol Nutr Food Res* (53) 1, 87-103
- (311) Trachootham, D., Alexandre, J. and Huang, P., (2009) Targeting cancer cells by ROS-mediated mechanisms: a radical therapeutic approach? *Nat Rev Drug Discov* (8) 7, 579-91
- (312) Tran, J., Rak, J., Sheehan, C., Saibil, S.D., Lacasse, E., Korneluk, R.G. and Kerbel, R.S., (1999) Marked induction of the IAP family antiapoptotic proteins survivin and XIAP by VEGF in vascular endothelial cells. *Biochem Biophys Res Commun* (264) 3, 781-8
- (313) Tran, J., Master, Z., Yu, J.L., Rak, J., Dumont, D.J. and Kerbel, R.S., (2002) A role for survivin in chemoresistance of endothelial cells mediated by VEGF. *Proc Natl Acad Sci U S A* (99) 7, 4349-54
- (314) Traynor, A.M., Thomas, J.P., Ramanathan, R.K., Mody, T.D., Alberti, D., Wilding, G. and Bailey, H.H., (2009) Phase I trial of motexafin gadolinium and doxorubicin in the treatment of advanced malignancies. *Invest New Drugs*
- (315) Turanov, A.A., Su, D. and Gladyshev, V.N., (2006) Characterization of alternative cytosolic forms and cellular targets of mouse mitochondrial thioredoxin reductase. *J Biol Chem* (281) 32, 22953-63
- (316) Urig, S. and Becker, K., (2006) On the potential of thioredoxin reductase inhibitors for cancer therapy. *Semin Cancer Biol* (16) 6, 452-65
- (317) Ursini, F., Maiorino, M., Valente, M., Ferri, L. and Gregolin, C., (1982) Purification from pig liver of a protein which protects liposomes and biomembranes from peroxidative degradation and exhibits glutathione peroxidase activity on phosphatidylcholine hydroperoxides. *Biochim Biophys Acta* (710) 2, 197-211
- (318) Volm, M., Koomagi, R. and Mattern, J., (1997) Prognostic value of vascular endothelial growth factor and its receptor Flt-1 in squamous cell lung cancer. *Int J Cancer* (74) 1, 64-8
- (319) Wakabayashi, T. and Spodnik, J.H., (2000) Structural changes of mitochondria during free radical-induced apoptosis. *Folia Morphol (Warsz)* (59) 2, 61-75

- (320) Wakabayashi, T., (2002) Megamitochondria formation - physiology and pathology. *J Cell Mol Med* (6) 4, 497-538
- (321) Walajtys, E.I., Gottesman, D.P. and Williamson, J.R., (1974) Regulation of pyruvate dehydrogenase in rat liver mitochondria by phosphorylation-dephosphorylation. *J Biol Chem* (249) 6, 1857-65
- (322) Wallace, D.C., (2005) A mitochondrial paradigm of metabolic and degenerative diseases, aging, and cancer: a dawn for evolutionary medicine. *Annu Rev Genet* (39) 359-407
- (323) Wang, G.L., Jiang, B.H., Rue, E.A. and Semenza, G.L., (1995) Hypoxia-inducible factor 1 is a basic-helix-loop-helix-PAS heterodimer regulated by cellular O₂ tension. *Proc Natl Acad Sci U S A* (92) 12, 5510-4
- (324) Wang, G.L., Jiang, B.H. and Semenza, G.L., (1995) Effect of altered redox states on expression and DNA-binding activity of hypoxia-inducible factor 1. *Biochem Biophys Res Commun* (212) 2, 550-6
- (325) Wang, G.L., Jiang, B.H. and Semenza, G.L., (1995) Effect of protein kinase and phosphatase inhibitors on expression of hypoxia-inducible factor 1. *Biochem Biophys Res Commun* (216) 2, 669-75
- (326) Warburg, O., (1956) On respiratory impairment in cancer cells. *Science* (124) 3215, 269-70
- (327) Warburg, O., (1956) On the origin of cancer cells. *Science* (123) 3191, 309-14
- (328) Warren, R.S., Yuan, H., Matli, M.R., Gillett, N.A. and Ferrara, N., (1995) Regulation by vascular endothelial growth factor of human colon cancer tumorigenesis in a mouse model of experimental liver metastasis. *J Clin Invest* (95) 4, 1789-97
- (329) Watabe, S., Hiroi, T., Yamamoto, Y., Fujioka, Y., Hasegawa, H., Yago, N. and Takahashi, S.Y., (1997) SP-22 is a thioredoxin-dependent peroxide reductase in mitochondria. *Eur J Biochem* (249) 1, 52-60
- (330) Watabe, S., Makino, Y., Ogawa, K., Hiroi, T., Yamamoto, Y. and Takahashi, S.Y., (1999) Mitochondrial thioredoxin reductase in bovine adrenal cortex its purification, properties, nucleotide/amino acid sequences, and identification of selenocysteine. *Eur J Biochem* (264) 1, 74-84
- (331) Watanabe, T., Sagisaka, H., Arakawa, S., Shibaya, Y., Watanabe, M., Igarashi, I., Tanaka, K., Totsuka, S., Takasaki, W. and Manabe, S., (2003) A novel model of continuous depletion of glutathione in mice treated with L-buthionine (S,R)-sulfoximine. *J Toxicol Sci* (28) 5, 455-69

- (332) Webb, C.P. and Vande Woude, G.F., (2000) Genes that regulate metastasis and angiogenesis. *J Neurooncol* (50) 1-2, 71-87
- (333) Wedge, S.R., Ogilvie, D.J., Dukes, M., Kendrew, J., Curwen, J.O., Hennequin, L.F., Thomas, A.P., Stokes, E.S., Curry, B., Richmond, G.H. and Wadsworth, P.F., (2000) ZD4190: an orally active inhibitor of vascular endothelial growth factor signaling with broad-spectrum antitumor efficacy. *Cancer Res* (60) 4, 970-5
- (334) Weichsel, A., Gasdaska, J.R., Powis, G. and Montfort, W.R., (1996) Crystal structures of reduced, oxidized, and mutated human thioredoxins: evidence for a regulatory homodimer. *Structure* (4) 6, 735-51
- (335) Weinberg, F. and Chandel, N.S., (2009) Mitochondrial metabolism and cancer. *Ann N Y Acad Sci* (1177) 66-73
- (336) Weinberg, R.A., (1996) How cancer arises. *Sci Am* (275) 3, 62-70
- (337) Weinberg, R.A., (2008) Mechanisms of malignant progression. *Carcinogenesis* (29) 6, 1092-5
- (338) Welsh, S.J., Bellamy, W.T., Briehl, M.M. and Powis, G., (2002) The redox protein thioredoxin-1 (Trx-1) increases hypoxia-inducible factor 1alpha protein expression: Trx-1 overexpression results in increased vascular endothelial growth factor production and enhanced tumor angiogenesis. *Cancer Res* (62) 17, 5089-95
- (339) Welsh, S.J., Williams, R.R., Birmingham, A., Newman, D.J., Kirkpatrick, D.L. and Powis, G., (2003) The thioredoxin redox inhibitors 1-methylpropyl 2-imidazolyl disulfide and pleurotin inhibit hypoxia-induced factor 1alpha and vascular endothelial growth factor formation. *Mol Cancer Ther* (2) 3, 235-43
- (340) Wenger, R.H., Kvietikova, I., Rolfs, A., Gassmann, M. and Marti, H.H., (1997) Hypoxia-inducible factor-1 alpha is regulated at the post-mRNA level. *Kidney Int* (51) 2, 560-3
- (341) White, M.A., Nicolette, C., Minden, A., Polverino, A., Van Aelst, L., Karin, M. and Wigler, M.H., (1995) Multiple Ras functions can contribute to mammalian cell transformation. *Cell* (80) 4, 533-41
- (342) Wieland, O.H., (1983) The mammalian pyruvate dehydrogenase complex: structure and regulation. *Rev Physiol Biochem Pharmacol* (96) 123-70
- (343) Wiener, C.M., Booth, G. and Semenza, G.L., (1996) In vivo expression of mRNAs encoding hypoxia-inducible factor 1. *Biochem Biophys Res Commun* (225) 2, 485-8
- (344) Wingler, K. and Brigelius-Flohe, R., (1999) Gastrointestinal glutathione peroxidase. *Biofactors* (10) 2-3, 245-9

- (345) Wood, J.M., Bold, G., Buchdunger, E., Cozens, R., Ferrari, S., Frei, J., Hofmann, F., Mestan, J., Mett, H., O'reilly, T., Persohn, E., Rosel, J., Schnell, C., Stover, D., Theuer, A., Towbin, H., Wenger, F., Woods-Cook, K., Menrad, A., Siemeister, G., Schirner, M., Thierauch, K.H., Schneider, M.R., Dreves, J., Martiny-Baron, G. and Totzke, F., (2000) PTK787/ZK 222584, a novel and potent inhibitor of vascular endothelial growth factor receptor tyrosine kinases, impairs vascular endothelial growth factor-induced responses and tumor growth after oral administration. *Cancer Res* (60) 8, 2178-89
- (346) Yagi, T. and Hatefi, Y., (1987) Thiols in oxidative phosphorylation: thiols in the F₀ of ATP synthase essential for ATPase activity. *Arch Biochem Biophys* (254) 1, 102-9
- (347) Yamaguchi, M., Belogradov, G.I. and Hatefi, Y., (1998) Mitochondrial NADH-ubiquinone oxidoreductase (Complex I). Effect of substrates on the fragmentation of subunits by trypsin. *J Biol Chem* (273) 14, 8094-8
- (348) Yamamoto, K., Takahashi, T., Asahara, T., Ohura, N., Sokabe, T., Kamiya, A. and Ando, J., (2003) Proliferation, differentiation, and tube formation by endothelial progenitor cells in response to shear stress. *J Appl Physiol* (95) 5, 2081-8
- (349) Yancopoulos, G.D., Davis, S., Gale, N.W., Rudge, J.S., Wiegand, S.J. and Holash, J., (2000) Vascular-specific growth factors and blood vessel formation. *Nature* (407) 6801, 242-8
- (350) Yoo, M.H., Xu, X.M., Carlson, B.A., Gladyshev, V.N. and Hatfield, D.L., (2006) Thioredoxin reductase 1 deficiency reverses tumor phenotype and tumorigenicity of lung carcinoma cells. *J Biol Chem* (281) 19, 13005-8
- (351) Yoo, M.H., Xu, X.M., Carlson, B.A., Patterson, A.D., Gladyshev, V.N. and Hatfield, D.L., (2007) Targeting thioredoxin reductase 1 reduction in cancer cells inhibits self-sufficient growth and DNA replication. *PLoS One* (2) 10, e1112
- (352) Yu, A.Y., Frid, M.G., Shimoda, L.A., Wiener, C.M., Stenmark, K. and Semenza, G.L., (1998) Temporal, spatial, and oxygen-regulated expression of hypoxia-inducible factor-1 in the lung. *Am J Physiol* (275) 4 Pt 1, L818-26
- (353) Zelzer, E., Levy, Y., Kahana, C., Shilo, B.Z., Rubinstein, M. and Cohen, B., (1998) Insulin induces transcription of target genes through the hypoxia-inducible factor HIF-1 α /ARNT. *EMBO J* (17) 17, 5085-94
- (354) Zhang, H., Luo, Y., Zhang, W., He, Y., Dai, S., Zhang, R., Huang, Y., Bernatchez, P., Giordano, F.J., Shadel, G., Sessa, W.C. and Min, W., (2007) Endothelial-specific expression of mitochondrial thioredoxin improves endothelial cell function and reduces atherosclerotic lesions. *Am J Pathol* (170) 3, 1108-20

- (355) Zhong, H., De Marzo, A.M., Laughner, E., Lim, M., Hilton, D.A., Zagzag, D., Buechler, P., Isaacs, W.B., Semenza, G.L. and Simons, J.W., (1999) Overexpression of hypoxia-inducible factor 1alpha in common human cancers and their metastases. *Cancer Res* (59) 22, 5830-5
- (356) Zhong, L., Arner, E.S., Ljung, J., Aslund, F. and Holmgren, A., (1998) Rat and calf thioredoxin reductase are homologous to glutathione reductase with a carboxyl-terminal elongation containing a conserved catalytically active penultimate selenocysteine residue. *J Biol Chem* (273) 15, 8581-91
- (357) Zhong, L., Arner, E.S. and Holmgren, A., (2000) Structure and mechanism of mammalian thioredoxin reductase: the active site is a redox-active selenolthiol/selenenylsulfide formed from the conserved cysteine-selenocysteine sequence. *Proc Natl Acad Sci U S A* (97) 11, 5854-9
- (358) Zhong, L. and Holmgren, A., (2000) Essential role of selenium in the catalytic activities of mammalian thioredoxin reductase revealed by characterization of recombinant enzymes with selenocysteine mutations. *J Biol Chem* (275) 24, 18121-8
- (359) Zhou, J., Damdimopoulos, A.E., Spyrou, G. and Brune, B., (2007) Thioredoxin 1 and thioredoxin 2 have opposed regulatory functions on hypoxia-inducible factor-1alpha. *J Biol Chem* (282) 10, 7482-90
- (360) Zhou, J., Eleni, C., Spyrou, G. and Brune, B., (2008) The mitochondrial thioredoxin system regulates nitric oxide-induced HIF-1alpha protein. *Free Radic Biol Med* (44) 1, 91-8
- (361) Zhu, X.Y., Rodriguez-Porcel, M., Bentley, M.D., Chade, A.R., Sica, V., Napoli, C., Caplice, N., Ritman, E.L., Lerman, A. and Lerman, L.O., (2004) Antioxidant intervention attenuates myocardial neovascularization in hypercholesterolemia. *Circulation* (109) 17, 2109-15
- (362) Zoratti, M. and Szabo, I., (1995) The mitochondrial permeability transition. *Biochim Biophys Acta* (1241) 2, 139-76

7. APPENDIX

7.1. Abbreviations

A	Adenine
ADP	Adenosine diphosphate
AG	Aktiengesellschaft
AMP	Adenosine monophosphate
Amp	Ampicillin
AmpR	Ampicillin resistance gene (β -lactamase)
Ang	Angiopoietin
APC	Adenomatosis polyposis coli gene
APS	Ammonium persulfate
ASK-1	Apoptosis stimulating kinase 1
ATP	Adenosine triphosphate
BCA	Bicinchoninic acid
Bcl-2	B-cell lymphoma 2 protein family
BNIP3	Bcl-2/adenovirus E1B 19kDa protein-interacting protein 3
BOOH	T-Buthylhydroperoxide
bp	Base pair
BSA	Bovine serum albumin
BSO	L-Buthionine sulfoximine
C	Cytosine
CD	Cluster of differentiation (e.g. CD4, CD19, CD31)
cDNA	Complementary DNA
c-Fos	FBJ murine osteosarcoma viral oncogene homolog (also AP-1)
c-Jun	Jun proto-oncogene
CO ₂	Carbon dioxide
Co.	Company
Cre	Cre recombinase
Cys	Cysteine
DAPI	4',6-Diamidino-2-phenylindole
DCFH-DA	Dichlorofluoescein
DMEM	Dulbecco's modified eagle's medium
DMSO	Dimethyl sulfoxide
DNA	Desoxyribonucleic acid

dNTPs	Desoxynucleoside triphosphate
DTNB	5,5'-Dithiobis-(2-nitrobenzoic acid)
E	Embryonic day
EDTA	Ethylenediaminetetraacetic acid
EGTA	Ethyleneglycoltetracetic acid
ELISA	Enzyme-linked immunosorbant assay
Env	Viral envelope gene
eEPCs	Embryonic endothelial progenitor cells
ER	Endoplasmatic reticulum
et al.	Et alii/et aliae
F	Farad, unit of capacitance
FACS	Fluorescence-activated cell sorting
FAD	Flavine adenine dinucleotide
FCS	Fetal calf serum
FGF	Fibroblast growth factor
FITC	Fluorescein isothiocyanate
fl	LoxP flanked allele
FL-1	Fluorescence channel 1 height (bandpass 530/30)
FL-2	Fluorescence channel 2 height (bandpass 585/42)
Flag-tag	Polypeptide protein tag
γ -GCS	γ -Glutamylcysteine synthetase
g	Units of gravity
G	Guanine
Gag	Viral capsid gene
GAPDH	Glyceraldehyde-3-phosphate dehydrogenase
GLUT	Glucose transporter
Gly	Glycine (G)
GmbH	Gesellschaft mit beschränkter Haftung
GPx	Glutathione peroxidase
GR	Glutathione reductase
GSH	Glutathione (reduced)
GSSG	Glutathione (oxidised)
H ₂ O ₂	Hydrogen peroxide
HO•	Hydroxyl radical
HO ₂ •	Hydroperoxyl radical
h	Hour
hCMVieE	Human cytomegalovirus modified chicken promoter

HEPES	(4-(2-Hydroxyethyl)-1-piperazineethanesulfonic acid
Hif	Hypoxia-inducible factor
HIV	Human immunodeficiency virus
HRE	Hypoxia-responsive element
HRP	Horseradish peroxidase
Hsp	Heat shock protein
Ig	Immunoglobulin
IGF2	Insulin-like growth factor 2
IL	Interleukin
iNOS	Inducible nitric oxide synthase
IRES	Internal ribosomal entry site
JNK	C-jun N-terminal kinases
kDa	Kilodalton
KGaA	Kommanditgesellschaft auf Aktien
l	Litre
LB	Luria-Bertani (agar or medium for bacteria)
LMP agarose	Low melting point agarose
Ltk	Leucocyte protein tyrosine kinase
LTR	Long terminal repeat
Lys	Lysin
M	Molar
MEFs	Murine embryonic fibroblasts
MFI	Mean fluorescence intensity
MGd	Motexafin gadolinium
min	Minutes
MLS	Mitochondrial leader sequence
MMP	Mitochondria membrane potential
MnSOD	Manganese superoxide dismutase
MOPS	3-(N-morpholino)propansulfonic acid buffer
mRNA	Messenger ribonucleic acid
MTT	Methylthiozolyldiphenyl-tetrazolium bromide
myc	Myelocytomatosis viral oncogene homolog, proto-oncogene
n	Number of individual measurements
n.s.	Not significant
NAC	N-acetylcysteine
NADPH	Nicotinamide adenine dinucleotide phosphate
NAO	Nonyl acridine orange

NaSe	Sodium selenite
NF κ B	Nuclear factor κ B
NO	Nitric oxide
NOS2	Nitric oxide synthase 2
N-TAPe	N-terminal tandem affinity purification enhanced tag
$^1\text{O}_2$	Singlet oxygen
O ₂	Oxygen
O ₂ ^{-•}	Superoxide anion
OD	Optical density
ODD	Oxygen-dependent degradation domain
p	Passage number (cell culture)
p53	Protein 53 / tumour protein 53
PAEC	Porcine aortic endothelial cells
PBS	Phosphate buffered saline
PCR	Polymerase chain reaction
PDGF	Platelet-derived growth factor
PECAM	Platelet endothelial cell adhesion molecule
PEITC	Phenylethyl isothiocyanate
PFA	Paraformaldehyde
PGC1 α	Peroxisome proliferator-activated receptor γ co-activator 1- α
PHD	Prolyl hydroxylase
PI3K	Phosphoinositide-3-kinase
PMSF	Phenylmethylsulfonyl fluoride
Pol	Viral polymerase gene
PP _i	Diphosphate
Pro	Proline
Prx	Peroxiredoxin
PT	Mitochondrial permeability transition pore
PTP1B	Protein tyrosine phosphatase, non-receptor type 1
PuroR	Purmomycin N-acetyltransferase gene
PX-12	1-Methylpropyl 2-imidazolyl disulfide, Txnrd inhibitor
ras	Rat sarcoma, proto-oncogene
RCC	Respiratory chain complex
Rev	Viral transcriptase gene
RNA	Ribonucleic acid
rRNA	Ribosomal ribonucleic acid
RO [•]	Alkoxy radical

RO ₂ •	Peroxyl radical
ROS	Reactive oxygen species
rpm	Revolutions per minute
s	Seconds
S	Sulfur
SD	Standard deviation
SDS	Sodium dodecylsulfate
SDS-Page	Sodium dodecylsulfate-polyacrylamide gel electrophoresis
Se	Selenium
Sec	Selenocysteine
SECIS	Selenocysteine insertion sequence
SelZ	Selenoprotein Z (e.g. SelZf1, SelZf2)
Ser	Serine
siRNA	Small interfering RNA
SOD	Superoxide dismutase
Strep-tag	Synthetic peptide sequence towards Strep-Tactin
TBE-buffer	Tris-borate-EDTA buffer
TBS-T	Tris-buffered saline with Tween
TCA	Tricarboxylic acid cycle
TCA	Trichloroacetic acid
TE-buffer	Tris-EDTA buffer
TEMED	N,N,N',N'-tetramethylethylenediamine
TFB	Standard transformation buffer
Tg	Transgenic
TGF	Transforming growth factor
TGR	Thioredoxin-glutathione reductase (Txnrd3)
TM	Melting temperature of primers
TMPD	Tetramethylphenylendiamin
TNF	Tumour necrosis factor
Tris	Tris(hydroxymethyl)aminomethane
Trx	Murine thioredoxin
Trx1	Murine thioredoxin, cytosolic isoform
Trx2	Murine thioredoxin, mitochondrial isoform
Trx-S ₂	Murine thioredoxin, oxidised
Trx-(SH) ₂	Murine thioredoxin, reduced
TSP1	Thrombospondin 1
Txnrd	Murine thioredoxin reductase

Txnrd1	Murine thioredoxin reductase, cytosolic isoform
Txnrd2	Murine thioredoxin reductase, mitochondrial isoform
Txnrd3	Murine thioredoxin-glutathione reductase (TGR)
U	Uracil
UGA	'Opal' stop codon
UTR	3'Untranslated region
UV	Ultra violet
Val	Valin (V)
VE-cadherin	Vascular endothelial cadherin
VEGF	Vascular endothelial growth factor
VHL	Von Hippel-Lindau gene
vs.	Versus
wt	Wild-type
μ	Micro
Ø	Diameter

7.2. Publications

7.2.1. Poster presentations

The impact of the mitochondrial thioredoxin reductase (Txnrd2) on tumour progression and tumour-associated angiogenesis.

Hrdina J., Perisic T., Schneider M., Conrad M., Beck H.

87th Annual Meeting of the German Society of Physiology, March 2-5, 2008
Cologne, Germany

Loss of mitochondrial thioredoxin reductase (Txnrd2) limits tumour growth.

Hrdina J., Perisic T., Esposito I., Schneider M., Conrad M., Beck H.

88th Annual Meeting of the German Society of Physiology, March 22-25, 2009
Giessen, Germany

Loss of mitochondrial thioredoxin reductase (Txnrd2) delays angiogenic switch and limits tumour growth.

Hellfritsch J., Perisic T., Esposito I., Schneider M., Conrad M., Beck H.

2nd International Seeon "Tumour-vessel" Meeting, SPP1190, DFG, September 19-22, 2009
Seeon, Germany

Loss of mitochondrial thioredoxin reductase (Txnrd2) delays angiogenic switch and limits tumour growth.

Hellfritsch J., Perisic T., Esposito I., Schneider M., Pohl U., Conrad M., Beck H.

Joint Meeting 2009 of the Society for Microcirculation and Vascular Biology and the Swiss Society of Microcirculation, October 8-10, 2009
Bern, Switzerland

7.2.2. Oral communication

Loss of mitochondrial thioredoxin reductase (Txnrd2) delays angiogenic switch and limits tumour growth.

Young Investigator Meeting SPP1190, May 19-21, 2010
Dresden, Germany

7.2.3. Original publication

Working title: Loss of mitochondrial thioredoxin reductase limits tumour growth by compromising tumour-associated angiogenesis.

Hellfritsch J., Perisic T., Esposito I., Lüdemann S., Eichhorn M., Kuhlencordt P., Koelle P., Schneider M., Pohl U., Conrad M., Beck H. (*in preparation*)

The gastrointestinal microbiota effects the selenium status and selenoprotein expression in mice. (2009) *Hrdina J., *Banning A., Kipp A., Loh G., Blaut M., Brigelius-Flohé R.

J Nutr Biochem. 20 (8): 638-48

*These authors contributed equally to this work.

7.3. Curriculum vitae

Personal data

Name	Juliane Hellfritsch, née Hrdina
Date of birth	February 27, 1983
Place of birth	Bad Schlema/Erzgebirge, Germany
Nationality	German
Marital status	Married

Academic education

Since 08/2007	Ph.D. thesis Walter-Brendel-Centre of Experimental Medicine, Prof. Dr. U. Pohl Medical Faculty, Ludwig-Maximilians-University Munich, Munich, Germany
07/2007	Diploma (nutritional scientist)
08/2006 – 06/2007	Diploma thesis Biochemistry of Micronutrients, Prof. Dr. R. Brigelius-Flohé German Institute of Human Nutrition, Potsdam-Rehbrücke, Germany
07/2006	Summer school “Epidemiology of nutrition“ Epidemiology, Prof. Dr. R. Boing German Institute of Human Nutrition Potsdam-Rehbrücke, Germany
04/2006 – 06/2006	Work experience Institute of Nutrition Research, Prof. Andrew Collins Faculty of Medicine, University of Oslo, Norway
10/2005 – 12/2006	Work experience Nutrition and Health, Prof. Dr. T. Remer Research Institute of Child Nutrition, Dortmund, Germany
06/2003	Preliminary diploma
10/2001 – 07/2007	Studies of Nutritional sciences Friedrich-Schiller University, Jena, Germany
1993 – 2001	Grammar School, ‘Christian Gottlieb Reichard’ Gymnasium, Bad Lobenstein, Germany

7.4. Acknowledgements

The work of this thesis was performed in the laboratories of the Walter-Brendel-Centre of Experimental Medicine in Munich. During the years I spent working on the mitochondrial thioredoxin reductase I learned so much and this thesis would not have been possible if it wasn't for a number of important people. At this point, I would like to take the opportunity and say `thank you`:

Prof. Dr. Ulrich Pohl for giving me the opportunity to perform this work at the Walter-Brendel-Centre. Thank you for fruitful discussions, helpful suggestions and suitable support.

My supervisor Dr. Heike Beck for overall support in many ways, introduction to the mitochondrial thioredoxin reductase, redox-regulation and tumour biology, limit-less time for interesting discussions but also relaxed chats, numerous suggestions and vivid ideas, sympathy and strong support during the final phase of my work.

Prof. Dr. Angelika Vollmar for accepting me as external Ph.D. student, thereby enabling the dissertation in natural sciences at the Ludwig-Maximilians-University in Munich.

The members of our working group, Dr. Manuela Schneider, Markus Wortmann and Matthias Semisch, for their help in the lab, technical assistance and supportive suggestions at any time. Thank you for uncomplicated support for me whenever I asked (especially at the end of my work).

Thank you Dr. Tamara Perisic for all the great help throughout my time in the lab but even in the beginning of my work and also for the funny times we spent outside the lab. Dr. Pankaj Kumar Mandal, thank you for your technical assistance with establishing new assays and your help in the lab at any time.

Dr. Marcus Conrad for great comments during my seminars. Thank you for all your bright ideas and interesting discussions. I also would like to put emphasis on the help and support by Heidi Förster and Alexander Mannes.

My roomies Dr. Theres Hennig, Juliane Behrens, Stefan Wallner, Angela Ritter, Julian Kirsch and Fabian Kellner for a great office atmosphere with helpful scientific and amusing everyday

discussions. Thank you for nice times we spent at congress visits and outside the lab. It has been a pleasure to work with you!

Thanks to all technicians of the Pohl group for technical support and help at any time in the lab.

Dr. Irene Esposito and Monika Tost (Institute of Pathology, Helmholtz Centre, Munich) for kindly performing and analysing immunohistological stainings of tumours and expert appraisal of the sections.

Dr. Holger Prokisch and Birgit Haberberger (Institut of Human Genetics, Helmholtz Centre, Munich) for kindly introducing me to High-resolution respirometry and giving me the opportunity to perform my analysis at the laboratories of the Helmholtz Centre.

Thanks to Sirii Lüdemann (Group of Dr. Martin Eichhorn, Surgical Clinic and Polyclinic Großhadern, Munich) for performing fascinating experiments using skinfold chambers and intravital microscopy to analyse tumour vascularisation.

Also, I would like to thank Pirkko Koelle (Group Dr. Peter Kuhlencordt, Department Angiology, Polyclinic LMU, Munich) for performing HPLC and ESR measurements.

My parents, Anette and Helmut, thank you for your unquestioning support at any time and all your love. Thanks to my sister Franziska for also being just a phone call away, listening and discussing open-end.

My husband Enrico for believing in me (even though I was thinking about to quit), standing behind me and having the time and patience when nobody would. Thank you for your limitless optimism and your constant positive thinking. With you by my side I had the feeling that I can beat the odds.